UNIVERSITY OF CALIFORNIA SAN DIEGO

Investigations into the mechanism of DNA binding and transcriptional regulation by the NF-κB subunit RelA

A Dissertation submitted in partial satisfaction of the requirements
for the degree Doctor of Philosophy

in

Chemistry

by

Shandy Shahabi

Committee in charge:

Professor Gourisankar Ghosh, Chair
Professor John E. Crowell
Professor Partho Ghosh
Professor Christopher K. Glass
Professor Patricia A. Jennings

2023

The Dissertation of Shandy Shahabi is approved, and it is acceptable in quality and form for publication on microfilm and electronically.

University of California San Diego

2023

DEDICATION

I dedicate this to thesis to my beloved parents, Shahriar Shahabi and Melle Shahabi. Words cannot express my gratitude for their unrelenting love and support. They are always on my mind and are my source of strength.

TABLE OF CONTENTS

LIST OF FIGURES

LIST OF TABLES

LIST OF ABBREVIATIONS

A	Adenine
bp	Base pair(s)
BSA	Bovine serum albumin
C	Cytosine
ChIP	Chromatin immunoprecipitation
DBD	DNA Binding Domain
DD	Dimerization Domain
DTT	Dithiotheirol
EMSA	Electrophoretic mobility shift assay
EV	Empty vector
FLAG	Peptide with sequence DYKDDDDK
G	Guanine
HEK293T	Human embryonic kidney, 293T
MEF	Mouse embryonic fibroblast
MD	Molecular dynamics
NE	Nuclear Extract
NF-κB	Nuclear Factor Kappa B
PCR	Polymerase chain reaction
PMSF	Phenylmethylsulfonyl fluoride
RE	Response element
RHR	Rel Homology Region
RNA-Seq	RNA sequencing

RT-qPCR	Reverse transcription with quantitative PCR
SDS-PAGE	Sodium dodecyl sulfate-polyacrylamide gel electrophoresis
T	Thymine
TF	Transcription factor
TAD	Transactivation Domain
TNFα	Tumor Necrosis Factor Alpha
WB	Western Blot
WT	Wild-type

ACKNOWLEDGEMENTS

I would like to thank my thesis advisor Dr. Gourisankar Ghosh for granting me the opportunity to conduct research under his guidance. His passion and dedication for science has been my source of motivation throughout the years and his teachings have, and will continue to, shape the scientist I am to become. It has been a privilege to work in his lab and couldn't have asked for a better mentor.

I would like to thank members of my dissertation committee, Dr. Partho Ghosh, Dr. Patricia Jennings, Dr. John Crowell, and Dr. Christopher Glass, for taking the time to read and critically evaluate my dissertation and provide helpful insight.

I would like to thank Dr. Kaushik Saha, Dr. Tapan Biswas, and Dr. Maria Carmen Mulero for providing me with guidance during my beginning years as a graduate student. Their teachings formed a foundation for my approach to science and have made me a better experimentalist and critical thinker.

I would also like to thank present lab members of the Gourisankar Ghosh lab, Zixing Liu, Yuting Shen, Diana Grada-Ibarra, Wyatt Miller, and Dr. Suborno Jati. It has been an absolute pleasure working with them and their help has dramatically advanced progression of my projects.

I would like to thank former lab members, Charles Lumba, Kyle Shumate, Dr. Myung Soo Ko, Dr. Sonjiala Hotchkiss, Emily Walters, William Suryajaya, and Weihan Huai for enriching my experiences at UCSD. I miss them deeply and I am often reminded of the times we shared in lab.

I would also like to thank the labs of Dr. Simpson Joseph, Dr. Kevin Corbett, Dr. Shankar Subramaniam, Dr. Alexander Hoffmann, Dr. Sushil Mahata, and Dr. Tapas Hazra for willingness to collaborate and technical help with experimental setup.

Lastly, and certainly not least, I would like to thank Kaushika Vayyala for her unrelenting support throughout my studies. Her patience and compassion cannot be overstated, and I will forever cherish the experiences we have shared.

Chapter 2, in part, has been submitted for publication of the material as it may appear in Nucleic Acids Research, 2023, Shahabi, Shandy; Ghosh, Gourisankar, Oxford Press, 2023. The dissertation author was the primary researcher and co-first author of this paper.

Chapter 3, in part is currently being prepared for submission for publication of the material. Shahabi, Shandy; Ghosh, Gourisankar. The dissertation author was the primary investigator and author of this material.

Chapter 4, in part, is currently being prepared for submission for publication of the material. Shahabi, Shandy; Ghosh, Gourisankar. The dissertation author was the primary investigator and author of this material.

VITA

EDUCATION

2023 Doctor of Philosophy in Chemistry, University of California San Diego

2015 Master of Science in Biochemistry and Molecular Biology, University of Southern California

2012 Bachelor of Science in Biochemistry, University of California, Los Angeles

PUBLICATIONS

Li T, **Shahabi S**, Biswas T, Tsodikov OV, Huang DB, Wang V, Wang Y, Ghosh G. Dynamicity of base-specific interactions determines binding stability of NF-κB complexes with κB DNA. *Submitted for publication*

Liu MA, **Shahabi S**, Jati S, Tang K, Gao H, Jin Z, Miller W, Meunier FA, Ying W, van den Bogaart G, Ghosh G, Mahata SK. Gut microbial DNA and immune checkpoint gene Vsig4/CRIg are key antagonistic players in healthy aging and age-associated development of hypertension and diabetes. Frontiers in Endocrinology. 2022; 13:1037465.

de Rozières CM, Pequeno A, **Shahabi S**, Lucas TM, Godula K, Ghosh G, Joseph S. PABP1 drives the selective translation of influenza A virus mRNA. Journal of Molecular Biology. 2022; 434(5):167460.

Tapryal N, **Shahabi S,** Chakraborty A, Hosoki K, Wakamiya M, Sarkar G, Sharma G, Cardenas VJ, Boldogh I, Sur S, Ghosh G, Hazra TK. Intrapulmonary administration of

purified NEIL2 abrogates NF-κB-mediated inflammation. Journal of Biological Chemistry. 2021; 296:100723.

Shahabi S, Kumaran V, Castillo J, Cong Z, Nandagopal G, Mullen DJ, Alvarado A, Correa MR, Saizan A, Goel R, Bhat A, Lynch SK, Zhou B, Borok Z, Marconett C. LINC00261 is an epigenetically regulated tumor suppressor essential for activation of the DNA damage response. Cancer Research. 2019; 79(12):3050-3062.

Mulero MC, **Shahabi S**, Ko MS, Schiffer JM, Huang DB, Wang VY, Amaro RE, Huxford T, Ghosh G. Protein cofactors are essential for high-affinity DNA binding by the nuclear factor κB RelA subunit. Biochemistry. 2018; 57(20):2943-2957.

ABSTRACT OF THE DISSERTATION

Investigations into the mechanism of DNA binding and transcriptional regulation by the NF-κB subunit RelA

by

Shandy Shahabi

Doctor of Philosophy in Chemistry

University of California San Diego, 2023

Professor Gourisankar Ghosh, Chair

The NF-κB family of dimeric transcription factors function as master regulators of inflammation and the innate immune response. Upon pathway activation, cytoplasmic NF-κB dimers translocate to the nucleus and bind DNA response elements, known as κB DNAs or κB sites, at the promoters or enhancers of pro-inflammatory genes to activate transcription. Like other transcription factors, NF-κB binding affinity to κB DNA is sequence-dependent, however *in vitro* binding affinity is not a determinant of transcriptional output in the cell. Further, recent reports suggest that nuclear cofactors influence NF-κB DNA binding to κB DNA. This thesis explores what factors contribute to DNA binding by the NF-κB subunit RelA. Chapter 1 introduces gene regulation by NF-κB and outlines current gaps in our understanding of DNA binding by NF-κB. Chapter 2 explores how the central nucleotide of κB DNA modulates RelA DNA binding affinity. Our results show that the central nucleotide of κB DNA dramatically influences RelA:κB DNA complex stability through transient and dynamic interactions not observed in crystal structures. Chapter 3 investigates how locally distributed low affinity κB sites contribute to DNA binding by RelA. Our results show that low affinity binding sites impact RelA DNA binding kinetics and overall affinity, and tandemly organized low affinity κB sites can synergistically activate RelA-dependent transcription. Additionally, DNA-dependent cofactors can associate with RelA on κB DNA to collectively increase promoter occupancy and activate transcription. Chapter 4 explores how nuclear cofactors contribute to RelA DNA binding affinity. Our results show that nuclear cofactors enhance RelA DNA binding *in vitro* and we identify NME1 as a κB site-specific nuclear cofactor for RelA.

Chapter 1: Introduction

Nuclear-Factor Kappa B (NF-κB) are a family of dimeric transcription factors that regulate a multitude of physiological processes in response to various extracellular stress signals (Zhang, 2017). Originally discovered in 1986 in the lab of David Baltimore, NF-κB was first identified as a nuclear factor with DNA binding specificity to the enhancer element of the kappa light chain gene in activated B cells (Sen, 1986). Subsequent research established that the NF-κB pathway plays a pivotal role in early activation of inflammatory signaling and the immune response (Hayden, 2012; Liu, 2017). Additionally, NF-κB signaling has also been implicated in many different cellular pathways which include cell survival, apoptosis, proliferation, differentiation, angiogenesis, and development (Xia, 2014). Consequently, aberrant NF-κB signaling contributes to various diseases, such as hyperinflammation, autoimmunity, and immunodeficiencies, and is involved in carcinogenesis and metastasis (Taniguchi, 2018; Lawrence, 2009).

The NF-κB transcription factors form homodimeric or heterodimeric complexes derived from five related polypeptides: RelA (p65), RelB, c-Rel, p100/p52, and p105/p50 (**Figure 1.1**) (Hoffmann, 2003). All members share a conserved stretch of approximately 300 amino acids at the N-terminus known as the Rel Homology Region, or RHR (Oeckinghaus, 2009; Ghosh, 2012). The RHR is responsible for sequence-specific DNA binding, subunit dimerization, and nuclear localization (Huxford, 1999). RelA, RelB, and c-Rel also contain a C-terminal transactivation domain (TAD) which allow them to act as transcriptional activators through coactivator recruitment. p52 and p50 are generated by partial proteolytic processing of p100 and 105, respectively, and do not have a TAD, leading them to function as transcriptional repressors in their homodimeric forms. p52 and p50 can however form transcriptionally active complexes

through heterodimerization with RelA, RelB, or c-Rel, or through association with non-Rel proteins, including the IκB family of proteins such as Bcl3 and IκBζ (Hayden, 2011).

Under resting conditions, most NF-κB dimers are maintained in an inactive state through association with the inhibitory IκB class of proteins (Baldwin, 1996). In canonical NF-κB signaling, the p50:RelA heterodimer is associated with IκBα through protein-protein interactions between the dimerization domain of RelA with IκBα, thus masking the nuclear localization signal of RelA (Huxford, 1998). Canonical pathway activation occurs following binding of an extracellular stimulatory molecule to the corresponding membrane associated receptor (**Figure 1.2**) (Glass, 2015). Stimuli can be derived from various sources, including proinflammatory cytokines, viral or bacterial components, UV-induced DNA damage, reactive oxygen species, and growth factors (Yu, 2020). Classic examples of ligand-receptor complexes in the canonical NF-κB signaling pathway include tumor necrosis factor alpha (TNFα) with TNFα receptor 1 (TNFR1), lipopolysaccharide (LPS) with toll-like receptor 4 (TLR4), interleukin-1 beta (IL-1β) with IL-1 receptor 1, and engagement of T-cell receptor (TCR) with antigen-associated major histocompatibility complex (MHC). Following ubiquitin-dependent adapter proteins recruitment, the central event in canonical NF-κB signaling is phosphorylation and activation of the IκB kinase (IKK) complex, which consists of IKK1/α, IKK2/β, and the regulatory subunit NF-κB essential modulator (NEMO) (Chen, 2013; Karin, 1999). The activated IKK complex then phosphorylates the substrate IκBα at Ser32 and Ser36, leading to subsequent K48-linked ubiquitination at Lys21 and Lys22 and 26S proteasome mediated degradation of IκBα (Karin, 2000). The liberated p50:RelA dimer is then shuttled to the nucleus through association of the nuclear localization signals with the adapter protein importin α, where it binds to the promoter or

enhancer regions of hundreds of downstream target genes and activates their transcription (Huang, 2000; Wong, 2011; Sharif, 2007).

NF-κB dimers engage in sequence specific interactions with double stranded DNA of the consensus: 5'-GGGRNNYYCC-3', where R = purine, Y = pyrimidine, and N = any nucleotide (**Figure 1.3**) (Chen, 1998; Wan, 2009; Mulero, 2019). Notably, the series of G and C nucleotides at the flanking ends of the 10 bp consensus display significant conservation and are a distinguishing feature of κB DNA, whereas the central region has higher variability. X-ray crystallographic studies of different NF-κB RHR dimers with many different κB DNAs reveal a shared structural architecture and mechanism of κB DNA recognition across all members (Ghosh, 1995; Muller, 1995; Ghosh, 2012). Overall, the RHR folds into two globular domains, the DNA binding domain (DBD) and dimerization domain (DD), connected by an approximate 10 amino acid linker. Both the DBD and DD are arranged into variations of the common immunoglobulin-like fold with a sandwich of antiparallel β-strands. Generally, each NF-κB monomer recognizes one half-site of the pseudosymmetric κB DNA that is separated by a central nucleotide, and contacts with DNA are made by both domains through loops that join the individual β-strands (Zabel, 1991). Each monomer makes contacts with both half-sites of κB DNA, however sequence specific DNA interactions are strictly mediated by a conserved stretch of amino acids within the DBD. In RelA, the corresponding residues are: Arg33, Arg35, and Arg41, which make contacts with flanking stretch of G, Tyr36 that makes van der Waals contacts with T of the reverse strand, and Glu39 that makes contacts with C on the reverse strand (**Figure 1.4**). In the case of p50 and p52, an additional His makes base-specific contacts with the 5'-G of the consensus, leading to preference for the 5-bp long half-site beginning with 5'-GGG. RelA, RelB, and c-Rel have an Ala substitution at this residue, allowing for variance in the

identity of the nucleotide at this position and recognition of the 4-bp half-site beginning with 5'-GG. Despite our structural understanding of the NF-κB and κB DNA complex, it has been observed that NF-κB dimers can also engage in promoters of target genes at DNA sequences with only a half site consensus or with sequences that substantially deviate from the consensus, such as CCND1 (GGGACTTTT), CCR7 (GGGGCTTTTT), IL1B (AGGGGGAAT), and Ccl3 (GGGAAAATTT) (Tong, 2016; Mulero, 2019). The mechanism by which NF-κB engages these sites, and sites lacking any similarity to the consensus κB DNA sequence, remains unclear.

Among all NF-κB members, the RelA subunit is the most extensively characterized due to its ubiquitous and constitutive expression and its involvement in nearly all NF-κB activity-dependent cellular functions (Smale, 2012). Predominantly associated with p50 to form the p50:RelA heterodimer, RelA also homodimerizes to form the RelA:RelA homodimer that regulates a nonredundant subset of NF-κB dependent genes (Tsui, 2015). Previous work established that the DNA binding propensity of RelA containing dimers can be influenced by the presence of specific protein cofactors, which include transcription factors such as IRF3, p53, E2F1, FOXM1, and KLF6, but also by non-transcription factor proteins, such as RPS3, SAM68, NPM1, OGG1, and HMGA1 (Mulero, 2019). Such cofactors enable recruitment of RelA to specific target genes under specific stimuli and in different cell-types, enabling a fine tuning of the RelA-dependent cellular response. Additionally, RelA has been shown to undergo different types of stimulus-specific post-translational modifications that alter RelA DNA binding activity. These modifications include phosphorylation, acetylation, methylation, SUMOylation, ubiquitination, O-GlcNAcylation, and deamidation. (Zhong, 1997; Chen, 2002; Ea, 2009; Liu, 2012; Allison, 2012; Zhao, 2020). Many layers of regulation control RelA recruitment to target

sites *in vivo.* However, a comprehensive and mechanistic understanding of how RelA binds DNA is lacking.

There is a fundamental disconnect between observed binding affinity of recombinant RelA *in vitro* compared to what is observed *in vivo.* First, despite measured differences in binding affinity of NF-κB dimers to sequences that deviate from the consensus motif, NF-κB nonetheless selectively engages in weaker binding sites despite the breadth of available sites present in the genome (Siggers, 2012; Martone, 2003; Zhao, 2014; Kolovos, 2016). Also, previous *in vitro* studies using techniques such as electrophoretic mobility shift assay (EMSA) and fluorescence-based assays reveal that cellular NF-κB complexes exhibit an approximate 100-fold greater affinity to κB DNA relative to purified components (Phelps, 2000; Leitner, 2021; Sanjabi, 2005). Lastly, purified NF-κB forms stable complexes on κB DNA with a half-life on the minute to hour timescale, whereas intracellular photobleaching and single molecule experiments reveal residence times of RelA on DNA for only a few seconds (Zabel, 1990; Chen-Park, 2002; Yie, 1999; Bosisio, 2006; Callegari, 2019). Currently, there is no clear explanation for the strong but short-lived interactions of NF-κB with DNA *in vivo* and how this mechanistically relates to transcriptional activation in the cell. Additionally, exactly what factors drive the discriminatory selection of NF-κB to specific κB sites in the genome is not known.

In this dissertation, I use *in vitro* biochemical and cell-based assays to address the current gaps in our understanding of κB DNA binding and transcriptional regulation by RelA. In Chapter 2, I explore the function of the central bp in κB DNA in influencing the affinity and specificity of RelA binding. Although structurally we observe no interaction of the central bp with RelA, binding analyses indicate that binding affinity of RelA has a high dependence on the identity of the central bp. Molecular dynamics (MD) simulations reveal differential dynamics of RelA with

respect to the identity of the central bp of κB DNA, and this was validated *in vitro*. This chapter explores how transient and dynamic interactions of RelA with κB DNA account for altered DNA binding specificity. In Chapter 3, I explore how low affinity κB sites contribute to RelA-mediated gene expression. I observe an unexpected presence of weak κB binding motifs colocalized with RelA ChIP-Seq peaks of TNFα stimulated mouse embryonic fibroblasts (MEF) and biochemically characterize the significance of weak sites. I identified the NFAT family of transcription factors, specifically NFATc1 and NFAT5, as contributors to regulation at the Cxcl2 promoter and explore the relation between RelA and NFATc1 on DNA. In Chapter 4, I explore how cofactors contribute to NF-κB mediated gene expression. I build upon the foundation of understanding for previously identified cofactors, such as p53 and RPS3, and develop an alternative approach to identify new cofactors. I identify NME1 as a cofactor that augments RelA binding to κB DNA in unstimulated nuclear extract and examine the biochemistry behind NME1-dependent κB DNA binding by RelA.

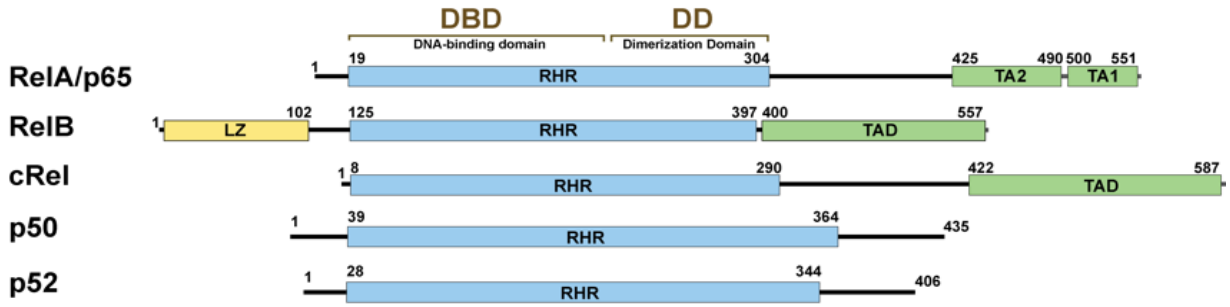

Figure 1.1: NF-κB family subunits
The mammalian NF-κB family consists of five distinct polypeptides, RelA (p65), RelB, c-Rel, p50, and p52. All members share a conserved N-terminal RHR domain that is responsible for DNA binding and subunit dimerization.

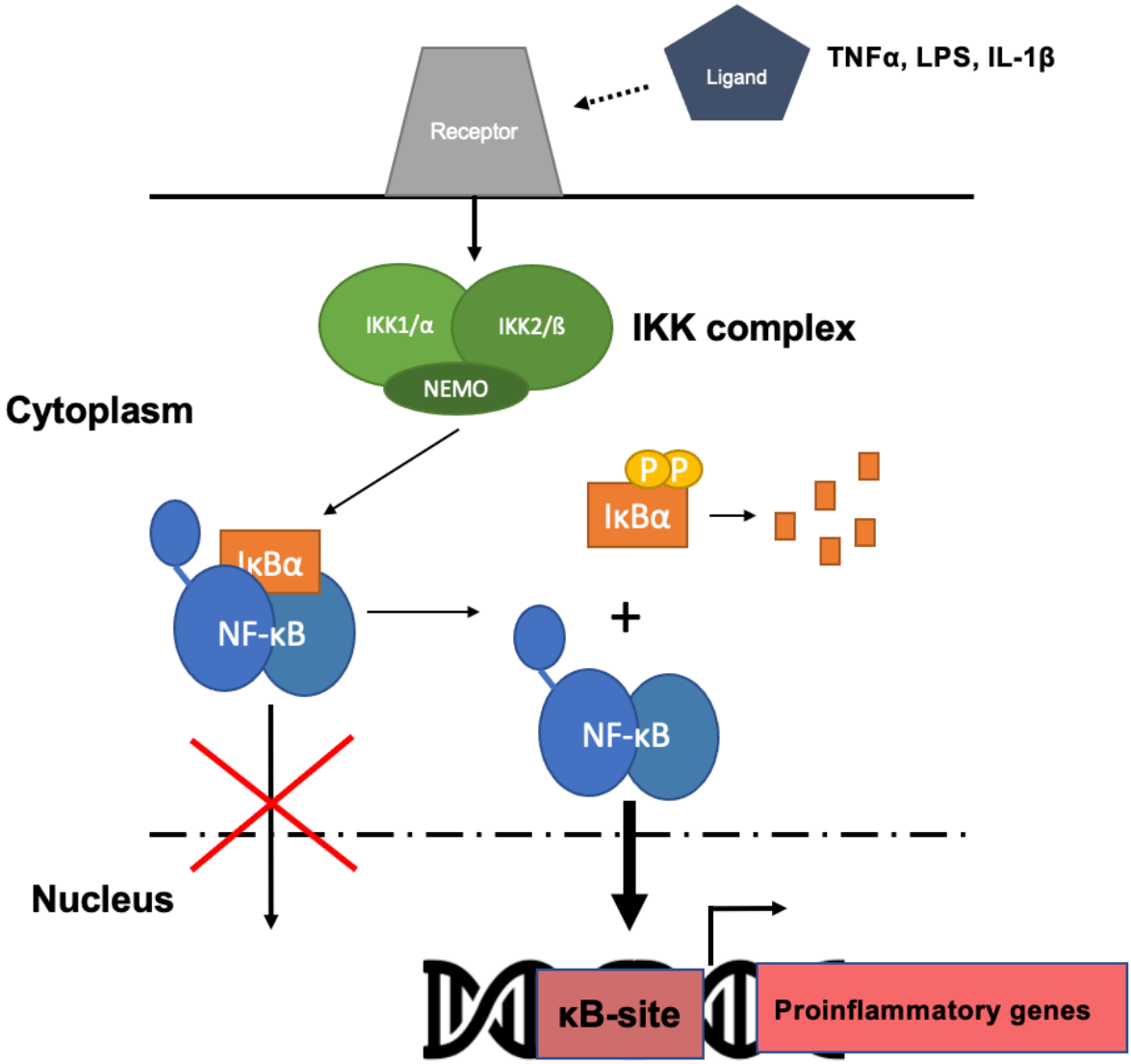

Figure 1.2: Canonical NF-κB signaling
In canonical NF-κB signaling, initially NF-κB dimers are sequestered as inactive cytoplasmic complexes through association with the inhibitory IκBα. Upstream ligand-receptor binding activates the IKK complex, leading to phosphorylation and degradation of IκBα. Liberated NF-κB will then translocate to the nucleus and bind κB sites at promoters or enhancer regions of inflammatory genes to activate transcription and initiate the immune response.

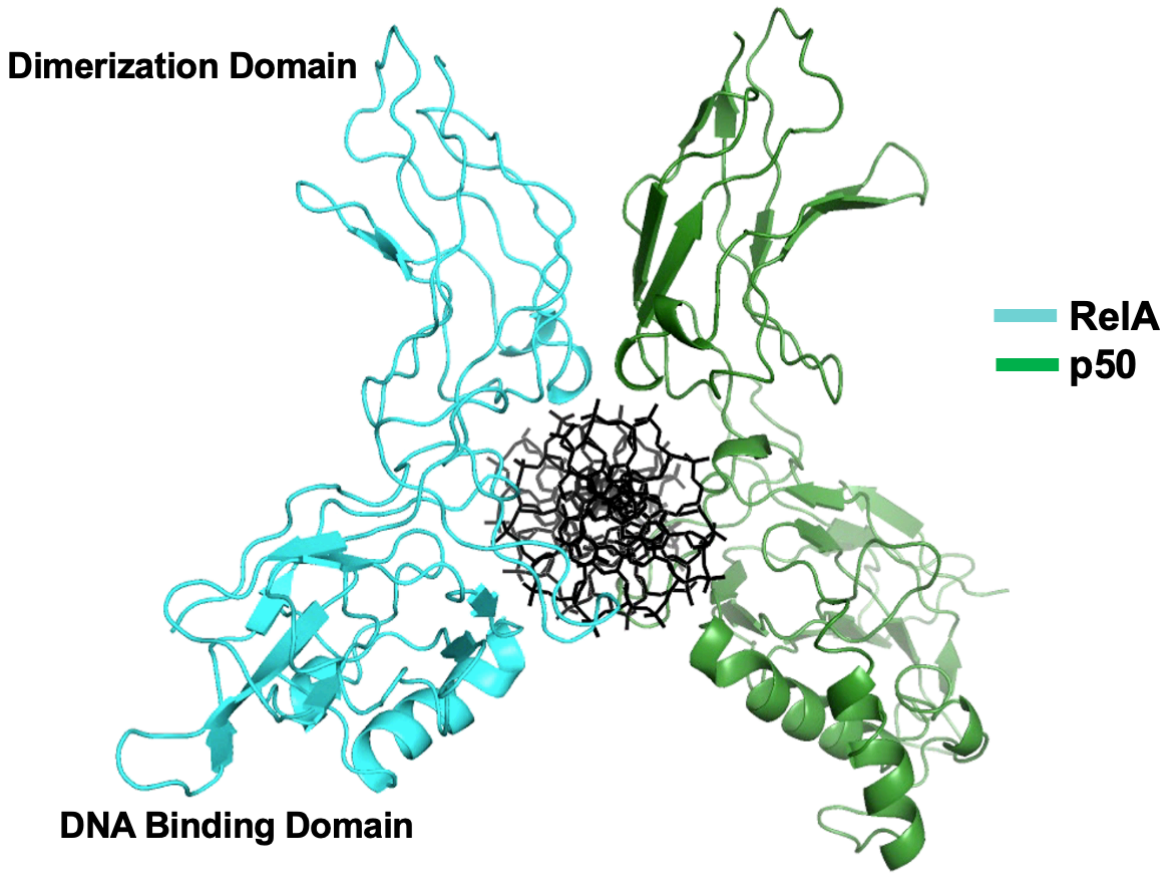

Figure 1.3: Structure of the p50:RelA heterodimer bound to κB DNA
NF-κB RHR folds into two globular domains, the DNA binding domain and dimerization domain. Both domains are arranged into variations of the common immunoglobulin-like fold with a sandwich of anti-parallel β-strands. Both domains make contacts with DNA, however the DNA binding domain is responsible for base-specific contacts.

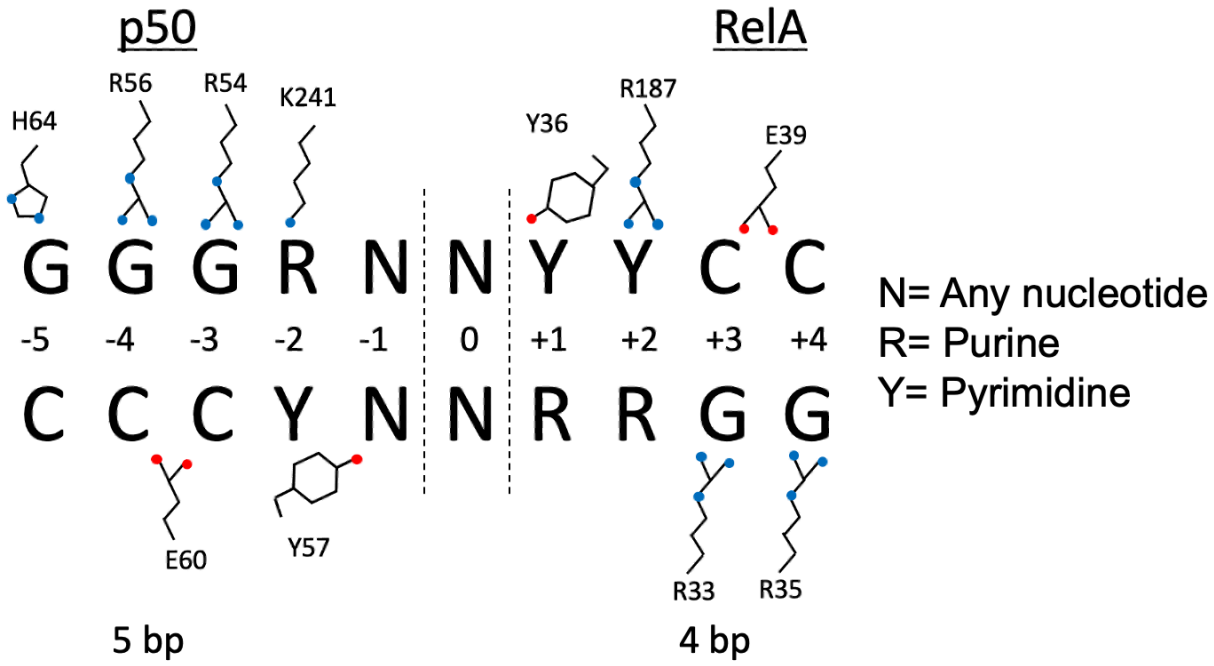

Figure 1.4: Consensus motif recognized by p50:RelA heterodimer
The consensus motif recognized by the p50:RelA heterodimer is mediated by conserved Arg, Tyr, and Glu residues present in all dimers. Whereas RelA recognizes the 4 bp half site, p50 contains an additional His making contacts with the $^{-5}$G, allowing recognition of the 5 bp half site. Altogether, the p50:RelA heterodimer recognizes the 9 bp pseudosymmetric consensus separated by a central uncontacted nucleotide.

Chapter 2: Dynamics of base-specific interactions determines binding stability of NF-κB:DNA complexes

A. Abstract

The dimeric NF-κB transcription factors regulate gene expression by binding to a variety of ~10 base pair long κB DNA elements with G:C-rich flanking sequences enclosing a variable central sequence. I investigated the function of the degenerate central region in influencing the affinity and specificity of NF-κB binding. The binding analyses indicate an unusual dependence of affinity on the identity of the central base pair, with A- and T-κB DNAs displaying ~10-fold higher affinities than G- and C-κB DNAs. The static crystal structures of neither the complexes nor the free κB DNAs explain the differences in affinity. Interestingly, differential dynamics of several DNA-interacting residues are revealed in MD simulations of κB DNAs and protein:DNA complexes. The most striking among these is the transient base-specific contacts of Arg124 with the A-κB DNA through the minor groove rarely observed in the G-κB DNA complex. Arg187 interacts with flanking G:C rich regions through the major groove of the DNA, and is regulated by an intricate network of several residues at the central region, suggesting dynamics at the central base pair and surrounding region influence protein:DNA contacts. Overall, this work provides a basic framework to understand how transient and dynamic interactions between residues in an ensemble of conformers, and not a particular predominant conformer of the NF-κB:κB DNA complex, could account for sequence specificity and affinity.

B. Introduction

Eukaryotic transcription factors regulate gene transcription by binding to their cognate DNA response elements. These factors often bind to an expanded repertoire of DNA sites with significant sequence variability (Inukai, 2017). Affinity of a transcription factor for its DNA binding sites above a threshold level is necessary for transcription, although affinity measured *in vitro* and transcription activation are not necessarily correlated (Cross, 1989; Mulero, 2017; Meijsing, 2009). Recognition elements in DNA for engaging transcription factors can be classified as direct or indirect. Direct are interactions between specific chemical groups of DNA bases and protein residues. In contrast, indirect are interactions between protein and DNA where the specificity originates from overall DNA structure or dynamics that are dictated by a particular sequence (Sarai, 2005). Indirect are often apparent when variation in a DNA sequence at a site not directly contacted by the transcription factor significantly alters the affinity. The NF-κB family of dimeric transcription factors bind DNA sequences that could be defined by a degenerate consensus sequence. Here I investigate how binding of NF-κB to DNA could be regulated through minor variations in sequence often observed in nature, and at times critical to the transcriptional output.

The NF-κB dimers regulate transcription of hundreds of target genes, influencing a broad spectrum of cellular programs, in particular immune and inflammatory responses, and cell survival and death (Hoffmann, 2006; Zhang, 2017; Ghosh, 2012; Hayden, 2012). Members of NF-κB share a conserved stretch of ~300 amino acids known as the Rel homology region (RHR) that is responsible for DNA binding and subunit dimerization (**Figure 2.1**). The discovery of a multitude of κB sites from genome-wide studies suggested that the consensus κB sequence was 5'- $G^{5}G^{4}G^{3}R^{2}N^{1}N^{0}Y^{-1}Y^{-2}C^{-3}C^{-4}$ -3' where N=any nucleotide, R=purine, and Y=pyrimidine, with

a partial two-fold symmetry around a central pair (Mulero, 2019; Siggers, 2011). The two sides of this central base are referred to as the half sites. The crystal structures of most NF-κB dimers observed in cells bound to various κB sites have been determined, which, along with corresponding biochemical studies, helped us define the DNA binding strategy of the dimers (Wang, 2012). These structures revealed that although each subunit of an NF-κB dimer contacts 7- to 8- bp, sequence-specific binding is confined to the 4- or 5-bp half-site. Interestingly, the specificity of binding in the central region is loose, whereas that in the flanking G/C-rich regions is strict. A host of publications suggest that sequence variations at the central region are linked to dimer specificity and gene regulation. For instance, κB sites in the promoters of cytokine genes frequently contain A/T bp at position -1, whereas those responsible for survival contain a G/C bp at that position. NF-κB dimers induced under stress fail to strongly bind κB DNA with G/C at -1, leading to cell death (Crawley, 2013). Sequence-specific DNA binding is also regulated by cofactors. The Src-associated substrate during mitosis of 68 kDa (SAM68) enhances binding of the p50:RelA heterodimer to the κB site present in the promoter of the alpha chain of the interleukin-2 receptor gene, with a G/C-bp at the +1 position instead of the consensus T/A-bp (Fu, 2013). The homodimer of p52 binds both A/T and G/C-centric κB sites with nearly equal affinities (Wang, 2012). Interestingly, the transcriptional activation by the p52 homodimer is observed primarily for G/C-centric κB sites, and it is dampened when the central bp is A/T. This difference likely originates from differential binding kinetics rather than affinity differences (Wang, 2023). A difference in transcriptional activity was also reported when an A/T-bp at the central position was changed to T/A in a κB site present in the promoter of the CXCL10 gene (Leung, 2004). These studies indicate a complex relationship between binding of NF-κB dimer to κB DNA of variable sequences and gene regulation.

In the cell, RelA appears to exist primarily as a heterodimer with p50. The noncovalent association of the p50:RelA heterodimer with IκBα, an IκB family inhibitor protein, retains the former in the cytoplasm and renders it transcriptionally inactive. The omnipresence of the p50:RelA heterodimer caused the field to initially overlook the existence and legitimate importance of the RelA homodimer. Only later was it discovered that the RelA homodimer regulated a distinct set of genes (Rao, 2010; Hoffmann, 2003). Moreover, the RelA homodimer is sequestered preferentially by IκBβ, and consequently, degradation of IκBβ selectively releases the RelA homodimer, allowing it to regulate genes independent of p50 and other NF-κB subunits (Tsui, 2015). This chapter provides an in-depth analysis of how NF-κB dimers, in particular RelA, could respond selectively to κB sites with different central base pairs by a combination of biochemical, structural, and *in silico* experiments. To assess functional dependence on the identity of the central base pair, I measured the binding affinities of RelA homodimer and p50:RelA heterodimer to four κB sites, where the central base pair was varied. I find that the RelA homodimer binds G- or C- centric κB DNA with a significantly lower affinity than the A- or T-centric DNA. Surprisingly, crystal structures of RelA bound to four different DNAs indicate nearly identical protein-DNA interactions. Furthermore, structures of free DNA also do not reveal any difference to infer an obvious effect of sequence in altering affinity. Since the central pair does not contact NF-κB residues directly, I then anticipated its effect on binding through an allosteric effect on structural dynamics. Molecular dynamics (MD) simulations of free κB DNAs and their complexes with RelA homodimer revealed that protein-DNA contacts around the central region of the DNA could confer sequence specificity of binding and coordinated interactions at both the central and flanking regions simultaneously dictate binding affinity.

These results reveal how dynamic interactions between NF-κB and κB DNA provide affinity-based DNA selection by the NF-κB dimers.

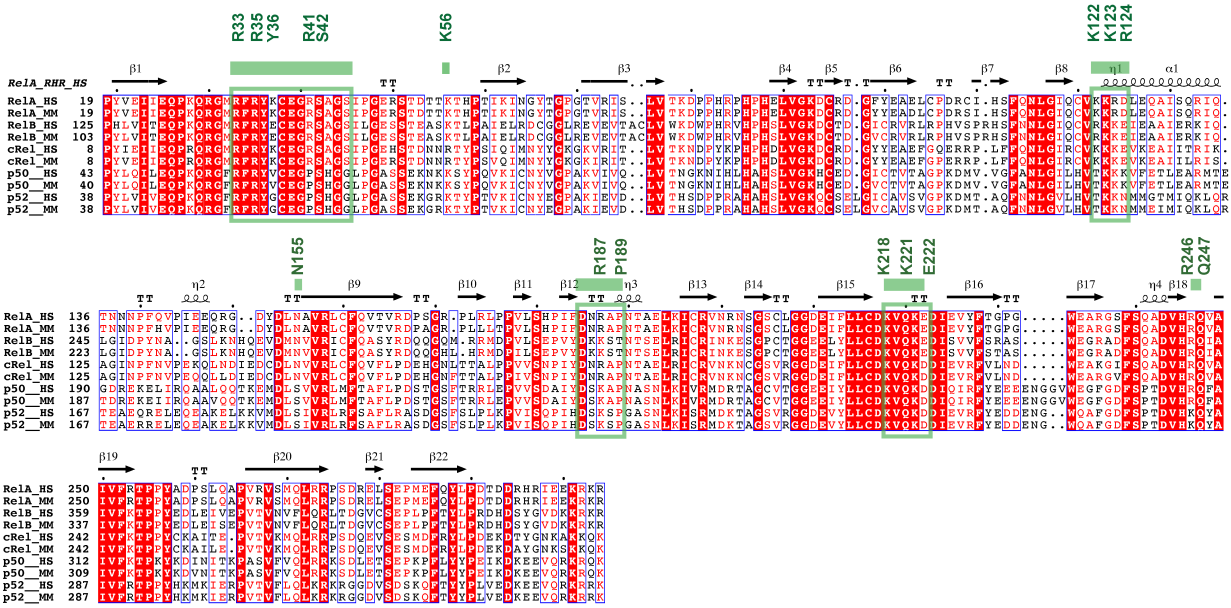

Figure 2.1: Sequence conservation of NF-κB RHR
Slight variations exist within the RHR regions of human and mouse NF-κB subunits which influence subunit specificity. However, key residues involved in mediating contacts with DNA are highly conserved (shown in green). The overall secondary structure of NF-κB RHR consists primarily of β-sheets connected by flexible linkers that contact DNA (shown above sequence).

C. Results

1. RelA homo- and heterodimers bind A- and T-centric κB sites with higher affinity than G- and C-centric sites

Most NF-κB driven promoter contain κB sites with an A or T at the central position, although recent studies indicate the presence of G- or C-centric κB DNA sites (Wang, 2012). Furthermore, the central position is obscure in some κB sites that deviate significantly from the consensus (Siggers, 2011). I tested binding of RelA:RelA homodimer to four κB sites with the core motif of GGGAANTTCC, where their sequences differ only in the central N position. I named these sequences A-κB, T-κB, G-κB, and C-κB DNA based on the identity of the central base on the forward strand. These κB sites mimic natural κB sites present in the promoters of four well-studied genes, namely, Cxcl10 (A-κB), Nfkbia (T-κB), Cxcl1 (G-κB), and Ccl2 (C-κB) (**Figure 2.2 and 2.3A**). I first tested the efficacy of these sites in activating transcription by a RelA-driven luciferase reporter assay in HEK293T (**Figure 2.3B**). I found that both A- and T-κB sites drive RelA-dependent transcription significantly stronger than the G- and C-κB sites, suggesting that the A- and T-centric κB sites bind the RelA:RelA homodimer significantly better than G- and C-centric κB DNA. I next assessed the binding of cellular NF-κB from TNFα-stimulated HEK293T nuclear extract (containing primarily p50:RelA and RelA:RelA dimers) to the four κB DNAs by EMSA (**Figure 2.3C**). The results show that binding of NF-κB dimers to both G- and C-κB DNA is much weaker than to A- and T-κB DNA. I next assessed the binding affinity of purified full-length RelA ($RelA^{FL}$) homodimer and p50:RelA heterodimer for all four κB by EMSA and observed a similar pattern of binding (**Figure 2.3D and 2.3E**). Further detailed analysis revealed the $RelA^{FL}$ bound A-κB DNA with a ~6-fold higher affinity relative to G-κB DNA (116 nM vs 699 nM) (**Figure 2.4A and 2.4B**). In addition to testing binding affinity for

$RelA^{FL}$ dimers, I investigated binding of RelA RHR dimers and found that the difference in affinity is nearly 10-fold between A- and G-κB DNA (16 nM vs 167 nM). Although RelA RHR dimers display stronger binding than $RelA^{FL}$ dimers in EMSA, due to the inhibitory effect of the activation domain, binding analysis of RHR to DNA allows convenient assessment of the effect of mutations of specific residues.

I also determined equilibrium binding affinity of $RelA^{FL}$ to the four different DNAs with fluorescence anisotropy assay (**Figure 2.5**). 5'-Fluorescein labeled κB DNAs of different centers were titrated with increasing amounts $RelA^{FL}$ in buffer containing 150 mM NaCl and fluorescence polarization was measured following incubation at room temperature for 10 minutes. The calculated equilibrium binding affinity of $RelA^{FL}$ for A- (34.7 nM) and T-κB DNA (32.6 nM) was significantly stronger than for G- (147.7 nM) and C-κB DNA (187.3 nM), which agreed with EMSA results.

For an in-depth binding analysis, I performed a biolayer interferometry (BLI) assay using biotin-tagged κB DNAs bound to a streptavidin chip to monitor the time course of association of $RelA^{FL}$ with the four κB DNA (**Figure 2.6**). The dependence of the plateau values of the BLI signal yield highly similar values for the apparent equilibrium constants (K_D) for binding of $RelA^{FL}$ to A- and T-κB DNA ($K_D \sim 25$ nM). The apparent binding affinities to the G- and C-κB DNA sites are also nearly equal but about 10-fold weaker ($K_D \sim 300$ nM) than to the A- and T-κB DNA sites. Detailed analysis shows that the association kinetics follow single-exponential accumulation of RelA-DNA complexes. The dissociation kinetics, performed by transferring the chip near equilibrium from the association experiment to binding buffer without protein, are double-exponential. However, while the initial, faster dissociation component is highly significant at and above 50 nM for RelA with A- and T-κB DNA, it is not prominent at low

protein concentrations and for less stable complexes. For example, for the RelA complex with T-κB DNA, the population of the rapidly dissociating complexes is undetectable at 12.5 nM and 25 nM protein concentrations, and the dissociation kinetics are apparently single-exponential. The dissociation kinetics of RelA complexes with G- and C- κB DNA, where the protein-DNA binding is much weaker than with A- and T-κB DNA and reaches only ~30% saturation at the highest RelA concentration, generally follow an apparent single-exponential behavior, where the faster component is not prominent.

I also performed BLI experiments with the p50:RelA heterodimer (**Figure 2.7**). Similarly to the RelA:RelA homodimer, the A- and T-κB DNA bound the heterodimer strongly (~25 nM) but binding to the G- and C-κB sites was approximately 8- to 10-fold weaker (~225 nM). Additionally, the heterodimer displayed single-exponential association and double-exponential dissociation kinetics. As observed with the RelA:RelA homodimer, the double-exponential kinetics likely reflect a second dimer bound at the specific site. Overall, the combined binding data reveal that RelA containing dimers bind significantly stronger to A- and T-κB DNA than C- and G-κB DNA despite no contacts in previous structural analyses.

`

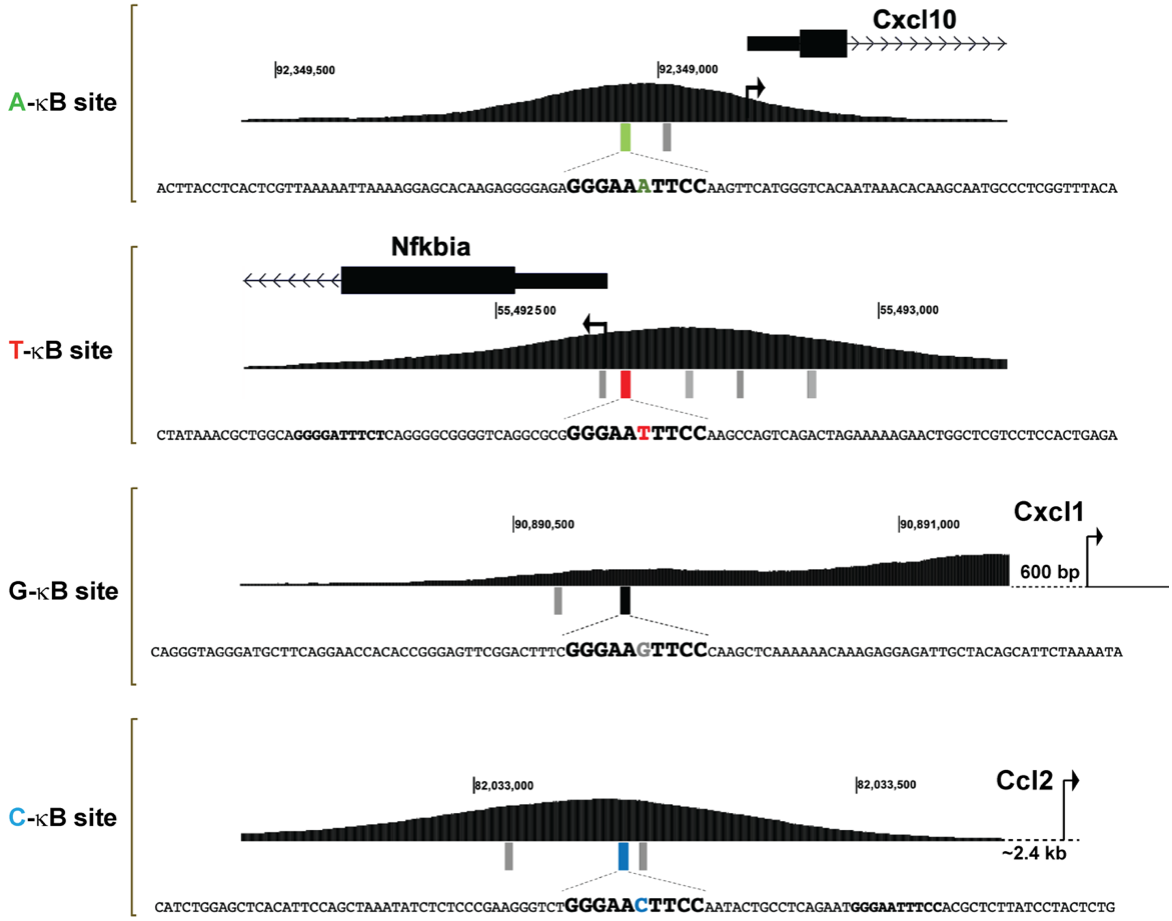

Figure 2.2: Central base pair variation at natural κB sites
UCSC genome browser view of the promoter regions for Cxcl10, Nfkbia, Cxcl1, and Ccl2. RelA ChIP-Seq peaks following 30 minutes of TNFα stimulation in MEF (Ngo, 2020) overlap at κB sites with different central nucleotides. Blocks below peaks represent identified κB sites from the JASPAR database (score > 300).

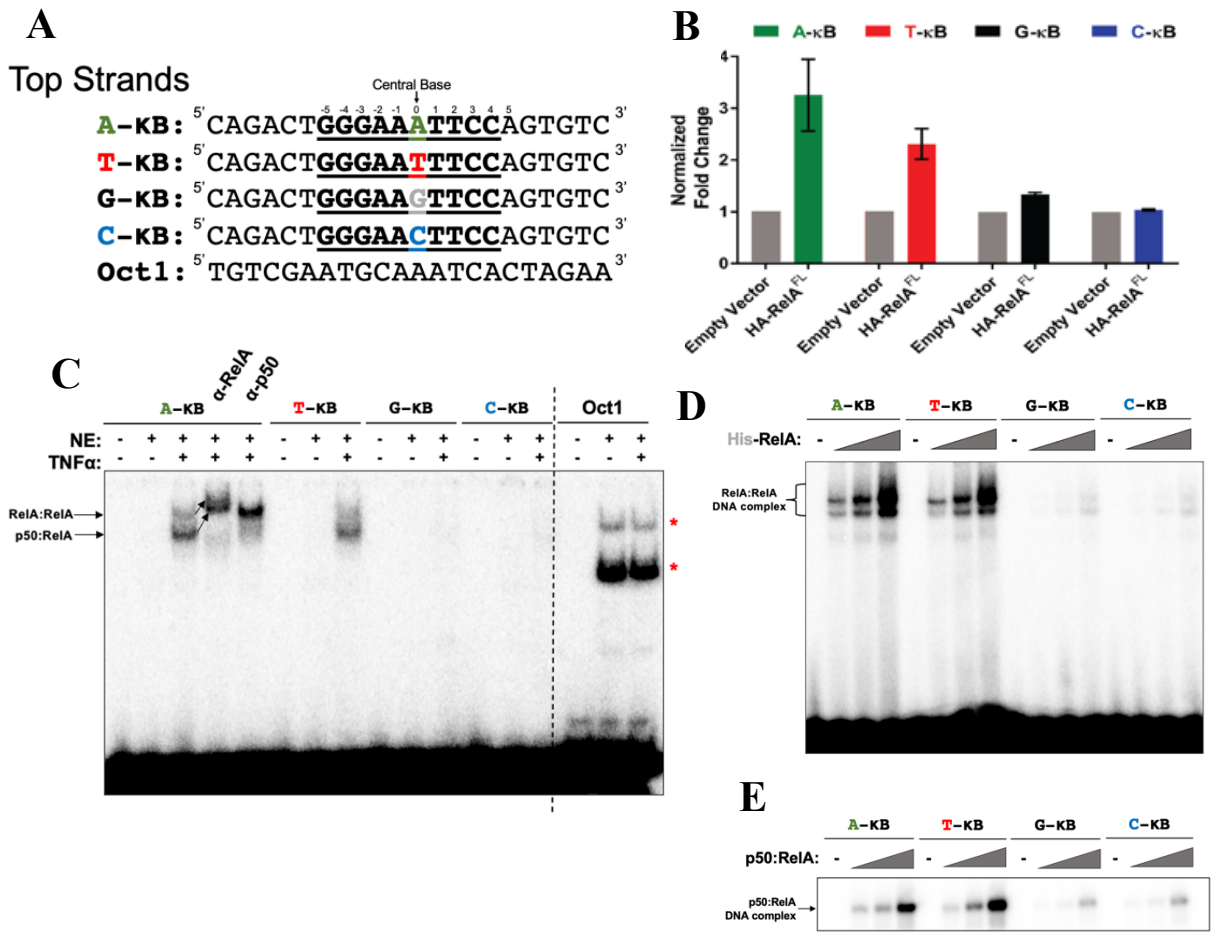

Figure 2.3: NF-κB binds A-/T-centric κB DNA with higher affinity than G-/C-centric κB DNA
A. The κB DNA sequence GGGAANTTCC, with N representing the single nucleotide variation, was used for *in vitro* binding assays. **B.** Luciferase reporter assay with empty vector or HA-RelA cotransfected with different κB-driven luciferase constructs in HEK293T. Luciferase readings were normalized to Renilla and data presented relative to empty vector control. **C.** EMSA from 30 minutes control or TNFα stimulated HEK293T nuclear extract. **D. and E.** EMSA showing differential binding affinity of 5, 10, and 20nM recombinant FL-RelA homodimer (**D.**) or 2.5, 5, and 10nM of p50:RelA heterodimer (**E.**) to the different κB DNAs.

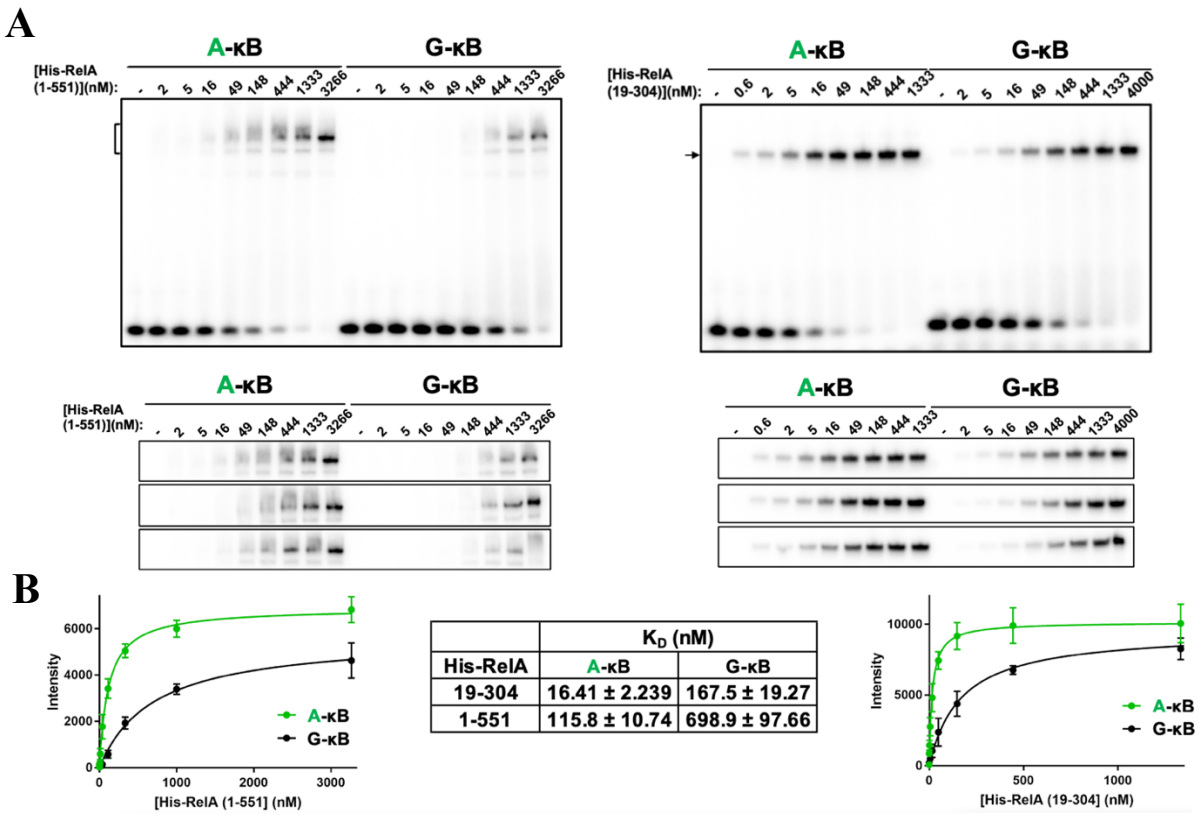

	K_D (nM)	
His-RelA	A-κB	G-κB
19-304	16.41 ± 2.239	167.5 ± 19.27
1-551	115.8 ± 10.74	698.9 ± 97.66

Figure 2.4: EMSA-determined binding affinity of FL-RelA and RelA-RHR
A. High range titration of recombinant FL-RelA (left) and RelA-RHR (right) to A- and G-centric κB DNA. Below are experimental triplicates used for quantitation. **B.** Plot of concentration dependent RelA:DNA complex formation for FL-RelA (left) and RelA-RHR (right) and exponential fit for K_D calculations. Data are represented as mean ± SD from three independent experimental replicates.

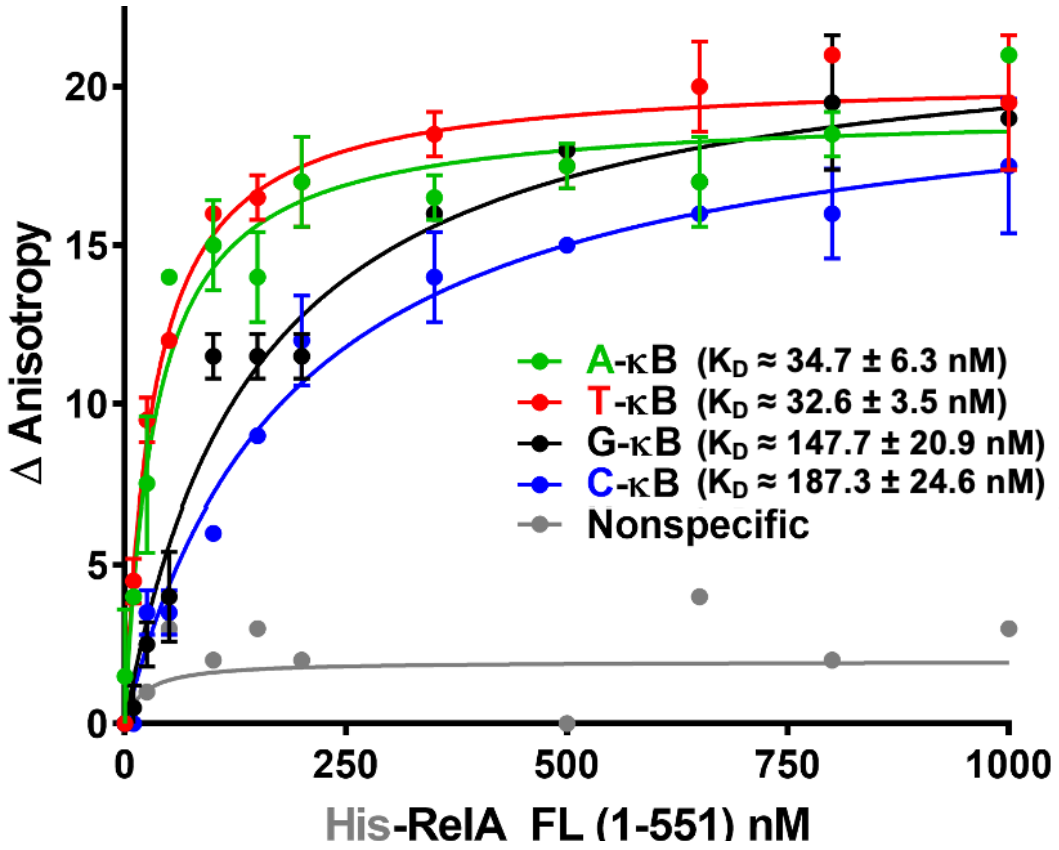

Figure 2.5: Fluorescence anisotropy of FL-RelA with different κB DNAs
Solution-based binding affinity determination of FL-RelA at physiological salt concentrations to κB DNA with different centers. Data was normalized to background and represented as mean ± SD from three independent experimental replicates.

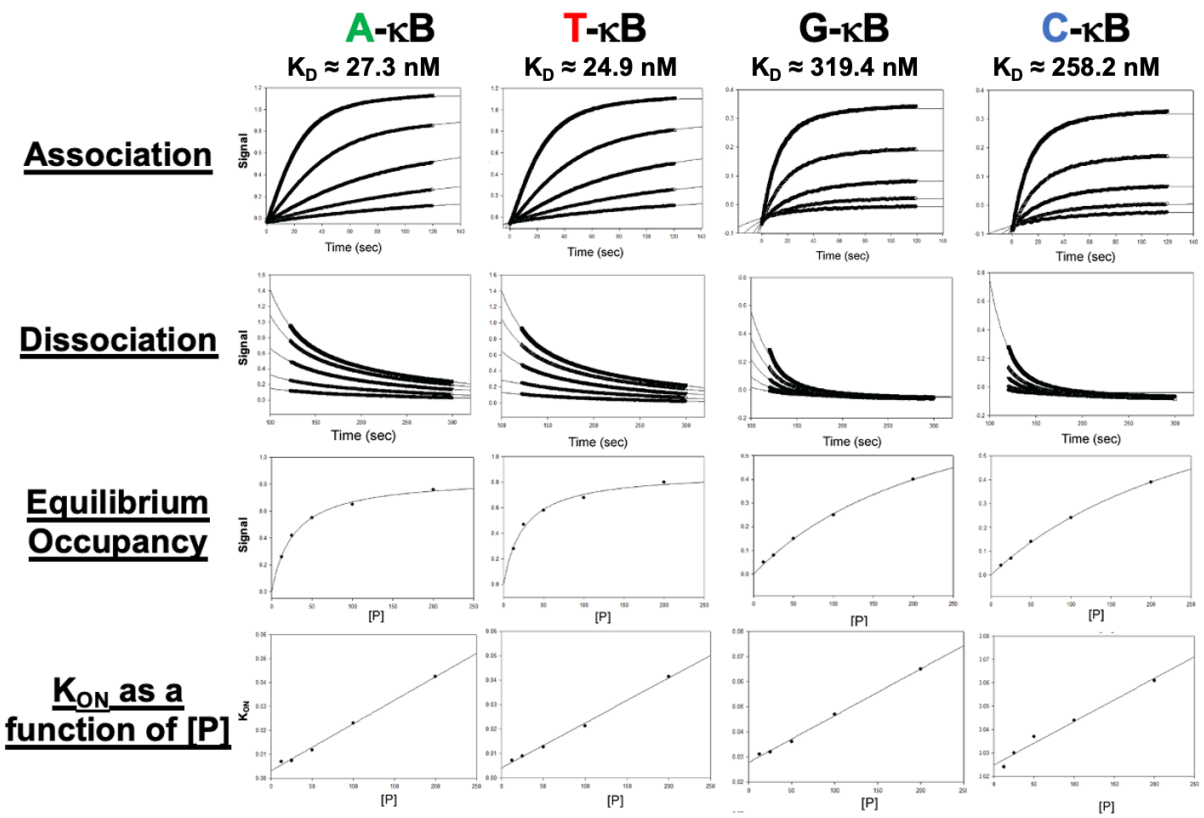

Figure 2.6: Biolayer interferometry of FL-RelA with different κB DNA
Biolayer interferometry (BLI) signals from purified full-length RelA homodimer for all four κB DNAs. The observed apparent K_D from plateau analysis of association data is presented above graphs.

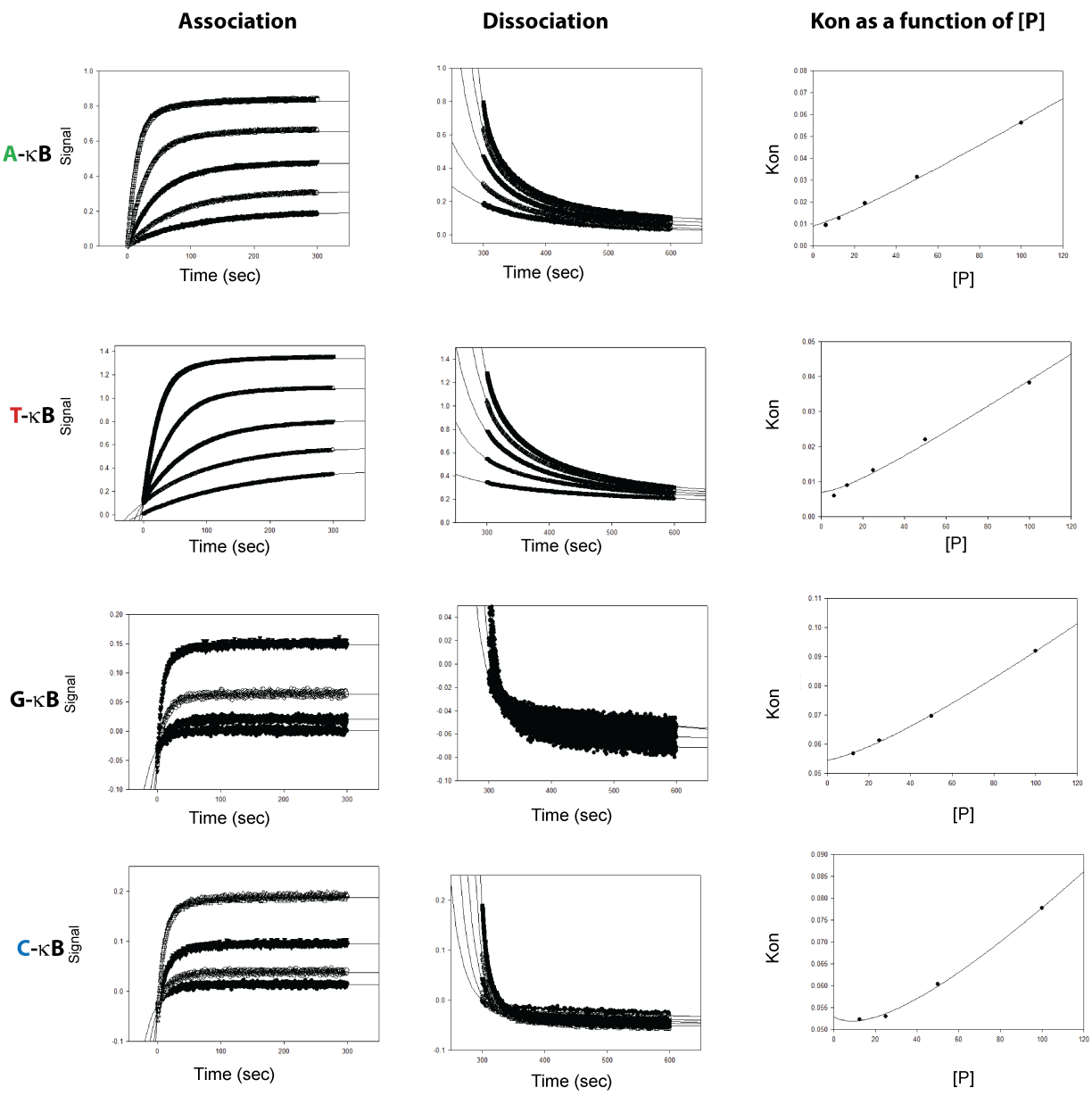

Figure 2.7: Biolayer interferometry of p50:RelA with different κB DNAs
Biolayer interferometry (BLI) signals from purified p50:RelA heterodimer for all four κB DNAs showing preference for A- and T-centric κB DNA over G- and C-centric.

2. Crystallographic analysis of RelA:κB DNA and free κB DNA reveal nearly identical structural states between A-, T-, G-, and C-κB DNA

To elucidate the physico-chemical properties behind the observed differences in binding affinities of RelA:RelA homodimer to various κB sites, we crystallized and determined the structures of the RelA RHR homodimer bound to the four aforementioned κB DNAs. The global architectures of all the four κB DNAs bound by RelA:RelA homodimer are highly similar (**Figure 2.8A**). Two of the four structures (RelA:RelA homodimer bound to the T- and G-κB DNA) were also resolved beyond 1.9Å, revealing finer structural details of the RelA:κB DNA complex. The structural models show that two half-sites separated by the central bp within the full κB site are located asymmetrically to engage with the interacting residues of the DNA-binding domains of the two RelA protomers (protomer I and II) (**Figure 2.8B**). The five bp half-site 5'-$^{-5}$G^{-4}G^{-3}G^{-2}A^{-1}A interacts with several amino acids of protomer I – R41, R35, and R33 recognize the G residues at positions -5, -4, and -3, respectively and Y36 forms van der Waals contacts with $^{-2}$T and $^{-1}$T of the reverse strand. E39, in addition to stabilizing R33 and R187, contacts $^{-3}$C of the reverse strand. All base-specific contacts, except for the R41 of protomer II are preserved in the four bp half-site (**Figure 2.8C**). Instead, R41 of protomer II contacts the phosphate of the DNA backbone. It is likely that the ^{5}T instead of ^{5}G triggers the elimination of base-specific contacts by R41, although, as elaborated later, even the presence of ^{5}G might not allow its efficient direct contact with R41 of protomer II due to the asymmetric positioning of RelA protomers on DNA. The interactions of R187 of protomer I and protomer II are also distinct and likely triggered by the asymmetric positioning of P189 in the global dimeric complex; R187 of protomer II (and not protomer I) contacts $^{-2}$A directly. Side chains of several

residues, some from the C-terminal DD make non-base specific contacts with the DNA backbone.

Overall, the protein-DNA interfaces are nearly identical in all four κB complexes, and several interactions are mediated by stably bound water molecules. The superposition of protomer I DNA-binding region (19-190) shows nearly identical binding with an RMSD of 0.87Å for backbone atoms. Similarly, an overlay of protomer II DNA-binding domains reveals little difference. However, it is noteworthy that the protomer I and II sub-complexes within the full complex have differences. The overlay of two half-complexes (e.g. in the T- or the G-κB complex) indicates that the primary source of asymmetry is generated due to a deviation from mirror symmetry in the positioning of the bases of the half-sites around the pseudo-dyad axis through the central base pair, which in turn creates differential strain in the linker region (loop L3) between the DD and DBD. P189 at the interface is positioned differently, likely interacting allosterically through R187 with R41, thereby differentiating the two half-site complexes. P189 makes van der Waals contacts with the base next to the central pair, and thus the stacking potential of the base pairs could possibly influence its position/interaction. The dynamicity is reflected in multiple positions of P189, R187, N186, and D185, thus allowing protomers to engage differently. Additionally, R124 of both protomers approaches DNA through the minor groove however does not make contacts. K218 of both protomers appears to make water mediated contact with the central base pair. To accommodate both protomers around the central base pair, P189 of protomer II must translate by about 4Å, a strain that is incorporated through the phosphodeoxyribose backbone of the central and ^{1}T base pair. This produces a strain on interactions of R187 such that in protomer I it interacts with E39 directly, but in protomer II it moves away and interacts with the carboxyl of F34. These subtle changes in turn influence the

K37-S45 loop area, the flexibility of which is allowed due to two appropriately placed glycine residues (G40 and G44), thereby modulating the positioning of R41. The movement about the center also has a long-range effect on binding since the domain movement allows for other DNA protein interactions, such as K56 interacting with the phosphate backbone in protomer I, where R41 of protomer II pulls the DNA from the opposite direction. These interactions create a distinct asymmetry in binding, the propensity of which is dictated by the sequence, including the identity of the central nucleotide.

We next analyzed differences in B-factors (a measure of thermal displacement) of interacting protein and DNA residues in these complexes, particularly for T- and G-κB complexes as these were resolved beyond 1.9Å. The most striking differences are observed with P189. P189 residues of both A- and T-κB complexes display higher average B-factor values compared to that in the G-κB complex. B-factor values of DNA nucleotides indicate that the nucleotides around the periphery (-4, -5, or beyond) are highly flexible compared to the central base pairs (56 vs 14), and the flexibility is more pronounced for the protomer I bound site. The crystallographic difference map also indicates a likely variation of the central base pair position, thus reflecting dynamics. Taken together, high-resolution structures of the RelA:κB DNA complexes reveal the details of protein-DNA contacts and the source of asymmetric binding to the two half sites as well as the differential side chain dynamics between the A/T- and G/C-κB DNA complexes.

We next determined crystal structures of all four κB DNA duplexes in the unbound state to investigate if a single base pair variation about the central nucleotide induces significant structural differences and what changes in DNA structure occur following binding by RelA. We obtained crystals with 12bp-long DNA duplexes, an observation tallying with numerous studies

indicating that similar lengths of DNA are conducive to packing in crystal lattices (**Figure 2.9A**). The crystal structures were determined by the single-wavelength anomalous diffraction method using the anomalous signal from Zn^{2+} atoms coordinated with the N7 atoms of guanine. The structures of all four DNAs were resolved in the resolution range of 2.15-2.5Å thus enabling a detailed comparison among them and with RelA-bound DNA. It is noteworthy that A- and T-κB DNA crystals diffracted less strongly than G- and C-κB DNA crystals, which could reflect flexibility of the A- and T-κB DNA. The structures of all four DNAs were highly similar, with the last base of each strand flipped out of base pairing to make lattice contacts. Interestingly, the placement of the two sides around the central base was striking symmetrical such that it caused a minor packing ambiguity in the crystal lattice. The unit cell contained 9 almost identical independent duplexes, out of which a row of 3 duplexes was positioned in shifted alternate lattices. A comparison of the DNA in the free and RelA-bound states indicates that in order to be accommodated within the protein-DNA complex, the DNA needs to be deformed around the central base pair (**Figure 2.9B and 2.9C**). The deformation is exhibited by the values of various DNA parameters in base pair and base pair steps all along the DNA axis. If the Gs at position -5, -4, and -3 interacting with protomer I are superimposed, the G3, G4, and T5 of unbound DNA are placed 3.5, 4.3, and 5.2Å away, respectively, to interact with protomer II. We reasoned that free κB DNA likely adopts various conformations, and stepwise engagement of the RelA dimer must deform and/or capture these target DNAs in the deformed state observed. The differential dynamics around the central base pair, which are dictated by the differential stacking of the central base with neighboring base pairs, must allow altered DNA deformation propensity to engage with RelA; and the energetic difference in forming complexes with RelA is reflected in the observed differences in binding affinity. We also noticed that the B factor values for unbound

DNAs were quite uniform in all areas, unlike for κB DNA bound to RelA. The flexibility was pronounced at positions $^{-4/4}$G and $^{-5/5}$G, indicating that the base specific interactions mediated by R41, R35, and R33 were likely highly dynamic.

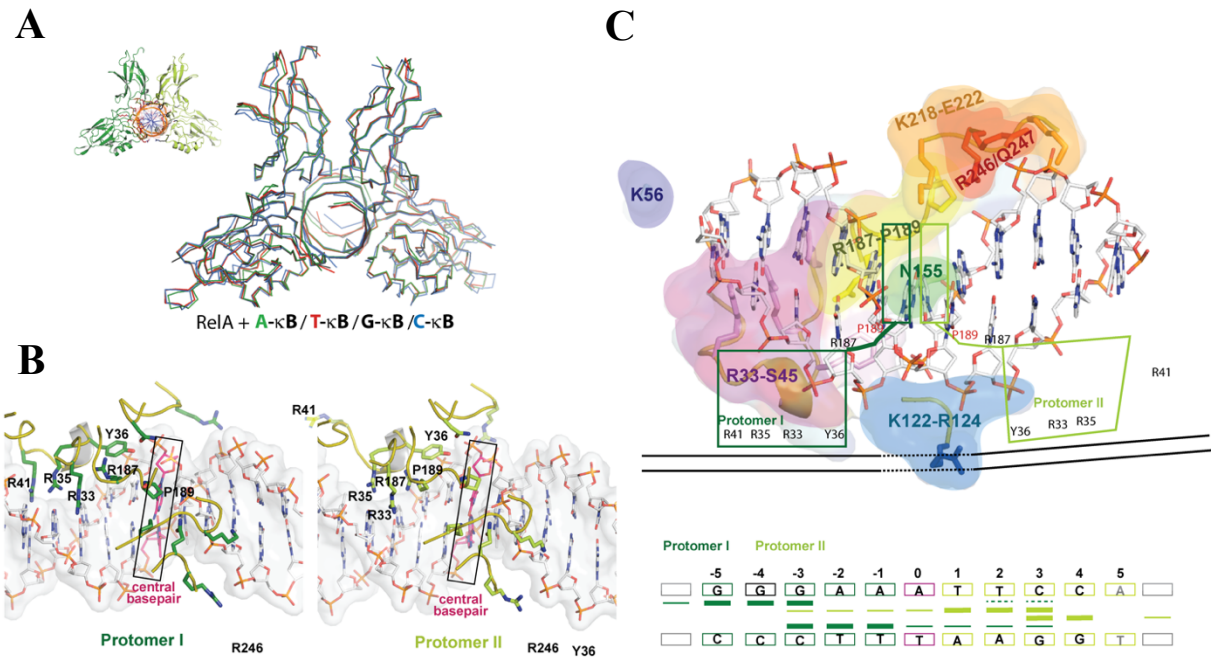

Figure 2.8: Structural analysis of RelA homodimer bound to different κB DNAs
A. View of RelA:κB DNA complex (representative T-κB) and superposition of A-, T-, G-, and C-centric κB DNA complexes with RelA homodimer. **B.** Interaction of protomer I and II in complex with T-κB site (similar orientation) highlighting key differences in interactions. Residues making base-specific contacts are marked. **C.** A schematic of asymmetry in positioning of the half-sites and that of the protomers, that triggers differential interactions of protomer I and II. Bottom panel: A schematic of base-specific (thick-bar) and non-base-specific (thin bar) interactions by protomer I (dark green) and II (light green).

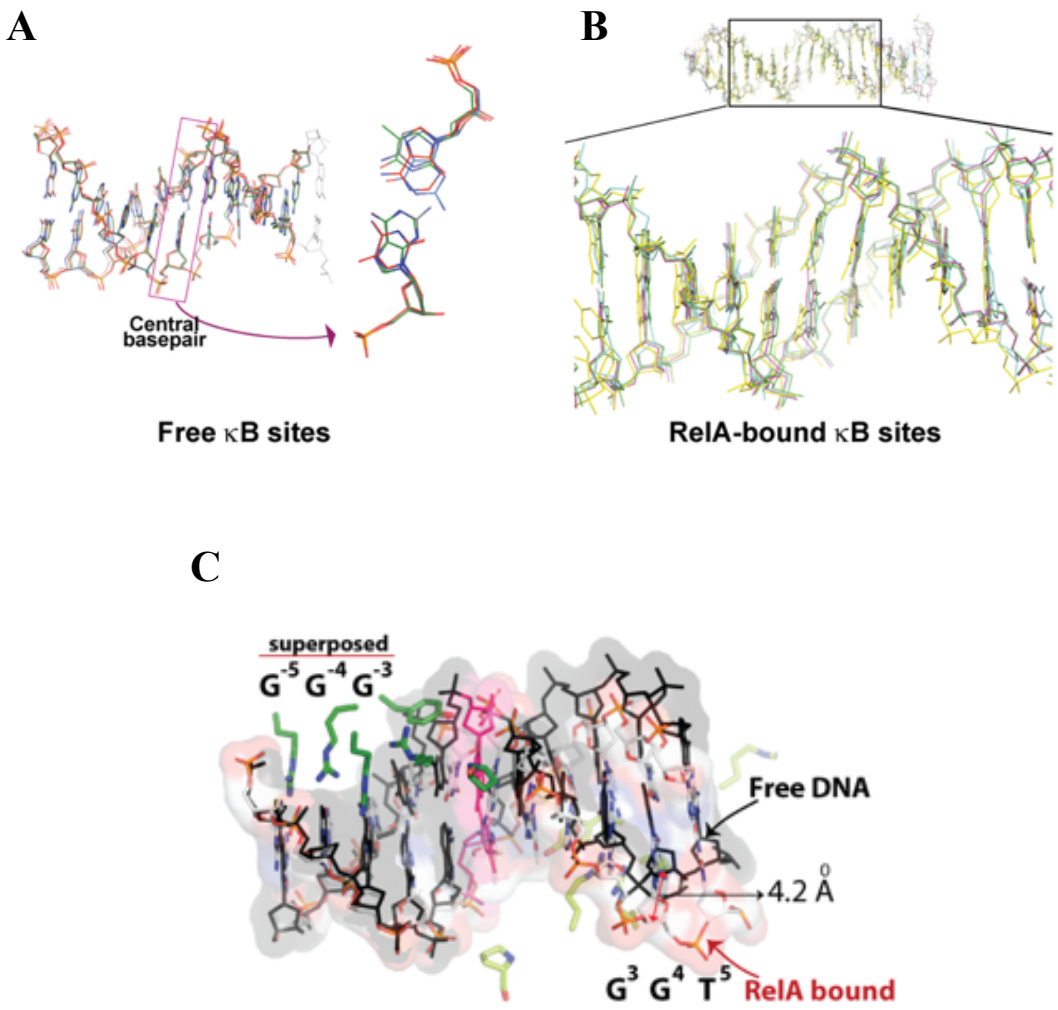

Figure 2.9: Structural analysis of free κB DNA
A. Structures of the unbound κB DNAs superimposed and a zoomed in view of the central base pair. **B.** Structure of RelA-bound κB DNA superimposed. **C.** Comparison of unbound vs RelA-bound κB DNA structures, superimposed by aligning Gs at positions -5, -4, and -3 of the 5-bp half-site.

3. Discriminatory recognition of κB DNA by RelA revealed through MD simulations

The high structural similarity is suggestive of additional factors underlying discriminatory affinities. To address the likelihood of sequence-specific differential dynamics at the atomic level, we performed all-atom molecular dynamics (MD) simulation of κB DNA both in the unbound and complexed with RelA:RelA homodimer. Five independent 2 μs simulations were performed for each of the four unbound κB DNAs, and five independent 3 μs simulations were performed for the A- and G-κB DNA:RelA dimer complexes, amounting to a total simulation time of 70 μs. MD simulations of unbound DNA reveal that A- and T-κB DNA have a narrower minor groove at -4 to +1 and -1 to +4 positions, indicative of a kink due to the A-tract in the central region. RelA binding causes a narrowing of the minor grove and widening of the major groove for both A- and G-κB DNA, and protomer I of RelA appears to form more hydrogen bonds to nucleobases and less to the DNA backbone in A-κB DNA bound form relative to G-κB DNA despite a similar number of total hydrogen bonds (**Figure 2.10**). R187 of protomer I (R187-I) binds predominantly D185-I in A-κB DNA to strengthen interactions of the R33, R35, and E39 patch with DNA, whereas R187-I in G-κB DNA binds E39 to reposition R35 away from making base specific contacts with DNA. Discriminatory minor groove binding of R124-I was also observed, where a state in which R124-I of RelA inserts into the minor groove to make base specific contacts with DNA is 4 times more populated in A-κB than in G-κB DNA (**Figure 2.11**). Altogether, the results from MD simulations suggest that specificity of RelA to A- over G-κB DNA may arise from differences in conformations and dynamics of specific residues that facilitate binding to κB DNA.

RelA R124 is substituted to lysine in p52. Since arginine and lysine display differential coordination in interacting with DNA, and we previously observed that p52:p52 homodimer

binds both A/T and G/C-κB DNA with near equal affinity, we were intrigued if the discriminatory specificity of RelA could be altered by swapping its sequence with that of p52. We replaced the KKRD sequence patch containing R124 in RelA with the corresponding TKKN region (containing K143) of p52. In addition, we generated the RelA R187K mutant, as the R187 corresponding position is a lysine in p52 (K221), and the RelA R187K/TKKN double mutant. WT and mutant $RelA^{FL}$ expression plasmids were transfected in HEK293T cells and TNFα stimulated nuclear extract was collected and assayed for binding to the variable center κB DNAs by EMSA. (**Figure 2.11**). We observed slightly enhanced affinity to G- and C-κB DNA for $RelA^{FL}$-TKKN relative to WT. In contrast, the binding to the A- and T-κB DNAs were slightly reduced for $RelA^{FL}$-TKKN relative to WT. The binding for the R187K mutant to all κB DNAs was reduced relative to WT, and the R187K/TKKN double mutant was severely defective in binding any of the κB DNAs. Furthermore, we generated the same mutants in the context of bacterially expressed RelA RHR and tested binding to A- and G-κB DNA following purification (**Figure 2.13**). As anticipated, the RelA RHR-TKKN bound the A-κB site with reduced affinity relative to WT RelA RHR but displayed slightly enhanced binding affinity for the G-κB site. The R187K mutant showed reduced binding for both A- and G-κB DNA, and the R187K/TKKN double mutant showed no difference relative to WT. In addition to R187K and TKKN, we tested the role of R41. Since the 9-bp sites retained a high affinity for the RelA homodimer, we postulated that R41 (making base-specific contacts with the first guanine of the GGGAA half-site) might not be critical for high affinity binding. However, we found the R41A mutant was highly defective in binding to both A- and G-κB DNAs, suggesting that R41 in addition to recognizing the $^{-5/5}$G, may be assisting in additional interactions that stabilize the RelA:κB DNA complex (**Figure 2.13A and 2.14**).

We further tested if the gain of function characteristic of the TKKN mutant is selective for G/C at the 0 position or if it could occur at other positions such as -1 or -2. We found that the TKKN mutant is defective in binding the well characterized IgκB sequence of GGGACTTTCC relative to WT, where the G/C-bp is at the -1 position instead of 0 (**Figure 2.15**). This suggests that the binding of the TKKN mutant can be linked to specific sequences of the central region (+2 to -2). Overall, these results suggest that residues of RelA interacting through the major and minor grooves within the variable central region may not be coupled and presence of a G/C in various positions of the central region could alter binding differently. In a much broader sense, while displaying a partial gain, the stability of the RelA-TKKN:G/C-DNA complex is still significantly lower than the RelA-TKKN:A/T-DNA complex. This suggests the presence of the G/C at the center regulates the conformational and electronic environment of the DNA in a manner that cannot be overcome by the base-specific contacts at the periphery.

Finally, we tested the reporter gene activation of WT and the TKKN mutant RelA to an A- or G-κB driven luciferase construct (**Figure 2.16**). Interestingly, we observed that the TKKN mutant reduced the reporter gene expression from both A- and G-κB driven luciferase relative to WT RelA, despite the observed increase in binding affinity of the TKKN mutant with G-κB DNA in EMSA. This reflects that binding affinity and transcriptional output are not necessarily correlated.

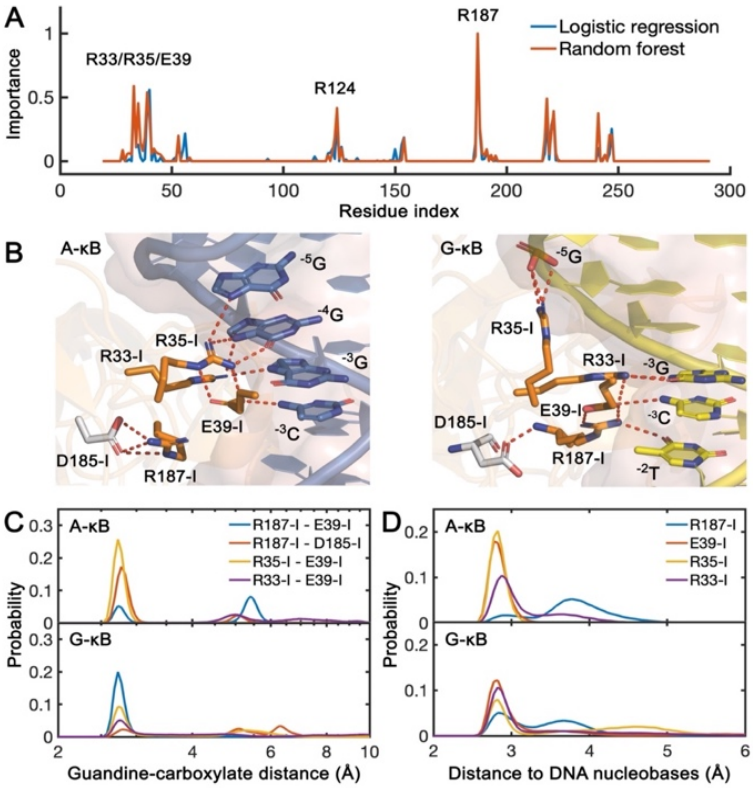

Figure 2.10: Dynamics of RelA bound to A- and G-κB DNAs from MD simulations
A. Key residues of protomer I differentiate the binding of A- versus G-κB DNAs. Logistic regression and random forest jointly identified two major patches, the first (R187, R33, R35 and E39) bound to the DNA major groove and the second (R124) bound to the DNA minor groove. **B.** Binding profiles of the first major patch (orange) on A- (blue) and G-κB (yellow) DNAs. Hydrogen bonds are presented as red dashed lines. **C.** Probability distributions of minimum guanidine-carboxylate distances between indicated interacting residues. **D.** Probability distributions of minimum distances between indicated residues and DNA nucleobases.

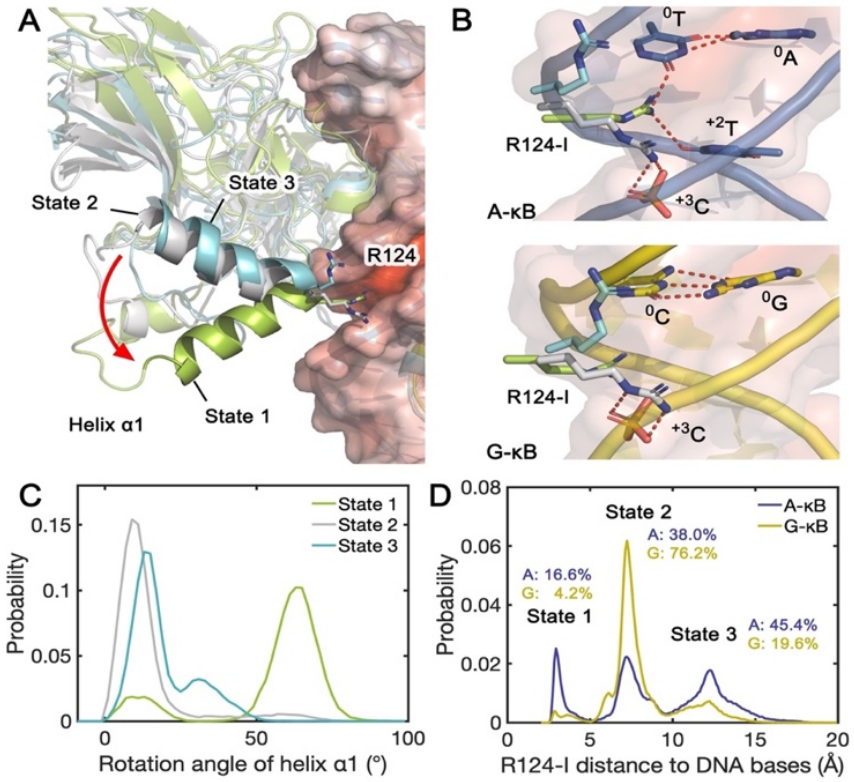

Figure 2.11: RelA R124 binding states and associated helix α1 dynamics
A. The swinging of helix α1 and the corresponding different binding states of R124-I in A-κB simulations. State 1 (lime): the guanidine of R124-I inserted into the minor groove; state 2 (grey): R124-I bound to the cross-strand phosphate; state 3 (cyan): R124-I unbound from DNA. **B**. The three binding states of R124-I to A- and G-κB (coloring scheme as in **A**). Hydrogen bonds are presented as red dashed lines. **C**. Probability distributions of rotation angles of helix α1 in A-κB simulations with respect to the crystal structure. **D**. Probability distributions of minimum distances between R124-I guanidine and DNA nucleobases. The populations of R124-I binding states in A- and G-κB are marked next to the corresponding labels.

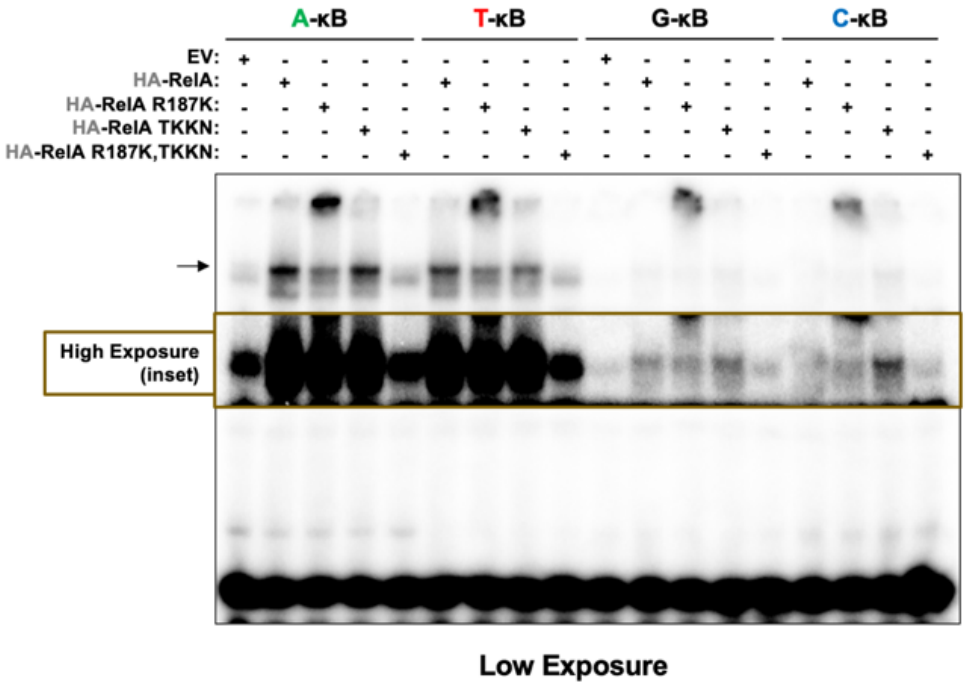

Figure 2.12: Binding of RelA mutants from transfected 293T nuclear extract
Qualitative assessment of WT and mutant RelA binding affinity in nuclear extract from transfected HEK293T. The day after transfection, cells were treated with TNFα for 30 minutes and nuclear extract was collected and mixed with radiolabeled A-, T-, G-, and C-κB sites for analysis by EMSA.

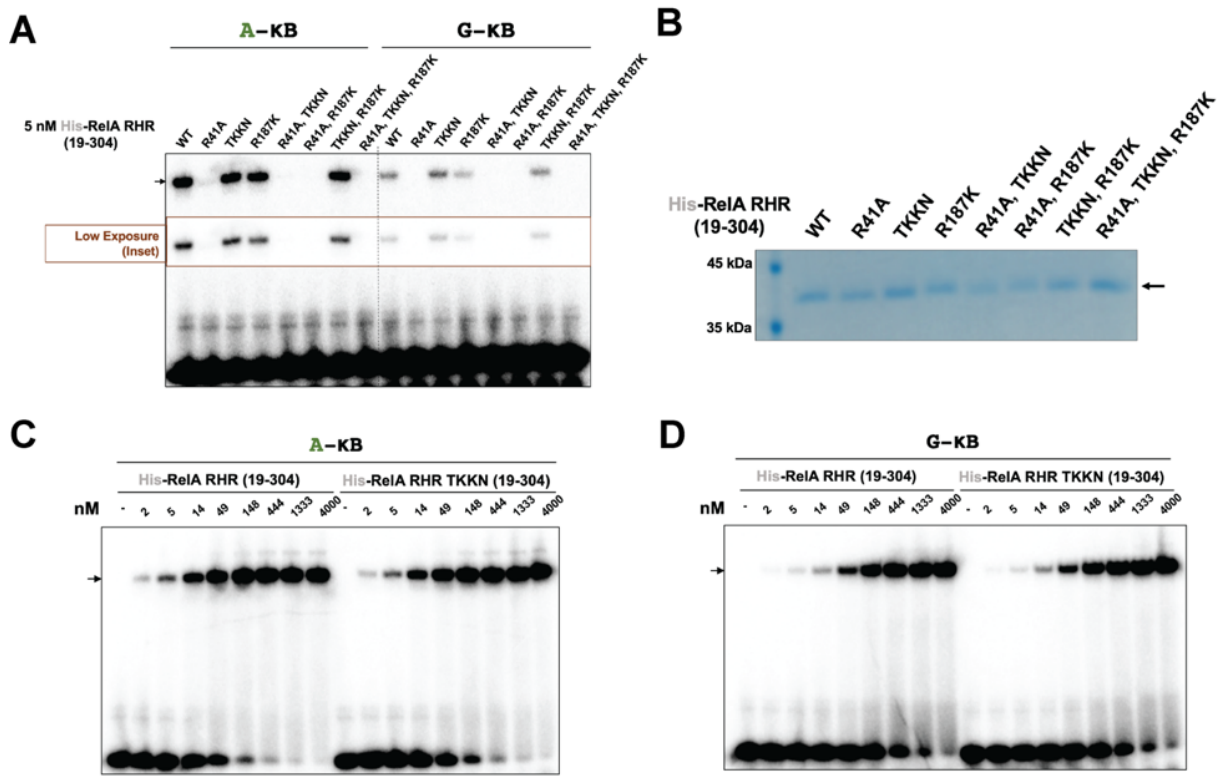

Figure 2.13: Binding of RelA RHR mutants to A- and G-κB DNA by EMSA
A. EMSA analysis of purified RelA RHR WT and R41A, R187K, and TKKN single, double, and triple mutants to A- (left) and G-κB (right) DNA. A lower exposure inset (brown) shows increased binding of the single TKKN mutant relative to wild type for G-κB DNA. **B.** Coomassie stained protein gel of WT and mutant RelA RHR proteins. **C. and D.** Full-spectrum titration of WT and TKKN mutant RelA RHR to both A- (**C.**) and G-κB (**D.**) DNA.

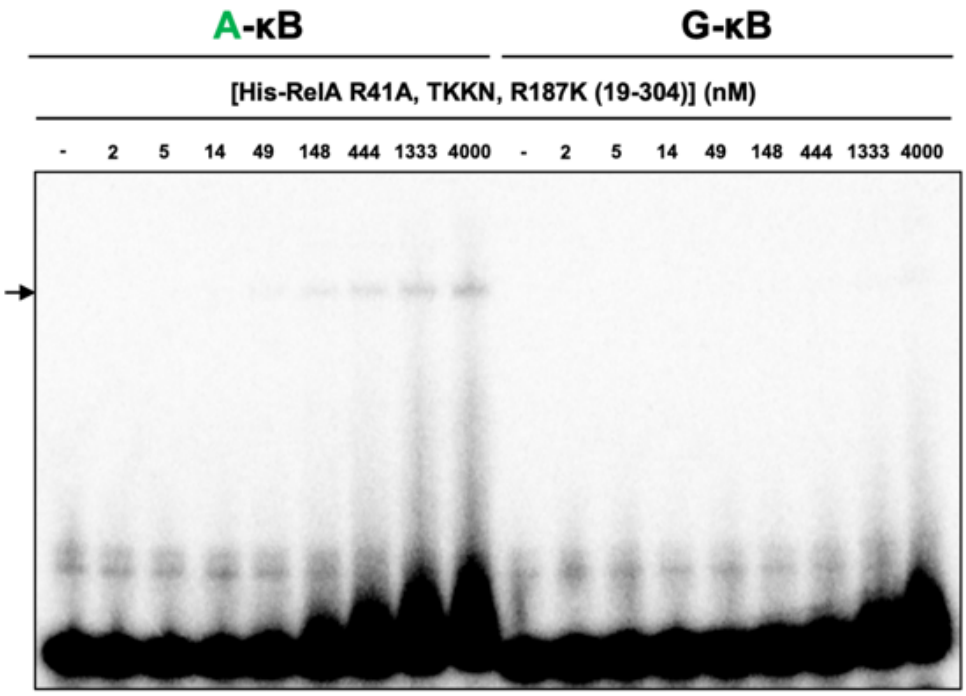

Figure 2.14: EMSA analysis of RelA RHR triple mutant DNA binding
A full-spectrum titration of R41A, TKKN, and R187K triple mutant RelA RHR to A- and G-κB DNA revealed severely defective DNA binding independent of the identity of the central nucleotide. Minimal binding can only be observed for A-κB at high levels of mutant RelA RHR.

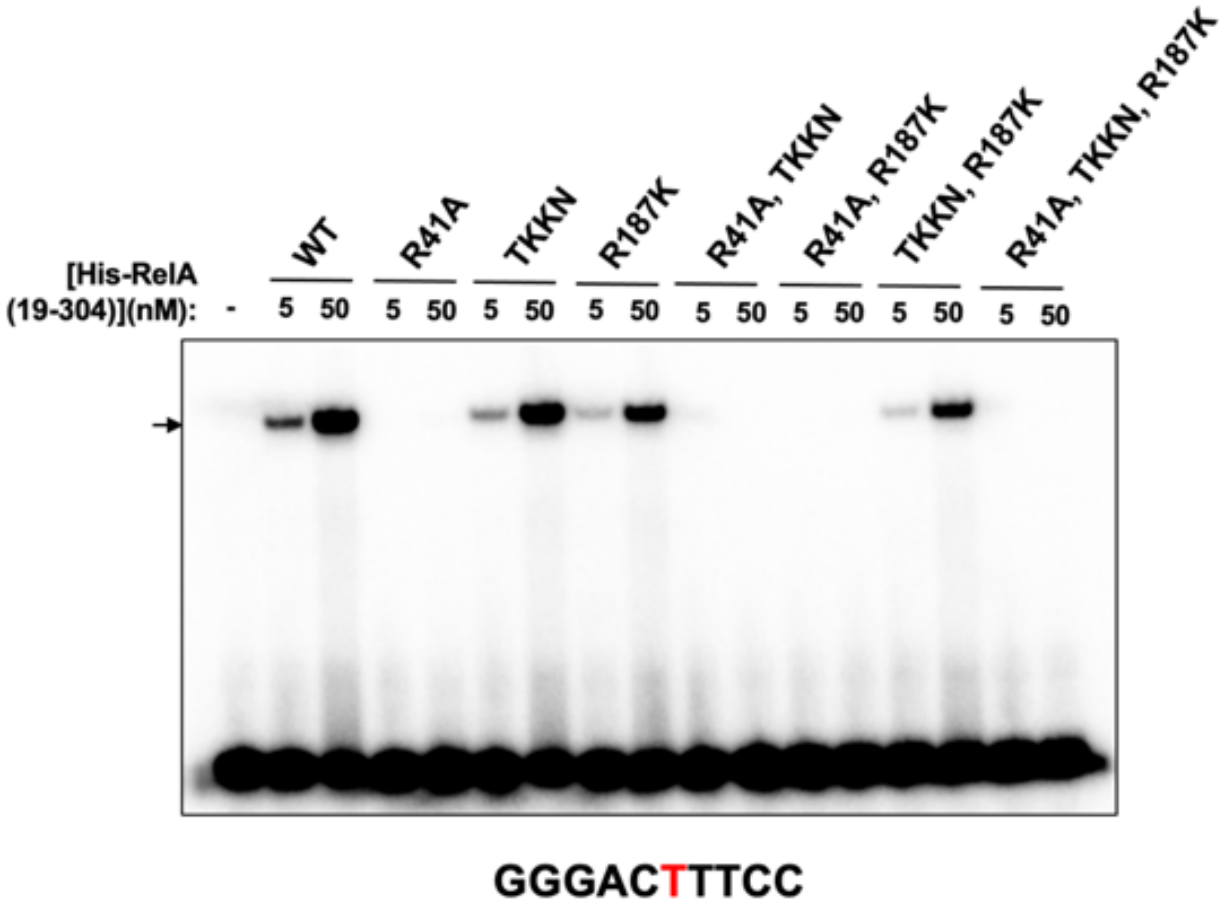

Figure 2.15: EMSA analysis of WT and mutant RelA RHR DNA binding to IgκB DNA
EMSA DNA binding analysis of RelA RHR WT and R41, TKKN, and R187K single, double, and triple mutants to IgκB DNA. The T-centric sequence of IgκB promoter DNA is shown below.

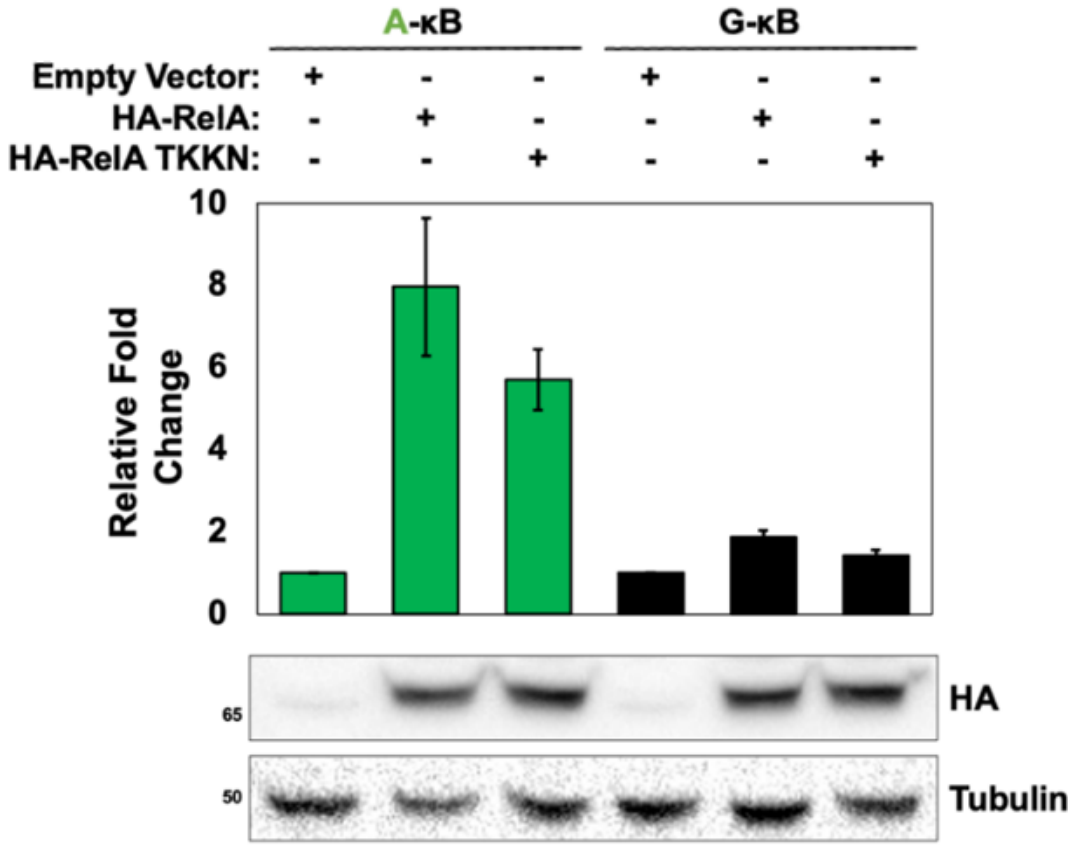

Figure 2.16: Luciferase assay of WT and TKKN mutant RelA with A- and G-κB DNA
HEK293T were transfected with empty vector control, WT, or TKKN mutant HA-tagged RelA with either A- or G-κB driven luciferase reporter construct. Data are present as mean ± SD of three independent experimental replicates.

D. Discussion

We revisited the question of how the NF-κB subunit RelA recognizes κB DNA and how variations in the DNA sequence affect both the binding affinity and specificity by focusing on four closely related and physiologically relevant κB DNAs with just a single bp variation at the center. We observed that, under similar conditions, the dimer of full-length RelA binds to the A- and T- centric κB sites significantly better than the G- and C-centric κB sites. In addition to the binding affinity at equilibrium, BLI kinetics experiments indicated an intriguing biphasic binding mode, where additional RelA dimers associate with κB DNAs.

The crystal structures of κB DNAs both in unbound and RelA-bound states revealed that the structural features of all four unbound κB DNAs were nearly identical. At first glance, the structures of the complexes also appeared nearly identical. However, an in-depth look at the B-factors revealed subtle differences in DNA and protein side chain dynamics between the two RelA protomers in the dimer, and among corresponding protomers of different RelA:κB DNA complexes. Remarkably, we found that the B-factors of R124 and P189 in the T-κB DNA complex were significantly higher than those in the G-κB DNA complex. A possible explanation could be that variable dynamics in these two classes of DNA is triggered due to the single bp difference at the central position, which drives RelA to bind them differently. Perhaps flexibility is necessary for higher stability, and higher rigidity of G- and C-κB DNAs constrains RelA from binding them efficiently. In contrast, A- and T-κB DNAs are more dynamic and/or RelA induces dynamicity in them for adjustable binding.

We observe no direct contact with the central bp at the dyad axis, which could have provided a simple explanation for why two identical RelA subunits cannot engage with two half-sites symmetrically. The static crystallographic structures revealed only non-base-specific and

water-mediated contacts with the central region at the minor groove side, and highly stabilized base-specific contacts with the flanking G:C bps at the major groove side. This has hitherto caused us to overlook the importance of the central region in κB DNA for NF-κB recognition. As discussed below, MD simulation studies revealed unexplored possibilities for sequence-specific regulation from the central region and their contextual significance.

Long time-scale simulations MD simulations have been successfully employed to uncover atomistic details in TF-DNA recognition, translocation of RNA polymerases, as well as other protein-DNA association processes. The tens-of-microseconds MD simulations of the unbound κB DNAs and two of the four RelA:DNA complexes presented here provided unprecedented insights into the mechanisms of differential binding. These simulations revealed that RelA could read subtle energetic and electronic structural differences in DNA, as exemplified by the increase of minor groove width at -1 and 0 positions in G-κB DNA relative to A-κB DNA, such difference being absent in the unbound DNAs. Moreover, multiple segments of RelA dynamically coordinate with each other through DNA to determine the final affinity and specificity. Two key residues for this coordination are minor groove binder R124 and major groove binder R187. In all eight DNA-bound RelA protomers from the four complexes resolved by crystallography, R124 is observed to mediate direct contacts only with the DNA backbone and not to specific bases. In contrast, the microsecond MD simulations reveal that R124 can interact with the thymine of the central A/T bp from the narrow minor groove side. The delocalized positive charge of the guanidino group of arginine has been suggested to allow its frequent insertion in the negatively charged minor groove of DNA from the aqueous phase. Such a direct contact by R124 not only confers particular conformational states that are not conducive to interactions between R187 and the $^{-2/2}$T sites through the major groove, but also competes with

R187 of the other protomer for binding to the $^{-2/2}$T sites. The lack of a direct contact by R187 in turn allows R33/R35/E39 to bind strongly to the base part of $^{\pm3/\pm4}$G/C sites. Thus, R187 appears to serve as a relay sensor from R124 in the minor groove at the center to R33/R35/E39 in the major groove at the edges of κB DNA. The guanidino group of arginine, with stronger electrostatic and hydrogen bonding potential, can propel itself to contact DNA if base pairs are unstacked. Thus, stacked sequences within an A-tract could prevent R187 from interacting/modulating the DNA structure. Instead, R187 could associate with D185, preventing it from contacting and stabilizing R33/R35/E39 for a stronger contact with DNA. Similarly, a higher G/C content at the center could restrain R187 from interacting with DNA, thereby weakening contacts between R33/R35/E39 and DNA. The net outcome of this could be a more finely tuned DNA-binding propensity of RelA. Since only RelA has an arginine at position 187 (all other NF-κB subunits have a lysine at the corresponding position), regulatory features of its DNA binding could be different than for other NF-κB subunits. Overall, the anti-correlative nature of DNA binding between Loop L3 residues and Loop L1 residues appears to be a critical aspect of specificity and affinity. The site farthest from the center is the G:C ($^{-5}$G) of the 5-bp half-site, which is contacted by R41. When R41 binds $^{-5}$G, R187 appears to move away completely from the DNA surface. In 4-bp κB half-sites, in the absence of a specific complementary base at ^{5}G, R41 swings away, making a path for R187 to interact. These observations suggest that affinity of macromolecular complexes is determined by both the number of contacts and the strength of these contacts. Some of these contacts may not be captured in static crystallographic structures, indicating its limitations. It is possible that a longer time-scale or improved simulation study can reveal details that explain how alterations in an apparently non-interacting bp could trigger such dramatic differences in binding affinity, and this

is supported by a recent NMR study of μs-ms transitions of DNA interacting loop residues of p50 (Singh, 2022).

In the cell, RelA is known to bind DNA segments in the promoter/enhancer or intergenic regions containing no strong κB sites but littered with weak κB binding motifs. However, not all DNA with a consensus or a non-consensus half-site is recognized by NF-κB dimers. It is possible that the sequence and dynamicity of only some of the non-consensus half-sites might allow NF-κB dimers to interact transiently with base-specificity. MD simulations of complexes with mutant κB sites could reveal how the specificity of NF-κB binding could be dictated by apparently non-consensus half sites, in turn regulating transcription. We found that the weak binding sites renders little transcriptional activity on its own, and a slight enhancement in binding affinity did not enhance reporter activity. Therefore, the role of low affinity κB sites in gene activation needs to be clarified.

How binding kinetics, dynamics, equilibrium binding affinity, and transcription are coupled is a subject for the future. The results of our DNA binding, structural, and computational studies sets a basis on which an understanding of the interaction dynamics of NF-κB dimers in selecting κB DNA sites can be developed. Furthermore, we believe that this work could help us understand how the regulatory scope of NF-κB is broadened by post-translational modifications of RelA or its interactions with other cofactors. Structural, MD simulation, and biophysical studies might shed light on discriminatory protein-DNA recognition in terms of affinity and specificity, and bridge the gap in our knowledge of correlating DNA binding by sequence specific transcription factors such as NF-κB *in vitro* to regulation of transcription in cells.

E. Materials and Methods

1. Luciferase Reporter Assay

Luciferase reporters were generated by cloning specific κB DNA promoter elements with different central base pairs in CMXTK-Luciferase vector (a kind gift from Dr. D. Chakravarti at Northwestern University Feinberg School of Medicine) using SalI and BamHI restriction enzymes (NEB). Sequences of oligonucleotides containing specific κB sites used are listed in **Table 2.1**. HEK293T cells were grown in 12-well plates at ~80 % confluency and transiently transfected with HA-RelA (1-551) or control empty HA-vector, and the luciferase reporter DNAs. Renilla luciferase expression plasmid was also co-transfected as an internal control. The total amount of plasmid DNAs was kept constant for all assays. Transient transfections were carried out using PEI. Cells were harvested 24 h after transfection. Luciferase activity assays were performed using the Dual-Luciferase Reporter Assay System (Promega) following the manufacturer's protocol. Data are represented as mean ± standard deviations (SD) of three or more independent experimental replicates.

2. Protein Expression and Purification

pET3a expression plasmid containing untagged mouse RelA (19-304) was transformed in *E. coli* Rosetta (DE3) and plated on LB media. A 10 mL overnight culture from a single colony was used to inoculate a 2 L LB culture. The cells were grown to an OD_{600} of 0.1 at 37°C and then induced with 0.1 mM isopropyl β-D-thiogalactopyranoside (IPTG) for 18 h at 25°C. Cells were harvested by centrifugation and the cell pellet was resuspended in lysis buffer containing 50 mM NaCl, 25 mM MES pH 6.5, 0.5 mM EDTA, 0.5 mM PMSF, and 10 mM β-mercaptoethanol. Cells were lysed by sonication and insoluble debris was removed by centrifugation. Streptomycin sulfate was slowly added to a final concentration of 1% and gently stirred for 20

minutes at 4°C. Precipitated DNA was removed by centrifugation and the clarified lysate was loaded onto a preequilibrated 5 mL HiTrap SP HP Sepharose (Cytiva) column. The column was washed with 40 column volumes of lysis buffer and eluted with 4 column volumes of 50 mM to 500 mM NaCl gradient in lysis buffer. RHR containing fractions were pooled, concentrated, and separated on a HiLoad 16/60 Superdex 75 (Cytiva) size-exclusion column with buffer containing 50 mM NaCl, 25 mM Tris-HCl pH 7.5, and 1 mM DTT. Peak fractions were pooled, concentrated, and flash frozen in liquid nitrogen until used for crystallography.

Expression of His-tagged mouse RelA(19-304) and its mutant versions was performed in *E.coli* Rosetta (DE3) similarly as for untagged RelA(19-304). The cell pellet was resuspended and sonicated in lysis buffer containing 150 mM NaCl, 25 mM Tris-HCl pH 7.5, 5% glycerol, 0.1% NP40, 10 mM imidazole, 0.25 mM PMSF, and 5 mM β-mercaptoethanol. Following centrifugation, the clarified lysate was incubated with preequilibrated Nickel-NTA agarose beads (BioBharati) for 2 h at 4°C with a rotary shaker. The beads were extensively washed with lysis buffer and eluted in lysis buffer containing 250 mM imidazole. Purified His-tagged RelA RHR was directly used for electrophoretic mobility shift assays.

Baculovirus expression construct for His-tagged RelA (1-551) was generated and used to produce full-length RelA in *Spodoptera frugiperda* Sf9 insect cells. A 300mL culture of Sf9 cells was grown in ESF 921 serum-free media (Expression Systems) to a density of 1 x 10^6 cells/mL for baculovirus infection. 48 hours post infection, cells were collected by centrifugation and sonicated in a lysis buffer containing 400 mM NaCl, 25 mM Tris-HCl pH 7.5, 10% glycerol, 0.1% NP-40, 10 mM imidazole, 0.5 mM PMSF, and 5 mM β-mercaptoethanol. The cell lysate was clarified by centrifugation and supernatant was incubated with preequilibrated Nickel-NTA agarose beads (BioBharati) for 2 hours at 4°C with gentle mixing. After batch binding, beads

were pelleted by centrifugation and washed twice with lysis buffer containing 300 mM NaCl and 30 mM imidazole, followed by two more washes with buffer containing 250 mM NaCl and 30 mM imidazole, then eluted in buffer containing 200 mM NaCl and 400 mM imidazole. The eluted RelA was concentrated and separated on a HiLoad 16/60 Superdex 200 (Cytiva) size-exclusion column with buffer containing 200 mM NaCl, 25 mM Tris-HCl pH 7.5, 5% glycerol, and 1 mM DTT. Peak fractions were pooled, concentrated, and flash frozen in liquid nitrogen for use in *in vitro* assays.

For preparation of recombinant p50:RelA heterodimer, first recombinant His-tagged p50(1-435) was purified by nickel affinity chromatography from *E. coli* Rosetta (DE3) as outlined for His-tagged RelA(19-304) except with the following modifications. The bacterial pellet was lysed in lysis buffer containing 25 mM Tris-HCl pH 7.5, 250 mM NaCl, 10% glycerol, 0.1% NP40, 10 mM imidazole, 0.25 mM PMSF, and 5 mM β-mercaptoethanol and recombinant His-tagged p50 was eluted from Nickel-NTA agarose beads in the same buffer except with 250 mM imidazole. The purified p50 was concentrated and incubated in a 1:1 molar ratio with His-tagged RelA(1- 551) at a final concentration of 0.1 mg/mL in buffer containing 25 mM Tris-HCl pH 7.5, 250 mM NaCl, 10% glycerol, and 1 mM DTT for 1 hour at room temperature. The p50:RelA heterodimer was then concentrated and separated on a HiLoad 16/60 Superdex 200 size-exclusion column with buffer containing 200 mM NaCl, 25 mM Tris-HCl, 5% glycerol and 1 mM DTT. Peak fractions were collected, concentrated, and flash frozen in liquid nitrogen.

3. Electrophoretic Mobility Shift Assay

Details of all oligonucleotides are provided in **Table 2.1**. Oligonucleotides were ^{32}P end radiolabeled using T4-polynucleotide kinase (New England Biolabs) and [γ-^{32}P]ATP

(PerkinElmer) and annealed with complementary DNA. Recombinant RelA or p50:RelA were incubated with radiolabeled DNA at room temperature for 15 minutes in binding buffer containing 10 mM Tris- HCl pH 7.5, 50 mM NaCl, 10% glycerol, 1% NP-40, 1 mM EDTA, and 0.1 mg/mL sonicated salmon sperm DNA. Proteins were diluted in dilution buffer containing 20 mM Tris-HCl pH 7.5, 50 mM NaCl, 10% glycerol, 1 mM DTT, and 0.2 mg/mL bovine serum albumin in preparation for the reaction mixture. Complexes were analyzed by electrophoresis in 5% non-denatured polyacrylamide gel at 200 V for 1 h at room temperature in 25 mM Tris base, 190 mM glycine, and 1 mM EDTA. Gel was then dried, exposed on a phosphor screen overnight, and scanned by Typhoon FLA 9000 imager (Cytiva).

For EMSA with 293T nuclear extract, cells were first harvested by scraping in chilled PBS, pelleted by centrifugation at 300 g, washed once with PBS, then resuspended in cytoplasmic lysis buffer consisting of PBS with 0.1% NP40. Nuclei were then pelleted by centrifugation at 3000 g, washed twice with PBS, and resuspended in nuclear extraction buffer consisting of 25 mM Tris-HCl pH 7.5, 420 mM NaCl, 10% glycerol, 0.2 mM EDTA, 1 mM DTT, and 0.5 mM PMSF. Nuclear extract was quantified by Bradford assay and 7 μg of extract was mixed with radiolabeled DNA in a binding reaction consisting of 25 mM Tris-HCl pH 7.5, 150 mM NaCl, 10% glycerol, 1 mM EDTA, and 0.1 mg/mL sonicated salmon sperm DNA. Complexes were analyzed by non-denaturing gel electrophoreses as outlined previously.

4. Biolayer Interferometry Assay and Analysis

Biotinylated oligonucleotides used for BLI experiments are listed in **Table 2.1**. Biotinylated oligonucleotides were annealed with complementary nonbiotinylated oligonucleotides by mixing at a ratio of 1:1.2 in buffer containing 10 mM Tris-HCl pH 7.5, 50 mM NaCl, and 1 mM EDTA and incubating in boiling water allowed to slowly cool to room

temperature. Biotinylated annealed DNA (200 nM) was then immobilized onto hydrated Octet Streptavidin (SA) biosensors (Sartorius) for 10 seconds in BLI buffer consisting of 25 mM Tris-HCl pH 7.5, 150 mM NaCl, 0.02% Tween 20, 0.1 mg/mL sonicated salmon sperm DNA, and 1 mM DTT using the Octet K2 system (ForteBio). Baseline signal for each binding condition was first measured by incubation of DNA-immobilized on sensor in BLI buffer for 60 seconds. Binding kinetics were then measured through an association phase of 120 seconds (or longer) in which 12.5, 25, 50, 100, or 200 nM of recombinant His-RelA(1-551) or p50:RelA was incubated with the biotinylated DNA-sensor complex, followed by a dissociation phase of 180 seconds (or longer) in BLI buffer without protein. Sensor was regenerated in BLI buffer containing 1 M NaCl for 5 seconds followed by wash in BLI buffer for another 5 seconds three times prior to each reading, and a reference sensor without biotinylated DNA was used for background subtraction.

The observed RelA-DNA association as a function of time follow single-exponential accumulation of the observed protein-DNA complexes. The single-exponential dependence of the background- corrected signal as a function of time, $S_{on}(t)$ is:

$$S_{\text{on}} = A\left(1 - e^{-k_{\text{on}}t}\right), \tag{1}$$

where A is signal change from time $t = 0$ to equilibrium and k_{on} is the observed association rate constant. The dissociation of the protein-DNA complexes in this experimental setup is initiated at the conclusion of the association experiment at $t = t_0$. The dissociation time course for RelA with A- and T-centric DNA are well described by double-exponential decay, with the exception to the two lowest protein concentrations, where they are single-exponential. The background-corrected double-exponential dependence of the signal used to fit the dissociation kinetics is:

$$S_{\text{off}} = A_1 e^{-k_{\text{off},1}\left(t - t_0\right)} + A_2 e^{-k_{\text{off},2}\left(t - t_0\right)}, \tag{2}$$

The best-fit values of A_1, A_2, $k_{off,1}$ and $k_{off,2}$ are calculated and the respective best-fit curves shown in Supplementary Fig. S1F. One can see that, as expected for first-order kinetics, $k_{off,1}$ and $k_{off,2}$ are independent of $[P]_T$. This double-exponential behavior indicates two types of complexes, one of which dissociates from the DNA much faster than the other ($k_{off,2} >> k_{off,1}$). The population of the rapidly dissociating complexes (proportional to A_2) increases in population nonlinearly as a function of protein concentration $[P]_T$, so that the relative population of these complexes decreases with decreasing $[P]_T$. For example, for the TA-centric DNA, the population of the rapidly dissociation complexes is undetectable at $[P]_T$ = 12.5 nM and 25 nM, and the dissociation kinetics are single-exponential at these concentrations. For RelA complexes with GC- and CG-centric DNA, where the protein-DNA binding is much weaker than for AT- and TA- centric DNA and reaches only ~30% of DNA saturation at the highest protein concentration, the dissociation kinetics generally follow a single-exponential behavior, where a faster dissociating component is not present. This behavior indicates that the faster dissociating complexes likely form by a second dimer of RelA binding to a nonspecific DNA site and interacting favorably with the specifically bound dimer.

The dependence of k_{on} on $[P]_T$ is approximately linear, indicating that RelA is in large excess of DNA ($[P]_T >> [D]$) and:

$$k_{on} = \alpha [P]_T + \beta, \quad (3)$$

For a one-step binding mechanism

$$P + D \underset{k_{-1}}{\overset{k_1}{\rightleftharpoons}} C, \quad (4)$$

$k_{off,1}$ (measured when $[P]_T = 0$) is equal to the microscopic rate constant k_{-1}, and

$$k_{on} = k_1 [P]_T + k_{-1}, \quad (5)$$

The y-axis intercept b (k_{on} extrapolated to $[P]_T = 0$) is, indeed, approximately equal to the smaller of the two observed dissociation rate constants, $k_{off,1}$, which describes the binding of the first RelA dimer to DNA at the specific recognition site, as deduced above. Because $k_{off,1}$ is measured directly and redundantly (for different $[P]_T$), it yields a more rigorous value of k_{-1}, than b does. The linearity of k_{on} as a function of $[P]_T$ indicates that k_{on} is a characteristic of these protein-DNA complexes. The slope of this dependence a is equal to k_1, as eq. (5) indicates. Therefore, the equilibrium constant for complex formation K_{eq} can be obtained as

$$K_{\mathrm{eq}} = \frac{k_1}{k_{-1}} = \frac{\alpha}{k_{\mathrm{off},1}}, \tag{6}$$

Another way of determining K_{eq} is from the dependence of A on $[P]_T$. However, signal A needs to be corrected by subtracting the rapidly dissociating complexes. Assuming that the ratio of rapidly to slowly dissociating complexes at equilibrium is A_2/A_1, we obtained K_{eq} by data fitting using the following dependence of the corrected signal A_{corr} on $[P]_T$:

$$A_{corr} = \frac{A_{\mathrm{corr},\infty} K_{\mathrm{eq}} [P]_{\mathrm{T}}}{1 + K_{\mathrm{eq}} [P]_{\mathrm{T}}}, \tag{7}$$

where $A_{corr,\infty}$ is the corrected equilibrium signal at saturation. This method of calculating K_{eq} involves more steps and approximations than eq. (6), but we also used it for comparison. The two methods yield very similar values, indicating a correct interpretation of the observed parameters in terms of mechanism (5).

5. Fluorescence Anisotropy Assays

The κB DNAs used for fluorescence anisotropy assay are listed in **Table 2.1**. Fluorescein-labeled oligos (IDT) were mixed at a 1:1.2 molar ratio with complementary unlabeled oligos at a final concentration of 1mM and annealed as previously outlined. A titration

of different concentrations of His-RelA^{FL} was mixed with 1 nM of labeled and annealed κB DNA at a total volume of 50 μL in buffer containing 25 mM Tris-HCl pH 7.5, 150 mM NaCl, 5% glycerol, 0.25 mg/mL BSA, 0.1 mg/mL sonicated salmon sperm DNA, and 0.5% NP-40. The reactions were incubated at room temperature for 15 minutes and transferred to a nonbinding 96-well black bottom plate (Greiner). Fluorescence anisotropy was measured using a Tecan Safire 2 plate reader in polarization mode with an excitation wavelength of 470 nm and an emission wavelength of 520 nm with a 20 nm bandwidth. To quantify binding affinity, the triplicate anisotropy data were normalized to baseline values without protein, plotted, and fit in GraphPad PRISM 4.0 (GraphPad Software) to the quadratic equation:

$$[\mathrm{RelA} + \mathrm{DNA}]/[\mathrm{DNA}] = \left[[\mathrm{RelA}] + [\mathrm{DNA}] + K_\mathrm{D} - \sqrt{([\mathrm{RelA}] + [\mathrm{DNA}] + K_\mathrm{D})^2 - 4[\mathrm{RelA}][\mathrm{DNA}]}\right]/\left(2[\mathrm{RelA}]\right).$$

6. Crystallization of κB DNAs and RelA:κB DNA Complexes

The κB DNAs used for crystallization are listed in **Table 2.1**. Complementary oligonucleotides were annealed at a 1:1 molar ratio at a final concentration of 0.5 mM by placing in boiling water and slowly cooling to room temperature. Crystals were formed by hanging drop vapor diffusion method at 18°C where 0.5 mM DNAs were mixed in 1:1 ratio with reservoir solution containing 100 mM sodium acetate-HCl pH 3.75, 8% PEG3350, and 50 mM zinc acetate. Crystals nucleated after three days and reached maximum size around the 7th day. Crystals were soaked in cryo-protectant buffer containing the mother liquor and 20% ethylene glycol and flash frozen with liquid nitrogen.

For RelA and κB DNA complex crystallization, κB DNA was first annealed in buffer containing 10 mM Tris-HCl pH 7.5, 50 mM NaCl, and 1 mM EDTA as outlined previously. Complex was formed by mixing untagged RelA(19-304) at a final concentration of 10 mg/mL

with κB DNA at a 1:1.2 molar ratio in buffer containing 25 mM Tris-HCl pH 7.5, 50 mM NaCl, and 1 mM DTT followed by incubation at room temperature for 15 minutes. Crystals of the complexes were formed by hanging drop vapor diffusion at 18°C by mixing in a 1:1 ratio with reservoir solution containing 100 mM MES pH 5.5, 2 mM calcium chloride, 50 mM ammonium chloride, 14% PEG3350, 1 mM spermine, and 0.05% octyl β-D-glucopyranoside. T-κB and C-κB complex crystals were grown under similar reservoir conditions except T-κB was supplemented with 2 mM ammonium sulfate and C-κB was supplemented with 1 mM spermidine. Crystals nucleated around the fourth day and reached a maximum size around the 10th day. A-κB, T-κB, and G-κB complex crystals were soaked in cryo-protectant buffer containing the mother liquor without DTT and supplemented with 15% glycerol and C-κB complex crystals were soaked in cryo-protectant buffer containing 20% ethylene glycol without DTT. Crystals were then flash frozen under liquid nitrogen.

7. Molecular Dynamics Simulations

Briefly, free-form structures of A-, T-, G- and C-κB DNAs were extracted from their corresponding crystal structures in the RelA-bound form. All DNAs in both free and RelA-bound structures were tailored to have an equivalent length of 18 base pairs (9+1+8). Free DNA (A-, T-, G- and C-κB) or DNA- RelA (A- and G-κB-RelA) complex was each placed in a dodecahedron box and solvated with TIP3P water models. Na^+ and Cl^- were added to retain an ionic concentration of 0.15 M. AMBER ff19SB force field with OL15 parameters for DNAs was employed, along with GROMACS 2021.4 for the all-atom MD simulations presented in this work. Five 2 μs simulations were carried out for each free κB DNAs, whereas five simulations of 3 μs were performed for each RelA-bound complex.

Table 2.1: Sequences of oligonucleotides used in experiments.

DNA	Experiment	Sequence (5' → 3')
A-κB-top	EMSA	CAGACTGGGAAATTCCAGTGTC
A-κB-bottom	EMSA	GACACTGGAATTTCCCAGTCTG
T-κB-top	EMSA	CAGACTGGGAATTTCCAGTGTC
T-κB-bottom	EMSA	GACACTGGAAATTCCCAGTCTG
G-κB-top	EMSA	CAGACTGGGAAGTTCCAGTGTC
G-κB-bottom	EMSA	GACACTGGAACTTCCCAGTCTG
C-κB-top	EMSA	CAGACTGGGAACTTCCAGTGTC
C-κB-bottom	EMSA	GACACTGGAAGTTCCCAGTCTG
A-κB-luciferase-top	Luciferase	TCGACGGGAAATTCCG
A-κB-luciferase-bottom	Luciferase	GATCCGGAATTTCCCG
T-κB-luciferase-top	Luciferase	TCGACGGGAATTTCCG
T-κB-luciferase-bottom	Luciferase	GATCCGGAAATTCCCG
G-κB-luciferase-top	Luciferase	TCGACGGGAAGTTCCG
G-κB-luciferase-bottom	Luciferase	GATCCGGAACTTCCCG
C-κB-luciferase-top	Luciferase	TCGACGGGAACTTCCG
C-κB-luciferase-bottom	Luciferase	GATCCGGAAGTTCCCG
A-κB-fluorescein-top	Fluorescence Anisotropy	(FAM)CAGACTGGGAAATTCCAGTGTC
T-κB-fluorescein-top	Fluorescence Anisotropy	(FAM)CAGACTGGGAATTTCCAGTGTC
G-κB-fluorescein-top	Fluorescence Anisotropy	(FAM)CAGACTGGGAAGTTCCAGTGTC
C-κB-fluorescein-top	Fluorescence Anisotropy	(FAM)CAGACTGGGAACTTCCAGTGTC
A-κB-BLI-top	Biolayer Interferometry	(Biotin)CAGACTGGGAAATTCCAGTGTC
T-κB-BLI-top	Bioayer Interferometry	(Biotin)CAGACTGGGAATTTCCAGTGTC
A-κB-BLI-top	Biolayer Interferometry	(Biotin)CAGACTGGGAAGTTCCAGTGTC
A-κB-BLI-top	Biolayer Interferometry	(Biotin)CAGACTGGGAACTTCCAGTGTC
A-κB-crystal-top	DNA crystallography	CGGGAAATTCCG
A-κB-crystal-bottom	DNA crystallography	CGGAATTTCCCG
T-κB-crystal-top	DNA crystallography	CGGGAATTTCCG
T-κB-crystal-bottom	DNA crystallography	CGGAAATTCCCG
G-κB-crystal-top	DNA crystallography	CGGGAAGTTCCG
G-κB-crystal-bottom	DNA crystallography	CGGAACTTCCCG
C-κB-crystal-top	DNA crystallography	CGGGAACTTCCG
C-κB-crystal-bottom	DNA crystallography	CGGAAGTTCCCG
A-κB-complex_crystal-top	RelA:DNA crystallography	ACTGGGAAATTCCAGTGAT
A-κB-complex_crystal-bottom	RelA:DNA crystallography	ATCACTGGAATTTCCCAGT
T-κB-complex_crystal-top	RelA:DNA crystallography	ACTGGGAATTTCCAGTGAT
T-κB-complex_crystal-bottom	RelA:DNA crystallography	ATCACTGGAAATTCCCAGT
G-κB-complex_crystal-top	RelA:DNA crystallography	ACTGGGAAGTTCCAGTGAT
G-κB-complex_crystal-bottom	RelA:DNA crystallography	ATCACTGGAACTTCCCAGT
C-κB-complex_crystal-top	RelA:DNA crystallography	ACTGGGAACTTCCAGTGAT
C-κB-complex_crystal-bottom	RelA:DNA crystallography	ATCACTGGAAGTTCCCAGT

Table 2.2: Crystallographic and refinement data of RelA:κB DNA complexes.

Structural Model	RelA:A-centric κB	RelA:T-centric κB	RelA:G-centric κB	RelA:C-centric κB
Deposition ID	D_1000269908	D_1000270087	D_1000270088	D_1000270089
Data Collection				
Wavelength (Å)	0.97929	0.97927	0.97927	0.97946
Resolution range (Å)	30-2.03 (2.06-2.03)	30-1.90(1.93-1.90)	30-1.87(1.90-1.87)	30-3.60(3.66-3.60)
Space group	P 21 21 2	P 21 21 2	P 21 21 2	P 21 21 2
Cell dimensions				
a, b, c (Å)	115.5160 133.5680 45.4430	118.654 132.682 45.663	119.263 133.084 45.670	113.953 132.182 66.577
α, β, γ (°)	90.0000 90.0000 90.0000	90.000 90.000 90.000	90.000 90.000 90.000	90.000 90.000 90.000
Total reflections	558216	448525	409360	147520
Unique reflections	46270	57610	60489	12133
Redundancy	12.1 (10.8)	7.8(7.7)	6.8(5.8)	12.2(9.0)
Completeness (%)	99.7 (99.1)	99.6(99.9)	99.5(99.8)	99.8(99.7)
I/σ(I)	312.7/11.7 (7.4/7.2)	522.1/23.7(23.9/15.6)	795.7/41.5(46.5/21.3)	4.2/1.8(5.7/3.0)
Rpim	0.030 (0.700)	0.047(0.985)	0.081(1.607)	0.325(0.547)
CC1/2 /(CC*)	0.993(0.644)/0.998 (0.885)	0.985(0.463)/0.996(0.795)	0.983(0.509)/0.996(0.821)	0.606(0.976)/0.869(0.994)
Refinement				
Resolution range (Å)	28.91-2.03	29.66-1.90 (1.949-1.90)	29.82-1.87(1.919-1.87)	29.75-3.60(3.694-3.60)
No. of reflections (work/test set)	33225/1739	49976/2577	56382/2947	11165/585
Rwork/Rfree	0.2232(0.268)/0.2733(0.309)	0.191(0.261)/0.230(0.301)	0.153(0.209)/0.227(0.301)	0.324(0.581)/0.374(0.609)
Number of non-hydroen atoms	5574	5747	5760	5082
r.m.s. deviations				
Bonds ()	0.0058	0.0025	0.0073	0.0138
Angles (*)	1.2042	0.9609	1.6758	2.092
Ramachandran plot				
Favored (%)/allowed(%)	95/4	96/4	96/3	79/16
Outliers (%)	1	0	1	6
Rotamer outliers (%)	4	1	4	6
Clashscore	9	2	12	14
Average B-factor ($Å^2$)	35.057	26.612	28.033	111.763

Table 2.3: Crystallographic and refinement data of κB DNAs.

Structural Model	A-centric κB	T-centric κB	G-centric κB	C-centric κB
Deposition ID	D_1000270091	D_1000270092	D_1000270093	D_1000270094
Data Collection				
Wavelength (Å)	1	1	1	1
Resolution range (Å)	50-2.5 (2.54-2.5)	50-2.5 (2.54-2.50)	50-2.15 (2.19-2.15)	50-2.2(2.24-2.2)
Space group	P 1	P 1	P 1	P 1
Cell dimensions				
a, b, c (Å)	46.479 46.447 98.381	46.078 46.233 98.646	46.857 46.850 99.289	46.999 47.031 98.682
α, β, γ (°)	90.012 89.915 60.013	89.904 89.860 60.098	90.136 90.200 60.019	90.031 89.957 59.993
Total reflections	72351	56953	135588	123764
Unique reflections	20950	21340	35776	33224
Redundancy	3.5 (3.5)	2.7(2.6)	3.8(3.8)	3.7(3.8)
Completeness (%)	86.1 (70.8)	89.9(74.1)	90.0(90.6)	89.9(91.8)
I/σ(I)	46.5/3.2 1.8/2.0	21.5?2.3(0.9/2.1)	54.2/3.8(2.2/3.9)	86.6/5.1 (1.8/4.0)
Rpim	0.077 (0.559)	0.114(1.217)	0.049(0.838)	.055(1.066)
CC1/2 /(CC*)	0.985(0.845)/0.996 (0.957)	0.970(0.340)/0.995(0.712)	0.989(0.617)/0.997(0.874)	1.037(0.531)/1.009(0.833)
Refinement				
Resolution range (Å)	37.31-2.51	37.17-2.52	37.63-2.15	37.66-2.19
No. of reflections (total/test set)	19959/1205	20366/1201	33938/1838	31524/1995
Rwork/Rfree	0.400(0.489)/0.482(0.473)	0.388/0.518 (0.457/0.496)	0.38(0.546)/0.413(0.570)	0.397(0.505)/0.412(0.464)
Number of non-hydroen atoms	5560	5562	5544	5562
r.m.s. deviations				
Bonds ()	0.0058	0.0268	0.014	0.021
Angles (*)	1.2042	1.533	1.462	2.121
Average B-factor (Å^2)	52.009	31.258	31.931	31.274

F. Acknowledgements

I would like to especially thank Dr. Tapan Biswas for contributions to DNA and RelA:DNA crystallization, structural analysis, and manuscript preparation. I would also like to thank Dr. Amar Deep and Dr. Kevin Corbett for help with BLI assay and Dr. Oleg Tsodikov for help with BLI analysis. I would like to thank Dr. Tianjie Li and Dr. Yi Wang for performing and analyzing MD simulations. Lastly, I would like to thank Emily Walters, Diana Grada-Ibarra, and Zixing Liu for help with purification of RelA-RHR mutants.

Chapter 2, in part, has been submitted for publication of the material as it may appear in Nucleic Acids Research, 2023, Shahabi, Shandy; Ghosh, Gourisankar, Oxford Press, 2023. The dissertation author was the primary researcher and co-first author of this paper.

Chapter 3: Low affinity κB sites direct RelA DNA binding and transcriptional activation with NFAT

A. Abstract

NF-κB family of inducible transcription factors control inflammatory gene expression by binding to κB sites located at the promoter or enhancer regions of target genes. I explore what factors promote recruitment of NF-κB to specific subsets of κB sites in the genome. TNFα-dependent rapidly activated genes displayed a surprising abundance of low affinity NF-κB motifs locally distributed around core κB binding sites. Biochemical characterization of low affinity κB sites reveal they modulate NF-κB DNA binding affinity and enhance overall occupancy on DNA to synergistically enhance transcriptional output. In the context of the Cxcl2 promoter, a low affinity κB site located downstream a well characterized core κB site impacted RelA binding and RelA-dependent transcriptional activation. Mass spectrometric analysis identified NFAT family as important transcriptional regulators at the Cxcl2 promoter. NFATc1 associated with NF-κB at the Cxcl2 promoter DNA, and this association was dependent on DNA binding of NFATc1 and both the core and low affinity κB elements. Overall, this work suggests that locally distributed low affinity κB elements contribute to NF-κB-dependent gene regulation.

B. Introduction

Like other transcription factors, NF-κB dimers recognize a degenerate consensus motif present in the promoter or enhancer region of target genes to activate transcription (Mulero, 2019; Zhang, 2017). Previous biochemical and structure-based approaches reveal sequence-dependence for NF-κB binding affinity, however *in vitro* binding affinity is not an absolute determinant for DNA binding *in vivo* (Chen, 1998; Siggers, 2012; Zhao, 2014). This is exemplified by the fact that NF-κB, like many other transcription factors, binds low affinity κB sites despite the breadth of available sites throughout the genome (Tong, 2016; Zhao, 2014; Wang, 2012). Chromatin accessibility is an important predictor of binding site availability, however the precise factors that dictate transcription factor recruitment to specific genomic regions is not clearly understood (Li, 2011; Spitz, 2012).

Current models of transcription factor DNA binding posit that transcription factors nonspecifically scan DNA for higher affinity DNA elements, thus leading to increased residency time and the experimentally observed DNA binding and transcriptional activation (Bonnet, 2008; Hammar, 2012; Blainey, 2009). This process, known as facilitated diffusion, is directly dependent on the identity of the DNA sequences locally surrounding a higher affinity DNA element (Berg, 1981; Cencini, 2017; Leven, 2019). Considering this, and recent observations that low affinity binding sites can promote transcription factor engagement and gene regulation, locally distributed low affinity elements may play an important role in influencing transcription factor binding at higher affinity elements (Crocker, 2015; Shahein, 2022). Most RelA genome-wide studies focus on identifying moderate to high affinity κB sites overlapping with stimulus-induced ChIP-Seq signals at induced genes, and neglect to interrogate the influence of locally distributed lower affinity sequences (Kasowski, 2010; Alizada, 2021; Borghini, 2018). The

extent to which weak κB elements contribute to DNA binding and transcriptional activation by NF-κB is not understood.

Cooperativity between multiple transcription factors is an emerging mechanism that explains locus-specific recognition by transcription factors (Yan, 2013; Ravasi, 2010; Mimy, 2010). Such cooperativity can be mediated through direct protein-protein between transcription factors contacts or facilitated by adjacent DNA elements and expands the potential binding repertoire of transcription factors (Morgunova, 2017; Rao, 2021; Jolma, 2015). Additionally, binding of one transcription factor may influence the genomic landscape to recruit binding of another transcription in a step-wise manner. Indeed, in the context of NF-κB signaling, RelA has been shown to cooperate with other transcription factors including E2F1, IRF, and FOXM1 to combinatorially influence transcriptional activation at specific genes (Ankers, 2016; Panne, 2007; Zhao, 2014; Csumita, 2019; Lim, 2007). DNA-dependent transcription factor cooperativity has been demonstrated to be an important aspect for gene regulation, however the underlying biochemical and biophysical mechanisms influencing transcriptional activation is not clearly understood (Sonmezer, 2020; Stefflova, 2013; Shen, 2022).

Nuclear factor of activated T cells (NFAT) is an important family of transcription factors involved in the regulation of T cell activation, cellular differentiation and development, and immune signaling (Muller, 2010; Shaw, 1988). The NFAT family consists of 5 members, NFATc1, NFATc2, NFATc3, NFATc4, and NFAT5, all of which share an N-terminal NFAT homology region, a highly conserved Rel-homology region (RHR), and a C-terminal activation domain. NFAT signaling is activated upon cell surface receptor-coupled calcium-mobilization and calcineurin-dependent dephosphorylation, thus leading to nuclear translocation and DNA binding. NFAT recognize the consensus sequence of GGAAA, which is similar to the NF-κB

consensus due to the shared DNA-binding mechanism of the RHR domain (Badran, 2002). NFAT can bind DNA in both monomeric and dimeric forms and has been shown dimerize with other transcription factors on DNA (Rao, 1997; Stroud, 2003; Soto-Nieves, 2009; Mognol, 2019; Ramirez-Carrozzi, 2001). Both NF-κB and NFAT have the capacity to bind overlapping regions, however the cooperativity between the two at target promoters has not been established.

In this chapter, I explore the how low affinity κB sites at promoter or enhancer regions of RelA-dependent genes influence DNA binding and transcription (**Figure 3.1**). I observe that weak κB sites are indeed prevalent at RelA-bound regions in promoters or enhancers of TNFα-dependent rapidly activated genes, and I biochemically investigate the influence of weak κB sites on DNA binding and transcriptional activation. I observe that a single κB site can only weakly induce transcription activation, however weak κB sites can combinatorially enhance RelA DNA binding and synergistically activate transcription. I also investigate RelA-dependent regulation at the Cxcl2 promoter following TNFα stimulation and observe that the NFAT family is induced to bind the Cxcl2 promoter in MEF. I observe that NFAT and NF-κB can associate together on DNA *in vitro*, and that Cxcl2 expression is dependent on both NF-κB and NFAT.

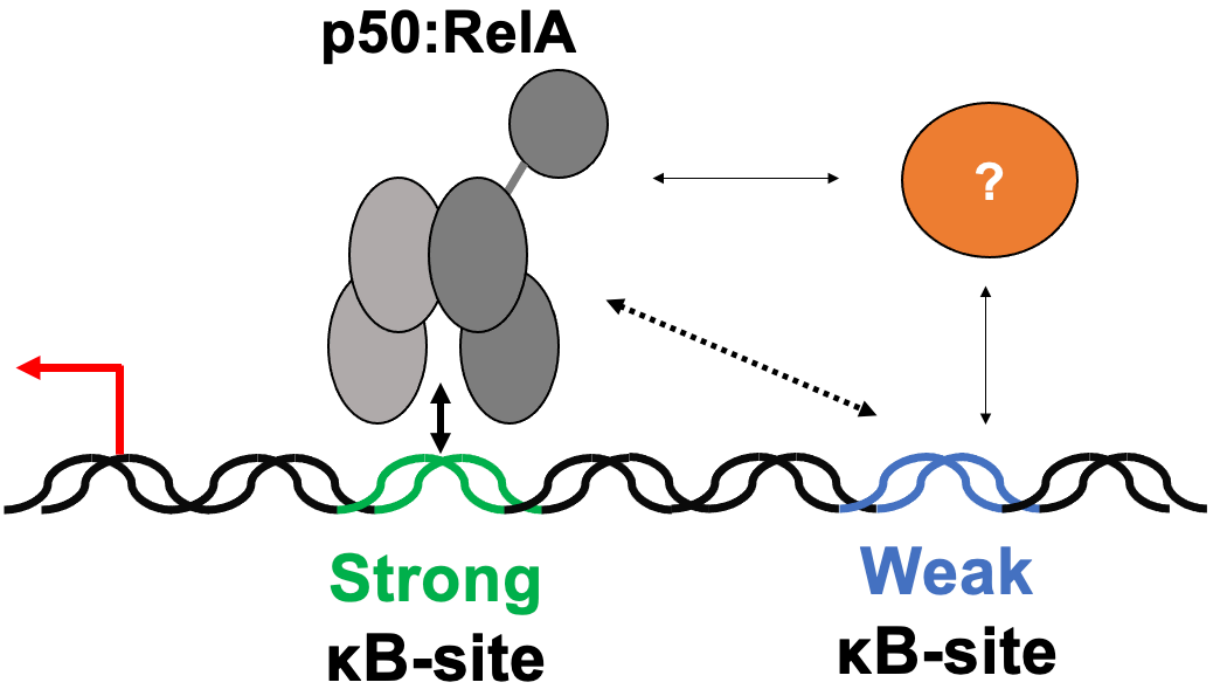

Figure 3.1: Schematic representation of how low affinity binding sites can contribute to transcription
Low affinity κB sites have been determined *in vitro* through previous high-throughput and biochemical assays. The effect of locally distributed "weak κB sites" on classical higher affinity κB sites has not been established. Weak κB sites can directly modulate NF-κB binding at target promoters but also influence activity of DNA-dependent cofactor proteins.

C. Results

1. Rapidly activated targets of RelA contain multiple weak κB motifs

I was curious if there existed a correlation between weak κB binding sites and NF-κB mediated transcriptional regulation. Using recently published RNA-Seq and ChIP-Seq data in TNFα stimulated MEF, I explored the presence of weak κB binding motifs at the promoters or enhancers of RelA-dependent targets using a reduced stringency search with the JASPAR database of predicted transcription factor binding sites (JASPAR score > 300; p-value < 10^{-3}) (Ngo, 2020; Fornes, 2020). Sequences throughout the genome were identified as potential weak κB sites through the extent of divergence from the established 10-mer κB consensus. Identified weak sites agree with previously published protein-binding microarray data that suggests NF-κB binds such sequences with reduced affinity (Siggers, 2011). I then identified the core κB site at the promoter or enhancer of RelA target genes as the strongest κB site that overlaps with the peak RelA ChIP-Seq signal following TNFα stimulation. Identified core κB sites agree with previously characterized RelA binding sites, examples of which include GGGAAATTCC in Tnf, GGGAATTTCC in Cxcl1, Cxcl2, and Cxcl10, and GGAAATTCCC in Nfkbiz. RelA-dependent genes were categorically separated into rapid or delayed activation following TNFα stimulation based on the timing of peak expression from RNA-Seq and 100bp upstream and downstream from the core κB site was analyzed for the presence of weak κB sites.

I observed a surprising overrepresentation of weak κB sites present in the RelA-associated promoter and enhancer regions of rapidly activated genes relative to genes that undergo delayed activation (**Figure 3.2**). An example promoter region is presented for Cxcl2, where the strong κB site with the sequence GGGAATTTCC is located 60 bp upstream of the transcription start site (TSS) and the associated weak κB site with the sequence GGGCTTTTCC

is 10 bp downstream of the strong κB site in mouse (**Figure 3.3A**). Both the strong and weak κB sites display high conservation between mouse and humans suggesting evolutionary importance (**Figure 3.3B**). I also observed a nonrandom enrichment of weak κB sites overlapping with RelA ChIP-Seq peak signals following TNFα stimulation of many rapidly activated genes despite the increase in potential κB sites from the unbiased and reduced stringency search. Representative RelA ChIP-Seq peaks and potential κB sites for Nfkbiz, Gadd45b, and Pim1 are presented in which the overlap of weak κB sites with RelA-ChIP signals can be observed (**Figure 3.4**).

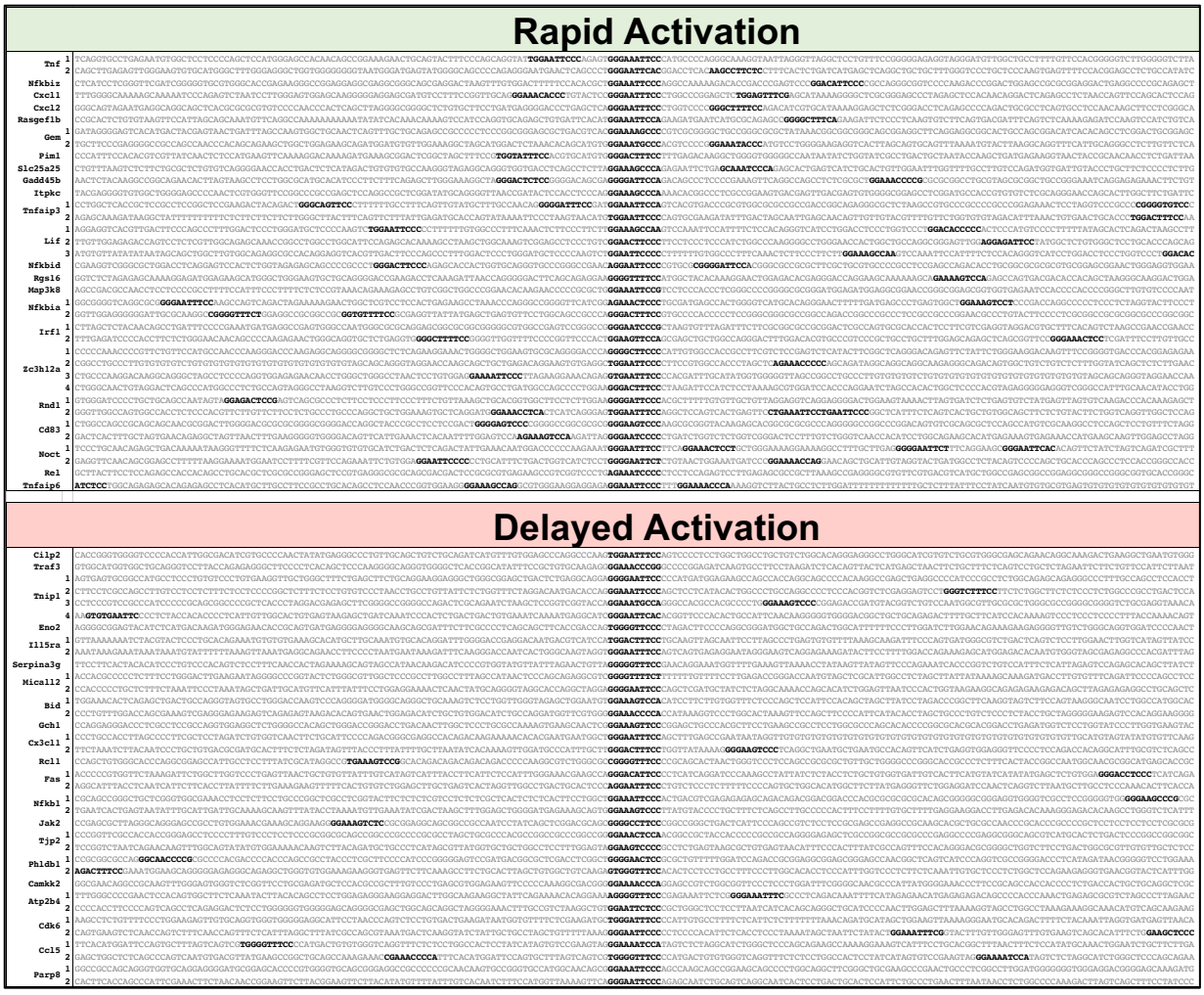

Figure 3.2: NF-κB binding sites of rapidly activated genes contain locally distributed weak κB sites
Graphic representation of genomic DNA sequence 100 bp upstream and downstream of κB sites of RelA-dependent genes. Genes are sorted by peak time of expression as presented in Ngo et al., 2020. Identified κB motifs from a reduced stringency JASPAR search (score > 300) are presented in bold, and sequences are centered around strongest κB motif overlapping with RelA ChIP-Seq signal following TNFα stimulation.

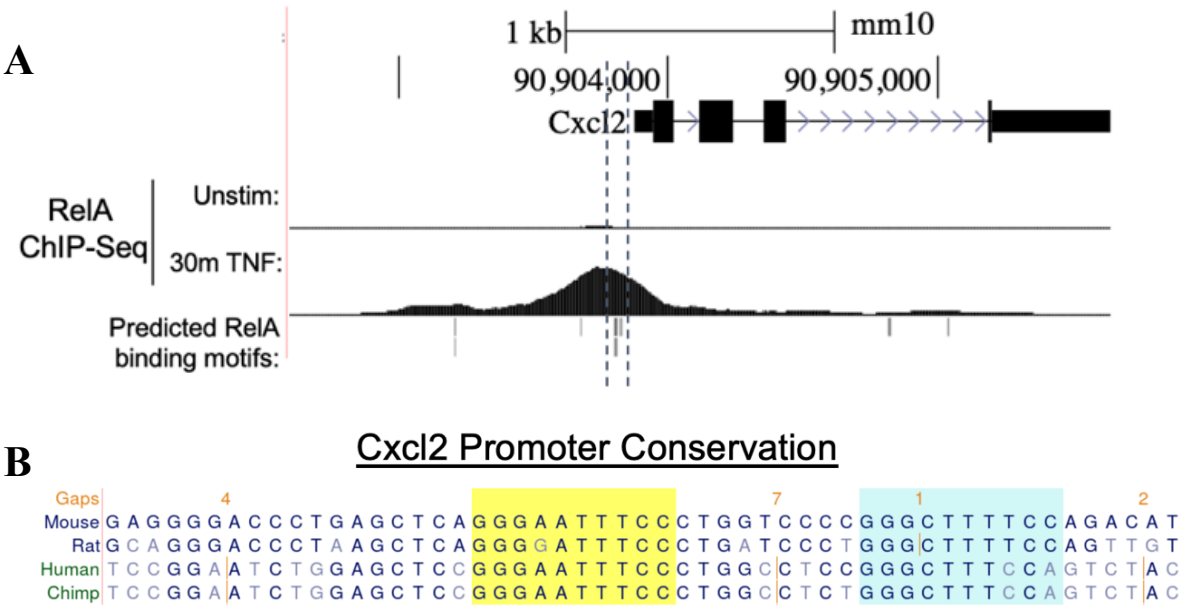

Figure 3.3: Sequence at the Cxcl2 promoter κB site
A. UCSC genome browser view of the Cxcl2 promoter with predicted κB motifs and induced RelA ChIP-Seq signal following 30 minutes of TNFα stimulation (Ngo, 2020). **B.** The strong κB site (yellow) and predicted weak κB site (cyan) at the Cxcl2 are conserved in human and mouse.

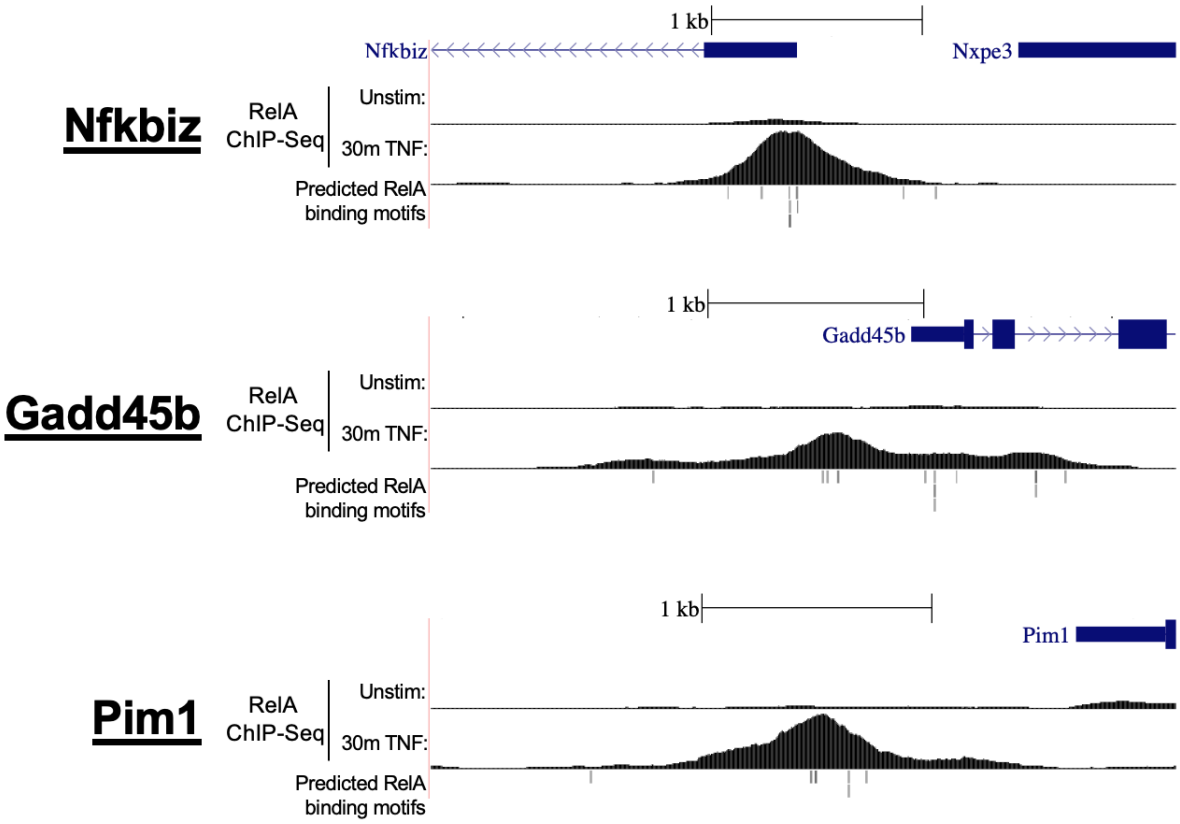

Figure 3.4: Predicted κB site distribution at promoters of RelA-dependent genes
UCSC genome browser view of the Nfkbiz, Gadd45b, and Pim1 promoters with predicted κB motifs and corresponding RelA ChIP-Seq signals in unstimulated and 30 minute TNFα stimulated MEF.

2. A weak κB element at the Cxcl2 promoter influences RelA-dependent transcriptional activation

To understand RelA-dependent transcriptional regulation of the Cxcl2 promoter, wild-type and mutant Cxcl2 promoters were cloned into a luciferase vector and activity was measured with RelA cotransfection in HEK293T cells (**Figure 3.5A and 3.5B**). Cotransfection of WT Cxcl2 (2WT) promoter driven luciferase construct with RelA resulted in an approximate 21-fold increase in activity relative to empty vector. A control mutation of the strong κB site (2M4) abolished RelA-dependent activation, suggesting that the strong κB site is imperative for RelA-mediated activation. Mutations that disrupt RelA binding were also introduced to the weak-κB site (2M1). I observed a significant decrease in RelA-dependent transcriptional activation of 2M1, with only an approximate 6-fold increase in luciferase activity relative to empty vector. This represents a 3.5-fold decrease in luciferase activity between 2WT and 2M1 and suggests that the associated weak κB site of Cxcl2 plays a role in RelA-dependent transcription.

The strong T-centric GGGAATTTCC κB site in Cxcl2 is also followed by an additional C in the human and mouse genome, allowing the strong site to be interpreted as the alternative A-centric GGGAAATTCC in the reverse direction. To investigate the importance of this bidirectionality in RelA-dependent transcriptional activation, single base substitutions were introduced that constrained the sequence to either the forward T-centric GGGAATTTCC (2M2) or the reverse A-centric GGGAAATTCC (2M3) sequence and luciferase activity was measured with RelA-cotransfection. I observed a slight reduction in luciferase activity for both 2M2 and 2M3 relative to 2WT, with a corresponding 19- and 16-fold increase in luciferase activity, respectively, with RelA cotransfection. This suggests that the bidirectionality of the strong κB

site plays a minor role in influencing RelA-mediated transcription, and the influence on RelA-dependent transcriptional activity are of lower magnitude than the weak κB site.

Cxcl2 is a known direct target of NF-κB, and RelA-dependence was first validated by RT-qPCR with WT and RelA-KO MEF cells (Tong, 2016; Burke, 2013) (**Figure 3.6A**). As expected, RelA-KO resulted in dramatically reduced Cxcl2 expression following 1 hour of TNFα stimulation. To understand regulation about the Cxcl2 promoter in the cell, the CRISPR-Cas9 system was used to introduce targeted mutations into the genome of MEF. Lentivirus for expression of Cas9 and a gRNA targeting Cxcl2 at either the strong κB site, weak κB site, or a closely localized control off-target were used to infect MEF, and stable cells with the modified genome were generated (**Figure 3.6B**). Bidirectional sanger sequencing of the Cxcl2 promoter in the different targeting constructs confirmed targeted disruption of the strong and weak κB sites and no off-targeted disruption around the Cxcl2 promoter (**Figure 3.6C**). Stable cells were then tested for expression of Cxcl2 following 1 hour of TNFα stimulation (**Figure 3.6D**). As expected, I observed that CRISPR mediated disruption of the Cxcl2 strong κB site resulted in a large reduction in TNFα induced expression relative to the off-target control, confirming the dependence of Cxcl2 expression on the strong κB site. Disruption of the weak κB site also significantly reduced Cxcl2 expression following TNFα stimulation relative to the off-target control, however to a lower extent than strong κB site disrupted cells. As a control, expression of Cxcl1 was measured in the Cxcl2-directed CRISPR cell lines with TNFα stimulation and I observed no significant change in Cxcl1 expression. This suggests that manipulation of the Cxcl2 promoter was direct and does not universally alter RelA-dependent transcription. Together these results suggest that the weak κB site at the Cxcl2 promoter is important for RelA-mediated transcriptional activation.

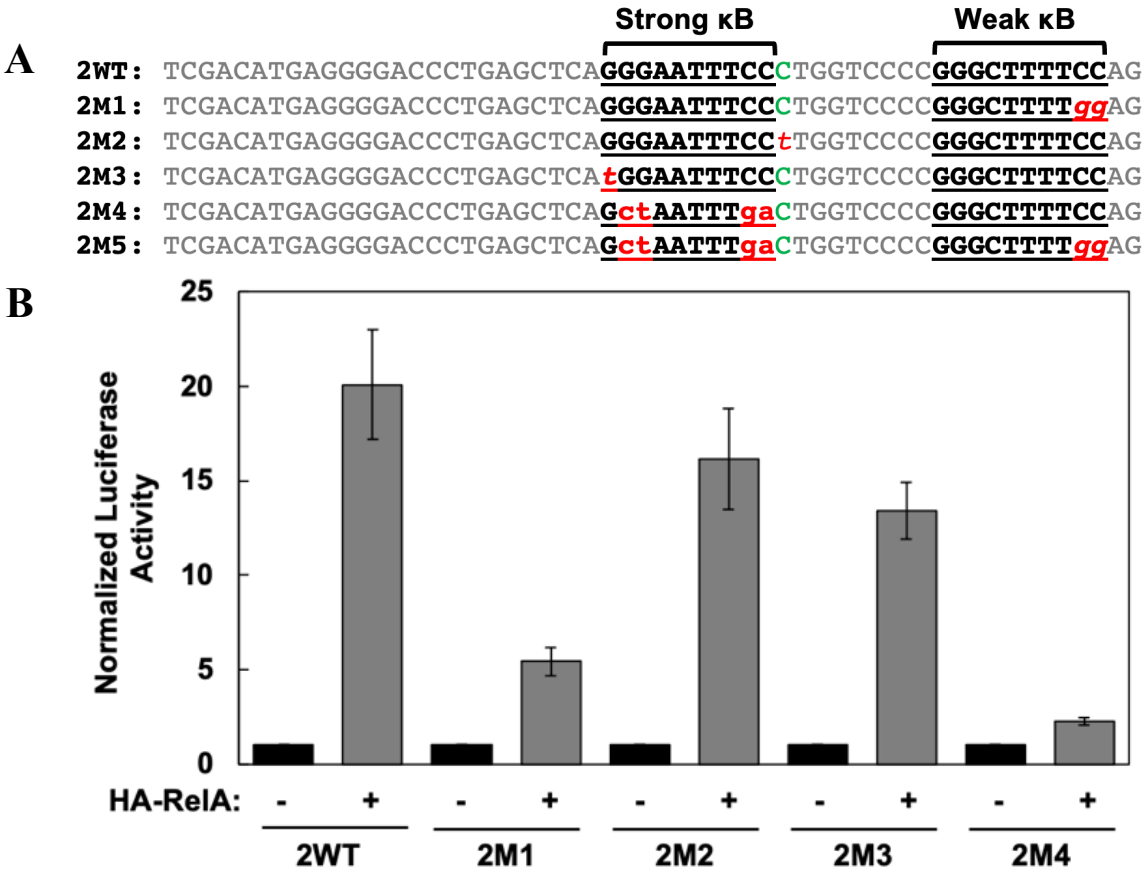

Figure 3.5: RelA-dependent luciferase activity assay of the Cxcl2 promoter
A. Sequences of Cxcl2 mutant promoters used in luciferase and *in vitro* binding assays. **B.** Renilla normalized luciferase activity of different Cxcl2 promoter mutants with HA-RelA cotransfection in HEK293T cells. Empty vector control was used for normalization. Data are presented as mean ± SD of three independent experimental replicates.

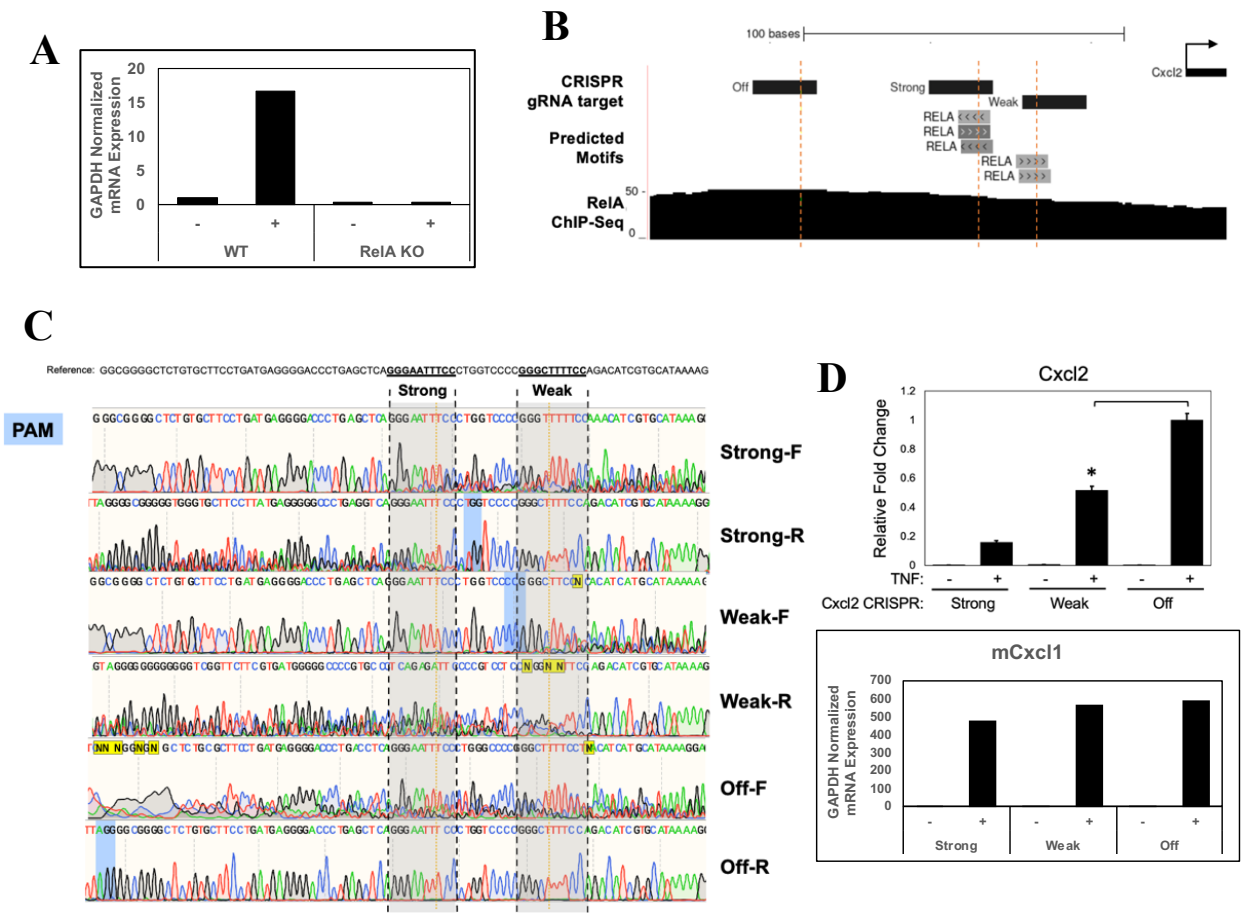

Figure 3.6: The weak κB site at the Cxcl2 promoter regulates expression following TNFα stimulation
A. RT-qPCR of Cxcl2 in WT and RelA-KO MEF establish RelA-dependence on Cxcl2 expression. Values presented are normalized to Gapdh. **B.** Guide RNA targeting specific regions of the Cxcl2 promoter were used to direct CRISPR-Cas9-mediated genome editing and disrupt the strong κB site, weak κB site, or off target control. **C.** Genomic DNA from CRISPR-Cas9 bulk-modified MEF cell lines were analyzed by Sanger sequencing to validate targeted disruption. Sanger sequencing was performed with forward or reverse primers targeting a 200 bp region of the Cxcl2 promoter DNA. **D.** RT-qPCR of Cxcl2 (top) and control Cxcl1(bottom) in Cxcl2-CRISPR modified MEF cell lines.

3. Weak κB sites in tandem are nearly as good as two strong sites in tandem to activate transcription

Based on the influence of the Cxcl2 weak κB site on regulating *in vivo* mRNA expression levels and RelA-dependent reporter activity, I generated several heterologous luciferase reporter constructs to test the transcriptional efficacy of weak κB sites (**Figure 3.7A**). I have previously shown that RelA binds G- and C- centric κB sites with much lower affinity relative to A- and T-centric κB sites, thus resulting in significantly reduced transcriptional activation. Using A- and T- centric κB sites to represent strong binding elements and G- and C- centric κB sites for weak binding elements, I generated different luciferase constructs where I altered the spacing and identity of the weak and strong κB sites and assayed luciferase activity following RelA cotransfection (**Figure 3.7B**). As expected, I observed less activation for G- and C- centric single κB sites relative to A- and T- centric κB sites, suggesting that stronger and weaker κB sites independently correspond to higher and lower NF-κB mediated transcription activation, respectively.

Using a two κB site dependent system, I observed that the combination of a strong and weak κB site (AG10) resulted in significantly elevated transcriptional activation following RelA cotransfection relative to a single strong or weak κB site. This elevation in transcriptional activity was dependent on the spacing of the strong and weak κB sites, as increasing the spacing between the strong and weak κB sites gradually reduced RelA-mediated activation. I also observed that inverting the position of the strong and weak κB site at a fixed distance of 16 nt did not significantly affect RelA-mediated activation (AG16 compared to GA16). Surprisingly, I also observed no difference in RelA-mediated transcriptional activation for two strong κB sites compared to a strong and weak κB site (AT16 compared to AG16). There was a slight reduction

in activation for two weak κB sites (CG16) compared to two strong or a strong and weak κB site, but the activation for the two weak κB sites was nonetheless significantly higher relative to a single strong κB site (CG16 compared to A or T).

I next investigated how RelA differentially binds multiple κB sites by EMSA to understand the observed differences in the RelA-mediated transcription assay. Using a radiolabeled DNA probe with a spacing of 16 nt between sites and fixed length (**Figure 3.8A**), I observed that RelA binds with much higher affinity to the strong A-centric κB site relative to the weak C-centric κB site when a second site is mutated (AX compared to CX), as expected (**Figure 3.8B**). When the strong A-centric κB site is associated with another strong or weak κB site (AX compared to AT and AG), I observed that binding of RelA was enhanced. Interestingly, I did not observe the formation of another shifted complex corresponding to a dimer of RelA:RelA homodimers on the two κB sites, suggesting that despite the presence of another potentially high affinity site, another RelA:RelA homodimer does not stably associate when the two sites are located 16nt apart. I also observed that RelA binds with higher affinity to two weak κB sites compared to a single weak κB site (CG compared to CX), however binding to two weak κB sites by RelA is weaker than binding to a single strong κB site (CG compared to AX). Altogether, this data suggests that a second κB site influences binding of RelA to κB DNA without formation of an additional RelA:DNA complex.

I next quantitatively examined binding of RelA to two κB sites by BLI to understand how secondary κB sites influence binding of RelA (**Figure 3.9A**). Double-stranded and biotinylated κB DNAs were immobilized onto streptavidin sensors and kinetics of RelA association and dissociation was calculated through wavelength interference of RelA binding using equations previously derived. Steady-state equilibrium K_D calculations revealed that RelA bound the single

strong A-κB DNA (AX) with an apparent K_D of 33.8 nM (**Figure 3.9B**). As expected, this was much higher than binding to the single weak C-κB DNA (CX), which did not yield a measurable K_D at the given concentrations of RelA. Comparison of the single strong A-κB DNA with the two strong site κB DNA (AX vs AT) revealed that the presence of the second strong site increased equilibrium binding affinity of RelA by approximately 3.5-fold (K_D ~9.64 nM for AT). Unexpectedly, addition of a weak κB site next the strong κB site slightly decreased equilibrium binding affinity of RelA by two-fold (K_D ~65.6 nM for AG). Also, the presence of two weak κB sites (CG) yielded a measurable equilibrium affinity of 88.2 nM, which was surprisingly close to the combined strong and weak AG DNA and much stronger than the unmeasurable single weak CX DNA. The secondary κB site altered kinetics of RelA DNA binding (**Figure 3.10A**), however there was no apparent correlation between binding affinity or kinetics and RelA-mediated transcriptional activation. Steady-state saturation, which is reflective of overall DNA occupancy, appeared to correlate with reporter assay results, suggesting that overall occupancy and not binding affinity at multiple sites may drive RelA-mediated transcription activation (**Figure 3.10B**).

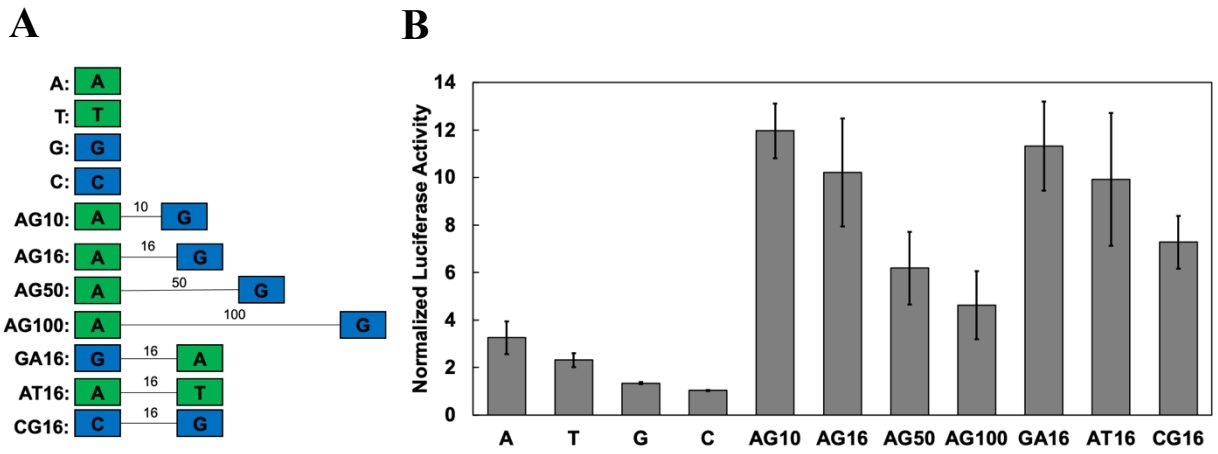

Figure 3.7: Luciferase activity assay of combinations of strong and weak κB sites
A. List of combinations and spacing used in luciferase assays. The A,T, G, or C corresponds to the identity of central nucleotide of the κB site GGGAANTTCC, and numbers between sites represent number of nucleotides between sites. Green denotes a high affinity κB site and blue represents a low affinity κB site. **B.** RelA-dependent luciferase activation assay with different synthetic promoter constructs. Values represent Renilla normalized fold induction with HA-RelA cotransfection relative to empty vector control in three independent experimental replicates.

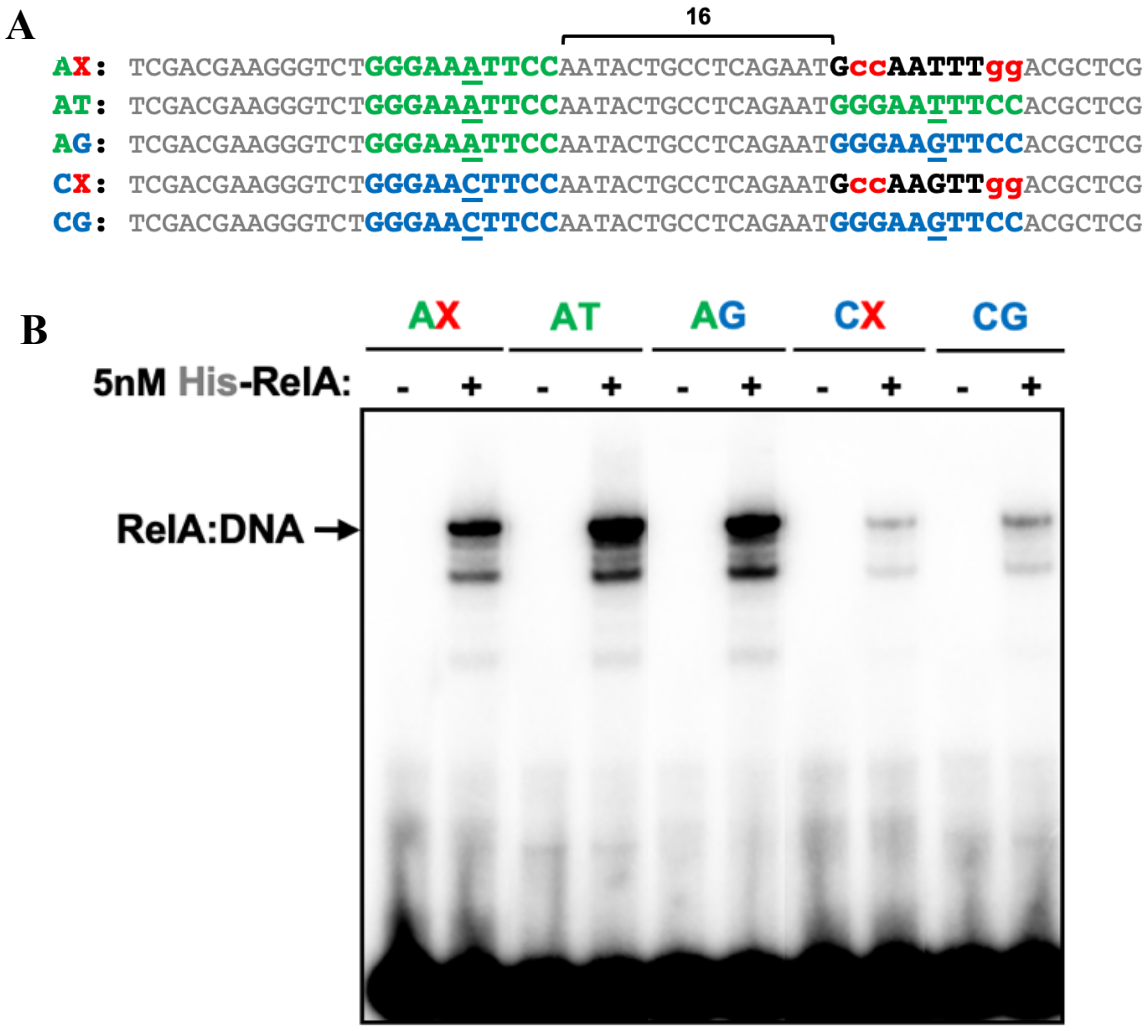

Figure 3.8: EMSA analysis of RelA binding to different combination of strong and weak κB sites
A. Sequence of κB DNAs used for *in vitro* binding assays. **B.** Qualitative analysis of RelA homodimer DNA binding affinity to different combinations of strong and weak κB sites by EMSA.

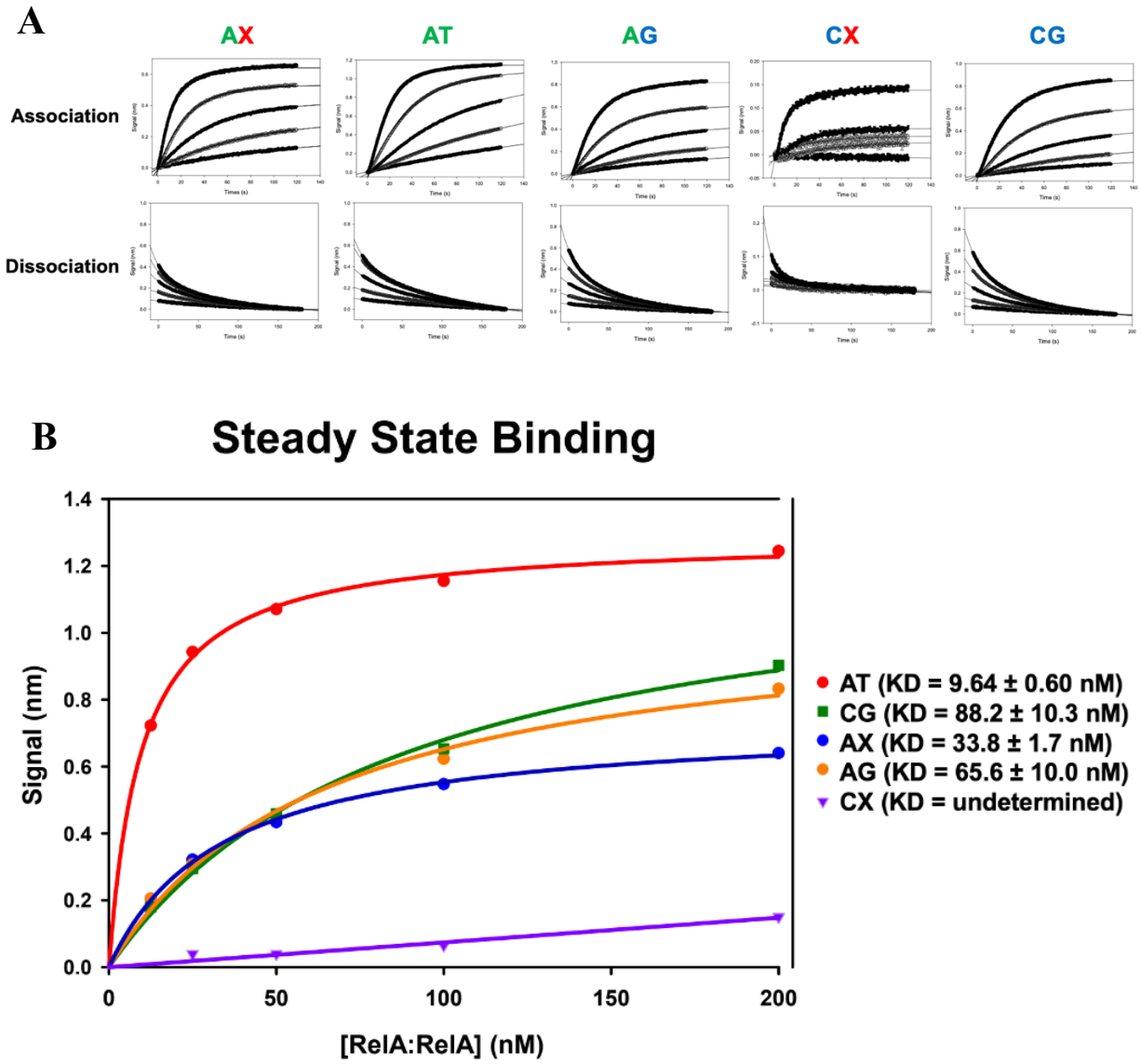

Figure 3.9: Biolayer interferometry analysis of RelA binding to combinations of strong and weak κB DNA

A. Representative association and dissociation signals for recombinant FL-RelA homodimer to different DNA. Concentrations of 12.5, 25, 50, 100, and 200 nM of RelA were used in assay. Signal intensity is adjusted to fit trace for specific DNAs and are not on same scale. **B.** Steady-state equilibrium binding affinity determined from RelA concentration-dependent signal saturation for different κB DNAs.

A

	Saturation (nm)	Steady State K_D (nM)	Luciferase Activation	k_{on}	k_{off1}	k_{off2}
AX	0.6402	33.8	3.25	0.0691	0.0108	0.0698
AT	1.2442	9.64	9.91	0.052	0.0078	0.0622
AG	0.8326	65.6	10.2	0.0443	0.011	0.0622
CX	0.1507	undetermined	1.04	0.0747	0.0158	0.1014
CG	0.9026	88.2	7.27	0.0363	0.0108	0.0589

B

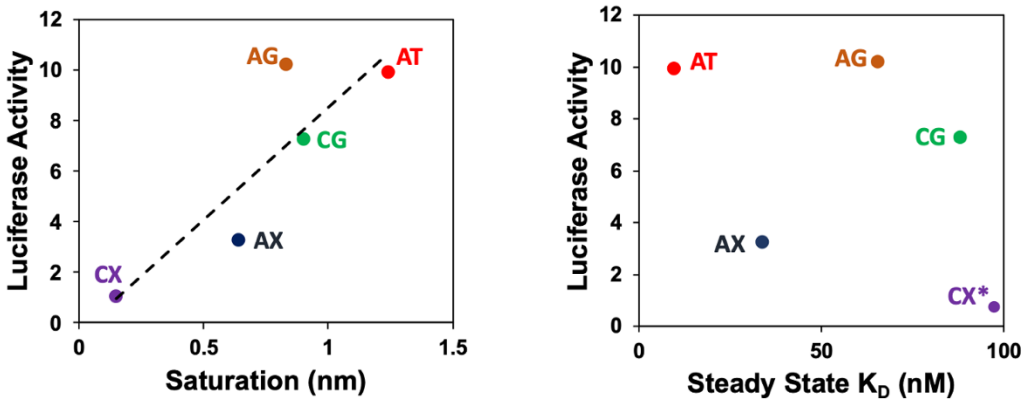

Figure 3.10: Kinetics of RelA binding combinations of κB DNA
A. Calculated steady state saturation, steady state K_D, and association and dissociation rates for 200 nM FL-RelA to the different combinations of κB DNA. Values for luciferase activation are from luciferase assays in transfected HEK293T cells. **B.** Plots for correlation between total saturation versus luciferase activity (left) and steady state K_D versus luciferase activity (right).

4. Characterization of RelA binding at the Cxcl2 promoter

Previous protein binding microarray data using different RHR dimers reveal relatively stronger binding for both p50:RelA heterodimer and RelA:RelA homodimer to the strong Cxcl2 GGGAATTTCC κB binding site (Z-score of 10.6 and 15.1, respectively) compared to the weak GGGCTTTTCC κB binding site (Z-score of 3.66 and 1.98, respectively) (Siggers, 2012). To investigate the influence of the associated weak-κB element on DNA binding by NF-κB, I radiolabeled WT and mutant Cxcl2 promoter probes and assayed binding of purified recombinant full-length RelA:RelA homodimer and p50:RelA heterodimer by EMSA (**Figure 3.11A**). EMSA binding analysis revealed stronger binding to WT Cxcl2 DNA (2WT) for the p50:RelA heterodimer relative to the RelA:RelA homodimer, with comparable DNA:NF-κB complex formation at concentrations of 2.5 nM and 20 nM, respectively. A supershift with RelA and p50-specific antibodies confirmed formation of the p50:RelA:DNA complex. It has been previously reported that binding affinity for κB DNA of p50:RelA heterodimer RHR is higher than RelA:RelA homodimer RHR for specific DNAs, and this was confirmed with full-length proteins to 2WT DNA (Phelps, 2000; Bergqvist, 2009).

I then explored differences in binding affinity of both p50:RelA heterodimer and RelA:RelA homodimer to Cxcl2 mutant DNA. As expected, mutation of the strong κB site (2M4) significantly reduced DNA binding for both p50:RelA heterodimer and RelA:RelA homodimer, however little binding can still be observed for both dimers at the given concentrations, suggesting that they bind with low affinity to the weak κB site of Cxcl2 promoter DNA. Mutation of only the weak κB site (2M1) surprisingly increased binding affinity for both p50:RelA heterodimer and RelA:RelA homodimer. Correlating this observation with luciferase activity of 2M1 and 2WT suggests that binding affinity is not the only determinant for

transcriptional activation by NF-κB, and these results are consistent with the synthetic luciferse constructs. Mutations that disrupt the bidirectionality about the strong κB site (2M2 and 2M3) significantly reduce binding for both p50:RelA heterodimer and RelA:RelA homodimer, with a larger decrease in binding for 2M2 relative to 2M3. The overall decrease in binding by NF-κB is consistent with the observed overall decrease in transcriptional output in luciferase assay, however the reduced DNA-binding for 2M2 relative to 2M3 is inconsistent with luciferase activity for 2M2 relative to 2M3. Additionally, the total reduction in binding of NF-κB for 2M2 relative to 2WT disagrees with the magnitude of reduction in luciferase promoter activity for 2M2 compared to 2WT. I also tested binding of FL-RelA in nuclear extract from HA-RelA transfected 293T cells with WT and mutant Cxcl2 DNA to test if binding of cellular RelA matches purified RelA-containing dimers (**Figure 3.11B**). Indeed, I observed a similar binding profile for transfected RelA to Cxcl2 DNA, with increased binding to 2M1 relative to 2WT and reduced binding for both 2M2 and 2M3 relative to 2WT, suggesting that *in vitro* binding by purified NF-κB matches binding of cellular RelA.

I next compared binding of purified p50:RelA heterodimer and RelA:RelA homodimer by EMSA with 2WT, both strong and weak κB site single mutants (2M1 and 2M4), and the double mutant (2M5) to test if the observed low affinity binding at the weak κB site was nonspecific (**Figure 3.12A**). I observed that the residual binding for both p50:RelA heterodimer and RelA:RelA homodimer with the strong κB site mutant 2M4 was abolished in the 2M5 double mutant, confirming that binding at the weak κB site was sequence specific. I also performed a DNA pulldown assay with streptavidin beads and biotinylated 2WT, 2M1, 2M4, and 2M5 with TNFα stimulated MEF and HA-RelA transfected 293T nuclear extract (**Figure 3.12B**). Western blotting for RelA revealed a similar profile of binding for RelA with the different Cxcl2

mutants, suggesting that the observed differential DNA binding affinity of RelA for the different Cxcl2 DNAs in EMSA was not an artifact of the assay. Taken together, these results suggest that the weak κB site and directionality about the strong κB site of the Cxcl2 promoter influence regulation by NF-κB and there is no direct correlation between binding affinity and transcriptional activation at the weak κB site by RelA-containing dimers.

To quantitatively analyze the influence of the weak κB site on binding affinity of RelA, I performed BLI with purified FL-RelA and biotinylated 2WT and mutant DNAs. As expected, the total concentration-dependent equilibrium occupancy of RelA correlated with affinity-based estimations of κB DNA strength, with highest RelA occupancy for the strong and weak κB site-containing 2WT DNA, followed by only the strong κB 2M1 DNA, then only the weak κB 2M4 DNA, and lastly the double mutant 2M5 DNA, which showed no binding. Steady-state equilibrium calculations of K_D revealed that RelA bound with significantly less affinity to 2WT DNA relative to 2M1 DNA, with a calculated K_D of 174.7 nM and 125.9 nM, respectively, which agreed with EMSA and solution-based pulldown assays (**Figure 3.13B**). Binding affinity did not correlate with higher 2WT transcription activation in RelA-dependent reporter assays, whereas overall RelA occupancy did. There was no calculable steady-state K_D value for 2M4 and 2M5 DNAs at the experimental RelA concentrations, however the relative BLI signal of 2M4 compared to 2M5 indicates that RelA is indeed binding to the weak κB element of 2M4, albeit to a small extent. Analysis of the association and dissociation kinetics for the highest concentration of RelA to 2WT, 2M1, and 2M4 DNAs reveal a surprising anticorrelation of k_{on} with κB DNA strength, with the highest k_{on} for only the weak κB 2M4 and lowest k_{on} for 2WT. The concentration dependent k_{on} of RelA is lower for 2WT relative to 2M1 (**Figure 3.13C**). Calculated k_{off} rates were proportionally correlated with κB DNA strength, and kinetics-derived

equilibrium calculations disagreed with experimental affinity observations. Altogether, this data suggests that RelA has significantly stronger equilibrium binding affinity for 2M1 relative to 2WT, and the weak κB element in the Cxcl2 promoter can indeed bind RelA. Additionally, the weak κB site at the Cxcl2 promoter can influence RelA binding kinetics, and total occupancy, not binding affinity or kinetics, correlated with RelA-mediated transcription activation.

I also performed similar experiments with the Cxcl1 promoter to assess the influence of another weak κB site in RelA-mediated transcriptional regulation. The Cxcl1 promoter is located 57nt upstream of the TSS and shares the same strong GGGAATTTCC κB site as Cxcl2 but has the weak GGGAAACACC κB site 9 bp upstream of the strong κB site (**Figure 3.14A**). RelA-dependence for Cxcl1 expression was first validated by RT-qPCR in RelA-KO MEF following TNFα stimulation (**Figure 3.14B**). A cell-based luciferase assay in 293T cells revealed that the WT Cxcl1 promoter (1WT) exhibited an 8-fold increase in promoter activity with RelA cotransfection and mutation of the strong Cxcl1 κB site (1M2) abolished RelA-dependent transcriptional activation (**Figure 3.14C**). Mutation of the Cxcl1 weak κB site (1M1) significantly reduced RelA-dependent activation to only 5-fold, suggesting that the weak κB site at the Cxcl1 promoter influences transcriptional activation by RelA. CRISPR targeted disruption of the strong and weak κB sites at the Cxcl1 promoter in MEF resulted in a 60% and 20% reduction in expression of Cxcl1, respectively, by RT-qPCR following 1 hour of TNFα stimulation (**Figure 3.14D**). I next testing binding for both recombinant p50:RelA heterodimer and RelA:RelA homodimer to the Cxcl1 promoter by EMSA (**Figure 3.14E**). As expected, both RelA-containing dimers displayed significantly reduced binding to 1M2 DNA relative to 1WT. However, unlike the Cxcl2 promoter, binding to the weak κB site mutant 1M1 slightly reduced binding for the dimers relative to 1WT. This observation was also recapitulated in HA-RelA

transfected 293T nuclear extract, suggesting that the effect on DNA binding of RelA by the weak κB site at the Cxcl1 promoter is different from the Cxcl2 weak κB site (**Figure 3.14F**). Altogether, I observe that like the Cxcl2 promoter, the Cxcl1 weak κB site influences RelA DNA-binding and transcriptional activation.

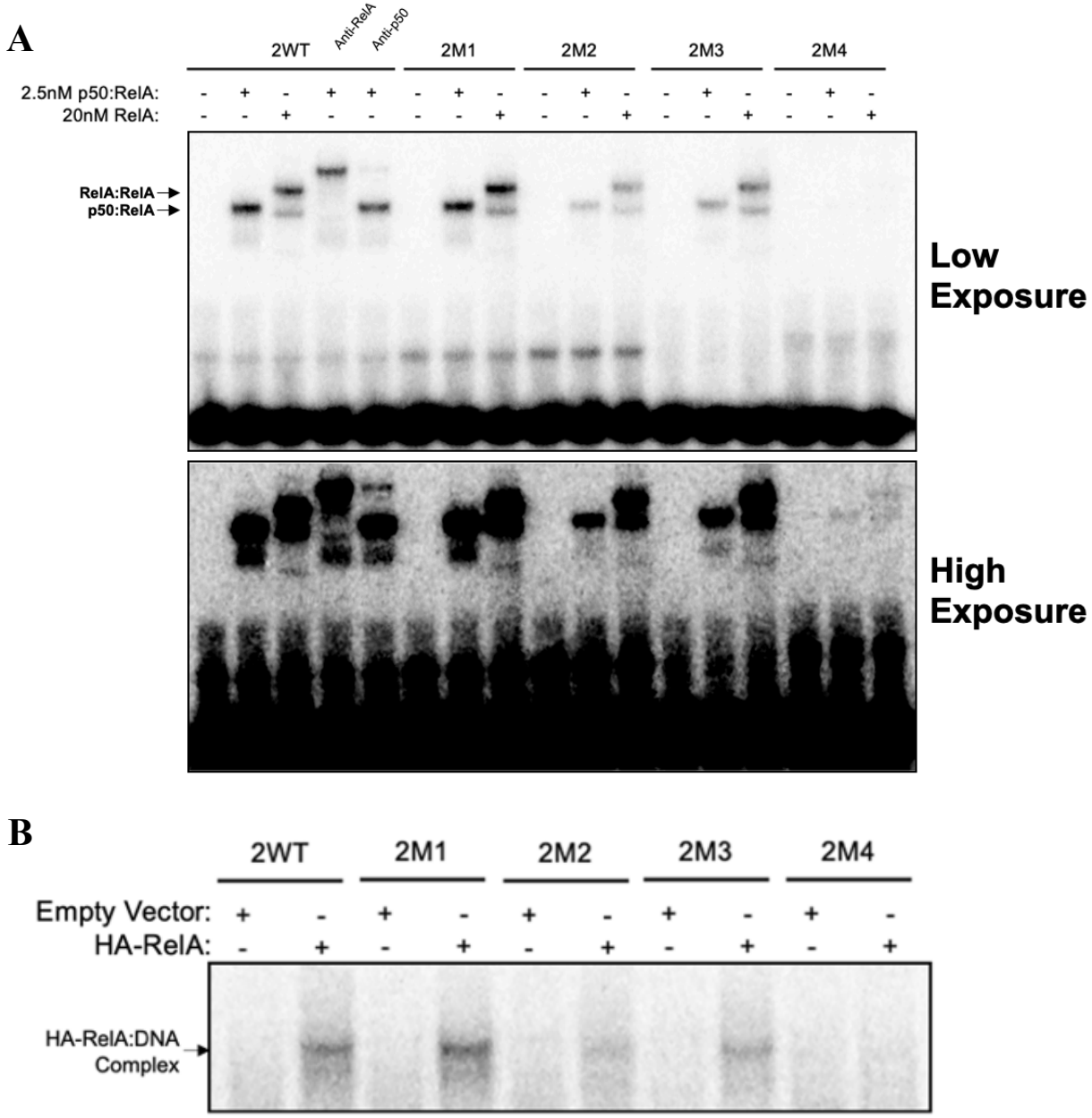

Figure 3.11: EMSA analysis of NF-κB binding at the Cxcl2 promoter DNA
A. Purified recombinant FL-RelA and p50:RelA were qualitatively analyzed for binding affinity to different Cxcl2 promoter DNAs by EMSA. A low exposure (top) and high exposure (bottom) image from the same gel are presented. Supershift with a RelA- or p50-specific antibody confirmed formation of the p50:RelA heterodimer complex to 2WT DNA. **B.** Binding of FL-RelA from empty vector or HA-RelA transfected HEK293T nuclear extract to different Cxcl2 promoter DNAs.

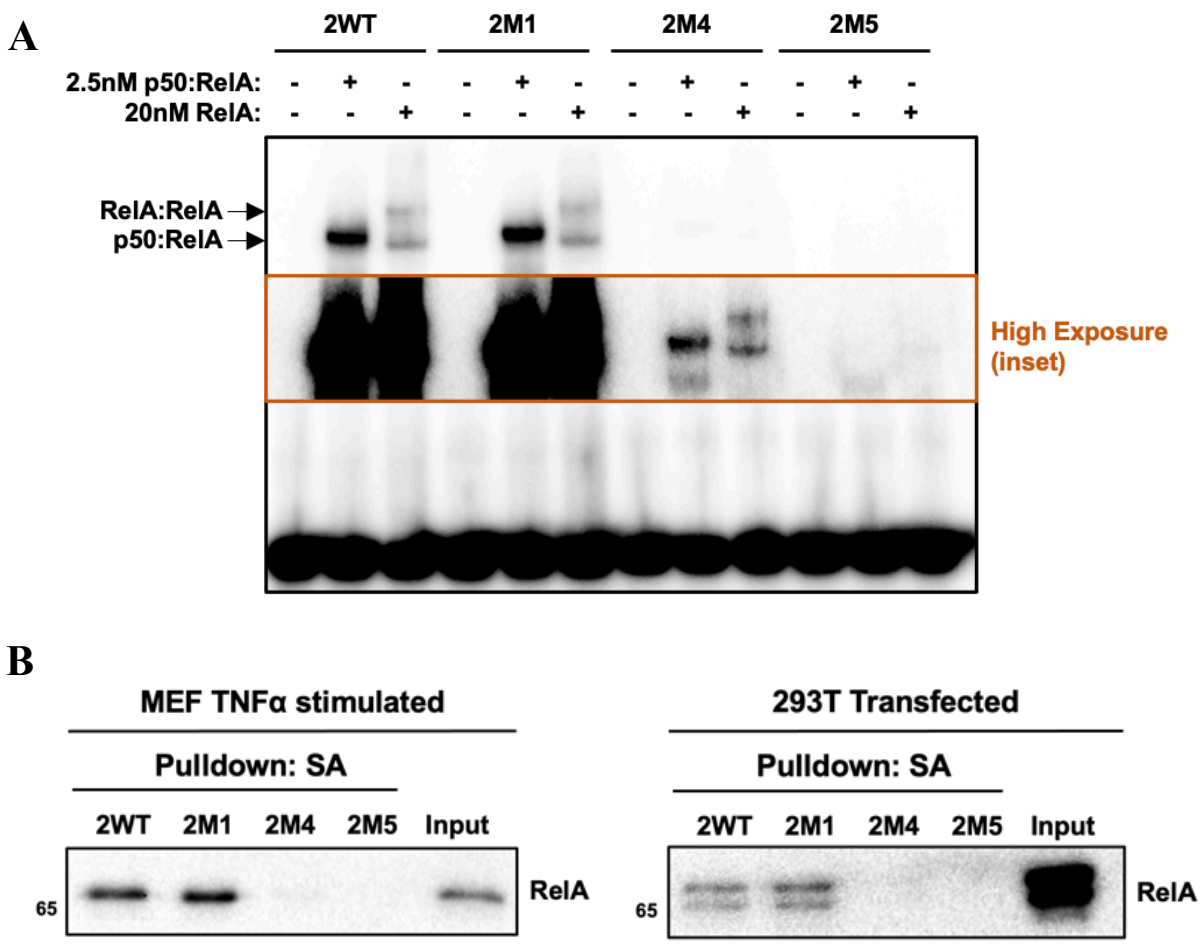

Figure 3.12: EMSA and pulldown assay binding of NF-κB to single and double mutant Cxcl2 DNA
A. Purified recombinant FL-RelA and p50:RelA were qualitatively analyzed for binding affinity to weak mutant, strong mutant, or double mutant Cxcl2 DNA. A high exposure inset (brown) confirms low affinity binding of both FL-RelA and p50:RelA to the weak κB site. **B.** Pulldown assay using biotinylated wild type and mutant Cxcl2 DNA immobilized onto streptavidin agarose beads with TNFα stimulated MEF (left) or HEK293T transfected nuclear extract (right). Precipitated proteins were separated by SDS-PAGE and analyzed by Western blot.

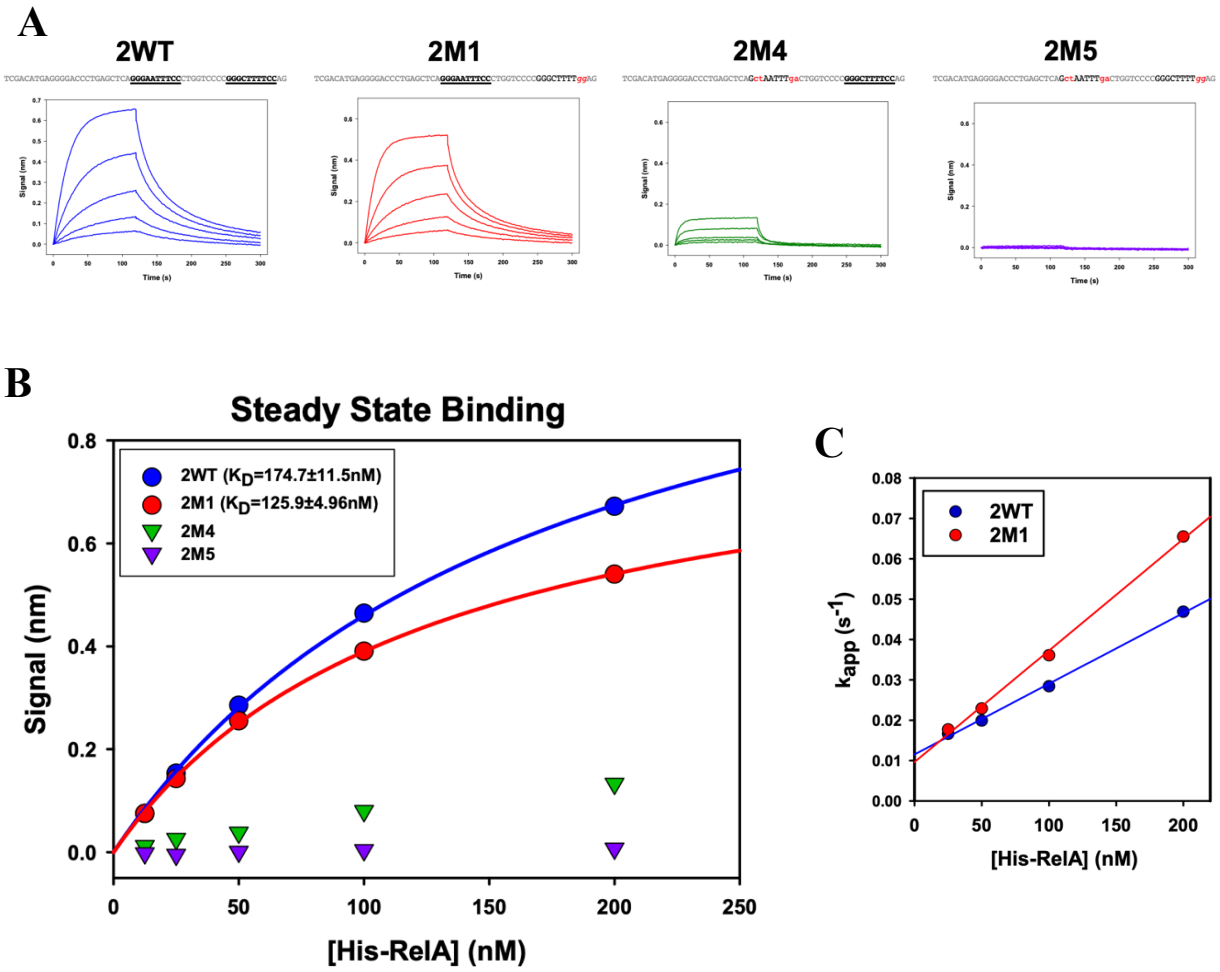

Figure 3.13: Biolayer interferometry analysis of FL-RelA binding to Cxcl2 promoter DNA
A. Representative signal traces from BLI experiments of RelA with Cxcl2 promoter DNAs. Traces are scaled identically for relative comparisons between DNAs. **B.** Steady state equilibrium binding affinity was determined for FL-RelA to 2WT and 2M1 DNAs. Marginal binding of RelA to 2M4 DNA and no binding to 2M5 did not yield measurable equilibrium affinity values. **C.** Plot of the concentration dependent association rate of FL-RelA to 2WT and 2M1 DNAs showing that the weak κB site influences FL-RelA DNA binding kinetics.

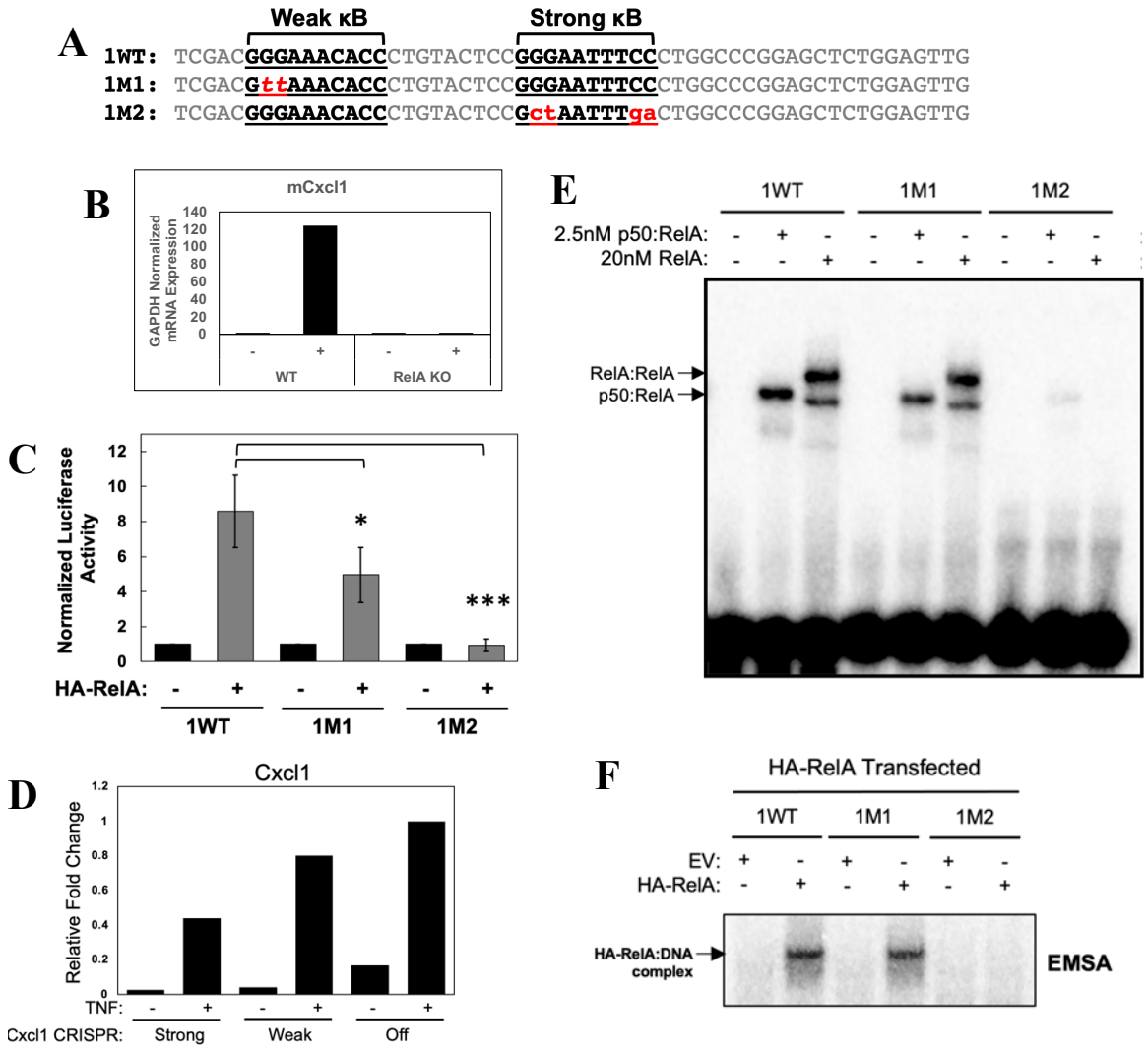

Figure 3.14: Cxcl1 promoter weak κB site modulates RelA-dependent transcription
A. Sequences of WT and mutant Cxcl1 promoter DNA used in luciferase and *in vitro* DNA binding assays. **B.** RT-qPCR of Cxcl1 in WT and RelA-KO MEF stimulated for 1 hour with TNFα. Values were normalized to Gapdh.
C. Luciferase activation assay with WT or mutant Cxcl1 promoter luciferase constructs cotransfected with empty vector or HA-RelA in HEK293T. Luciferase readings were normalized to Renilla control and fold induction was calculated relative to empty vector. **D.** RT-qPCR of CRISPR modified MEF stable cell lines following stimulation for 1 hour with TNFα. Guide RNA targeting the Cxcl1 strong κB site, weak κB site, or off target control were used to generate stable cell lines. Values are normalized to Gapdh and presented relative to off target stimulated cells. **E.** Qualitative analysis of DNA binding by EMSA of recombinant p50:RelA heterodimer and FL-RelA homodimer to wild-type and mutant Cxcl1 promoter DNAs. **F.** Pulldown assay with biotinylated Cxcl1 promoter DNAs immobilized onto streptavidin agarose beads and empty vector control or HA-tagged RelA transfected HEK293T nuclear extract.

4. Multiple factors associate with RelA at the Cxcl2 promoter to regulate transcription

I postulated that the observed discrepancy between RelA DNA-binding affinity and transcriptional regulation at the Cxcl2 promoter may be coordinated by the activity of additional protein cofactors. To identify proteins that associate at the Cxcl2 promoter, biotinylated 2WT DNA was immobilized onto streptavidin agarose beads, and a pulldown was performed with TNFα stimulated MEF nuclear extract in two independent experimental replicates. Control pulldowns were also performed in tandem with the double mutant 2M5 biotinylated DNA. In comparing 2WT with 2M5 pulldowns, the NF-κB members RelA, Nfkb2 (p52), and Nfkb1 (p50) were among the top enriched proteins, suggesting that pulldown assay can successfully capture proteins that occupy the Cxcl2 promoter (**Figure 3.15A**). Additionally, I observed a surprising enrichment of the NFAT family transcription factor members Nfatc1, Nfat5, and Nfatc4 in 2WT relative to 2M5, suggesting they also occupy the Cxcl2 promoter with NF-κB. I also observed enrichment of several other proteins that include transcription factors (Tead1 and Tead3), RNA binding proteins (Srsf2 and Pabpn1), DNA damage repair proteins (Pnkp), and enzymes (Ogt).

It has been previously shown that NFAT can associate with other transcription factors to coordinate transcriptional activation on DNA, and indeed NFAT and NF-κB have been shown to associate at target promoters under specific stimulatory conditions (Chen, 1998; Jain, 1992; Macian, 2001; Sica, 1997; Conboy, 1999; Bardran, 2002; Pham, 2005; Liu, 2012). Additionally, both NFAT and NF-κB recognize the same consensus sequence of GGAAA through the shared DNA-binding mechanism of their corresponding RHR (Ray, 2021). However, the cooperativity between NFAT and NF-κB on DNA and mechanism of transcription activation is not clearly understood.

I was particularly interested in Nfatc1 as previous reports suggest TNFα regulates Nfatc1 activity and nuclear occupancy of Nfatc1 has been implicated in regulating inflammatory signaling (Pan, 2007; Yarilina, 2011; Peng, 2001). I first tested if TNFα stimulation alters Nfatc1 nuclear localization and binding to 2WT DNA in MEF (**Figure 3.15B**). Following 30 minutes of TNFα stimulation, I observed an increased abundance of nuclear Nfatc1 and RelA and binding of both to 2WT DNA, suggesting that binding of Nfatc1 to the Cxcl2 promoter element is induced upon TNFα stimulation in MEF. I next tested if binding to 2WT by Nfatc1 is influenced by RelA. Using TNFα stimulated nuclear extract from both WT and RelA-KO MEF, I observed a reduction in both nuclear Nfatc1 and binding to 2WT in nuclear extract derived from RelA-KO MEF relative to wild-type MEF (**Figure 3.15C**). Surprisingly, I observed more nuclear Nfatc1 in RelA-KO MEF following TNFα stimulation despite the higher levels of total cellular Nfatc1 in RelA-KO MEF, which suggests that RelA expression is involved in regulating Nfatc1 activity. Altogether, there results suggest that TNFα induces binding of both RelA and Nfatc1 to the Cxcl2 promoter element.

I next examined the coordination between RelA and Nfatc1 at the Cxcl2 promoter by EMSA. I overexpressed increasing amounts of FLAG-tagged Nfatc1 in HEK293T cells and tested the effect on binding of p50:RelA to 2WT in TNFα stimulated nuclear extract (**Figure 3.16A**). As expected, I observed formation of a discrete band representing the p50:RelA:DNA complex upon TNFα induction in empty vector transfected control extract. Overexpression of Nfatc1 resulted in the concentration-dependent formation of a low electrophoretic mobility complex between Nfatc1 and 2WT. Formation of the Nfatc1:2WT-DNA complex was TNFα-independent at high Nfatc1 expression levels and induced smearing of the p50:RelA:2WT-DNA complex before gradually displacing binding of NF-κB to 2WT DNA in TNFα stimulated

extract. This suggest that Nfatc1 may associate with NF-κB on DNA before eventually outcompeting binding of NF-κB at higher concentrations.

Following the observed association of Nfatc1 and NF-κB on 2WT DNA in stimulated nuclear extract, I next tested how Nfatc1 and NF-κB bound DNA *in vitro.* I purified recombinant FLAG-tagged Nfatc1 from 293T and tested binding with purified p50:RelA heterodimer to 2WT and mutant DNAs by EMSA (**Figure 3.16B and 3.16C**). I observed that purified Nfatc1 formed the same low mobility complex with 2WT DNA as observed in nuclear extract. Formation of this complex can only be observed for 2WT DNA and not 2M1 or 2M4, suggesting that Nfatc1 binds both the strong and weak κB sites of Cxcl2. The p50:RelA heterodimer formed the expected complex with 2WT DNA, and a shifted complex is formed in the presence of Nfatc. The p50:RelA heterodimer also bound to the weak site mutant 2M1 DNA, however there was no induction of a shifted complex in the presence of Nfatc1. The strong site mutant 2M4 DNA largely reduced binding of p50:RelA relative to 2WT, and Nfatc1 did not induce the formation of the shifted complex that was observed in 2WT. Altogether, these results suggest that Nfatc1 and p50:RelA can associate on Cxcl2 DNA and this association is mediated by both the strong and weak κB sites.

I next tested if DNA binding of Nfatc1 is necessary for formation of the shifted complex with p50:RelA and 2WT DNA. I expressed and purified both WT and the DNA binding defective mutant R439E Nfatc1from HEK293T and assayed binding to 2WT DNA with p50:RelA in EMSA (**Figure 3.17A and 3.17B**). As expected, I observed that the R439E Nfatc1 mutant displayed no binding to 2WT DNA. I also observed that the R439E Nfatc1 mutant no longer formed the shifted complex with p50:RelA and 2WT DNA as was observed with WT

Nfatc1. These results suggest that DNA binding of Nfatc1 is necessary for association with RelA on 2WT DNA.

Following the observed association of Nfatc1 and p50:RelA on DNA, I next tested if RelA and Nfatc1 can physically interact in the cell. I transiently overexpressed FLAG-tagged Nfatc1 or EV control in HEK293T and performed a pulldown assay to test for coimmunoprecipitation of RelA with anti-FLAG agarose beads (**Figure 3.18A**). I observed that RelA coprecipitated with pulldown of FLAG-Nfatc1, suggesting that Nfatc1 and RelA physically interact. I then extended my examination of the interaction between Nfatc1 and RelA to test if the interaction is influenced by TNFα induction or DNA binding of Nfatc1. I observed that TNFα stimulation enhanced coprecipitation of RelA with WT Nfatc1 and not with R439E mutant Nfatc1 (**Figure 3.18B**). This suggests that TNFα simulation enhances the interaction between Nfatc1 and RelA and DNA binding by Nfatc1 is involved in this interaction.

I next tested if Nfatc1 is involved in regulating the expression of Cxcl1 and Cxcl2 in TNFα stimulated MEF. To study this, I generated stable shRNA-mediated Nfatc1 knockdown (Nfatc1 KD) and scramble control cell lines in MEF and assayed expression of Cxcl1 and Cxcl2 by RT-qPCR following 1 hour of TNFα treatment (**Figure 3.18C and 3.18D**). I observed that knockdown of Nfatc1 resulted in a significant reduction of TNFα induced expression of Cxcl1 and Cxcl2. I also tested if upstream NF-κB signaling was altered in Nfatc1 KD relative to scramble control by analyzing IκBα degradation and nuclear translocation of RelA following TNFα stimulation (**Figure 3.18E**). I observed that Nfatc1 KD did not affect neither IκBα degradation, total RelA expression levels, or nuclear abundance of RelA. This suggests that Nfatc1 regulates TNFα-induced expression of Cxcl1 and Cxcl2 following without influencing upstream NF-κB signaling.

Collectively these results demonstrate that Nfatc1 can associate with NF-κB on Cxcl2 promoter DNA, and this association is dependent on both the strong and weak κB sites of the Cxcl2 promoter. TNFα stimulation increased the nuclear abundance and binding to Cxcl2 DNA for both RelA and Nfatc1 and the interaction between RelA and Nfatc1. Knockdown of Nfatc1 reduced expression of Cxcl2 following TNFα stimulation, suggesting that Nfatc1 recruitment to the promoter of Cxcl2 with RelA is important for TNFα-induced expression.

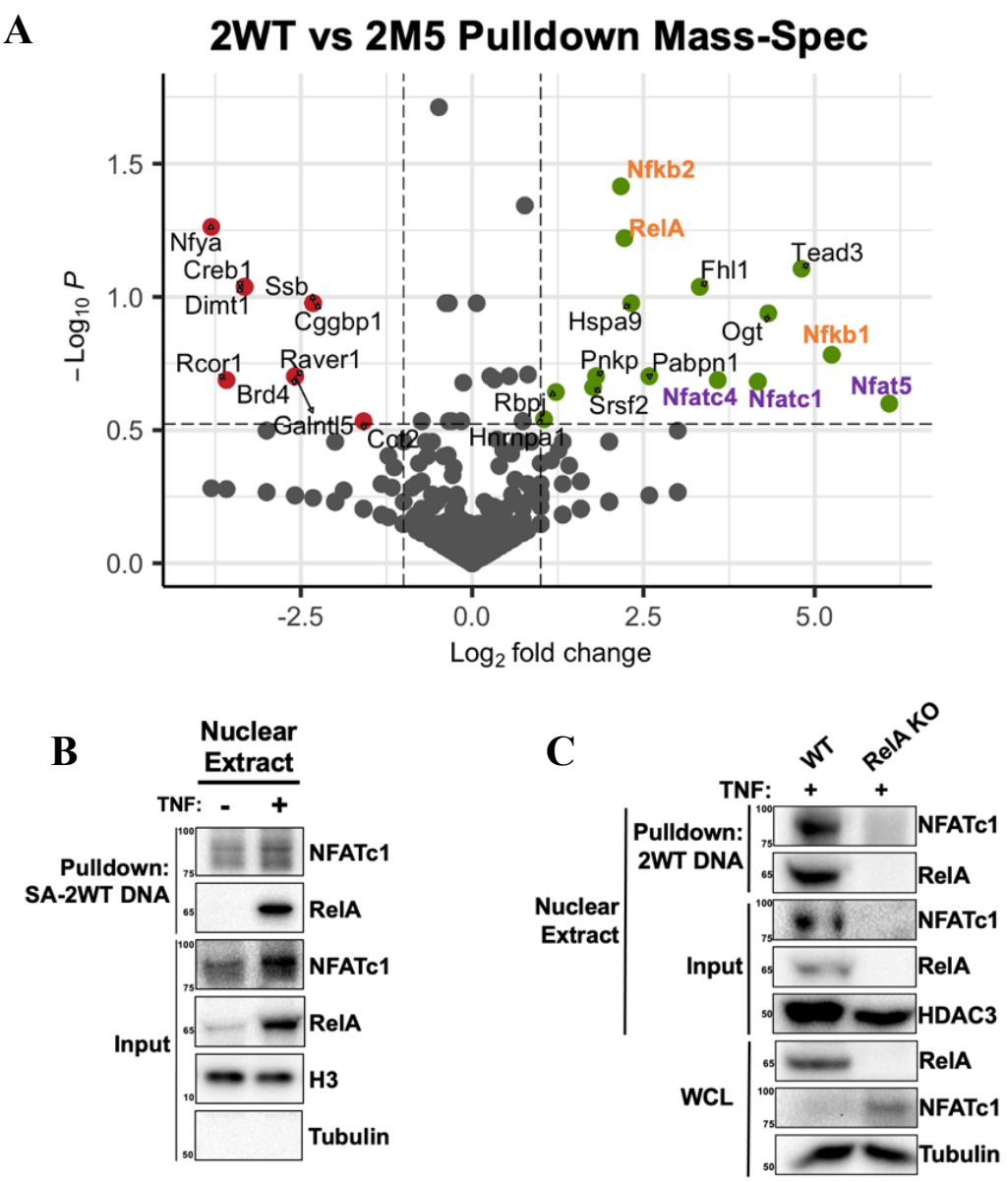

Figure 3.15: NF-κB and NFAT bind Cxcl2 promoter DNA following TNFα stimulation
A. Volcano plot of total peptides identified by mass-spec from pulldown of biotinylated Cxcl2 promoter DNA- streptavidin agarose beads with 30 minutes TNFα stimulated MEF nuclear extract. Fold change was calculated from pulldown of wild type Cxcl2 DNA relative to double mutant M5 DNA. Log transformed p-value was calculated from two independent experimental replicates. **B.** Pulldown with biotinylated Cxcl2 promoter DNA-streptavidin beads and 30 minutes control or TNFα stimulated MEF nuclear extract. Nuclear extract input and precipitated proteins were analyzed by Western blot using indicated antibodies. **C.** Pulldown with biotinylated Cxcl2 promoter DNA-streptavidin beads and 30 minutes TNFα stimulated wild type or RelA-KO MEF nuclear extract. Whole cell lysate, nuclear extract input, and precipitated proteins were analyzed by Western blot using indicated antibodies.

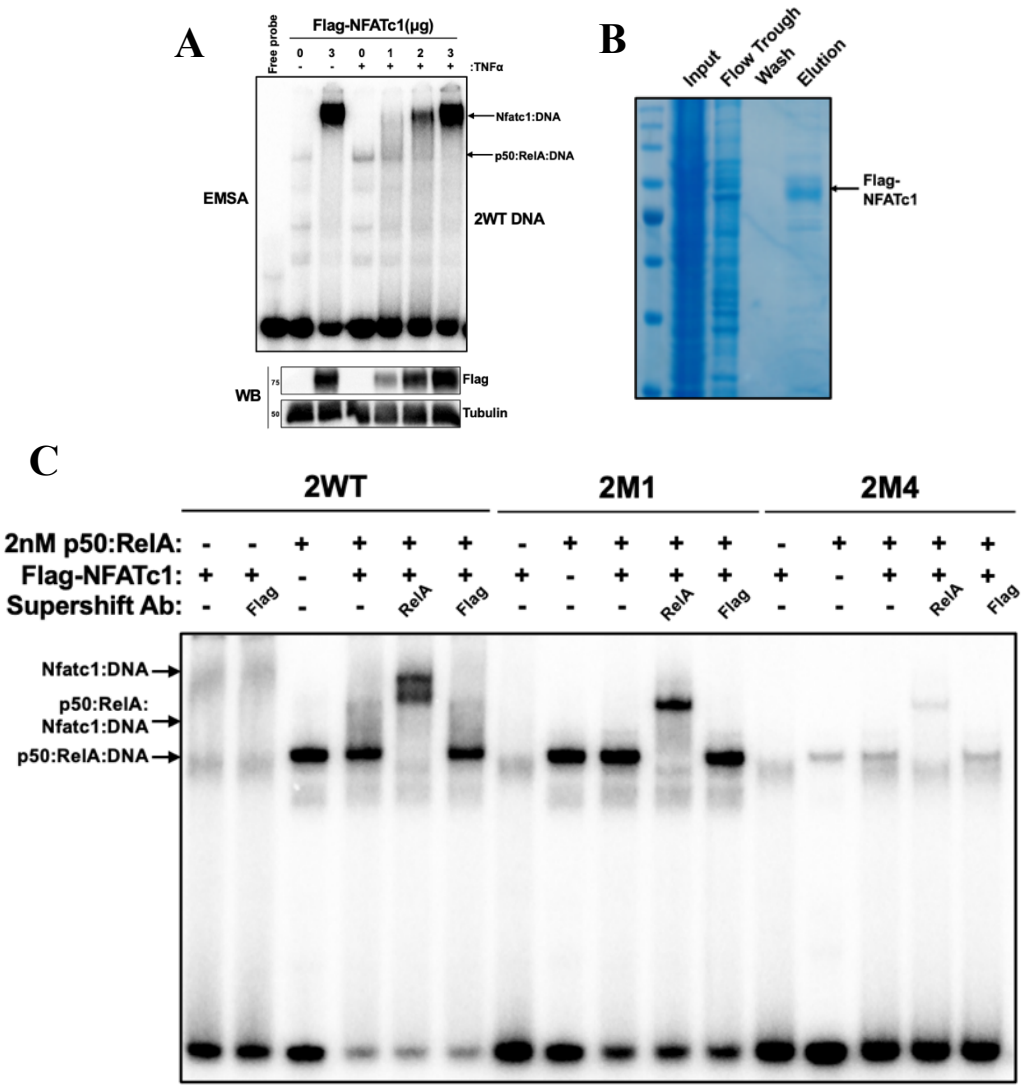

Figure 3.16: EMSA analysis of NF-κB and NFAT binding to Cxcl2 promoter DNA
A. Different concentrations of FLAG-tagged NFATc1 was transfected in HEK293T and nuclear extract was collected and assayed for binding to Cxcl2 promoter DNA by EMSA. Cells were stimulated for 30 minutes with DMSO or TNFα prior to collection of nuclear extract. Western blot showing relative expression levels of FLAG-tagged NFATc1 is presented below. **B.** Coomassie stained protein gel of purified FLAG-tagged NFATc1 from HEK293T. FLAG-tagged NFATc1 was transfected in HEK293T and cells were stimulated for 30 minutes with TNFα prior to purification. **C.** EMSA DNA binding analysis with recombinant p50:RelA heterodimer and purified FLAG-tagged NFATc1 to wild type and mutant Cxcl2 promoter DNAs. Supershift was performed using the indicated antibodies.

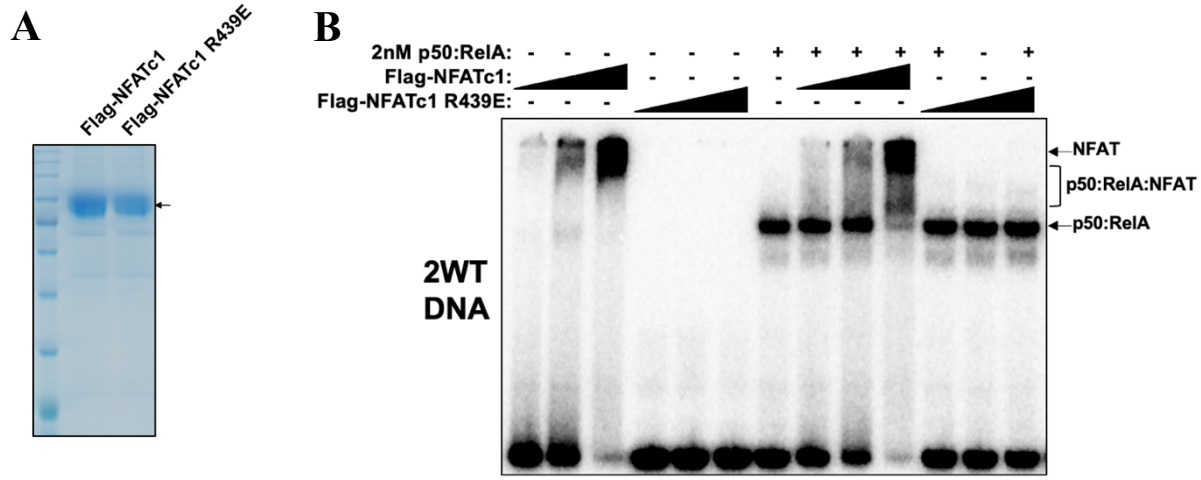

Figure 3.17: EMSA analysis of DNA binding mutant NFATc1 with NF-κB to Cxcl2 promoter DNA
A. Coomassie stained protein gel of FLAG-tagged wild or R439E mutant NFATc1 purification from transfected HEK293T. Cells were stimulated for 30 minutes with TNFα prior to purification **B.** EMSA DNA binding analysis with recombinant p50:RelA heterodimer and purified wild type or R439E NFATc1 to different Cxcl2 promoter DNAs.

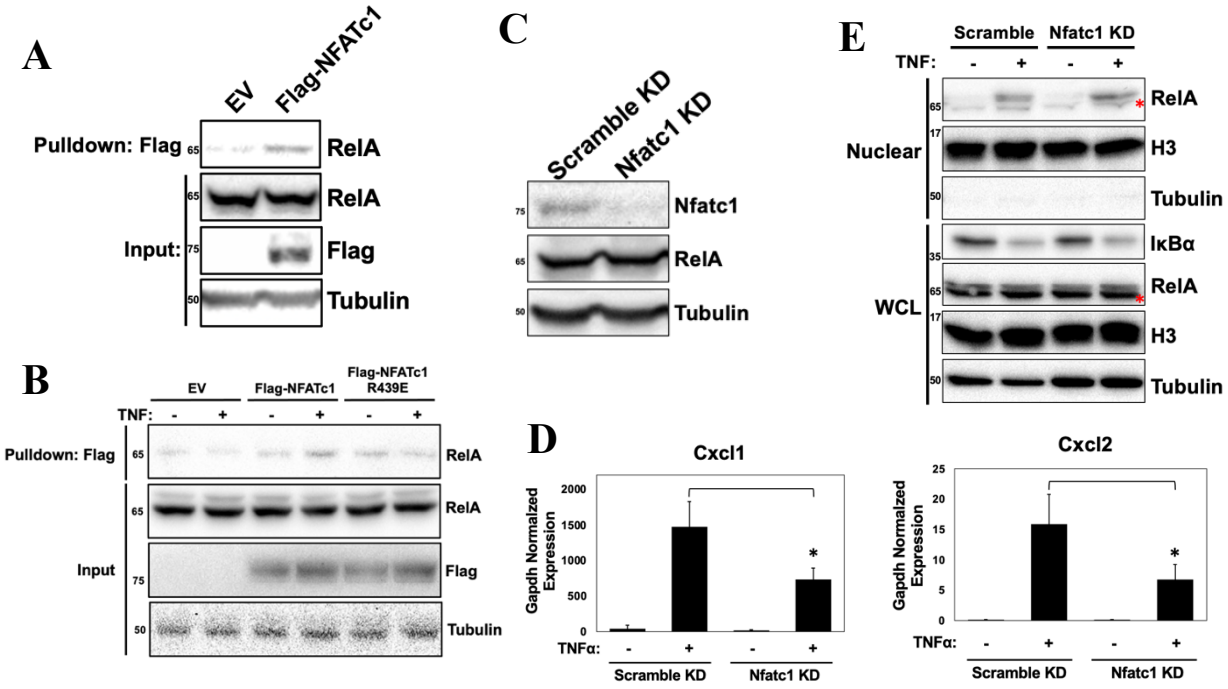

Figure 3.18: NFATc1 interacts with RelA and regulates Cxcl1 and Cxcl2 expression in MEF
A. FLAG pulldown of empty vector or FLAG-tagged NFATc1 transfected in HEK293T. **B.** FLAG pulldown of empty vector, wild type, or R439E mutant NFATc1 transfected in HEK293T. Cells were treated for 30 minutes with control DMSO or TNFα prior collection of cell lysate. **C.** Stable scramble or Nfatc1 knockdown MEF cell lines were generated and expression levels of the indicated proteins were analyzed from whole cell lysate by Western blot. **D.** RT-qPCR of Cxcl1 (top) and Cxcl2 (bottom) in stable scramble and Nfatc1 knockdown MEF cell lines. Cells were treated for 1 hour with TNFα and expression levels were normalized to Gapdh. Values are represented as mean ± SD from three independent experimental replicates. **E.** RelA nuclear translocation and IκBα degradation were assayed in stable scramble and Nfatc1 knockdown MEF cell lines. Cells were treated for 30 minutes with TNFα and nuclear extract and whole cell lysate was analyzed by Western blot using the indicated antibodies. The red asterisk indicates nonspecific protein.

D. Discussion

The question I attempted to address in this section is what contributes to NF-κB specificity for target κB sites in the cell and if locally distributed weak κB elements are involved. Further, do associated weak κB sites combinatorially influence NF-κB DNA binding and transcription activation. I found that weak κB sites are functionally significant and may play an important role in transcriptional synergy. I also surprisingly observed that multiple TFs can bind the same promoter DNA fragment to assist binding, while also competing for promoter binding. Weak interactions between these TFs play a role in recruiting each other, implying cooperation, despite the fact they cannot bind concurrently, implying competition. That is, the binding of these TFs to a promoter is both cooperative and competitive.

In addition to TFs, I also observe many other factors are recruited to the promoters. These include DNA damage repair proteins, RNA binding proteins, and enzymes. I have not investigated how these factors regulate TF binding to their respective sites. These factors may interact with only one or multiple TFs to facilitate DNA binding and transcriptional activation. These factors may also act as protein or DNA modifying enzymes to regulate TF DNA binding through enzymatic modifications. But the most intriguing thought is that they too can directly associate onto DNA, acting as a noncanonical TF. Future experiments are required to examine these possibilities.

The most surprising observation is that based on total peptides identified by mass-spec, the NF-κB family members are not the most abundant group to bind the Cxcl2 promoter DNA. The NFAT family of transcription factors appear to bind Cxcl2 promoter DNA and are important for activating transcription of cytokine genes following TNFα stimulation. Perhaps, NF-κB's role in the nuclear localization of NFAT family members is the reason why NF-κB appeared to be the

most important factor for the regulation of TNFα-induced cytokine gene expression. Nonetheless, my data suggest that it is the combined actions of several TFs to activate gene transcription. This work also addresses another long-standing question: Why does the number of DNA REs for each transcription factor family vary to such a great extent? There are at least several hundred active κB DNA REs known to exist and some of them only loosely fit the kB DNA consensus. Indeed, only one bp in the entire 10-bp sequence is invariant, resulting in a large possibility of potential κB sites with a wide range of affinities that bind NF-κB dimers. Based on two promoters (CCL2 promoter data not shown) that consist of a locally associated strong and weak κB site , I found that each site can be recognized by a selective group of other TFs that are not structurally related. Since each κB DNA accommodates a specific number of TFs, larger sequence variations seen cross different NF-κB-regulated promoters allow more TF to bind to these collective groups of κB sites. This also implies that these DNA response elements respond not only to NF-κB dimers, but also to many non-NF-κB TFs. Therefore, κB sites and DNA REs for all other TFs are highly promiscuous, and most likely there is no RE that selects only a single TF. In other words, a single DNA site can be specific to many TFs for binding. Many TFs can bind with high frequency and specificity over a length of as short as only 30-40 bp. It will be an important question for the future if longer stretches of promoter sequence recruits more TFs and if they all contribute to the transcription.

The DNA binding promiscuity provides a greater regulatory benefit than a highly specific site for one TF. The duration and amplitude of transcription will not be dictated by a single factor or a single family but by a collective group of factors. Thus, a better way to accomplish transcriptional regulation is not through DNA RE elements, but rather the factors that are available through cell signaling processes.

I made another important observation. In addition to known transcriptionally competent TFs, such as NF-κB and NFAT, several known transcriptional repressors are also recruited to the promoters. Since both coactivators, such as mediator and p300, and corepressors, such as HDAC and Sin3, are also recruited to these promoters, this suggests that transcription is stochastic where activation and repression can occur in phases. The duration of such phases is determined by the frequency in which activators and repressors bind the promoters. These findings could explain the disparity between resident time and transcriptional bursting. It is known that transcriptional bursts last for minutes, whereas TF resident time is only about 10 seconds. I propose rapid exchange of multiple TFs (at least 10 TFs at any given time) with little down time in-between akin to a single continuous binding event leading to continuous transcriptional initiation. So, why do we observe phases? We can only see the binding phase of TFs binding because only one or two factors are labeled, leaving the rest bound but invisible to us. The most likely explanation of transcriptional burst phase is that transcription pauses due to the binding of TFs that represses transcription, such as CUX1 and BEND3 which recruit HDAC and Sin3 complexes that block Pol II recruitment. However, the overwhelming presence of activating TF during the productive phase of transcription results in the accumulation of transcripts.

E. Materials and Methods

1. Antibodies and Reagents

The RelA (8242), H3 (9715), HDAC3 (3949) and p50 (13586) antibodies used in Western Blots and EMSA supershifts were purchased from Cell Signaling Technology. The IκBα (0040) and tubulin (0119) antibodies were purchased from BioBharati LifeScience. The FLAG (F1804) antibody was purchased from Sigma-Aldrich. The NFATc1 (7294) antibody was purchased from Santa Cruz Biotechnology. Mouse TNFα (BioBharati) was used at a final concentration of 20 ng/mL for the indicated timepoints.

2. Mammalian Cell Culture and Generation of Stable Cell Lines

WT MEF, RelA-KO MEF, and 293T cells were cultured in Dulbecco's modified Eagle's medium (Corning) supplemented with 10% FBS and antibiotics.

The list of oligonucleotides used for gRNA and shRNA cloning is outlined in **Table 3.3**. For generation of stable CRISPR-modified MEF cell lines, gRNA targeting a 20 nt genomic region adjacent to a Cas9 protospacer adjacent motif (PAM) was first annealed and cloned into BsmbI (NEB) digested pLentiCRISPRv2 vector. Sanger sequencing was performed verify cloning. The different pLentiCRISPRv2 gRNA constructs were then cotransfected with pMDLg/pRRE, pCMV-VSV-G, and pRSV-Rev expression constructs into HEK293T using TransIT-Lenti transfection reagent (Mirus) for generation of lentiviral particles. After 24 hours, viral supernatant was harvested and filtered through a 0.4 μm filter and used to infect MEF at a dilution of 1:10 in the presence of 10 ng/μL polybrene (MilliporeSigma) for 48 hours. MEF was then selected and grown in media containing 5 μg/mL puromycin. Generation of stable shRNA knockdown MEF cells was carried out similarly, with the exception that annealed oligoes for

shRNA targets were cloned into the pLKO.1 TRC vector digested with AgeI and EcoRI, which was then cotransfected in HEK293T for generation of viral particles.

3. Protein Expression and Purification

Expression and purification of His-tagged full-length RelA from Sf9 cells was performed as outlined in Chapter 2. Additionally, expression of His-tagged p50 from *E.coli* Rosetta (DE3) and formation of the p50:RelA heterodimer was performed as outlined in Chapter 2.

FLAG-tagged WT and R439E NFATc1 expression constructs were cloned into modified pEYFP-c1 with EYFP removed and replaced with a FLAG tag. Constructs were then transfected with TransIT-Lenti (Mirus) into HEK293T following manufacturer's recommendations. After 24 hours, cells were stimulated with 20 ng/mL mouse TNFα for 30 minutes then lysed in lysis buffer containing 25 mM Tris-HCl pH 7.5, 150 mM NaCl, 1% NP40, 5% glycerol, 1 mM DTT, and 0.5 mM PMSF. Lysate was clarified by centrifugation at 13,000 rpm for 10 minutes at 4°C and incubated with anti-FLAG M2 agarose beads (Sigma) at 4°C for 2 hours with gentle rotation. Beads were then extensively washed with lysis buffer and NFATc1 was eluted in lysis buffer contain 0.1 mg/mL 3xFLAG peptide (Sigma). Soluble FLAG-tagged NFATc1 was separated from beads by centrifugation, quantified by Bradford, analyzed by SDS-PAGE with Coomassie staining, and used directly for *in vitro* assays.

4. Luciferase Assays

The list of primers used for generation of different luciferase constructs is listed in **Table 3.1**. Complementary primers of specific promoters were first annealed by mixing at a final concentration of 2μM in buffer containing 10 mM Tris-HCl pH 7.5, 50 mM NaCl, and 1 mM EDTA and incubating in boiling water allowed to slowly cool to room temperature. Annealed promoters were then cloned into the CMXTK-Luciferase vector (a kind gift from Dr. Chakravarti

at Northwestern University Feinberg School of Medicine) at the SalI and BamHI restriction sites. HEK293T were grown in 12-well plates and transiently transfected using PEI with HA-RelA (1-551) or control empty HA-vector, the luciferase reporter DNAs, and control CMV-driven Renilla. Cells were collected 24 h post-transfection and lysate was collected and used for luciferase activity assay using the Dual-Luciferase Reporter Assay System (Promega). Data are represented as mean ± standard deviations (SD) of three or more independent experimental replicates.

5. Elecrophoretic Mobility Shift Assays

The list of primers used for generation of radiolabeled probes is listed in **Table 3.2**. Oligonucleotides were ^{32}P end radiolabeled using T4-polynucleotide kinase (New England Biolabs) and [γ-^{32}P]ATP (PerkinElmer), purified from free [γ-^{32}P]ATP using a Microspin G-25 column (Cytiva), and annealed with complementary DNA. Recombinant RelA or p50:RelA were incubated with radiolabeled DNA at room temperature for 15 minutes in binding buffer containing 10 mM Tris- HCl pH 7.5, 50 mM NaCl, 10% glycerol, 1% NP-40, 1 mM EDTA, and 0.1 mg/mL sonicated salmon sperm DNA. Proteins were diluted in dilution buffer containing 20 mM Tris-HCl pH 7.5, 50 mM NaCl, 10% glycerol, 1 mM DTT, and 0.2 mg/mL bovine serum albumin in preparation for the reaction mixture. Complexes were analyzed by electrophoresis in a pre-ran 5% non-denatured polyacrylamide gel at 200 V for 1 h at room temperature in 25 mM Tris base, 190 mM glycine, and 1 mM EDTA. Gel was then dried, exposed on a phosphor screen overnight, and scanned by Typhoon FLA 9000 imager (Cytiva).

For EMSA with 293T nuclear extract, cells were first transfected with either empty vector or HA-tagged full-length RelA overexpression plasmid using TransIT-Lenti (Mirus) following the manufacturers recommendations. 24 hours after transfection, cells were harvested

by scraping and lysed in cytoplasmic lysis buffer consisting of PBS with 0.1% NP40, 0.25 mM PMSF, and 1 mM DTT. Nuclei were then pelleted by centrifugation at 300 g, washed twice with PBS, and resuspended in nuclear extraction buffer consisting of 25 mM Tris-HCl pH 7.5, 420 mM NaCl, 10% glycerol, 0.2 mM EDTA, 1 mM DTT, and 0.5 mM PMSF. Nuclear extract was quantified by Bradford assay and 7 μg of extract was mixed with radiolabeled DNA in a binding reaction consisting of 25 mM Tris-HCl pH 7.5, 150 mM NaCl, 10% glycerol, 1 mM EDTA, and 0.1 mg/mL sonicated salmon sperm DNA. Complexes were analyzed by non-denaturing gel electrophoreses as outlined previously.

6. RNA Isolation and Real-Time qPCR

Total RNA was isolated from cultured cells by isopropanol precipitation with TRIzol (Invitrogen) following manufacturers recommendations. RNA concentration was determined by nanodrop, and 1 μg of total RNA was used for cDNA synthesis using Maxima H Minus Master Mix (Thermo Scientific) in a reaction volume of 5 μL. Synthesized cDNA was then diluted 4-fold and 1 μL was used as template for real-time qPCR using Luna Master Mix (NEB). Values were normalized to GAPDH, and data was represented at mean ± standard deviation (SD) from three independent experimental replicates. The list of primers used in RT-qPCR analysis are listed in **Table 3.3**.

7. *In vitro* Pulldown Assays and Mass Spectrometry

For FLAG pulldown assays in HEK93T, cells were transfected with empty vector or FLAG-NFATc1 overexpression constructs using TransIT-Lenti. After 24 hours, cells were stimulated with mouse TNFα for 30 minutes, washed once with ice-cold PBS, and lysed in lysis buffer containing 25 mM Tris-HCl pH 7.5, 150 mM NaCl, 5% glycerol, 1% NP-40, 1 mM DTT, and 0.25 mM PMSF. Lysate was clarified by centrifugation and incubated for 2 hours at 4°C

with anti-FLAG M2 agarose beads (Sigma) with gentle rotation. Beads were extensively washed with lysis buffer before adding 4x SDS gel loading dye to a final concentration of 1x. Beads were incubated on a 95°C heatblock for 5 minutes and loaded on gel for Western blot analysis.

For streptavidin-DNA pulldown assays, 5' biotinylated oligonucleotides (IDT) were annealed with corresponding nonbiotinylated reverse complement oligonucleotides at a final concentration of 45 μM as previously outlined. For each pulldown reaction, 40 μL of 45 μM annealed DNA was mixed with 100 μL of Neutravidin agarose resin (Thermo) at a total volume of 400 μL in buffer containing 10 mM Tris-HCl pH 7.5, 50 mM NaCl, and 0.5 mM EDTA. Biotinylated DNA was immobilized onto beads by incubation for 1 hour at room temperature with gentle rotation. Beads were then washed extensively with pulldown buffer containing 25 mM Tris-HCl pH 7.5, 150 mM NaCl, 5% glycerol, 0.1% NP-40, and 1 mM DTT with final resuspension in 50 μL per pulldown. MEF nuclear extract was prepared following 30 minutes of 20 ng/mL mouse TNFα treatment as previously outlined. Approximately 250 μg of nuclear extract was diluted 2.8-fold with pulldown buffer without NaCl but supplemented with 0.5 mM PMSF to reduce the final NaCl concentration from 420 mM to 150 mM. The diluted extract was then mixed with the double mutant M5 beads and precleared by gentle rotation at 4°C for 2 hours. Mutant beads were then pelleted and discarded, and the precleared lysate was mixed with the corresponding beads overnight at 4°C with gentle rotation. For Western analysis, beads were extensively washed and resuspended in 4x SDS gel loading dye to a final concentration of 1x. Beads were then incubated on a 95°C heatblock for 5 minutes and analyzed by Western blot. Microcapillary LC/MS/MS for peptide identification was conducted at the Taplin Biological Mass Spectrometry Facility at Harvard Medical School using Orbitrap mass spectrometers (Thermo).

8. Biolayer Interferometry Assay and Analysis

The list of primers used for BLI analysis are listed in **Table 3.4**. Biotinylated oligonucleotides were annealed with complementary nonbiotinylated oligonucleotides by mixing at a ratio of 1:1.2 in buffer containing 10 mM Tris-HCl pH 7.5, 50 mM NaCl, and 1 mM EDTA and incubating in boiling water allowed to slowly cool to room temperature. Biotinylated annealed DNA (200 nM) was then immobilized onto hydrated Octet Streptavidin (SA) biosensors (Sartorius) for 10 seconds in BLI buffer consisting of 25 mM Tris-HCl pH 7.5, 150 mM NaCl, 0.02% Tween 20, 0.1 mg/mL sonicated salmon sperm DNA, and 1 mM DTT using the Octet K2 system (ForteBio). A reference sensor without DNA was used for background subtraction. Baseline was first measured by incubation of sensors in BLI buffer for 60 seconds. Binding kinetics were then measured through an association phase of 120 seconds in which 12.5, 25, 50, 100, or 200 nM of recombinant His-RelA(1-551) was incubated with the biotinylated DNA-sensor complex, followed by a dissociation phase of 180 seconds in BLI buffer without protein. Sensor was regenerated in BLI buffer containing 1 M NaCl for 5 seconds followed by wash in BLI buffer for another 5 seconds three times prior to each reading. Analysis of BLI data was carried out using equations derived in Chapter 2.

9. Genomic DNA Isolation and Sanger Sequencing

Genomic DNA was isolated from stable MEF cell lines by phenol-chloroform precipitation. Plated cells were washed once with ice-cold PBS and collected by scraping. Cells were then pelleted by centrifugation at 300 g and resuspended in 100 µL of PBS. 100 µL of phenol:chloroform:isoamyl alcohol (25:24:1) (Invitrogen) was then added and thoroughly mixed. Following centrifugation at 13,000rpm for 5 minutes at room temperature, the upper aqueous phase was transferred to a new tube and mixed with 20 ng/µL RNAse A with incubation at 37°C

for 20 minutes. A 1/10 volume of 3M sodium acetate pH 4.8 and 2.5 volumes of ethanol were added to precipitate genomic DNA with incubation at -20°C for 30 minutes. The genomic DNA pellet was collected by centrifugation, washed once with 75% ethanol, and resuspended in water. Genomic DNA concentrations were determined by nanodrop, and DNA served as a template for PCR with primers specific to the Cxcl2 promoter (sequence of primers provided in **Table 3.3**). PCR products were separated and visualized by agarose gel electrophoresis and bands of the expected size were extracted from the gel and purified using the Zymoclean Gel DNA Recovery Kit (Zymo). Purified DNA was then sequenced by Sanger sequencing (Genewiz) in both the forward and reverse direction using the same primers used in PCR.

Table 3.1: Sequences of oligonucleotides used for generation of luciferase constructs. κB sites are indicated in bold. Restriction sites are indicated in blue. Mutated κB sites are indicated in red.

κB Promoter	Sequence
A	5'- TCGAC**GGGAAATTCC**G -3' 3'- G**CCCTTTAAGG**CCTAG -5'
T	5'- TCGAC**GGGAATTTCC**G -3' 3'- G**CCCTTAAAGG**CCTAG -5'
G	5'- TCGAC**GGGAAGTTCC**G -3' 3'- G**CCCTTCAAGG**CCTAG -5'
C	5'- TCGAC**GGGAACTTCC**G -3' 3'- G**CCCTTGAAGG**CCTAG -5'
2WT	5'- TCGACATGAGGGGACCCTGAGCTCA**GGGAATTTCC**CTGGTCCCC**GGGCTTTTCC**AG -3' 3'- GTACTCCCCTGGGACTCGAGT**CCCTTAAAGG**GACCAGGGG**CCCGAAAAGG**TCCTAG -5'
2M1	5'- TCGACATGAGGGGACCCTGAGCTCA**GGGAATTTCC**CTGGTCCCC**GGGCTTTTgg**AG -3' 3'- GTACTCCCCTGGGACTCGAGT**CCCTTAAAGG**GACCAGGGG**CCCGAAAAcc**TCCTAG -5'
2M2	5'- TCGACATGAGGGGACCCTGAGCTCA**GGGAATTTCC**tTGGTCCCC**GGGCTTTTCC**AG -3' 3'- GTACTCCCCTGGGACTCGAGT**CCCTTAAAGG**aACCAGGGG**CCCGAAAAGG**TCCTAG -5'
2M3	5'- TCGACATGAGGGGACCCTGAGCTCA**t**GGAATTTCC**t**TGGTCCCC**GGGCTTTTCC**AG -3' 3'- GTACTCCCCTGGGACTCGAGT**a**CCTTAAAGG**a**ACCAGGGG**CCCGAAAAGG**TCCTAG -5'
2M4	5'- TCGACATGAGGGGACCCTGAGCTCAG**ct**AATTT**ga**CTGGTCCCC**GGGCTTTTCC**AG -3' 3'- GTACTCCCCTGGGACTCGAGT**Cga**TTAAA**ct**GACCAGGGG**CCCGAAAAGG**TCCTAG -5'
1WT	5'- TCGAC**GGGAAACACC**CTGTACTCCG**GGAATTTCCC**TGGCCCGGAGCTCTGGAGTTG -3' 3'- G**CCCTTTGTGG**GACATGAGGC**CCTTAAAGGG**ACCGGGCCTCGAGACCTCAACCTAG -5'
1M1	5'- TCGAC**G**tt**AAACACC**CTGTACTCCG**GGAATTTCCC**TGGCCCGGAGCTCTGGAGTTG -3' 3'- GC**aa**T**TTGTGG**GACATGAGGC**CCTTAAAGGG**ACCGGGCCTCGAGACCTCAACCTAG -5'
1M2	5'- TCGAC**GGGAAACACC**CTGTACTCCG**ct**AATTT**ga**CTGGCCCGGAGCTCTGGAGTTG -3' 3'- G**CCCTTTGTGG**GACATGAGGC**ga**T**TAAAct**GACCGGGCCTCGAGACCTCAACCTAG -5'
AG10	5'- TCGACGAAGGGTACTGCTCT**GGGAAATTCC**AACTCAGAAT**GGGAAGTTCC**ACGCTCG -3' 3'- GCTTCCCATGACGAGA**CCCTTTAAGG**TTGAGTCTTA**CCCTTCAAGG**TGCGAGCCTAG -5'
AG16	5'- TCGACGAAGGGTCT**GGGAAATTCC**AATACTGCCTCAGAAT**GGGAAGTTCC**ACGCTCG -3' 3'- GCTTCCCAGA**CCCTTTAAGG**TTATGACGGAGTCTTA**CCCTTCAAGG**TGCGAGCCTAG -5'
GA16	5'- TCGACGAAGGGTCT**GGGAAGTTCC**AATACTGCCTCAGAAT**GGGAAATTCC**ACGCTCG -3' 3'- GCTTCCCAGA**CCCTTCAAGG**TTATGACGGAGTCTTA**CCCTTTAAGG**TGCGAGCCTAG -5'
AT16	5'- TCGACGAAGGGTCT**GGGAAATTCC**AATACTGCCTCAGAAT**GGGAATTTCC**ACGCTCG -3' 3'- GCTTCCCAGA**CCCTTTAAGG**TTATGACGGAGTCTTA**CCCTTAAAGG**TGCGAGCCTAG -5'
CG16	5'- TCGACGAAGGGTCT**GGGAACTTCC**AATACTGCCTCAGAAT**GGGAAGTTCC**ACGCTCG -3' 3'- GCTTCCCAGA**CCCTTGAAGG**TTATGACGGAGTCTTA**CCCTTCAAGG**TGCGAGCCTAG -5'
AG50	5'- TCGACGAAGGGTCT**GGGAAATTCC**AATACTGCGGGTCTGATTCATTATCCCAGTCTGCCACTACAGCTCAGAAT**GGGAAGTTCC**ACGCTCG -3' 3'- GCTTCCCAGA**CCCTTTAAGG**TTATGACGCCCAGACTAAGTAATAGGGTCAGACGGTGATGTCGAGTCTTA**CCCTTCAAGG**TGCGAGCCTAG -5'
AG100	5'- TCGACGAAGGGTCT**GGGAAATTCC**AATACTGCGGGTCTGATTCATTATCAATACTGCGGGTCTGATTCATTATCCCAGTCTGCCACTACAGCTCAGAATCCAGTCTGCCACTACAGCTCAGAAT**GGGAAGTTCC**ACGCTCG -3' 3'- GCTTCCCAGA**CCCTTTAAGG**TTATGACGCCCAGACTAAGTAATAGTTATGACGCCCAGACTAAGTAATAGGGTCAGACGGTGATGTCGAGTCTTAGGTCAGACGGTGATGTCGAGTCTTA**CCCTTCAAGG**TGCGAGCCTAG -5'

Table 3.2: Sequences of oligonucleotides used in EMSA assays. κB sites are indicated in bold and mutated κB sites are indicated in red.

κB DNA	Sequence
AX	5'– TCGACGAAGGGTCT**GGGAAATTCC**AATACTGCCTCAGAAT**GccAATTTgg**ACGCTCG –3' 3'– GCTTCCCAGA**CCCTTTAAGG**TTATGACGGAGTCTTA**CggTTAAAcc**TGCGAGCCTAG –5'
AT	5'– TCGACGAAGGGTCT**GGGAAATTCC**AATACTGCCTCAGAAT**GGGAATTTCC**ACGCTCG –3' 3'– GCTTCCCAGA**CCCTTTAAGG**TTATGACGGAGTCTTA**CCCTTAAAGG**TGCGAGCCTAG –5'
AG	5'– TCGACGAAGGGTCT**GGGAAATTCC**AATACTGCCTCAGAAT**GGGAAGTTCC**ACGCTCG –3' 3'– GCTTCCCAGA**CCCTTTAAGG**TTATGACGGAGTCTTA**CCCTTCAAGG**TGCGAGCCTAG –5'
CX	5'– TCGACGAAGGGTCT**GGGAACTTCC**AATACTGCCTCAGAAT**GccAATTTgg**ACGCTCG –3' 3'– GCTTCCCAGA**CCCTTCAAGG**TTATGACGGAGTCTTA**CggTTAAAcc**TGCGAGCCTAG –5'
CG	5'– TCGACGAAGGGTCT**GGGAACTTCC**AATACTGCCTCAGAAT**GGGAAGTTCC**ACGCTCG –5' 3'– GCTTCCCAGA**CCCTTGAAGG**TTATGACGGAGTCTTA**CCCTTCAAGG**TGCGAGCCTAG –5'
2WT	5'– TCGACATGAGGGGACCCTGAGCTCA**GGGAATTTCC**CTGGTCCCC**GGGCTTTTCC**AG –3' 3'– GTACTCCCCTGGGACTCGAGT**CCCTTAAAGG**GACCAGGGG**CCCGAAAAGG**TCCTAG –5'
2M1	5'– TCGACATGAGGGGACCCTGAGCTCA**GGGAATTTCC**CTGGTCCCC**GGGCTTTTgg**AG –3' 3'– GTACTCCCCTGGGACTCGAGT**CCCTTAAAGG**GACCAGGGG**CCCGAAAAcc**TCCTAG –5'
2M2	5'– TCGACATGAGGGGACCCTGAGCTCA**GGGAATTTCC**tTGGTCCCC**GGGCTTTTCC**AG –3' 3'– GTACTCCCCTGGGACTCGAGT**CCCTTAAAGG**aACCAGGGG**CCCGAAAAGG**TCCTAG –5'
2M3	5'– TCGACATGAGGGGACCCTGAGCTCAt**GGAATTTCC**CTGGTCCCC**GGGCTTTTCC**AG –3' 3'– GTACTCCCCTGGGACTCGAGTA**CCTTAAAGG**GACCAGGGG**CCCGAAAAGG**TCCTAG –5'
2M4	5'– TCGACATGAGGGGACCCTGAGCTCA**Gct**AATTT**ga**CTGGTCCCC**GGGCTTTTCC**AG –3' 3'– GTACTCCCCTGGGACTCGAGT**Cga**TTAAA**ct**GACCAGGGG**CCCGAAAAGG**TCCTAG –5'
2M5	5'– TCGACATGAGGGGACCCTGAGCTCA**Gct**AATTT**ga**CTGGTCCCC**GGGCTTTTgg**AG –3' 3'– GTACTCCCCTGGGACTCGAGT**Cga**TTAAA**ct**GACCAGGGG**CCCGAAAAcc**TCCTAG –5'
1WT	5'– TCGAC**GGGAAACACC**CTGTACTCCG**GGAATTTCCC**TGGCCCGGAGCTCTGGAGTTG –3' 3'– G**CCCTTTGTGG**GACATGAGGC**CCTTAAAGGG**ACCGGGCCTCGAGACCTCAACCTAG –5'
1M1	5'– TCGAC**Gtt**AAACACCCTGTACTCCG**GGAATTTCCC**TGGCCCGGAGCTCTGGAGTTG –3' 3'– G**Caa**TTTGTGGGACATGAGGC**CCTTAAAGGG**ACCGGGCCTCGAGACCTCAACCTAG –5'
1M2	5'– TCGAC**GGGAAACACC**CTGTACTCC**GctAATTTga**CTGGCCCGGAGCTCTGGAGTTG –3' 3'– G**CCCTTTGTGG**GACATGAGG**CgaTTAAAct**GACCGGGCCTCGAGACCTCAACCTAG –5'

Table 3.3: Sequences of oligonucleotides used in RT-qPCR, Sanger sequencing, shRNA cloning, and CRISPR cloning.

Target	Assay	Primer	Sequence (5' → 3')
Cxcl1	RT-qPCR	Forward	ACCCAAACCGAAGTCATAGCC
		Reverse	TTGTCAGAAGCCAGCGTTCA
Cxcl2	RT-qPCR	Forward	CCAGACAGAAGTCATAGCCACT
		Reverse	GGTTCTTCCGTTGAGGGACA
Gapdh	RT-qPCR	Forward	TACGGCCAAATCCGTTCACA
		Reverse	CCCTTAAGAGGGATGCTGCC
Cxcl2 genomic DNA promoter	Sanger sequencing	Forward	AATGAGGCAGGCAGCTCACG
		Reverse	GCCCGAGGAAGCTTGTTGGA
Scramble-pLKO	shRNA cloning	Forward	CCGGCCTAAGGTTAAGTCGCCCTCGCTCGAGCGAGGGCGACTTAACCTTAGGTTTTTG
		Reverse	AATTCAAAAACCTAAGGTTAAGTCGCCCTCGCTCGAGCGAGGGCGACTTAACCTTAGG
Nfatc1-pLKO	shRNA cloning	Forward	CCGGGCCGCAGAACACTACAGTTATCTCGAGATAACTGTAGTGTTCTGCGGCTTTTTG
		Reverse	AATTCAAAAAGCCGCAGAACACTACAGTTATCTCGAGATAACTGTAGTGTTCTGCGGC
Cxcl2 strong κB site	CRISPR cloning	Forward	CACCGCTGAGCTCAGGGAATTTCCC
		Reverse	AAACGGGAAATTCCCTGAGCTCAGC
Cxcl2 weak κB site	CRISPR cloning	Forward	CACCGGCACGATGTCTGGAAAAGCC
		Reverse	AAACGGCTTTTCCAGACATCGTGCC
Cxcl2 off-target site	CRISPR cloning	Forward	CACCGGTCCCCAACCCACTCAGCTT
		Reverse	AAACAAGCTGAGTGGGTTGGGGACC

Table 3.4: Sequences of oligonucleotides used in BLI assays. κB sites are indicated in bold and mutated κB sites are indicated in red.

κB DNA	Sequence
biotin-AX	5'- (Biotin)CGAAGGGTCT**GGGAAATTCC**AATACTGCCTCAGAAT**Gcc**AATTT**gg**ACGCTCGGATC -3' 3'- GCTTCCCAGA**CCCTTTAAGG**TTATGACGGAGTCTTA**Cgg**TTAAA**cc**TGCGAGCCTAG -5'
biotin-AT	5'- (Biotin)CGAAGGGTCT**GGGAAATTCC**AATACTGCCTCAGAAT**GGGAATTTCC**ACGCTCGGATC -3' 3'- GCTTCCCAGA**CCCTTTAAGG**TTATGACGGAGTCTTA**CCCTTAAAGG**TGCGAGCCTAG -5'
biotin-AG	5'- (Biotin)CGAAGGGTCT**GGGAAATTCC**AATACTGCCTCAGAAT**GGGAAGTTCC**ACGCTCGGATC -3' 3'- GCTTCCCAGA**CCCTTTAAGG**TTATGACGGAGTCTTA**CCCTTCAAGG**TGCGAGCCTAG -5'
biotin-CX	5'- (Biotin)CGAAGGGTCT**GGGAACTTCC**AATACTGCCTCAGAAT**Gcc**AATTT**gg**ACGCTCGGATC -3' 3'- GCTTCCCAGA**CCCTTGAAGG**TTATGACGGAGTCTTA**Cgg**TTAAA**cc**TGCGAGCCTAG -5'
biotinCG	5'- (Biotin)CGAAGGGTCT**GGGAACTTCC**AATACTGCCTCAGAAT**GGGAAGTTCC**ACGCTCGGATC -3' 3'- GCTTCCCAGA**CCCTTGAAGG**TTATGACGGAGTCTTA**CCCTTCAAGG**TGCGAGCCTAG -5'
biotin-2WT	5'- (Biotin)CATGAGGGGACCCTGAGCTCA**GGGAATTTCC**CTGGTCCCC**GGGCTTTTCC**A 3'- GTACTCCCCTGGGACTCGAGT**CCCTTAAAGG**GACCAGGGG**CCCGAAAAGG**TCCTAG -5'
biotin-2M1	5'- (Biotin)CATGAGGGGACCCTGAGCTCA**GGGAATTTCC**CTGGTCCCC**GGGCTTTT**gg**A** 3'- GTACTCCCCTGGGACTCGAGT**CCCTTAAAGG**GACCAGGGG**CCCGAAAA**cc**TCCTAG -5'
biotin-2M4	5'- (Biotin)CATGAGGGGACCCTGAGCTCA**G**ct**AATTT**ga**CTGGTCCCC**GGGCTTTTCC**A** 3'- GTACTCCCCTGGGACTCGAGT**C**ga**TTAAA**ct**GACCAGGGG**CCCGAAAAGG**TCCTAG -5'
biotin-2M5	5'- (Biotin)CATGAGGGGACCCTGAGCTCA**G**ct**AATTT**ga**CTGGTCCCC**GGGCTTTT**gg**A** 3'- GTACTCCCCTGGGACTCGAGT**C**ga**TTAAA**ct**GACCAGGGG**CCCGAAAA**cc**TCCTAG -5'

F. Acknowledgements

I would like to thank Yuting Shen and Zixing Liu for help with generating and maintaining cell lines, cloning, *in vitro* assays, RT-qPCR, and Western blotting. I would like to thank Dr. Tapan Biswas and Dr. Kaushik Saha for helpful discussions and experimental design suggestions. I would like to thank Dr. Catera Wilder and Dr. Alexander Hoffmann for providing the pLenti-CRISPRv2 plasmid. I would like to thank Dr. Oleg Tsodikov for help with BLI analysis.

Chapter 3, in part is currently being prepared for submission for publication of the material. Shahabi, Shandy; Ghosh, Gourisankar. The dissertation author was the primary investigator and author of this material.

Chapter 4: Protein cofactors are essential for high-affinity DNA binding by RelA

A. Abstract

Dimeric NF-κB transcription factors bind κB sites distributed at the promoter or enhancer regions of target genes to facilitate transcriptional activation and proinflammatory signaling. The κB site sequence directs NF-κB binding affinity *in vitro*, however binding affinity is not the absolute determinant for site-specific NF-κB binding *in vivo*. Protein cofactors, which include RPS3 and p53, direct cellular RelA-containing NF-κB dimers to specific κB sites and facilitate transcriptional activation. I observe that RelA binds κB DNA poorly at physiological salt concentrations *in vitro* and purified RPS3 and p53 augment RelA DNA binding affinity without forming stable ternary complexes, suggesting dynamic interactions. NME1 was identified as a constitutive RelA-specific cofactor through fractionation of unstimulated nuclear extract. NME1 interacted directly with RelA to enhance DNA binding affinity *in vitro* and facilitate transcriptional activation. NME1 altered RelA recruitment and transcriptional activation of a distinct subset of TNFα-dependent target genes, suggesting that NME1 contributes to promoter specificity. Altogether, these observations suggest that nuclear protein cofactors modulate NF-κB DNA binding affinity and direct NF-κB target site specificity.

B. Introduction

NF-κB dimers are sequence-specific DNA binding transcription factors that regulate target gene expression levels by binding to DNA response elements known collectively as "κB sites" or "κB DNAs". The fundamental principles that direct NF-κB:DNA complex formation have been determined through elucidation of three-dimensional structures of several NF-κB:DNA complexes, identification of *cis*-acting regulatory sequences coupled to reporter activity assays, *in vitro* DNA binding activity assays using EMSA, and gene expression microarray experiments. The κB site consensus is 5'-GGGRNNNYCC-3' (R, Y, and N denote purine, pyrimidine, and any base, respectively), where each NF-κB dimer subunit binds either 4 or 5 bp half-sites separated by a single base pair. Although this consensus accommodates many DNA sequences, NF-κB dimers have repeatedly been found to bind DNA that falls outside the consensus, as well. For example, NF-κB dimers have been shown to bind DNA that retains only one half-site consensus (Guttridge, 1999; Huang, 2001; Wong, 2011). The modular architecture of the NF-κB subunit DNA-binding domain allows NF-κB dimers to bind DNA with minimal sequence conservation (Chen, 1998) . Additionally, even a single nucleotide variation within a κB site can switch a gene regulatory program from activation to repression (Wang, 2012; Leung, 2004). This suggests that κB sites are not merely passive placeholders that function to tether NF-κB to a promoter. Instead, κB sites play an active role in influencing gene regulation.

Genome-wide ChIP-Seq studies revealed unexpected modes of DNA binding by NF-κB. The first genome-wide study investigated RelA targets within chromosome 22 and revealed two surprising observations: more than one-third of the RelA target genes do not contain a κB site, and often RelA binds stably to intergenic regions far away from an active gene (Martone, 2003). Since that report, several other genome-wide studies have been performed with RelA, as well as

other transcription factors, and the results are consistent with nonconsensus DNA binding (Heinz, 2013; Jin, 2013; Heldring, 2011). The degree of nonconsensus site binding varies from 15-50% depending on the transcription factor, stimulus, and cell-type.

Consistent with these reports, a recent study of the NF-κB DNA binding landscape in lymphoid B cell lines (LCL) revealed that one-third of all DNA bound NF-κB was at non-κB sites (Zhao, 2014). The nonconsensus NF-κB binding sites were, however, enriched for recognized gene regulatory elements such as E-box, ZNF143, PU.1/IRF4, and CTCF motifs. Such DNAs are known to recruit their own respective direct binding transcription factor proteins, and it is possible that NF-κB acts at these sites as a non-DNA binding cofactor to regulate target gene expression. It was also determined that a significant fraction of κB sites requires the accessory transcription factor FOXM1. Reduction of FOXM1 levels correlates with reduced expression levels of NF-κB target genes, suggesting that FOXM1 may function as a cofactor for RelA.

E2F1 was reported as the first global NF-κB cofactor (Lim, 2007). In response to LPS stimulation, E2F1 was shown to play an important role in NF-κB-mediated activation of inflammatory genes. Some of the target genes contain both a κB site and E2F1 site, but many others contained only a κB site. Despite this, E2F1 knockdown resulted in reduced induction of genes with only a κB site, suggesting a DNA-independent influence of E2F1 for RelA-mediated transcriptional activation. Similarly, ribosomal protein S3 (RPS3), p53, SAM68, NPM1, and OGG1 have also been found to enhance activation of NF-κB target genes in response to different stimuli (Wan, 2007; Choy, 2010; Fu, 2013; Lin, 2017; Pan, 2017). Overall, these studies suggest that many transcription factors, or nucleic acid binding proteins in general, can function in a manner independent of their own DNA binding propensities as cofactors that direct DNA

binding of other transcription factors. Additionally, negative regulatory cofactors have also been shown to reduce DNA binding of RelA under specific conditions (Jin, 2019; Tapyral, 2021). Although the *in vivo* functional significance for the "cofactor" activity of NF-κB, FOXM1, and E2F1 is beginning to come to light, a mechanism for how cofactors modulate DNA binding of transcription factors has not been thoroughly investigated.

NME1 is a member of the nucleoside diphosphate kinase family of enzymes (Lascu, 2000). This family catalyzes the transfer of phosphate from nucleoside triphosphates to nucleoside diphosphates through a high-energy phosphohistidine intermediate (Boissan, 2009; Norman, 1965). Originally discovered as a suppressor of tumor metastasis, NME1 is versatile in that it also functions as a protein-histidine kinase, 3'-5' exonuclease, and geranyl and farnesyl pyrophosphate kinase (Steeg, 1998; Lecroisey, 1995; Ma, 2004; Wagner, 2000). Previous studies demonstrate that NME1 has the capacity to occupy chromatin and cooperate with transcription factors at target promoters to regulate gene expression (Curtis, 2007; Pamidimukkala, 2018; Subramaniam, 2002; Choudhuri, 2006; Egistelli, 2009). NME1 has also been previously implicated in NF-κB signaling, however a defined function in the regulation of RelA DNA binding has not been established (You, 2014; Mohanty, 2022).

In this chapter, I explore how cofactors influence RelA DNA binding *in vitro* (**Figure 4.1**). I observe that factors present in nuclear extract enhance binding of RelA to κB DNA, and explore if cofactors can enhance DNA binding of RelA *in vitro*. I also develop an approach to identify new RelA-specific cofactors and identify NME1 as a novel cofactor that augments RelA DNA binding. I observed that NME1 can physically interact with RelA and enhance DNA-binding *in vitro*. I also observed that NME1 contributes to RelA DNA binding and

transcriptional activation *in vivo*. Taken together, this expands our current understanding of how cofactors contribute to gene regulation by NF-κB.

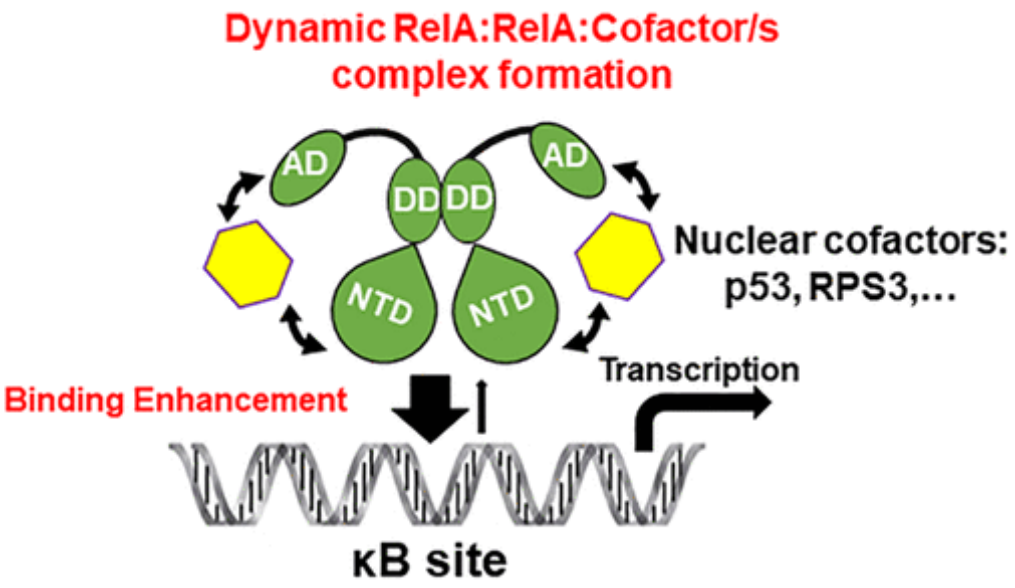

Figure 4.1: Schematic representation of cofactor-mediated DNA binding by NF-κB
Nuclear cofactors, such as p53 and RPS3, transiently interact with NF-κB to enhance DNA binding affinity and direct κB site specificity.

C. Results

1. RPS3 and p53 enhance binding affinity of RelA to κB DNA *in vitro*

I first explored if factors constitutively present in the nucleus have the capacity to augment DNA binding of recombinant FL-RelA *in vitro*. I tested DNA binding of FL-RelA in the presence or absence of unstimulated HeLa nuclear extract by EMSA and observed that FL-RelA formed a discrete complex with κB only in the presence of nuclear extract (**Figure 4.2A**). No shifted complex was observed with nuclear extract alone, and the complex formed with RelA and nuclear extract was validated as RelA-dependent with a supershift using a RelA-specific antibody. I also explored if nuclear extract could enhance binding of FL-RelA in solution by biotinylated-DNA streptavidin pulldown assay (**Figure 4.2B**). FL-RelA was incubated with biotinylated-κB DNA immobilized onto streptavidin agarose beads in the presence or absence of nuclear extract. I observed that nuclear extract enhanced precipitation of RelA with κB DNA, which agreed with EMSA results. Collectively, these results suggest that unstimulated nuclear extract enhances DNA binding of FL-RelA.

I next assessed the influence of two previously identified cofactors, RPS3 and p53, on the κB DNA binding affinity of RelA *in vitro*. I purified recombinant FL-RelA, RelA-RHR, RPS3, and p53 and tested DNA binding by EMSA (**Figure 4.3A**). Using the HIV κB DNA as a probe, I observed a concentration dependent enhancement of DNA binding for FL-RelA to κB DNA in the presence of RPS3 or p53 (**Figure 4.3B**). Both p53 and RPS3 enhanced binding of RelA without themselves binding to κB DNA, suggesting that the binding enhancement observed is a result of protein-protein interactions between RelA and these cofactors (**Figure 4.4A**). Surprisingly, neither p53 nor RPS3 enhanced binding affinity of RelA-RHR to κB DNA, suggesting that the activation domain of RelA plays an important role in cofactor mediated DNA

binding enhancement (**Figure 4.4B**). As a control nonspecific protein, BSA was used at an equivalent molar amount and no effect on DNA binding of FL-RelA was observed (**Figure 4.5A**). Further, two other previously established cofactors, OGG1 (8-oxo-guanine glycosylase 1) and HMGA1 (high-mobility group protein 1) were tested for their ability to enhance DNA binding of FL-RelA by EMSA (Pan, 2017; Yie, 1997). Neither OGG1 nor HMGA1 enhanced FL-RelA DNA binding, however this may be attributed to other factors. For instance, OGG1 facilitates NF-κB:DNA complex formation by binding damaged DNA that is absent in the EMSA probe (Pan, 2017). Also, previous reports suggest that HMGA1 may require a specific A/T rich segment central to the κB DNA to exert its function (Yie, 1997). Nevertheless, I observe that purified RPS3 and p53 enhance binding of FL-RelA to κB DNA in EMSA.

Since EMSA is conducted in low salt and non-physiological conditions, enhancement of DNA binding affinity for FL-RelA to κB DNA was also verified through an *in vitro* pulldown assay at physiological salt concentration in solution. Biotinylated κB DNA was immobilized to streptavidin beads, followed by incubation with FL-RelA in the presence or absence of RPS3 (**Figure 4.6A**). Following extensive washing, I observed increased FL-RelA being precipitated in the presence of RPS3, suggesting that RPS3 enhances DNA binding of FL-RelA *in vitro* beyond the constraints imposed in EMSA. To correlate the observed increase in κB DNA binding affinity of FL-RelA with transcriptional output, a κB-dependent luciferase reporter assay was performed in transiently transfected HEK293T (**Figure 4.6B**). I observed that following 8 hours of TNFα stimulation, ectopic overexpression of FLAG-RPS3 significantly increased luciferase activity for the κB DNA driven reporter construct. Taken together, this data suggests that RPS3 has the capacity to enhance binding of FL-RelA to κB DNA at physiological salt concentration and this can lead to increased transcriptional activation.

I aimed to further characterize RelA:DNA complex formation in solution under conditions that more closely mimic cellular salt concentrations. It was previously shown that the RHR of the purified p50:RelA heterodimer bound κB DNA very weakly at near a physiological salt concentration 150mM NaCl (Phelps, 2000). I performed binding affinity measurements using fluorescence anisotropy in which the HIV-κB DNA was labeled with a fluorescein molecule at the 5'-end (F-HIV-κB DNA). I observed that the F-HIV-κB DNA does not bind BSA at above 4 μM, and therefore all binding assays were completed with a final concentration of 4 μM BSA and a >200-fold molar excess of nonspecific DNA (**Figure 4.8A**). Consistent with previous reports, I found that RelA-RHR homodimer does not bind F-HIV-κB DNA at room temperature in a solution containing 150 mM NaCl, at pH 7.5. The presence of 500 nM RPS3 in the solution also had no impact on DNA binding by RelA-RHR (**Figure 4.7A**).

I then examined DNA binding by FL-RelA, which has never been tested in solution. At 150 mM NaCl/KCl, FL-RelA bound DNA weakly ($K_D \approx 630$ nM) but significantly better than RelA-RHR did. This was a surprise because according to our EMSA result, the RelA RHR was expected to bind stronger relative to FL-RelA. I then tested the effect of RPS3 on DNA binding by FL-RelA. In the presence of constant 500 nM RPS3, FL-RelA bound F-HIV-κB DNA with a K_D of ~10 nM, representing an approximate 60-fold enhancement in binding affinity. Anisotropy did not change when a single-stranded fluoresceinated DNA containing the κB site was used for titration against increasing concentrations of FL-RelA, indicating that the fluorophore itself does not interact with FL-RelA (**Figure 4.8B**). Additionally, heat-inactivated RPS3 had no effect on RelA:DNA complex formation, suggesting that the RPS3 mediated enhancement of DNA binding by RelA is dependent on the globular structure of RPS3 (**Figure 4.8C**).

I next tested the effect of p53. Surprisingly, I found that p53 could enhance the affinity of FL-RelA by only 2-4 fold (**Figure 4.7A**). Moreover, I need to use slightly different binding conditions to obtain an optimal effect of p53 (see details in the corresponding section of Materials and Methods). These results suggest that p53 has much less impact on the stability of the RelA:DNA complex in solution. It is possible that the effect of the cofactors is DNA-specific, where RPS3 might affect binding of RelA to a broad spectrum of κB DNA sequences and p53 affects a narrower subclass of sequences.

Although NaCl and KCl are popularly used to test the effect of the electrolyte on protein:DNA complex formation, a high chloride (Cl^-) concentration might pose a problem for the complex to form. The cellular Cl^- ion concentration is much lower than 150 mM in most cells, and Cl^- is known to impose a negative effect on the binding of protein to DNA. Potassium (K^+) ion, which is present at levels higher than that of Na^+, partly associates with glutamate and acetate ions *in vivo*. While differential effects between glutamate and chloride ions are established for prokaryotic processes, eukaryotic biochemical processes such as splicing are also reported to be more efficient in the presence of acetate and glutamate ions relative to chloride. Therefore, I tested the effects of potassium chloride (KCl), potassium glutamate (KGlu), and potassium acetate (KOAc) on RelA:DNA complex formation in the presence or absence of RPS3 (**Figure 4.7B**). DNA binding by FL-RelA in KCl was nearly identical to that in NaCl. However, binding was significantly enhanced in 150 mM KOAc or KGlu, even in the absence of RPS3. The binding was even further improved in the presence of RPS3. In all cases, the affinity was enhanced ~8 to >50-fold when RPS3 was present in the binding buffer. Therefore, both KGlu and KOAc enabled binding more efficiently than NaCl and KCl did. This suggests that glutamate

and acetate ions somehow stabilize the interactions between RPS3 and RelA such that RelA could bind DNA better.

The precise ion composition and the concentration of each ion in mammalian cells are not known. Cellular glutamate and acetate concentrations are only around 20 mM, which is much lower than the level of 150mM used in our assay. Therefore, the high affinity of the RelA:DNA complex observed in the presence of 150 mM KOAc or KGlu does not represent the true *in vivo* affinity. Similarly, in the complex ionic environment *in vivo*, RPS3 alone may not be sufficient for optimal RelA:DNA complex formation. It is likely that other cofactors work along with RPS3 to fulfill this role.

In summary, my binding studies show that RelA binds DNA differently under different salt conditions. Surprisingly, FL-RelA binds better than RelA-RHR in solution, suggesting that the activation domain of RelA participates as a key partner in the process of complex stabilization and does not inhibit RelA:DNA binding as was previously reported. Moreover, cofactors such as RPS3 and, to a lesser extent, p53 impact the stability of the RelA:DNA complex in solution.

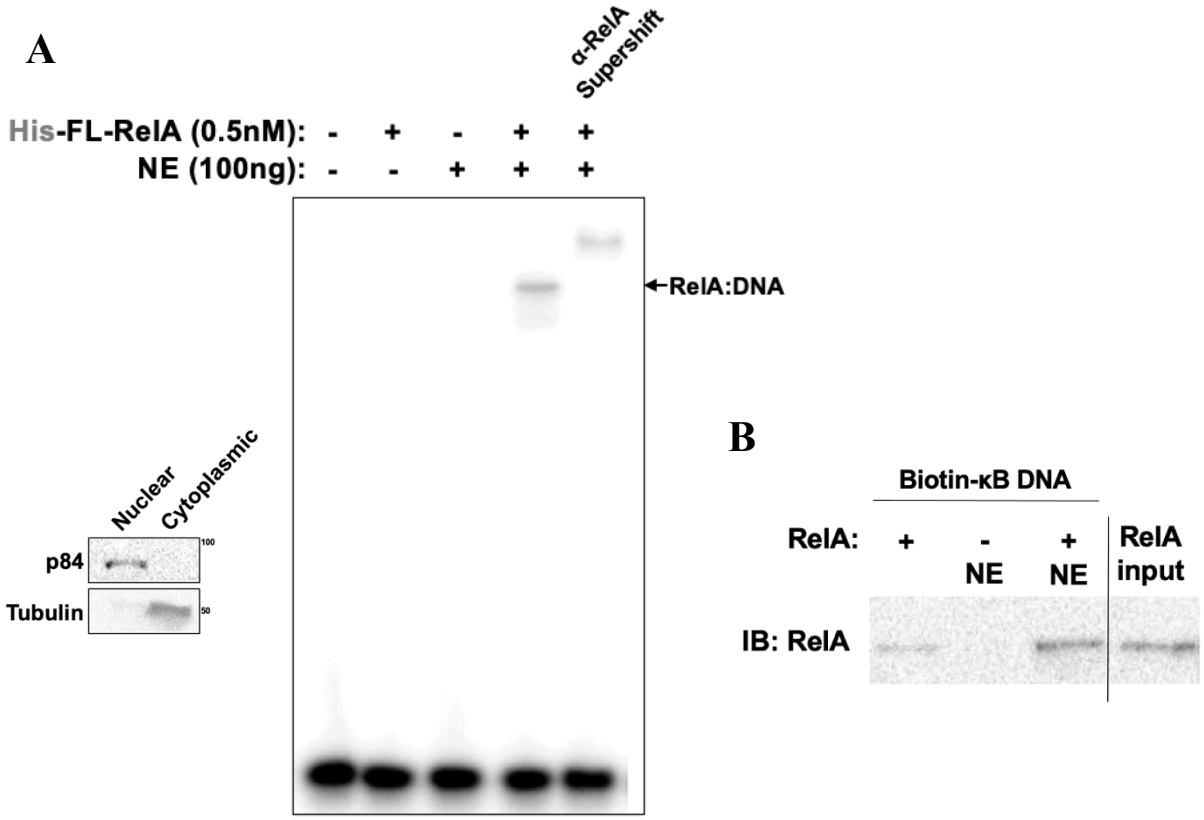

Figure 4.2: Unstimulated nuclear extract enhances recombinant FL-RelA DNA binding affinity
A. EMSA analysis of purified recombinant FL-RelA homodimer and unstimulated HeLa nuclear extract. The radiolabeled probe κB DNA sequence GGGAAATTCC was used for binding assays. Efficiency of HeLa nuclear fractionation was analyzed by Western blot using indicated antibodies (bottom left). **B.** Pulldown assay with biotinylated HIV-κB DNA-streptavidin beads and recombinant FL-RelA in the presence or absence of unstimulated HeLa nuclear extract. Precipitated proteins were analyzed by Western blot using RelA antibody.

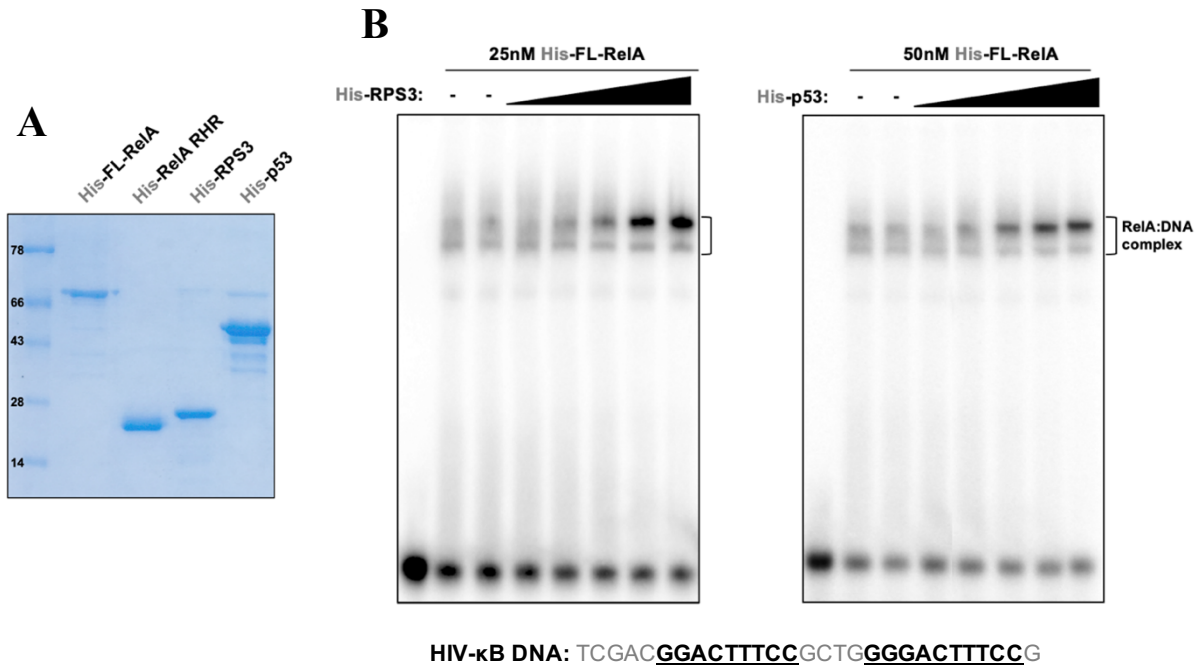

Figure 4.3: Recombinant RPS3 and p53 enhance RelA DNA binding affinity *in vitro*
A. Coomassie stained protein gel of purified proteins. His-tagged proteins were purified by Ni-affinity chromatography **B.** EMSA analysis showing a concentration-dependent enhancement of FL-RelA DNA binding for recombinant RPS3 (left) and p53 (right). The HIV-κB DNA probe was used in assays and sequence is shown below.

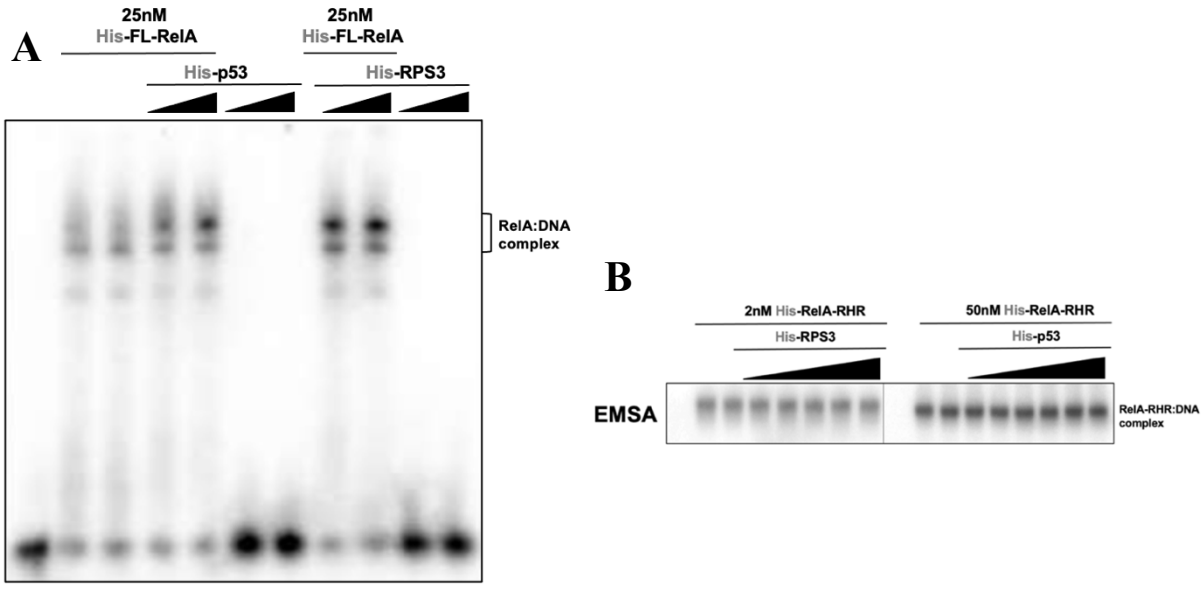

Figure 4.4: RPS3 and p53 enhance DNA binding of FL-RelA without binding DNA
A. EMSA analysis showing that both p53 and RPS3 enhance binding of FL-RelA homodimer without independently forming shifted complexes with DNA. **B.** EMSA analysis of DNA binding by RelA-RHR in the presence of increasing concentrations of RPS3 or p53. The HIV-κB DNA probe was used for gel shift assays.

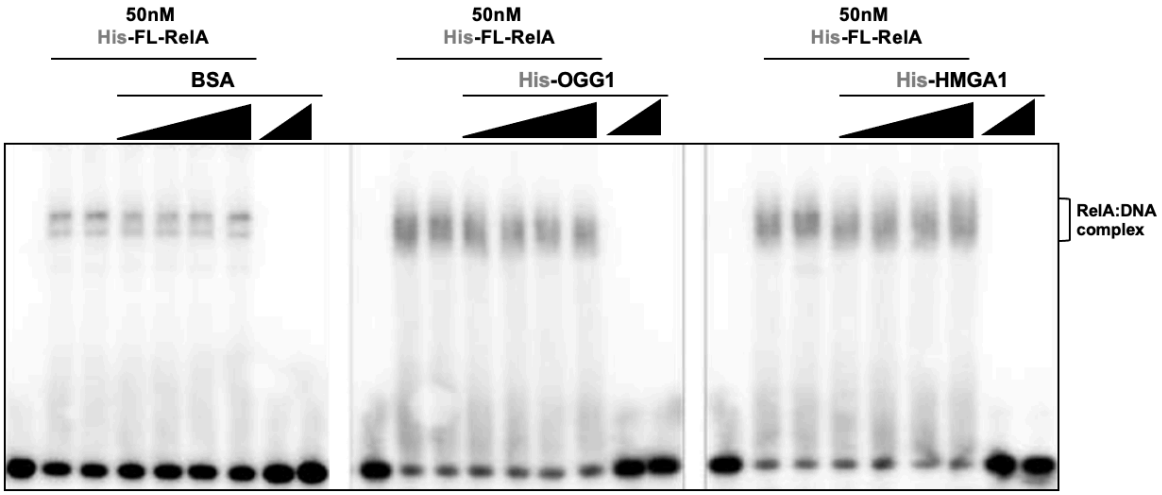

Figure 4.5: Control BSA, OGG1, and HMGA1 do not enhance DNA binding of RelA
EMSA analysis with recombinant FL-RelA and titrations with BSA (left), purified OGG1 (center), and purified HMGA1 (right). The HIV-κB DNA probe was used for gel shift assays.

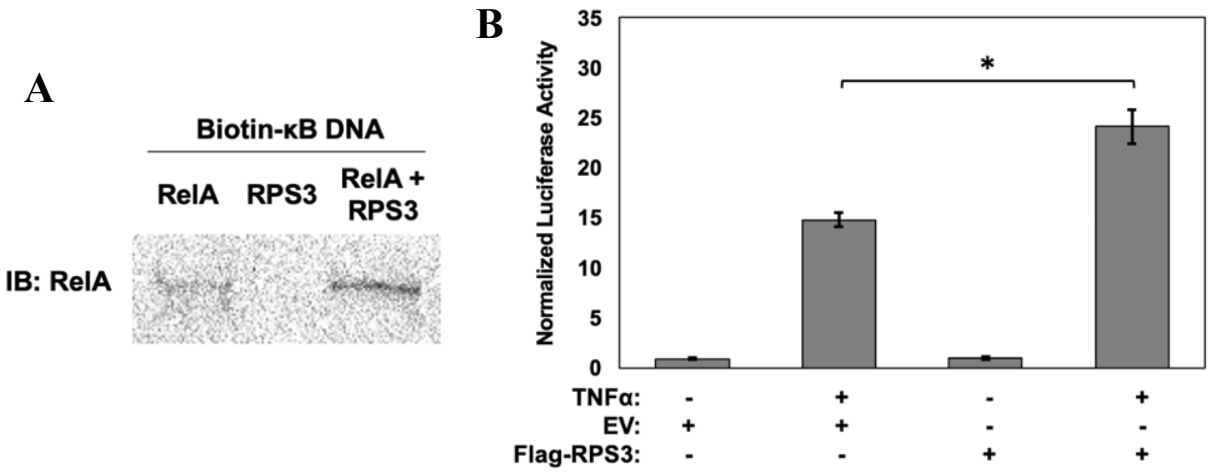

Figure 4.6: RPS3 enhances RelA DNA binding affinity and RelA-dependent transcription activation
A. Pulldown assay with biotinylated HIV-κB DNA-streptavidin agarose beads with recombinant FL-RelA and RPS3. Precipitated proteins were analyzed by Western blot with RelA antibody. **B.** Luciferase activation assay with empty vector or FLAG-tagged RPS3 transfected in HEK293T. Cells were stimulated with TNFα for 8 hours prior to assay. AT16 κB DNA was used luciferase construct. Luciferase values were normalized to Renilla and values are represented as mean ± SD from three independent experimental replicates.

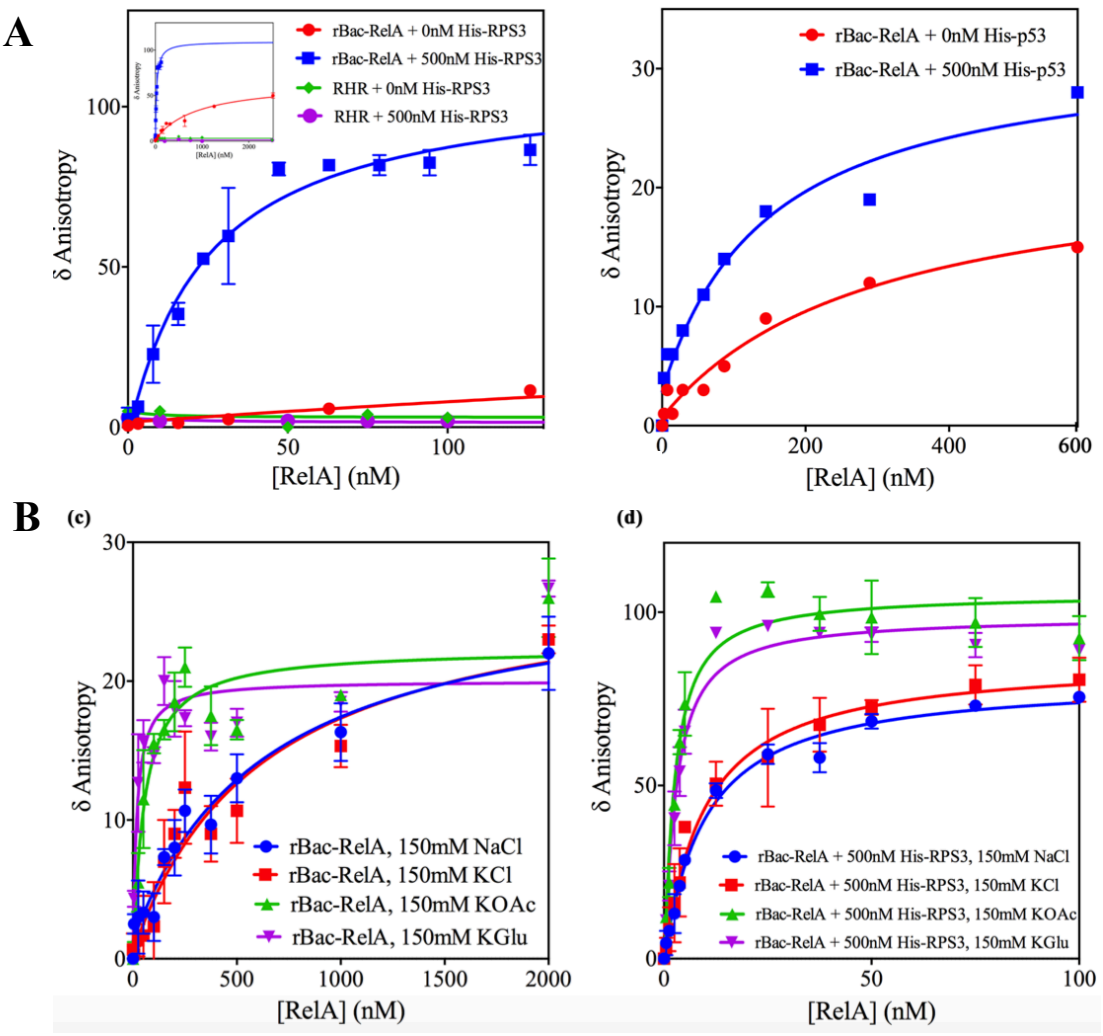

Figure 4.7: DNA binding by RelA in the presence or absence of cofactors by fluorescence anisotropy
A. Graphical representation of FL-RelA and RelA-RHR binding to 1 nM fluorescein-labeled HIV-κB DNA in the presence or absence of 500 nM RPS3 (left) or p53 (right). Binding reactions were performed at 150 mM NaCl. Polarization values were normalized to background and data is presented from three independent experimental replicates. **B.** Binding of FL-RelA to HIV-κB DNA in the absence (left) or presence of 500nM RPS3 (right) with different salts at a final concentration of 150 mM.

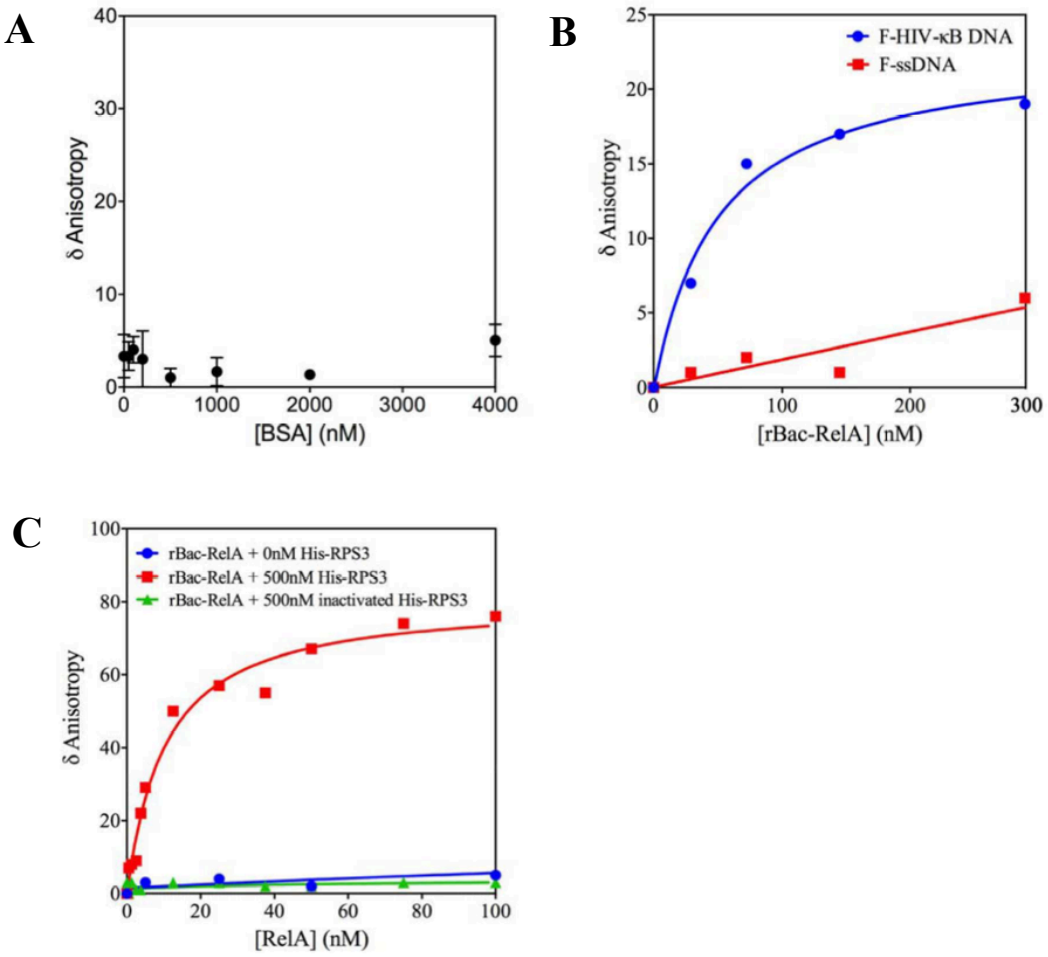

Figure 4.8: Control fluorescence anisotropy assays of FL-RelA
A. Increasing concentrations of nonspecific BSA was incubated with 1 nM fluorescein-labeled HIV-κB and fluorescence polarization was assayed as outlined for FL-RelA. **B.** Fluorescence polarization was measured for FL-RelA to 1 nM single-stranded fluorescein-labeled HIV-κB DNA. **C.** Recombinant RPS3 was heat inactivated by incubation at 95°C for 10 minutes, and fluorescence polarization was measured with FL-RelA and 1 nM fluorescein-labeled HIV-κB DNA.

2. Identification of NME1 as a RelA-specific cofactor

I sought to develop a κB sequence dependent approach for enriching and identifying nuclear cofactor(s) responsible for the observed increase in binding of FL-RelA to κB DNA in EMSA. Previous approaches for cofactor identification utilize a minimally stringent protocol for enrichment prior to mass-spec analysis or identify DNA-binding cofactors based on overlapping ChIP-Seq motifs, thus increasing the likelihood of false positives or RelA-independent coregulatory proteins. RPS3, for example, was identified through a DNA-independent pulldown and mass-spec analysis of an overexpressed RelA fusion construct in 293T cells following TNFα stimulation. Further, IRF3 and E2F1 are transcription factors that were identified to co-occupy genomic regions with RelA in response to viral infection or LPS stimulation, respectively, based on motif analysis of RelA associated genomic loci (Freaney, 2013; Lim, 2007). Due to the high observed activity of HeLa nuclear extract for enhancing RelA:DNA binding in EMSA, I postulated that it would be possible to observe the diminishing activity following two purification steps before mass spectrometry analysis for protein identification (**Figure 4.9**).

With unstimulated HeLa nuclear extract as input, the first step for clarification was size exclusion chromatography (**Figure 4.10A**). Using EMSA as an activity assay for enhancement of DNA binding by FL-RelA, I observed most activity contained within the fractions corresponding to an average molecular weight between 100-400 kDa (**Figure 4.10B**). Some activity was observed in fractions corresponding to a lower molecular weight of around 50 kDa, however these were excluded to limit the abundance of proteins for input into subsequent steps. The pooled fractions were then subject to MonoQ anion exchange chromatography, followed by the same EMSA activity assay. The elution profile from MonoQ revealed a differential abundance of proteins contained within the elution fractions upon increasing salt concentration based on

absorbance at 280 nm (A280) (**Figure 4.10C**). The elution fractions corresponding to a salt concentration between 300-400 mM NaCl yielded the most residual activity, with fractions Q23 and Q26 showing the highest activity. There was no correlation between RelA DNA-binding enhancement activity and A280 of the fractions. Fractions corresponding to a salt concentration between 250-500 mM NaCl were also tested for their capacity to enhance binding of FL-RelA to biotinylated κB DNA immobilized to streptavidin beads (**Figure 4.10D**). A similar pattern of enhancement across the MonoQ fractions was observed in the biotin-DNA pulldown assay, with fractions Q23 and Q26 providing the most enhancement for RelA binding, suggesting that the observed enhancement across fractions in EMSA was not an artifact of the assay.

Fraction Q23 displayed slightly higher activity than fraction Q26 in the biotin-DNA pulldown assay and was therefore pursued further. The same biotin-DNA pulldown assay was performed with fraction Q23 and recombinant FL-RelA, and precipitated proteins were subject to mass-spec for peptide identification. A control pulldown was also performed in parallel using fraction Q23 and the same biotin-DNA except in the absence of FL-RelA. A list of identified proteins unique to the biotin-DNA pulldown in the presence of RelA is listed in **Figure 4.11A**. As expected, RelA was the top identified protein as recombinant RelA was used as the bait protein in the assay. Additionally, MED12, a component of the Mediator complex that is known to interact with NF-κB, was also identified, suggesting that the pulldown assay has the capacity to capture RelA specific targets. (Taatjes, 2012; Freaney, 2013). Many structural proteins, such as collagen-alpha-1(XXIV) chain, vimentin, dynein heavy chain 8 axonemal, synemin, and nuclear envelope pore membrane protein 121 and 121C, were identified and excluded in downstream analysis.

The candidate proteins for further investigation were E3 ubiquitin-protein ligase CBL-B (CBLB), DENN domain-containing protein 2A (DENND2A), glial fibrillary acidic protein (GFAP), nucleoside diphosphate kinase A (NME1), RIB43A-like with coiled-coils protein 1 (RIBC1), Tonsoku-like protein (TONSL), and regulator of nonsense transcripts 3A (UPF3A). NME1 stuck out as potential cofactor as recent reports suggest NME1 can associate on DNA to facilitate transcription factor recruitment (Pamidimukkala, 2018; Curtis, 2007; Subramanian, 2002).

To preliminarily assess if the candidate proteins influence binding affinity of FL-RelA, stable shRNA-mediated knockdown cell lines of each target and a scramble control (scramble KD) were generated in HeLa. Crude nuclear extract was collected from each cell line and tested for the capacity to augment DNA-binding of FL-RelA by EMSA as previously performed (**Figure 4.11B**). Nuclear extract derived from the NME1 knockdown stable cell line (NME1 KD) displayed the largest reduction in enhancement of RelA:DNA binding relative to the scramble KD. CBLB, GFAP, TONSL, and UPF3A knockdown displayed no effect on RelA:DNA binding relative to scramble KD, and DENND2A and RIBC1 knockdown displayed only a moderate effect. This data suggests that NME1 may function as a cofactor for DNA binding of FL-RelA to κB DNA from the fractionated nuclear extract.

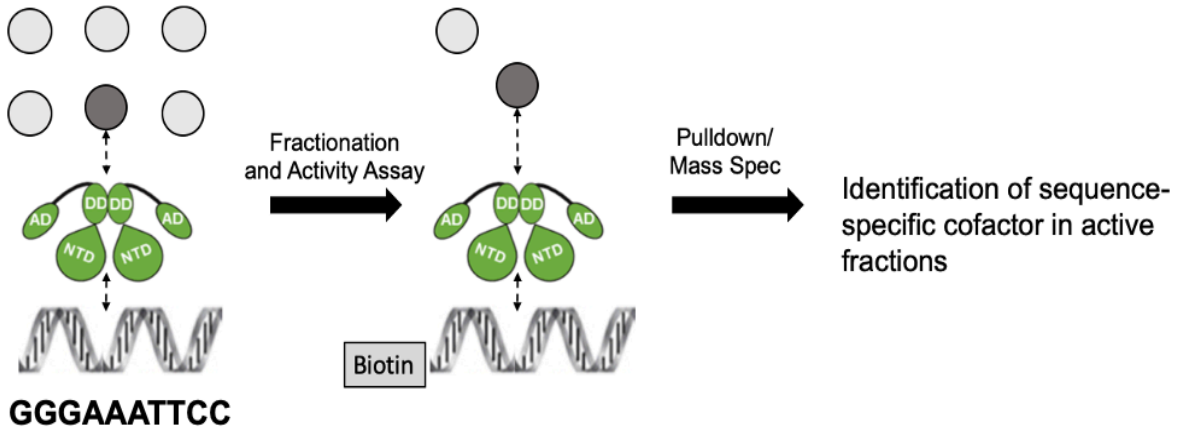

Figure 4.9: Schematic representation of strategy for identification of RelA-specific cofactors
Unstimulated HeLa nuclear extract underwent chromatographic fractionation with EMSA activity assay in parallel to enrich for cofactors that enhance RelA DNA-binding affinity. Purified fractions were then pulled down with biotinylated κB DNA-streptavidin agarose beads in the presence or absence of FL-RelA for mass spectrometry identification.

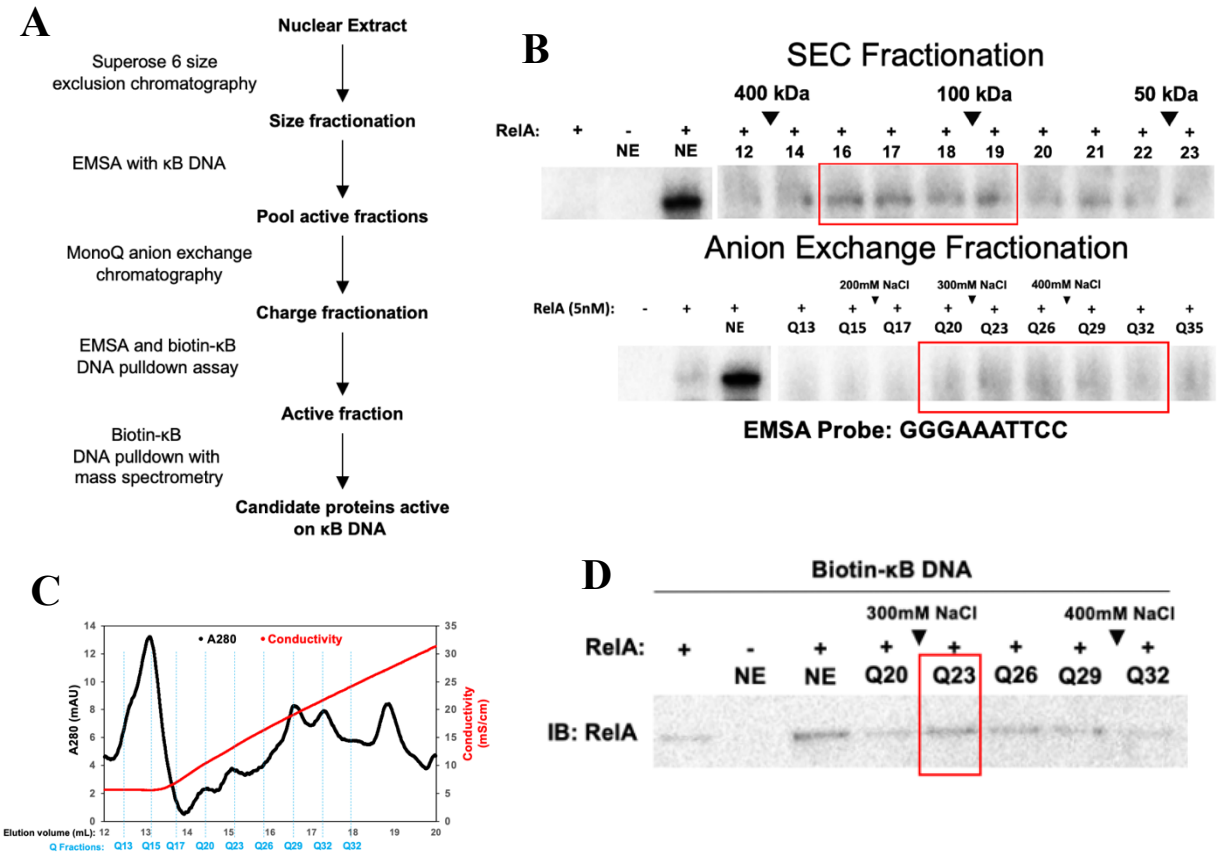

Figure 4.10: Fractionation and activity assays of unstimulated nuclear extract
A. Unstimulated HeLa nuclear extract from 3 15cm plates was collected and first fractioned by size-exclusion chromatography. Fractions were assayed by EMSA and active fractions were pooled and further fractionated by anion exchange chromatography. **B.** EMSA binding analysis of recombinant FL-RelA with nuclear extract fractioned by size-exclusion (top) and anion exchange (middle). **C.** Elution profile from MonoQ anion exchange fractionation. 280 nm absorbance readings for protein quantification is on left axis (black), NaCl dependent conductivity is on right axis (red), and elution volume and corresponding fractions are indicated on bottom axis. **D.** Active anion exchange fractions were assayed by biotinylated DNA-streptavidin agarose pulldown with recombinant FL-RelA, and precipitated RelA was analyzed by Western blot with RelA antibody.

A

RelA
Glial fibrillary acidic protein; GFAP
Mediator of RNA polymerase II transcription subunit 12; MED12
Collagen alpha-1(XXIV) chain; COL24A1
Vimentin; VIM
Dynein heavy chain 8 axonemal; DNAH8
Synemin; SYNM
Nuclear envelope pore membrane protein POM 121C; POM121C
Nuclear envelope pore membrane protein POM 121; POM121
DENN domain-containing protein 2A; DENND2A
E3 ubiquitin-protein ligase CBL-B; CBLB
Tonsoku-like protein; TONSL
RIB43A-like with coiled-coils protein 1; RIBC1
Protocadherin Fat 4; FAT4
Regulator of nonsense transcripts 3A; UPF3A
Nucleoside diphosphate kinase A; NME1
Serine/arginine repetitive matrix protein 2; SRRM2

B

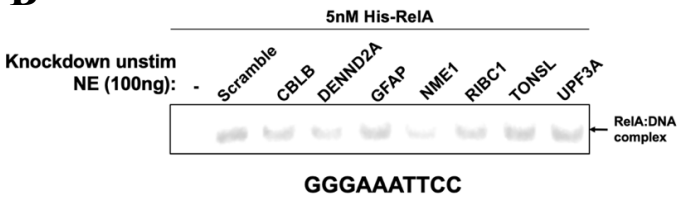

Figure 4.11: Identification of NME1 as a RelA-specific DNA binding cofactor
A. List of RelA-specific proteins identified by mass-spec **B.** EMSA analysis with recombinant FL-RelA and unstimulated nuclear extract from stable knockdown HeLa cell lines.

3. NME1 augments RelA binding to κB DNA to activate transcription

Knockdown of NME1 was first confirmed by RT-PCR and western blotting (**Figure 4.12A**). I then tested if the differences in RelA:DNA binding enhancement by EMSA can be observed using different amounts of nuclear extract, and indeed I observed an overall reduction in the concentration dependent enhancement of RelA:DNA binding in NME KD nuclear extract relative to scramble KD (**Figure 4.12B**). I next tested if NME1 KD altered binding of cellular p50:RelA heterodimer to κB DNA following TNFα stimulation by EMSA (**Figure 4.12C**). I observed that NME KD reduced binding of p50:RelA to κB DNA at 15 and 30 minutes following TNFα stimulation relative to scramble KD, however there was no observed difference after 1 hour of TNFα stimulation. This suggests that NME1 functions early in NF-κB signaling to enhance binding of p50:RelA to κB DNA when less p50:RelA is present in the nucleus relative to the later stages of NF-κB activation.

To further investigate if NME1 KD influences RelA DNA binding, I overexpressed HA-tagged RelA in both scramble KD and NME1 KD cell lines and analyzed HA-RelA DNA binding by EMSA (**Figure 4.12D**). As expected, I observed that NME1 KD resulted in reduced binding of HA-RelA to κB DNA. I next tested if NME1 expression contributes to NF-κB dependent transcriptional activation using a κB-driven luciferase reporter construct in 293T cells (**Figure 4.13**). Following 8 hours of TNFα stimulation, I observed increased luciferase activity for both empty vector and FLAG-NME1 transfected cells. However, the increase in luciferase activity was significantly elevated in FLAG-NME1 overexpressing cells, suggesting that NME1 enhances NF-κB-dependent transcription activation.

Two hallmarks of the canonical NF-κB pathway activation are IκBα degradation and RelA nuclear translocation, both of which are necessary events prior to RelA DNA binding. It is

possible that the observed differences in RelA:DNA complex formation and transcriptional activation may be due to NME1 acting upstream in the NF-κB pathway. I tested if NME1 KD altered IκBα degradation by Western blot (**Figure 4.14A**). As expected, I observed time-dependent degradation of IκBα upon TNFα stimulation, with nearly complete degradation at 30 minutes of stimulation. However, there was no observed difference in IκBα degradation in NME1 KD compared to scramble KD. I also tested if there was a difference in the overall nuclear abundance of RelA upon TNFα stimulation (**Figure 4.14B**). I observed that following 30 minutes of TNFα stimulation, there was an increase in nuclear RelA in both scramble KD and NME1 KD, but no difference between the two. Additionally, there was no difference in total cytoplasmic RelA between scramble KD and NME1, suggesting that NME1 does not alter the overall cellular levels or nuclear abundance of RelA. Taken together, this data suggests that NME1 enhances DNA binding of RelA to enhance transcriptional activation without acting upstream in the NF-κB signaling pathway.

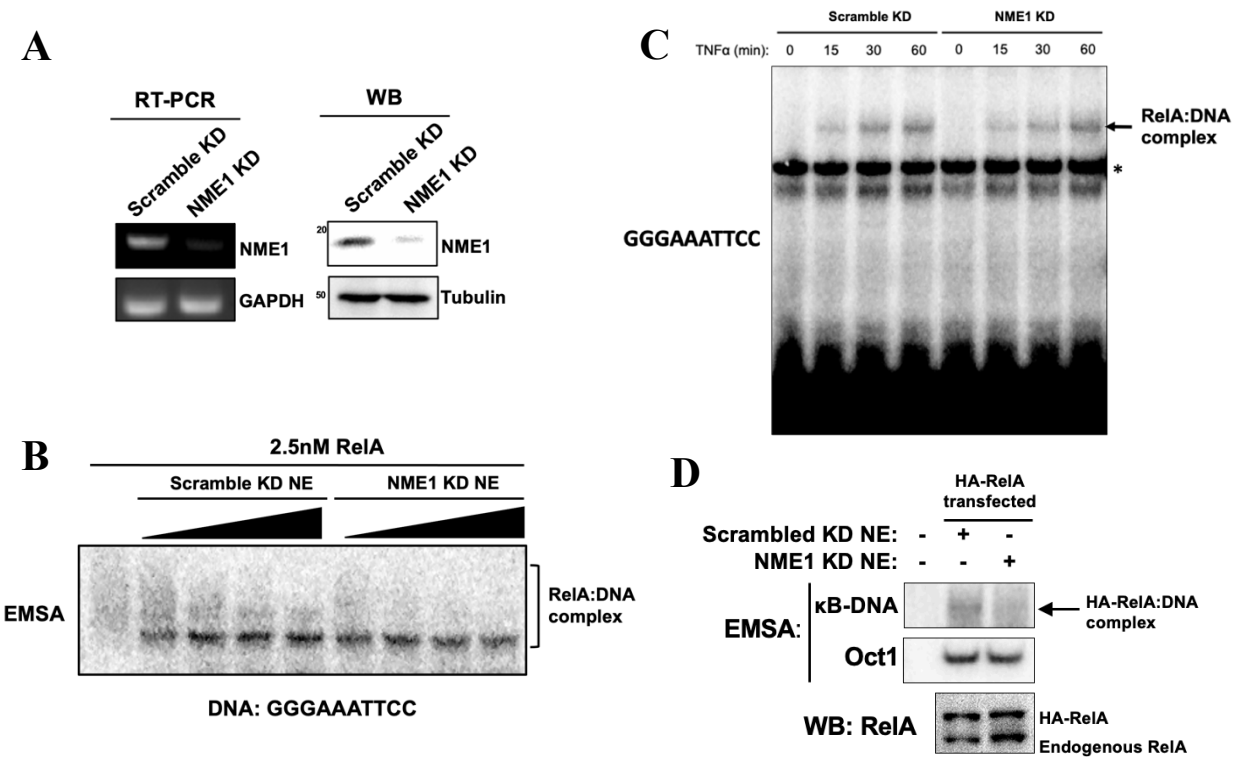

Figure 4.12: Knockdown of NME1 reduces RelA DNA binding
A. RT-PCR (left) and Western blot (right) analysis of scramble and NME1 knockdown stable HeLa cell lines. **B.** EMSA with recombinant FL-RelA and increasing amounts of unstimulated nuclear extract from scramble or NME1 knockdown HeLa cell lines. **C.** EMSA analysis of endogenous NF-κB binding in nuclear extract from stable scramble or NME1 knockdown HeLa cell lines. Cells were stimulated with 20 ng/mL TNFα for the indicated timepoints prior to preparation of nuclear extract. **D.** EMSA analysis of nuclear extract from stable scramble or NME1 knockdown HeLa cell lines transfected with HA-tagged RelA.

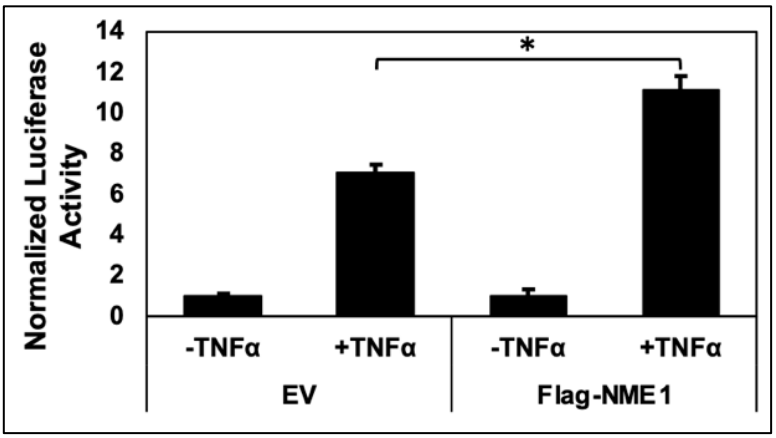

Figure 4.13: NME1 enhances RelA-dependent transcriptional activation
Luciferase activation assay with a NF-κB driven luciferase construct cotransfected with empty vector or FLAG-tagged NME1 in HEK293T. Cells were stimulated for 8 hours with control DMSO or TNFα prior to preparation of lysate. AT16 κB DNA was used luciferase construct. Luciferase reading were normalized to Renilla internal control and values are represented as mean ± SD of three independent experimental replicates.

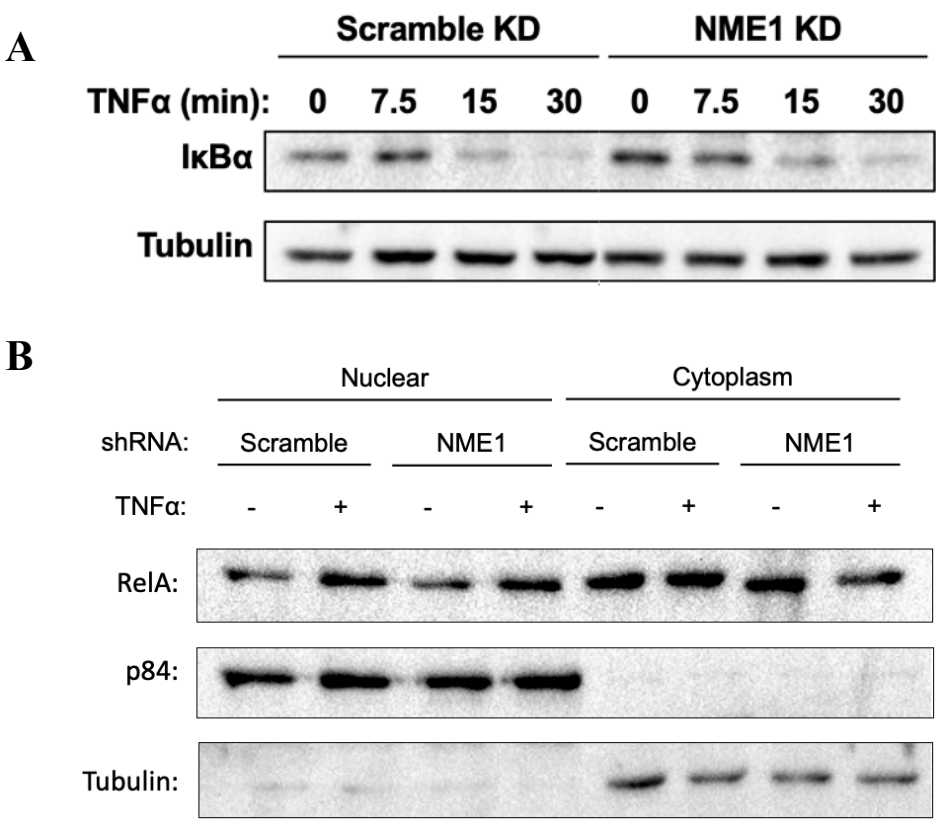

Figure 4.14: Knockdown does not impact upstream NF-κB signaling
A. Stable scramble and NME1 knockdown HeLa cell lines were stimulated with TNFα for the indicated timepoints and IκBα degradation was analyzed by Western blot of whole cell lysate. **B.** Stable scramble and NME1 knockdown HeLa cell lines were stimulated with TNFα for 15 minutes. Cells were then fractionated and nuclear and cytoplasmic fractions were analyzed by Western blot using the indicated antibodies.

4. NME1 interacts with RelA to enhance DNA binding *in vitro*

Based on the observed NME1-mediated DNA binding enhancement of RelA, I next tested if NME1 and RelA physically interacted. I overexpressed HA-tagged RelA with FLAG empty vector control or FLAG-tagged NME1 in 293T cells and performed a pulldown assay using anti-FLAG agarose beads (**Figure 4.15A**). I observed that HA-RelA coprecipitated with FLAG-NME1 upon FLAG pulldown but not with empty vector control. This suggests that RelA and NME1 can interact.

I next questioned if NME1 acts directly on RelA to enhance binding to κB DNA or if this was mediated by other factors present in the cell. I purified His-tagged NME1 to near homogeneity from Rosetta BL21 DE3 *E. coli* and performed an EMSA with recombinant FL-RelA (**Figure 4.15B**). I observed a concentration-dependent increase in binding of FL-RelA to κB DNA in the presence of NME1, suggesting that NME1 acts directly on RelA to enhance κB DNA binding affinity (**Figure 4.15C**). Following this observation, I tested if FL-RelA can physically interact with NME1 *in vitro* to further reinforce that the observed effects between RelA and NME1 are direct. I purified GST-tagged NME1 and control GST and performed an *in vitro* GST pulldown assay with FL-RelA using glutathione beads (**Figure 4.15D**). Indeed, I observed increased coprecipitation of FL-RelA with GST-NME1 relative to GST control, suggesting a direct physical interaction between RelA and NME1 *in vitro*. However, the interaction with FL-RelA with NME1 was weak, as evidenced by the relatively low amount of FL-RelA precipitated with GST-NME1 in the pulldown. This was expected as cofactors are hypothesized to transiently and dynamically associate with RelA to enhance binding affinity without forming a discrete stable complex with κB DNA. This is further supported by the observation that NME1 enhances binding of FL-RelA to κB DNA in EMSA without forming a

discrete shifted complex. This pattern of enhancement in EMSA was also observed for the previously discovered cofactors RSP3, SAM68, OGG1, and NPM1.

Upon stimulation, nuclear RelA and NME1 interact in the presence of genomic DNA. I speculated that NME1 and RelA only weakly associate *in vitro* in the absence of DNA and questioned if the presence of κB DNA can enhance the interaction through the transient ternary association between NME1:RelA:κB DNA. I performed the same pulldown experiment with GST and GST-NME1 with FL-RelA in the presence or absence of κB DNA (**Figure 4.15E**). A control mutated κB DNA that is known to not bind RelA was used as a negative control. As previously observed, there was no interaction with RelA and the GST control and only a weak interaction between RelA and NME1 in the absence of κB DNA. There was no increased interaction between RelA and NME1 with control mutated κB DNA pulldown, however the interaction was increased in the presence of κB DNA. This suggests that the interaction between RelA and NME1 is κB DNA mediated, perhaps through the formation of the transient complex. Altogether, I observe that NME1 can enhance κB DNA binding of RelA *in vitro* through direct protein-protein interactions, and these interactions are facilitated by κB DNA.

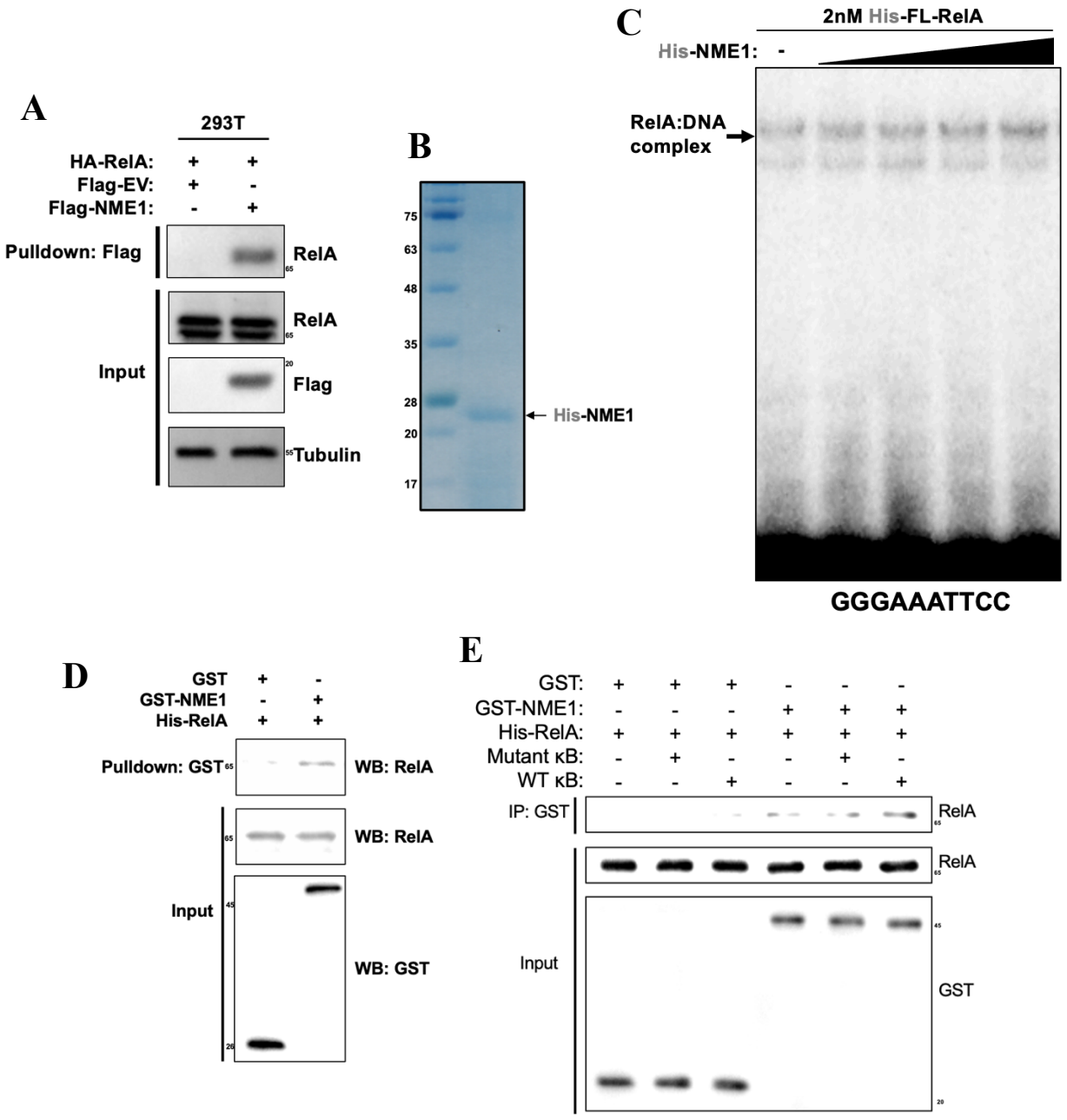

Figure 4.15: NME1 interacts directly with RelA and enhances binding affinity *in vitro*
A. FLAG pulldown assay in whole cell lysate from empty vector or FLAG-NME1 transfected HEK293T. Cells were cotransfected with HA-tagged RelA and precipitated proteins were analyzed by Western blot using the indicated antibodies. **B.** Coomassie stained protein gel of His-tagged NME1 purification from *E. coli.* **C.** EMSA assay with recombinant FL-RelA and increasing amounts of recombinant His-NME1. The sequence of the radiolabeled κB DNA probe is indicated below. **D.** GST-pulldown assay with purified GST or GST-NME and FL-RelA. **E.** GST-pulldown assay with GST or GST-NME1 and FL-RelA in the presence or absence mutated κB DNA or wild type κB DNA.

5. NME1 regulates NF-κB-dependent gene expression

I next examined if NME1 knockdown altered NF-κB-dependent gene expression in scramble KD compared to NME1 KD HeLa cells by RNA-seq. Duplicate mRNA libraries were prepared from scramble KD and NME1 KD HeLa with or without 1 hour of TNFα stimulation. As expected, the most significantly down regulated gene between scramble KD and NME1 KD irrespective of TNFα stimulation was NME1 (**Figure 4.16A**). Using a p-value cutoff of 0.01 and fold change cutoff of 2, I observed that NME1 KD increased expression of 244 genes relative to scramble KD and decreased expression of 108 genes in the unstimulated condition, suggesting that NME1 knockdown influences a broad spectrum of genes in the unstimulated context. TNFα stimulation induced the expression of 112 genes and decreased the expression of 7 genes in scramble KD cells, compared to an increased expression of 72 genes and decreased expression of 11 genes in NME1 KD cells. TNFα induced genes in both scramble KD and NME1 KD were enriched for known direct NF-κB targets, such as CXCL1, CXCL2, CXCL8, CCL2, TNFAIP3, IL6, and NFKBIA. In comparing scramble KD vs NME1 KD gene expression following TNFα stimulation, an increase in 222 genes and decrease in 145 genes was observed, suggesting that NME1 may play a role in regulating TNFα-dependent gene expression (**Figure 4.16B**). Examples of TNFα-dependent genes that had increased expression following NME1 KD were ZNF331, NR4A2, ATF3, PTGS2, and KLF10.

Of interest were TNFα-dependent genes with reduced expression upon NME1 KD as this set represents RelA-regulated genes that may be coactivated in the presence of NME1. Examples of genes include IL1A, CCL20, CXCL8, TNFAIP2, and NFKBIA. I validated the expression of IL1A, CCL20, CXCL8, TNFAIP2, and NFKBIA by RT-qPCR and observed that these genes were indeed induced upon TNFα treatment in both scramble KD and NME1 KD cells (**Figure**

4.16C). I also observed an overall reduction in expression following TNFα treatment when comparing NME1 KD to scramble KD in agreement with RNA-Seq data. A control RelA knockdown HeLa cell line (RelA KD) was generated to validate RelA-dependent expression of the target genes, and indeed I observed that total expression following TNFα treatment was significantly reduced in the absence of RelA. Altogether this data suggests that NME1 KD reduces a subset of RelA-dependent gene expression upon TNFα treatment.

I next tested if NME1 knockdown impacted RelA recruitment to target promotors as a mechanism for the observed downregulation of target genes. Using chromatin immunoprecipitation with qPCR (ChIP-qPCR), I tested TNFα-dependent RelA recruitment to CCL20, CXCL8, and NFKBIA in scramble KD and NME1 KD HeLa cells (**Figure 4.16D**). As expected, I observed very little RelA occupancy at target promoters in unstimulated cells but increased recruitment following 30 minutes of TNFα stimulation in both scramble KD and NME1 KD relative to control IgG. I also observed that RelA recruitment to target promoters was significantly reduced in NME1 KD relative to scramble KD following TNFα stimulation, suggesting that NME1 influences RelA recruitment to target promoters.

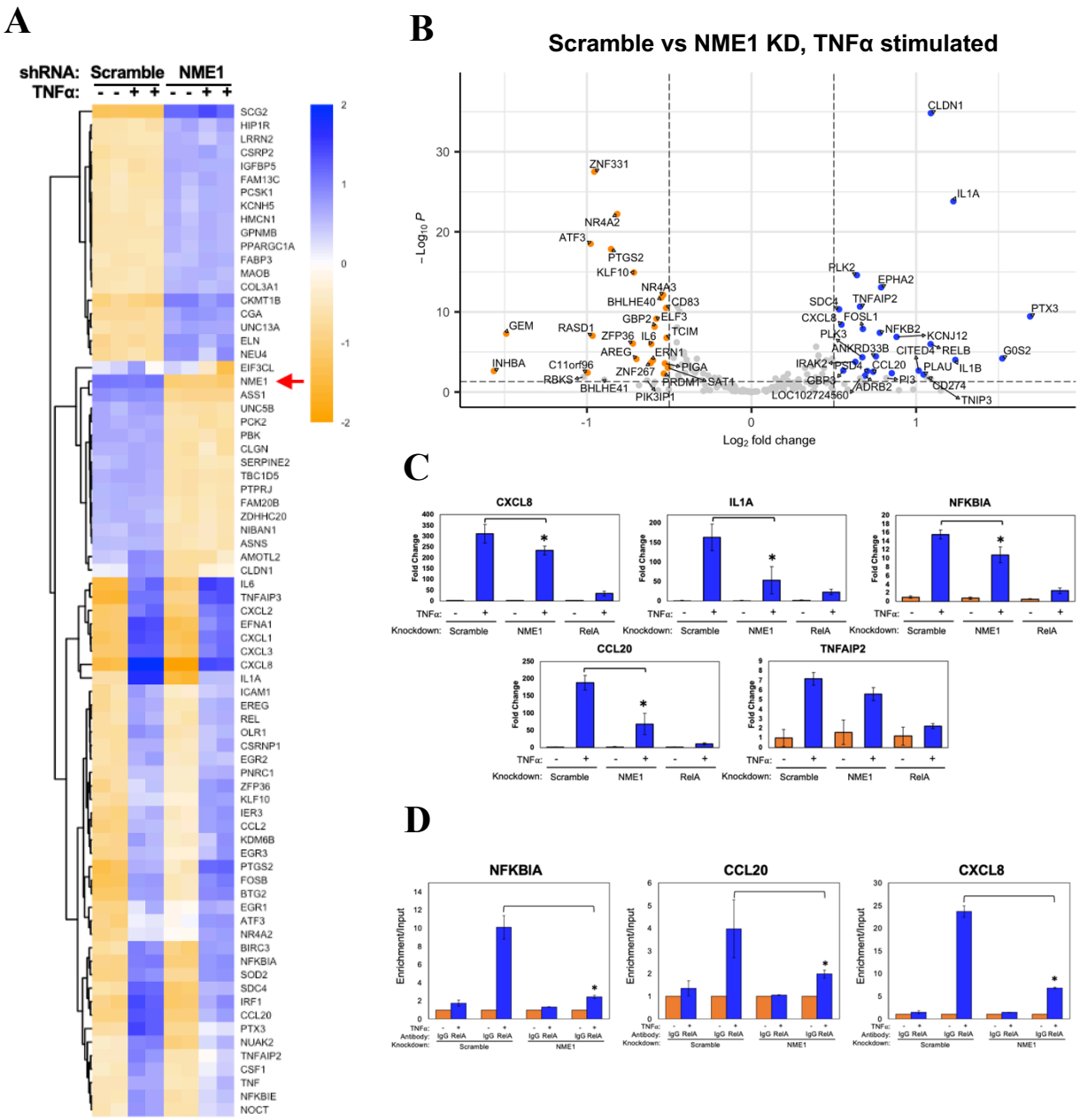

Figure 4.16: Genome-wide analysis of NME1-knockdown HeLa cells
A. Unsupervised hierarchical clustering of top 75 differentially expressed genes from RNA-seq of scramble and NME1 knockdown HeLa cells stimulated with TNFα for 1 hour. The red arrow indicates NME1 expression across cell lines. **B.** Volcano plot representing differentially expressed genes between scramble and NME1 knockdown HeLa cells following 1 hour TNFα stimulation. Genes were filtered to include only TNFα inducible genes (log_2 fold change > 0.5, p-value < 0.01). **C.** RT-qPCR analysis of differentially expressed genes in stable scramble, NME1, and RelA knockdown HeLa cell lines following 1 hour TNFα stimulation. Expression levels were normalized to GAPDH and values are represented as mean ± SD of three independent experimental replicates. **D.** RelA ChIP-qPCR in scramble and NME1 knockdown HeLa cells stimulated with TNFα for 30 minutes. Enrichment was normalized to input and values are represented relative IgG in three replicates.

D. Discussion

There has been a long-standing disconnect between binding affinity of purified recombinant NF-κB dimers and endogenous nuclear NF-κB. I initially set out to determine if factors constitutively present in the nucleus have the capacity to enhance κB DNA binding of recombinant NF-κB dimers. Indeed, I observed that unstimulated HeLa nuclear extract can significantly enhance κB DNA binding of recombinant FL-RelA *in vitro*, suggesting that factors within the nucleus play an important role in determining RelA binding affinity. Furthermore, I observed that nuclear extract enhances binding of FL-RelA without forming a discrete shifted complex, suggesting that transient and not stable interactions may facilitate this enhancement. This is further supported by previous gel shift studies of RelA and my data of RPS3, p53, and NME1. The nature of these transient interactions and how they combinatorially contribute to endogenous nuclear NF-κB binding to specific κB sites in the genome remains to be answered. It is likely that a single purified cofactor is not sufficient to recapitulate observed cellular NF-κB DNA binding affinity, and it is the DNA-mediated combination of several factors that collectively generate the transcriptionally competent RelA:κB DNA complex in the cell. This is supported by my observations that high relative molar concentrations of a single cofactor are generally required to significantly enhance FL-RelA DNA binding *in vitro*. Considering that the nuclear environment hosts a wide variety proteins at relatively low individual concentrations, it is unlikely that a single cofactor functions independently to enhance DNA binding of RelA. Also, my luciferase-based transcription assays show that overexpressed cofactors RPS3 and NME1 significantly enhance NF-κB-mediated transcriptional output, however only to a relatively modest extent.

Previously identified cofactors, such as RPS3 and p53, were not identified in my mass-spec analysis, suggesting a noncomprehensive identification of RelA-specific cofactors. One possibility is that these and other previously described cofactors were present and excluded during purification of nuclear extract. Another possibility is that cofactor mediated regulation is specialized and context-specific, with unique cofactors exerting cell-type and stimulus-dependent activity in specific κB sites. This is supported by the fact that previously described cofactors are active under specific stimulatory conditions in different cell types. For example, RPS3 was identified with a tandem affinity peptide fused RelA in HEK293T, and RPS3 modulated a specific subset of RelA-dependent genes under specific stimulatory conditions. SAM68 was identified in the constitutively active NF-κB T-cell lymphoma cell line HUT102 and displayed specificity to the CD25 promoter κB site. I identified NME1 in fractionated and unstimulated HeLa nuclear extract with the κB DNA sequence of GGGAAATTCC and observed that NME1 altered TNFα-dependent expression of a subset of RelA-dependent genes, further supporting the notion of context-specificity. Additionally, I observed that the recombinant cofactors OGG1 and HMGA1 did not alter binding of recombinant FL-RelA *in vitro*, suggesting that underlying cellular factors influence their activity towards RelA. These observations collectively outline the complexity of cofactor-mediated regulation of RelA DNA-binding and suggest that the context with regards to κB site, stimulation, and cell-type are important factors that motivate cofactor specificity.

As described in Chapter 2, I observed that dynamic and transient interactions play an important role in determining NF-κB DNA-binding affinity. Further, structural studies reveal that the modular architecture of NF-κB allows conformational alterations that enable NF-κB to engage κB DNA with minimal sequence conservation (Chen, 2000; Chen-Park, 2002; Cheng,

2011). This dynamic nature of κB DNA binding by NF-κB dimers creates an additional regulatory component that may influence DNA-binding affinity, and it is possible cofactors facilitate conformational alterations of NF-κB to guide κB-site specificity. It is also possible that one cofactor is not sufficient to promote such processes, and a comprehensive biophysical investigation would necessitate the proper combination of cofactors and appropriate κB DNA. A deeper understanding of cofactor-mediated regulation is required to design the appropriate experiments.

Because the interactions involving the RelA activation domain, RHR, and cofactors are dynamic, the activation domain can simultaneously contact other downstream effectors required for transcription initiation, including the histone acetylase CBP/p300, the Mediator complex, and RNA polymerase II. Interaction of RelA with cofactors can directly or allosterically influence transactivation domain dynamics. An additional potential role of the interaction of nuclear cofactors with RelA can be observed in recent work that demonstrated that the RelA activation domain is not essential for transcription of all RelA-dependent genes (van Essen, 2009). Transcriptional activation from these promoters requires other factors in addition to RelA, such as members of the AP1 transcription factor family. It is possible that not only the interaction between NF-κB and AP1 on these sites promote RelA:DNA binding, but also that AP1 activation domain cooperates to recruit RNA polymerase and initiate target gene transcription. This work thus leads to several novel ideas surrounding the mechanism of nuclear proteins cofactors. The hypotheses will direct the design of new experiments aimed at addressing the poorly understood but fundamental processes in the initiation of eukaryotic transcription.

E. Materials and Methods

1. Antibodies and Reagents

The GST (0020), β-tubulin (0119), and IκBα (0040) antibodies were purchased from BioBharati LifeScience. The RelA (sc-372) antibody used in Western blots, EMSA supershift, and ChIP assays was purchased from Santa Cruz Biotechnology. The FLAG (F1804) and control IgG ((12-371) antibodies were purchased from Sigma. The p84 (C1C3) antibody was purchased from GeneTex. The NME1 (3345) antibody was purchased from Cell Signaling. Mouse TNFα (BioBharati) was used at a final concentration of 20ng/mL for the indicated timepoints.

2. Mammalian Cell Culture and Transient Transfection

HeLa and HEK293T cell lines were maintained in Dulbecco's modified Eagle's medium (Corning) supplemented with 10% FBS and antibiotics.

For transient transfection of HEK293T, cells were plated in 6-well dishes at 80% confluence the day before transfection. The next day, 2 μg of DNA was mixed with 8μg of polyethylenimine (PEI) in OptiMEM (Gibco) at a total reaction volume of 50 μL. After incubation at room temperature for 15 minutes, cell media was exchanged to DMEM without FBS or antibiotics and DNA:PEI complexes were added dropwise over cells and left to incubate for 4 hours at 37°C. Media was then exchanged back to DMEM supplemented with 10% FBS and antibiotics and incubated for 16 hours before harvesting.

For preparation of HeLa nuclear extract, plated cells were harvested by scraping in PBS and lysed in hypototonic lysis buffer consisting of PBS supplemented with 0.1% (v/v) NP-40, 1 mM DTT, and 0.25mM PMSF. Nuclei were pelleted by centrifugation at 3000g, washed twice with ice-cold PBS, and resuspended in nuclear extraction buffer containing 25 mM Tris-HCl pH 7.5, 420 mM NaCl, 10% glycerol, 0.2 mM EDTA, 1 mM DTT, 0.5 mM PMSF, and mammalian

protease inhibitor cocktail (Sigma). After incubation on ice for 30 minutes, nuclei were centrifuged at 13,000 rpm for 15 minutes at 4°C. The supernatant containing nuclear extract was collected, snap frozen on liquid nitrogen, and stored at -80°C.

The list of oligonucleotides used for generation of stable knockdown HeLa cells are listed in **Table 4.1**. First, forward and reverse oligonucleotides for specific targets were annealed in buffer containing 10 mM Tris-HCl pH 7.5, 50 mM NaCl, and 1 mM EDTA by incubating in boiling water allowed to slowly cool to room temperature. Annealed DNA duplex was then ligated into the pLKO.1 TRC vector using the AgeI and EcoRI restriction sites. Lentivirus was then generated in 293T cells by cotransfecting the pLKO.1 construct with pMDLg/pRRE, pCMV-VSV-G, and pRSV-Rev expression constructs. After 48 hours, virus-containing supernatant was harvested, filtered through a 0.4 μm filter, and used to infect HeLa at a 1:10 dilution in the presence of 10 ng/μL polybrene (MilliporeSigma). After 48 hours, stably infected cells were selected by treatment of 1 μg/mL puromycin in culture media and continuously maintained in the presence of 1 μg/mL puromycin.

3. Protein Expression and Purification

Expression and purification of His-tagged full-length RelA from Sf9 cells and His-tagged RelA RHR (19-304) in *E. coli* Rosetta (DE3) was performed as outlined in Chapter 2.

Recombinant His-RPS3 was expressed in *E. coli* Rosetta (DE3) cells by growing cells to an OD_{600} of 0.2 followed by induction with 1 mM IPTG overnight at 16°C. Cells were lysed with lysis buffer containing 40 mM Tris-HCl pH 8.0, 150 mM NaCl, 10% glycerol, 0.2% Triton X-100, 2.5 mM β-mercaptoethanol, 1 mM PMSF, and 10 mM imidazole and sonicated. The lysate was clarified by centrifugation at 13000 rpm for 30 min at 4 °C. The supernatant was mixed with nickel-NTA resin (BioBharati) pre-equilibrated with lysis buffer in batch for 2 hours at 4 °C in a

rotary shaker. Then, the resin was washed four times with wash buffer (same as lysis buffer but with 30 mM imidazole), and protein was eluted with elution buffer containing 40 mM Tris-HCl pH 8.0, 150 mM NaCl, 10% glycerol, 2.5 mM β-mercaptoethanol, and 400 mM imidazole. Peak fractions were pooled and stored at 4 °C.

His-tagged p53 was cloned into the pET-24d vector and expressed in *E. coli* Rosetta (DE3) cells by growing cells to an OD_{600} of 0.2 followed by induction with 0.1 mM IPTG overnight at room temperature. Cells were lysed with lysis buffer containing 25 mM sodium phosphate pH 7.5, 300 mM NaCl, 5% glycerol, 0.2% Triton X-100, 10mM imidazole, 5 mM β-mercaptoethanol and 0.5mM PMSF and sonicated. The lysate was clarified by centrifugation at 13000 rpm for 30 min at 4°C. The supernatant was loaded onto a nickel-NTA resin (BioBharati) column pre-equilibrated with lysis buffer. Then, the resin was washed with 10 column volumes of wash buffer (same as lysis buffer but with 500 mM NaCl and 45mM imidazole), and protein was eluted with elution buffer (same as lysis buffer but without PMSF and with 250 mM imidazole). Peak fractions were pooled and filtered through a 0.22 μm filter. Then, the sample was loaded onto a Superdex 200 size exclusion column (Amersham Biosciences) pre-equilibrated with SEC buffer containing 25 mM sodium phosphate pH 7.5, 300 mM NaCl, 5% glycerol, 5 mM DTT, and 0.5 mM EDTA. Peak fractions were pooled and concentrated using a Centriprep 30 kDa cutoff membrane concentrator unit (Millipore). Lastly, aliquots were snap frozen in liquid nitrogen and stored at -80°C.

His-tagged NME1 was cloned into the pET-24d vector and expressed in *E. coli* Rosetta (DE3) by growing cells to an OD_{600} of 0.4 and inducing with 0.25 mM IPTG overnight at room temperature. Cells were pelleted by centrifugation and lysed by sonication in lysis buffer containing 25 mM Tris-HCl pH 7.5, 300 mM NaCl, 5% glycerol, 0.1% NP-40, 10 mM

imidazole, 5 mM β-mercaptoethanol, and 0.25 mM PMSF. Lysate was clarified by centrifugation at 14,000 rpm for 30 minutes at 4°C and incubated with nickel-NTA agarose beads (BioBharati LifeScience) for 2 hours at 4°C on a rotary shaker. Beads were then extensively washed with lysis buffer and His-tagged NME1 was eluted in lysis buffer without PMSF but supplemented with 250 mM imidazole. Protein quality was assessed by SDS-PAGE with Coomassie staining and peak fractions were pooled, snap frozen on liquid nitrogen, and stored at -80°C.

NME1 was cloned into the pGEX-4T2 GST vector and both GST and GST-tagged NME1 were expressed in *E. coli* Rosetta (DE3). Cells were grown to an OD_{600} of 0.3 and induced with 0.25 mM IPTG overnight at 16°C. Cells were then pelleted by centrifugation and lysed by sonication in lysis buffer containing 50 mM Tris-HCl pH 7.5, 200 mM NaCl, 5% glycerol, 0.1% NP-40, 0.5 mM EDTA, 1 mM DTT, and 0.25 mM PMSF. The lysate was then clarified by centrifugation at 14,000 rpm for 30 minutes at 4°C and incubated with pre-equilibrated glutathione agarose beads (BioBharati LifeScience) for 2 hours at 4°C on a rotary shaker. Beads were then extensively washed with lysis buffer and eluted lysis buffer without PMSF but with 25 mM reduced glutathione (Sigma-Aldrich). Eluted protein was then dialyzed in a 6-8 kDa MWCO membrane three times in 1L of dialysis buffer containing 50 mM Tris-HCl pH 7.5, 200 mM NaCl, 5% glycerol, 0.5 mM EDTA, and 1 mM DTT and dialyzed once in 200 mL of dialysis buffer containing 50% glycerol. The dialyzed 50% glycerol stock protein was then stored at -20°C.

4. Electrophoretic Mobility Shift Assay

Radiolabeled probes were incubated with the proteins under study for 20 minutes at room temperature in binding buffer containing 10 mM Tris-HCl pH 7.5, 50 mM NaCl, 10% glycerol, 1% NP-40, 1 mM EDTA, and 0.1 mg/mL poly(dI-dC). When needed, proteins were diluted in

dilution buffer containing 20 mM Tris-HCl pH 7.5, 50 mM NaCl, 10% glycerol, 1 mM DTT, and 0.2 mg/mL BSA. Samples were run through a 4% nondenatured polyacrylamide gel in TGE buffer (24.8 mM Tris base, 190 mM glycine, and 1 mM EDTA) at 200V for 1 hour. Gel was then dried, exposed on a phosphor screen overnight, and scanned by Typhoon FLA 9000 imager (Cytiva).

5. Fractionation and Identification of RelA-Specific Cofactors

Unstimulated HeLa nuclear extract was collected from three 15 cm dishes in a total volume of 500 µL and cleared by centrifugation at 13,000 rpm for 15 minutes at 4°C. Supernatant was collected and fractionated through a pre-equilibrated 24 mL Superose 6 (Cytiva) size-exclusion column in SEC buffer containing 25 mM Tris-HCl pH 7.5, 420 mM NaCl, 10% glycerol, 0.2 mM EDTA, 1 mM DTT, and 0.5 mM PMSF. 42 fractions at a volume of 330 µL (14 mL total volume) were collected starting 8 mL after injection, and 2 µL from fractions were tested for activity by EMSA with 5 nM of recombinant full-length RelA. Fractions 16-19 showed the most activity and were therefore combined and diluted in SEC buffer without NaCl to a final 100 mM NaCl concentration. The pooled extract was then centrifuged at 13,000 rpm for 15 minutes at 4°C and supernatant was passed through a 3 mL Mono Q (Cytiva) anion exchange column. The column was then washed with 10 mL of buffer containing 25 mM Tris-HCl pH 7.5, 100 mM NaCl, 10% glycerol, and 1 mM DTT and bound proteins were eluted with 10 mL of the same buffer but with an increasing NaCl gradient up to 700 mM NaCl. A total of 40 250 µL fractions were collected and 2 µL from fractions were tested for activity by EMSA with recombinant full-length RelA.

The fractions corresponding to Q20, Q23, Q26, Q29, and Q32 showed the highest activity and were further tested for RelA DNA-binding enhancement in an *in vitro* biotinylated

DNA-pulldown assay. Biotinylated DNA was annealed as outlined previously in buffer containing 10 mM Tris-HCl pH 7.5, 50 mM NaCl, and 1 mM EDTA and immobilized onto streptavidin agarose beads (BioBharati LifeSciences) in buffer containing 25 mM Tris-HCl pH 7.5, 150 mM NaCl, 5% glycerol, 0.1% and 1 mM DTT. Beads were then washed to remove unbound DNA and mixed with 100 ng of recombinant full-length RelA at a total volume of 200 μL. 10 μL of the corresponding Mono Q fractions were added and samples were rotated for 2 hours at 4°C. Beads were then pelleted by centrifugation and washed 4 times with the same pulldown buffer. After the final wash, 4x SDS gel loading dye was added to the beads at a final dilution of 1x and beads were boiled for 10 minutes. Samples were centrifuged at 13,000 rpm for 5 minutes and supernatant was separated by SDS-PAGE and analyzed by Western blot.

Fraction Q23 showed the highest activity in both EMSA and the DNA pulldown assay and was therefore further investigated by mass-spec for peptide identification. A final pulldown was performed in buffer containing 25 mM Tris-HCl pH 7.5, 150 mM NaCl, 5% glycerol, and 1 mM DTT with 100 ng of recombinant full-length RelA, fraction Q23, and biotinylated-DNA immobilized onto streptavidin agarose beads. A control pulldown was also prepared in parallel without recombinant RelA added. The reactions were incubated overnight at 4°C with gentle rotation. Beads were then washed with the pulldown buffer 3 times and precipitated peptides were identified by liquid chromatography with mass spectrometry (LC-MS) at the UCSD Biomolecular and Proteomics Mass Spectrometry Facility.

6. Fluorescence Polarization Assay

RelA dimers or other proteins were titrated against 1nM fluorescein-labeled HIV-κB DNA. Fluorescence anisotropy was measured on a nonbinding 96-well black bottom plate (Greiner) using a Tecan Safire 2 plate reader in polarization mode with an excitation wavelength

of 470nm and an emission wavelength of 520 nm with a 2 nm bandwidth. Most measurements were taken in anisotropy buffer containing 25 mM Tris-HCl pH 7.5, 150 mM NaCl, 5% glycerol, 0.25 mg/mL BSA, 200 nM nonspecific DNA, and 0.5% NP-40, with an incubation of 15 min at room temperature. Measurements with KCl, KOAc, and KGlu were performed in anisotropy buffer, except with NaCl substituted with the corresponding salt. For heat-inactivated RPS3, His-RPS3 was diluted in anisotropy buffer without nonspecific DNA and incubated for 10 min at 90°C, followed by cooling on ice for 5 min. Samples containing p53 were measured in buffer containing 25 mM Tris-HCl pH 8.0, 125 mM NaCl, 5% glycerol, 0.25 mg/mL BSA, 200 nM nonspecific DNA, and 0.1% NP-40, with a 90 min incubation at 4 °C. The sequence ATCGTGCATATTGCTACTAGCGTTTTTGGA was used as nonspecific DNA for the binding assays, and the fluorescein-labeled single-stranded DNA ATCGTGGGAAAGTTTCTGGATA-TTCCCTTGGA was used as a negative control. To quantify the binding affinity between RelA and DNA, the anisotropy data from each binding assay were normalized to the initial value without protein, plotted, and fit to the quadratic equation below to calculate the equilibrium dissociation constant (K_D) as described previously. GraphPad PRISM 4.0 (GraphPad Software, San Diego, CA) was used to perform the curve fits. All experiments were performed a minimum of two or three times to determine the standard deviations.

7. Luciferase Assays

Complementary oligonucleotides were first annealed by mixing at a final concentration of 2 μM in buffer containing 10 mM Tris-HCl pH 7.5, 50 mM NaCl, and 1 mM EDTA and incubating in boiling water allowed to slowly cool to room temperature. Annealed promoters were then cloned into the CMXTK-Luciferase vector (a kind gift from Dr. Chakravarti at Northwestern University Feinberg School of Medicine) at the SalI and BamHI restriction sites.

HEK293T were grown in 12-well plates and transiently transfected with the FLAG-tagged overexpression construct or empty vector control, luciferase reporter DNA, and control CMV-driven Renilla. After 24 hours, cells were stimulated for 8 hours with 20 ng/mL mouse TNFα. Lysate was then collected and used for luciferase activity assay using the Dual-Luciferase Reporter Assay System (Promega). Data are represented as mean ± standard deviations (SD) of three or more independent experimental replicates.

8. Pulldown Assays

NME1 was cloned into a modified pEYFP-c1 vector with YFP removed and substituted for an N-terminal FLAG tag. The day before transfection, HEK293T was plated on a 6-well plate. The next day, the cells were at approximately 80% confluence and transfected with either FLAG empty vector or FLAG-tagged NME1 with PEI. The next day, cells were washed with ice-cold PBS and lysed directly on the plate in buffer containing 25 mM Tris-HCl pH 7.5, 150 mM NaCl, 5% glycerol, 1% NP-40, 1 mM DTT, and 0.5 mM PMSF by gentle rocking at 4°C for 15 minutes. Lysate was then collected and centrifuged at 13,000 rpm for 15 minutes at 4°C. Supernatant was then collected and mixed with 50 µL of preequilibrated anti-FLAG M2 beads (Sigma) for 2 hours at 4°C on a rotary shaker. Beads were then extensively washed and mixed with 4x SDS gel loading dye to a final dilution of 1x. Samples were boiled for 5 minutes and centrifuged for 5 minutes at 13,000rpm. Supernatant was then resolved by SDS-PAGE and analyzed by Western blot.

For GST pulldown assays, first 1µg of GST or GST-tagged NME1 was mixed with 50 µL of preequilibrated glutathione agarose beads (BioBharati LifeScience) in 200 µL of pulldown buffer containing 25 mM Tris-HCl pH 7.5, 150 mM NaCl, 5% glycerol, 0.1% NP-40, and 1 mM DTT. Samples were mixed for 1 hour at 4°C with gentle rotation. Beads were then washed 4

times with pulldown buffer to wash unbound proteins and brought to a final volume of 200 μL after the last wash. 1 μg of recombinant full-length RelA and 1 μM of annealed κB or mutant κB DNA was then added and the reaction was incubated for 2 hours at 4°C with gentle rotation. Beads were then extensively washed and mixed with 4x SDS gel loading to a final dilution of 1x. Samples were then boiled for 5 minutes and centrifuged at 13,000rpm for 5 minutes. Supernatant was then resolved by SDS-PAGE and analyzed by Western blot.

9. RNA Isolation and Real-Time qPCR

A list of oligonucleotides used in RT-qPCR reactions is listed in **Table 4.1**. HeLa was plated in 6 well dishes and total RNA was isolated the next day with TRIzol (Invitrogen) and purified by isopropanol precipitation following the manufacturers recommendations. RNA concentration was determined by nanodrop and cDNA was synthesized in a 5 μL reaction from 500 ng of RNA using SuperScript IV VILO Master Mix (ThermoFisher). The cDNA was then diluted 1:4 to a total volume of 20 μL and 1 μL was used as template for qPCR with the Luna qPCR Master Mix (New England Biolabs) in a total reaction volume of 10 μL. Values were normalized to GAPDH and data are represented as mean ± standard deviation of three independent experimental replicates.

10. Chromatin Immunoprecipitation qPCR

A list of oligonucleotides used in ChIP-qPCR experiments is listed in **Table 4.1**. For every two immunoprecipitation reactions, a confluent 10 cm dish of HeLa was used. Cells were first treated with TNFα or DMSO for 30 minutes. Formaldehyde was then added directly to the media at a final concentration of 1% and incubated on the cells for 10 minutes at room temperature with gentle rocking. Crosslinking was then quenched by addition of 125 mM glycine and incubation at room temperature for 5 minutes with gentle rocking. Cells were then washed

twice with ice-cold PBS and collected by scraping in 1mL of PBS. Cells were then pelleted by centrifugation and resuspended in 1 mL of PBS supplemented with 0.1% NP-40, 1 mM DTT, and 0.25 mM PMSF. The cell pellet was then gently pipetted 5 times to facilitate cytoplasmic lysis and nuclear fractionation, and nuclei was then pelleted by centrifugation. The nuclear pellet was then resuspended in 1 mL of RIPA buffer containing 50 mM Tris-HCl pH 7.5, 150 mM NaCl, 2 mM EDTA, 1% NP-40, 0.1% sodium deoxycholate, 0.1% SDS, 0.5 mM PMSF, and mammalian protease inhibitor cocktail (Sigma). Resuspended nuclei were sonicated on ice with a micro tip sonicator (Branson) to generate DNA fragments with an average length of 500 bp. Sonicated nuclear extract was then centrifuged at 13,000 rpm for 15 minutes at 4°C and supernatant was precleared with 25 µL protein AG PLUS agarose beads (BioBharati LifeScience) and 500 ng of IgG control antibody (ThermoFisher) for 1 hour at 4°C with rotation. Extract was then centrifuged at 13,000 rpm for 10 minutes at 4°C, and precleared supernatant was divided into two equal reactions and mixed with 25 µL of protein AG PLUS agarose beads and 500 ng of either IgG or anti-RelA antibody. Immunoprecipitation reactions were incubated at 4°C overnight with gentle rotation. Beads were then washed three times for 5 minutes each with 1 mL of RIPA buffer, then RIPA buffer supplemented with 500 mM NaCl, RIPA buffer with NaCl substituted with 250 mM LiCl, and lastly with TE buffer containing 10 mM Tris-HCl pH 7.5 and 1 mM EDTA. Immune complexes were then eluted from beads in 150 µL of elution buffer containing 1% SDS and 100 mM sodium bicarbonate pH 8.0 for 30 minutes at room temperature with rotation. Eluted complex was then mixed to 6 µL of 5 M NaCl and 2 µL of 100 mg/mL RNase A (Qiagen) and incubated overnight at 65°C to reverse cross-linking and digest RNA. The next morning, 2 µL of Proteinase K (Invitrogen) was added and incubated at 60°C for 1 hour. DNA was then extracted with phenol:chloroform:isoamyl alcohol (25:24:1) (Invitrogen)

and isopropanol precipitation following manufacturers recommendation. DNA pellet was resuspended in 50 μL of TE buffer and 1 μL was used in qPCR reaction with Luna qPCR Master Mix (New England Biolabs).

11. RNA Sequencing and Analysis

Scramble and NME1 knockdown HeLa cell lines were initially plated on 6 well plates. The next day, duplicate wells from each cell line were treated for 1 hour with either DMSO or 20 ng/mL TNFα. Cells were then washed once with ice-cold PBS and RNA was isolated with TRIzol (Invitrogen) following manufacturers recommendations. RNA quality was then assessed by TapeStation (Agilent) and RNA with a RIN score greater than 8.0 was further processed. Poly-A enriched libraries were prepared from 1 μg of total RNA using the mRNA HyperPrep Kit (KAPA) with unique dual-indexed adapters (KAPA) following manufacturers recommendations. Library quality was assessed by DNA TapeStation (Agilent) and quantified with Qubit 2.0 fluorometer (Life Technologies). Libraries were pooled and underwent paired-end sequencing using the NovaSeq6000 (Illumina) at the UCSD Institute for Genomic Medicine (IGM).

For analysis of sequencing data, read quality was first checked by FASTQC. Reads were then mapped to human genome using OSA/Oshell (Omicsoft). Reads were then normalized and differentially expressed genes were analyzed using DESeq2 (v1.38.3).

Table 4.1: Sequences of oligonucleotides used in shRNA cloning, RT-qPCR, and ChIP-qPCR.

Target	Assay	Primer	Sequence (5' → 3')
Scramble-pLKO	shRNA cloning	Forward	CCGGCCTAAGGTTAAGTCGCCCTCGCTCGAGCGAGGGCGACTTAACCTTAGGTTTTTG
		Reverse	AATTCAAAAACCTAAGGTTAAGTCGCCCTCGCTCGAGCGAGGGCGACTTAACCTTAGG
NME1-pLKO	shRNA cloning	Forward	CCGGGCTCAGAACTGGATCTATGAACTCGAGTTCATAGATCCAGTTCTGAGCTTTTTG
		Reverse	AATTCAAAAAGCTCAGAACTGGATCTATGAACTCGAGTTCATAGATCCAGTTCTGAGC
NME1	RT-qPCR	Forward	GTAGTTGCCATGGTCTGGGA
		Reverse	GAAACCACAAGCCGATCTCC
GAPDH	RT-qPCR	Forward	GTCTCCTCTGACTTCAACAGCG
		Reverse	ACCACCCTGTTGCTGTAGCCAA
CCL20	RT-qPCR	Forward	CGAATCAGAAGCAGCAAGCA
		Reverse	TGATGTCACAGCCTTCATTGG
CXCL8	RT-qPCR	Forward	TGGCAGCCTTCCTGATTTCT
		Reverse	AATTTCTGTGTTGGCGCAGT
TNFAIP2	RT-qPCR	Forward	CACAGATAAAGCGGGTGCTG
		Reverse	TAATTCGTCAGCTGCTTGCC
NFKBIA	RT-qPCR	Forward	TCCTGAGCTCCGAGACTTTC
		Reverse	CACGTGTGGCCATTGTAGTT
TNF	RT-qPCR	Forward	CTGCACTTTGGAGTGATCGG
		Reverse	AGGGTTTGCTACAACATGGG
NFKBIA	ChIP-qPCR	Forward	AAGAGAACTGGCTTCGTCCT
		Reverse	ATCAAAAAGTTCCCTGTCCGT
CCL20	ChIP-qPCR	Forward	TTCGCACCTTCCCAATATGAG
		Reverse	TGTACACAGAAGGCGTGTTG
CXCL8	ChIP-qPCR	Forward	GTGTGATGACTCAGGTTTGC
		Reverse	TTTGTGCCTTATGGAGTGCT

F. Acknowledgements

I would like to especially thank Dr. Maria Carmen Mulero Roig for help with EMSA, assays with RPS3 and p53, and guidance throughout experiments. I would like to thank Dr. Mano Maurya and Dr. Shankar Subramaniam for help with RNA sequencing and analysis. I would like to thank Dr. Majid Ghassemian for help with mass spectrometry. I would like to thank Dr. Kaushik Saha and Dr. Tapan Biswas for help with experimental design. I would like to thank Dr. Youssi Athar and Dr. Simpson Joseph for help with fluorescence polarizations assays.

Chapter 4, in part, is currently being prepared for submission for publication of the material. Shahabi, Shandy; Ghosh, Gourisankar. The dissertation author was the primary investigator and author of this material.

Chapter 5: Discussion

Research presented in this thesis uncovered three new attributes that are important regulatory niches in transcription; 1) Discriminatory contacts between NF-κB and κB DNAs can occur on short timescales that cannot be visualized by x-ray structural models. 2) Multiple cofactors are required to enable the NF-κB:DNA complex formation. 3) Promoter κB sites are continuously recognized by a vast number of nucleic acid binding proteins, including sequence-specific TFs. Collectively, these factors influence TF-DNA binding to regulate gene expression.

MD simulations and structural analyses allowed me to propose a stereochemical principle for NF-κB:κB DNA complex formation at different timescales. Although no base-specific interactions were observed at the central nucleotide, a single nucleotide substitution at this position profoundly impacts NF-κB DNA binding affinity and kinetics. I found that dynamic interactions not observed in x-ray crystal structures can induce structural changes that propagate throughout the NF-κB-DNA interface to influence discriminatory DNA binding. These results suggests that structurally unobserved transient interactions and transcription factor dynamics can influence TF:DNA complex formation to facilitate transcription activation. Additional biophysical experiments, such as NMR, would be useful in understanding the influence of the central nucleotide and dynamic interactions with RelA on a longer different timescale.Further, binding assays with nucleotide analogs at the central base of κB DNA would be useful in probing how dynamic interactions influence binding affinity.

I also found that promoters of rapidly activated NF-κB-dependent genes contain several low affinity κB sites. Transcription activation assays reveal that promoters containing a single high affinity κB site cannot be fully activated by RelA, and two κB sites can activate transcription synergistically even if they are low affinity sequences or spaced 100 bp apart. Our lab has previously reported that transcriptional activity by NF-κB to κB DNA is not correlated

with binding affinity, and I observed that the magnitude of transcription activation is correlated with the concentration-dependent DNA occupancy, not binding affinity, at multiple κB sites. Interestingly, I also observed that κB sites can bind several other TFs with specificity. That is, the κB sites are not just the binding sites for NF-κB, but other TFs can also use κB sites or overlapping sites. Therefore, through variations in the sequences of κB sites, this expands the diversity of alternate TFs that bind at κB site-containing promoters. Although competitive interactions prevent simultaneous binding of TFs on the same DNA molecule, DNA can be cooperatively occupied by several factors within a time window, thus leading enhanced collective promoter occupancy. I propose that TF-DNA binding is both cooperative and competitive and overall promoter occupancy is critical for transcriptional output. Establishing this requires further experimental investigation, and future work is directed towards understanding the biochemical mechanism of cooperativity between multiple TFs. Mutagenesis and luciferase activation assays will be performed to probe the interactions between RelA and Nfatc1 on κB sites. Additionally, ChIP will be performed to understand how RelA binding to promoters is affected upon knockdown of cofactors or CRISPR-mediated genome editing of weak κB sites. Lastly, pulldown experiments with different κB sites and in different cell-types will be performed to understand specificity of cooperative TF regulation.

Cofactor-mediated transcription factor DNA-binding is recently emerging as an important layer of gene regulation. However, the mechanisms underlying this process is still unclear. In this work, I found that NME1 is a RelA-specific cofactor that is required for inducible transcription by RelA. Although NME1 directly stabilizes the RelA:κB DNA complex, it is still unclear if NME1 can also directly contact DNA. If NME1 binds DNA to augment RelA DNA-binding affinity, then NME1 can be categorically considered as a noncanonical DNA binding

transcription factor. However, it is also possible that NME1 allosterically enhances RelA DNA binding through DNA-independent protein-protein interactions. Altogether, I observe that NME1, like other nuclear cofactors, can stabilize the NF-κB:DNA complex through transient interactions to influence transcription at specific κB sites. Future experiments will be directed towards understanding mechanistically how NME1 influences RelA DNA binding affinity. Deletion mapping and mutagenesis will be performed to understand where RelA and NME1 interact. Additionally, the combinatorial influence of NME1 and other cofactors will be explored to understand how multiple cofactors influence RelA DNA binding. Lastly, mass spectrometry will be performed with IL1A promoter DNA and unstimulated nuclear extract to identify additional cofactors that modulate basal IL1A expression.

REFERENCES

Allison, D. F., Wamsley, J. J., Kumar, M., Li, D., Gray, L. G., Hart, G. W., Jones, D. R., & Mayo, M. W. (2012). Modification of RelA by O-linked N-acetylglucosamine links glucose metabolism to NF-κB acetylation and transcription. *Proceedings of the National Academy of Sciences of the United States of America*, *109*(42), 16888–16893. https://doi.org/10.1073/pnas.1208468109

Ankers, J. M., Awais, R., Jones, N. A., Boyd, J., Ryan, S., Adamson, A. D., Harper, C. V., Bridge, L., Spiller, D. G., Jackson, D. A., Paszek, P., Sée, V., & White, M. R. (2016). Dynamic NF-κB and E2F interactions control the priority and timing of inflammatory signalling and cell proliferation. *ELife*, *5*, e10473. https://doi.org/10.7554/eLife.10473

Badran, B. M., Wolinsky, S. M., Burny, A., & Willard-Gallo, K. E. (2002). Identification of three NFAT binding motifs in the 5'-upstream region of the human CD3gamma gene that differentially bind NFATc1, NFATc2, and NF-kappa B p50. *The Journal of Biological Chemistry*, *277*(49), 47136–47148. https://doi.org/10.1074/jbc.M206330200

Baldwin, A. S. (1996). THE NF-κB AND IκB PROTEINS: New Discoveries and Insights. *Annual Review of Immunology*, *14*(1), 649–681. https://doi.org/10.1146/annurev.immunol.14.1.649

Berg, O. G., Winter, R. B., & von Hippel, P. H. (1981). Diffusion-driven mechanisms of protein translocation on nucleic acids. 1. Models and theory. *Biochemistry*, *20*(24), 6929–6948. https://doi.org/10.1021/bi00527a028

Bergqvist, S., Alverdi, V., Mengel, B., Hoffmann, A., Ghosh, G., & Komives, E. A. (2009). Kinetic enhancement of NF-κB·DNA dissociation by IκBα. *Proceedings of the National Academy of Sciences*, *106*(46), 19328–19333. https://doi.org/10.1073/pnas.0908797106

Blainey, P. C., Luo, G., Kou, S. C., Mangel, W. F., Verdine, G. L., Bagchi, B., & Xie, X. S. (2009). Nonspecifically bound proteins spin while diffusing along DNA. *Nature Structural & Molecular Biology*, *16*(12), 1224–1229. https://doi.org/10.1038/nsmb.1716

Boissan, M., Dabernat, S., Peuchant, E., Schlattner, U., Lascu, I., & Lacombe, M.-L. (2009). The mammalian Nm23/NDPK family: From metastasis control to cilia movement. *Molecular and Cellular Biochemistry*, *329*(1–2), 51–62. https://doi.org/10.1007/s11010-009-0120-7

Bonnet, I., Biebricher, A., Porté, P.-L., Loverdo, C., Bénichou, O., Voituriez, R., Escudé, C., Wende, W., Pingoud, A., & Desbiolles, P. (2008). Sliding and jumping of single EcoRV restriction enzymes on non-cognate DNA. *Nucleic Acids Research*, *36*(12), 4118–4127. https://doi.org/10.1093/nar/gkn376

Burke, S. J., Lu, D., Sparer, T. E., Masi, T., Goff, M. R., Karlstad, M. D., & Collier, J. J. (2014). NF-κB and STAT1 control CXCL1 and CXCL2 gene transcription. *American Journal of*

Physiology-Endocrinology and Metabolism, *306*(2), E131–E149. https://doi.org/10.1152/ajpendo.00347.2013

Chen, J., & Chen, Z. J. (2013). Regulation of NF-κB by ubiquitination. *Current Opinion in Immunology*, *25*(1), 4–12. https://doi.org/10.1016/j.coi.2012.12.005

Chen, L., Glover, J. N. M., Hogan, P. G., Rao, A., & Harrison, S. C. (1998). Structure of the DNA-binding domains from NFAT, Fos and Jun bound specifically to DNA. *Nature*, *392*(6671), 42–48. https://doi.org/10.1038/32100

Chen, Y. Q., Sengchanthalangsy, L. L., Hackett, A., & Ghosh, G. (2000). NF-kappaB p65 (RelA) homodimer uses distinct mechanisms to recognize DNA targets. *Structure (London, England: 1993)*, *8*(4), 419–428. https://doi.org/10.1016/s0969-2126(00)00123-4

Chen, Y.-Q., Ghosh, S., & Ghosh, G. (1998). A novel DNA recognition mode by the NF-κB p65 homodimer. *Nature Structural Biology*, *5*(1), 67–73. https://doi.org/10.1038/nsb0198-67

Cheng, C. S., Feldman, K. E., Lee, J., Verma, S., Huang, D.-B., Huynh, K., Chang, M., Ponomarenko, J. V., Sun, S.-C., Benedict, C. A., Ghosh, G., & Hoffmann, A. (2011). The Specificity of Innate Immune Responses Is Enforced by Repression of Interferon Response Elements by NF-κB p50. *Science Signaling*, *4*(161). https://doi.org/10.1126/scisignal.2001501

Chen-Park, F. E., Huang, D.-B., Noro, B., Thanos, D., & Ghosh, G. (2002). The κB DNA Sequence from the HIV Long Terminal Repeat Functions as an Allosteric Regulator of HIV Transcription. *Journal of Biological Chemistry*, *277*(27), 24701–24708. https://doi.org/10.1074/jbc.M200007200

Choudhuri, T., Verma, S. C., Lan, K., & Robertson, E. S. (2006). Expression of alpha V integrin is modulated by Epstein-Barr virus nuclear antigen 3C and the metastasis suppressor Nm23-H1 through interaction with the GATA-1 and Sp1 transcription factors. *Virology*, *351*(1), 58–72. https://doi.org/10.1016/j.virol.2006.03.031

Choy, M.-K., Movassagh, M., Siggens, L., Vujic, A., Goddard, M., Sanchez, A., Perkins, N., Figg, N., Bennett, M., Carroll, J., & Foo, R. (2010). High-throughput sequencing identifies STAT3 as the DNA-associated factor for p53—NF-kappaB - complex-dependent gene expression in human heart failure. *Genome Medicine*, *2*(6), 37. https://doi.org/10.1186/gm158

Conboy, I. M., Manoli, D., Mhaiskar, V., & Jones, P. P. (1999). Calcineurin and vacuolar-type H^+-ATPase modulate macrophage effector functions. *Proceedings of the National Academy of Sciences*, *96*(11), 6324–6329. https://doi.org/10.1073/pnas.96.11.6324

Crawley, C. D., Raleigh, D. R., Kang, S., Voce, D. J., Schmitt, A. M., Weichselbaum, R. R., & Yamini, B. (2013). DNA damage-induced cytotoxicity is mediated by the cooperative interaction of phospho-NF-κB p50 and a single nucleotide in the κB-site. *Nucleic Acids Research*, *41*(2), 764–774. https://doi.org/10.1093/nar/gks1120

Crocker, J., Abe, N., Rinaldi, L., McGregor, A. P., Frankel, N., Wang, S., Alsawadi, A., Valenti, P., Plaza, S., Payre, F., Mann, R. S., & Stern, D. L. (2015). Low affinity binding site clusters confer hox specificity and regulatory robustness. *Cell*, *160*(1–2), 191–203. https://doi.org/10.1016/j.cell.2014.11.041

Cross, S. L., Halden, N. F., Lenardo, M. J., & Leonard, W. J. (1989). Functionally distinct NF-kappa B binding sites in the immunoglobulin kappa and IL-2 receptor alpha chain genes. *Science (New York, N.Y.)*, *244*(4903), 466–469. https://doi.org/10.1126/science.2497520

Csumita, M., Csermely, A., Horvath, A., Nagy, G., Monori, F., Göczi, L., Orbea, H.-A., Reith, W., & Széles, L. (2020). Specific enhancer selection by IRF3, IRF5 and IRF9 is determined by ISRE half-sites, 5′ and 3′ flanking bases, collaborating transcription factors and the chromatin environment in a combinatorial fashion. *Nucleic Acids Research*, *48*(2), 589–604. https://doi.org/10.1093/nar/gkz1112

Curtis, C. D., Likhite, V. S., McLeod, I. X., Yates, J. R., & Nardulli, A. M. (2007). Interaction of the Tumor Metastasis Suppressor Nonmetastatic Protein 23 Homologue H1 and Estrogen Receptor α Alters Estrogen-Responsive Gene Expression. *Cancer Research*, *67*(21), 10600–10607. https://doi.org/10.1158/0008-5472.CAN-07-0055

Egistelli, L., Chichiarelli, S., Gaucci, E., Eufemi, M., Schininà, M. E., Giorgi, A., Lascu, I., Turano, C., Giartosio, A., & Cervoni, L. (2009). IFI16 and NM23 bind to a common DNA fragment both in the *P53* and the *cMYC* gene promoters. *Journal of Cellular Biochemistry*, *106*(4), 666–672. https://doi.org/10.1002/jcb.22053

Fornes, O., Castro-Mondragon, J. A., Khan, A., van der Lee, R., Zhang, X., Richmond, P. A., Modi, B. P., Correard, S., Gheorghe, M., Baranašić, D., Santana-Garcia, W., Tan, G., Chèneby, J., Ballester, B., Parcy, F., Sandelin, A., Lenhard, B., Wasserman, W. W., & Mathelier, A. (2019). JASPAR 2020: Update of the open-access database of transcription factor binding profiles. *Nucleic Acids Research*, gkz1001. https://doi.org/10.1093/nar/gkz1001

Freaney, J. E., Kim, R., Mandhana, R., & Horvath, C. M. (2013). Extensive Cooperation of Immune Master Regulators IRF3 and NFκB in RNA Pol II Recruitment and Pause Release in Human Innate Antiviral Transcription. *Cell Reports*, *4*(5), 959–973. https://doi.org/10.1016/j.celrep.2013.07.043

Fu, K., Sun, X., Zheng, W., Wier, E. M., Hodgson, A., Tran, D. Q., Richard, S., & Wan, F. (2013). Sam68 modulates the promoter specificity of NF-κB and mediates expression of CD25 in activated T cells. *Nature Communications*, *4*(1), 1909. https://doi.org/10.1038/ncomms2916

Ghosh, G., Duyne, G. V., Ghosh, S., & Sigler, P. B. (1995). Structure of NF-κB p50 homodimer bound to a κB site. *Nature*, *373*(6512), 303–310. https://doi.org/10.1038/373303a0

Ghosh, G., Wang, V. Y.-F., Huang, D.-B., & Fusco, A. (2012). NF-κB regulation: Lessons from structures: NF-κB regulation: lessons from structures. *Immunological Reviews*, *246*(1), 36–58. https://doi.org/10.1111/j.1600-065X.2012.01097.x

Giffin, M. J., Stroud, J. C., Bates, D. L., von Koenig, K. D., Hardin, J., & Chen, L. (2003). Structure of NFAT1 bound as a dimer to the HIV-1 LTR κB element. *Nature Structural & Molecular Biology*, *10*(10), 800–806. https://doi.org/10.1038/nsb981

Glass, C. K., & Natoli, G. (2016). Molecular control of activation and priming in macrophages. *Nature Immunology*, *17*(1), 26–33. https://doi.org/10.1038/ni.3306

Guttridge, D. C., Albanese, C., Reuther, J. Y., Pestell, R. G., & Baldwin, A. S. (1999). NF-kappaB controls cell growth and differentiation through transcriptional regulation of cyclin D1. *Molecular and Cellular Biology*, *19*(8), 5785–5799. https://doi.org/10.1128/MCB.19.8.5785

Hammar, P., Leroy, P., Mahmutovic, A., Marklund, E. G., Berg, O. G., & Elf, J. (2012). The lac repressor displays facilitated diffusion in living cells. *Science (New York, N.Y.)*, *336*(6088), 1595–1598. https://doi.org/10.1126/science.1221648

Hayden, M. S., & Ghosh, S. (2011). NF-κB in immunobiology. *Cell Research*, *21*(2), 223–244. https://doi.org/10.1038/cr.2011.13

Hayden, M. S., & Ghosh, S. (2011). NF-κB in immunobiology. *Cell Research*, *21*(2), 223–244. https://doi.org/10.1038/cr.2011.13

Heinz, S., Romanoski, C. E., Benner, C., Allison, K. A., Kaikkonen, M. U., Orozco, L. D., & Glass, C. K. (2013). Effect of natural genetic variation on enhancer selection and function. *Nature*, *503*(7477), 487–492. https://doi.org/10.1038/nature12615

Heldring, N., Isaacs, G. D., Diehl, A. G., Sun, M., Cheung, E., Ranish, J. A., & Kraus, W. L. (2011). Multiple Sequence-Specific DNA-Binding Proteins Mediate Estrogen Receptor Signaling through a Tethering Pathway. *Molecular Endocrinology*, *25*(4), 564–574. https://doi.org/10.1210/me.2010-0425

Hoffmann, A. (2003). Genetic analysis of NF- B/Rel transcription factors defines functional specificities. *The EMBO Journal*, *22*(20), 5530–5539. https://doi.org/10.1093/emboj/cdg534

Hoffmann, A., & Baltimore, D. (2006). Circuitry of nuclear factor kappaB signaling. *Immunological Reviews*, *210*, 171–186. https://doi.org/10.1111/j.0105-2896.2006.00375.x

Huang, D.-B., Chen, Y.-Q., Ruetsche, M., Phelps, C. B., & Ghosh, G. (2001). X-Ray Crystal Structure of Proto-Oncogene Product c-Rel Bound to the CD28 Response Element of IL-2. *Structure*, *9*(8), 669–678. https://doi.org/10.1016/S0969-2126(01)00635-9

Huang, T. T., Kudo, N., Yoshida, M., & Miyamoto, S. (2000). A nuclear export signal in the N-terminal regulatory domain of IκBα controls cytoplasmic localization of inactive NF-κB/IκBα complexes. *Proceedings of the National Academy of Sciences*, *97*(3), 1014–1019. https://doi.org/10.1073/pnas.97.3.1014

Huxford, T., Huang, D. B., Malek, S., & Ghosh, G. (1998). The crystal structure of the IkappaBalpha/NF-kappaB complex reveals mechanisms of NF-kappaB inactivation. *Cell*, *95*(6), 759–770. https://doi.org/10.1016/s0092-8674(00)81699-2

Huxford, T., Malek, S., & Ghosh, G. (1999). Structure and Mechanism in NF- B/I B Signaling. *Cold Spring Harbor Symposia on Quantitative Biology*, *64*(0), 533–540. https://doi.org/10.1101/sqb.1999.64.533

Inukai, S., Kock, K. H., & Bulyk, M. L. (2017). Transcription factor–DNA binding: Beyond binding site motifs. *Current Opinion in Genetics & Development*, *43*, 110–119. https://doi.org/10.1016/j.gde.2017.02.007

Jain, J., McCaffrey, P. G., Valge-Archer, V. E., & Rao, A. (1992). Nuclear factor of activated T cells contains Fos and Jun. *Nature*, *356*(6372), 801–804. https://doi.org/10.1038/356801a0

Jin, F., Li, Y., Dixon, J. R., Selvaraj, S., Ye, Z., Lee, A. Y., Yen, C.-A., Schmitt, A. D., Espinoza, C. A., & Ren, B. (2013). A high-resolution map of the three-dimensional chromatin interactome in human cells. *Nature*, *503*(7475), 290–294. https://doi.org/10.1038/nature12644

Jin, X., Ding, D., Yan, Y., Li, H., Wang, B., Ma, L., Ye, Z., Ma, T., Wu, Q., Rodrigues, D. N., Kohli, M., Jimenez, R., Wang, L., Goodrich, D. W., de Bono, J., Dong, H., Wu, H., Zhu, R., & Huang, H. (2019). Phosphorylated RB Promotes Cancer Immunity by Inhibiting NF-κB Activation and PD-L1 Expression. *Molecular Cell*, *73*(1), 22-35.e6. https://doi.org/10.1016/j.molcel.2018.10.034

Jolma, A., Yin, Y., Nitta, K. R., Dave, K., Popov, A., Taipale, M., Enge, M., Kivioja, T., Morgunova, E., & Taipale, J. (2015). DNA-dependent formation of transcription factor pairs alters their binding specificity. *Nature*, *527*(7578), 384–388. https://doi.org/10.1038/nature15518

Karin, M. (1999). How NF-κB is activated: The role of the IκB kinase (IKK) complex. *Oncogene*, *18*(49), 6867–6874. https://doi.org/10.1038/sj.onc.1203219

Karin, M., & Ben-Neriah, Y. (2000). Phosphorylation Meets Ubiquitination: The Control of NF-κB Activity. *Annual Review of Immunology*, *18*(1), 621–663. https://doi.org/10.1146/annurev.immunol.18.1.621

Kasowski, M., Grubert, F., Heffelfinger, C., Hariharan, M., Asabere, A., Waszak, S. M., Habegger, L., Rozowsky, J., Shi, M., Urban, A. E., Hong, M.-Y., Karczewski, K. J., Huber, W., Weissman, S. M., Gerstein, M. B., Korbel, J. O., & Snyder, M. (2010). Variation in Transcription Factor Binding Among Humans. *Science*, *328*(5975), 232–235. https://doi.org/10.1126/science.1183621

Kolovos, P., Georgomanolis, T., Koeferle, A., Larkin, J. D., Brant, L., Nikolicć, M., Gusmao, E. G., Zirkel, A., Knoch, T. A., van Ijcken, W. F., Cook, P. R., Costa, I. G., Grosveld, F. G., & Papantonis, A. (2016). Binding of nuclear factor κB to noncanonical consensus sites reveals its

multimodal role during the early inflammatory response. *Genome Research*, *26*(11), 1478–1489. https://doi.org/10.1101/gr.210005.116

Lascu, I., & Gonin, P. (2000). The catalytic mechanism of nucleoside diphosphate kinases. *Journal of Bioenergetics and Biomembranes*, *32*(3), 237–246. https://doi.org/10.1023/A:1005532912212

Lawrence, T. (2009). The nuclear factor NF-kappaB pathway in inflammation. *Cold Spring Harbor Perspectives in Biology*, *1*(6), a001651. https://doi.org/10.1101/cshperspect.a001651

Lecroisey, A., Lascu, I., Bominaar, A., Veron, M., & Delepierre, M. (1995). Phosphorylation Mechanism of Nucleoside Diphosphate Kinase: 31P-Nuclear Magnetic Resonance Studies. *Biochemistry*, *34*(38), 12445–12450. https://doi.org/10.1021/bi00038a043

Leung, T. H., Hoffmann, A., & Baltimore, D. (2004). One nucleotide in a kappaB site can determine cofactor specificity for NF-kappaB dimers. *Cell*, *118*(4), 453–464. https://doi.org/10.1016/j.cell.2004.08.007

Leven, I., & Levy, Y. (2019). Quantifying the two-state facilitated diffusion model of protein–DNA interactions. *Nucleic Acids Research*, *47*(11), 5530–5538. https://doi.org/10.1093/nar/gkz308

Li, X.-Y., Thomas, S., Sabo, P. J., Eisen, M. B., Stamatoyannopoulos, J. A., & Biggin, M. D. (2011). The role of chromatin accessibility in directing the widespread, overlapping patterns of Drosophila transcription factor binding. *Genome Biology*, *12*(4), R34. https://doi.org/10.1186/gb-2011-12-4-r34

Lim, C.-A., Yao, F., Wong, J. J.-Y., George, J., Xu, H., Chiu, K. P., Sung, W.-K., Lipovich, L., Vega, V. B., Chen, J., Shahab, A., Zhao, X. D., Hibberd, M., Wei, C.-L., Lim, B., Ng, H.-H., Ruan, Y., & Chin, K.-C. (2007). Genome-wide Mapping of RELA(p65) Binding Identifies E2F1 as a Transcriptional Activator Recruited by NF-κB upon TLR4 Activation. *Molecular Cell*, *27*(4), 622–635. https://doi.org/10.1016/j.molcel.2007.06.038

Lin, J., Kato, M., Nagata, K., & Okuwaki, M. (2017). Efficient DNA binding of NF-κB requires the chaperone-like function of NPM1. *Nucleic Acids Research*, *45*(7), 3707–3723. https://doi.org/10.1093/nar/gkw1285

Liu, Q., Chen, Y., Auger-Messier, M., & Molkentin, J. D. (2012). Interaction Between NFκB and NFAT Coordinates Cardiac Hypertrophy and Pathological Remodeling. *Circulation Research*, *110*(8), 1077–1086. https://doi.org/10.1161/CIRCRESAHA.111.260729

Liu, T., Zhang, L., Joo, D., & Sun, S.-C. (2017). NF-κB signaling in inflammation. *Signal Transduction and Targeted Therapy*, *2*(1), 17023. https://doi.org/10.1038/sigtrans.2017.23

Liu, Y., Bridges, R., Wortham, A., & Kulesz-Martin, M. (2012). NF-κB repression by PIAS3 mediated RelA SUMOylation. *PloS One*, *7*(5), e37636. https://doi.org/10.1371/journal.pone.0037636

Ma, D., McCorkle, J. R., & Kaetzel, D. M. (2004). The Metastasis Suppressor NM23-H1 Possesses 3′-5′ Exonuclease Activity. *Journal of Biological Chemistry*, *279*(17), 18073–18084. https://doi.org/10.1074/jbc.M400185200

Macián, F., López-Rodríguez, C., & Rao, A. (2001). Partners in transcription: NFAT and AP-1. *Oncogene*, *20*(19), 2476–2489. https://doi.org/10.1038/sj.onc.1204386

Martone, R., Euskirchen, G., Bertone, P., Hartman, S., Royce, T. E., Luscombe, N. M., Rinn, J. L., Nelson, F. K., Miller, P., Gerstein, M., Weissman, S., & Snyder, M. (2003). Distribution of NF-κB-binding sites across human chromosome 22. *Proceedings of the National Academy of Sciences*, *100*(21), 12247–12252. https://doi.org/10.1073/pnas.2135255100

Meijsing, S. H., Pufall, M. A., So, A. Y., Bates, D. L., Chen, L., & Yamamoto, K. R. (2009). DNA binding site sequence directs glucocorticoid receptor structure and activity. *Science (New York, N.Y.)*, *324*(5925), 407–410. https://doi.org/10.1126/science.1164265

Mirny, L. A. (2010). Nucleosome-mediated cooperativity between transcription factors. *Proceedings of the National Academy of Sciences*, *107*(52), 22534–22539. https://doi.org/10.1073/pnas.0913805107

Mognol, G. P., González-Avalos, E., Ghosh, S., Spreafico, R., Gudlur, A., Rao, A., Damoiseaux, R., & Hogan, P. G. (2019). Targeting the NFAT:AP-1 transcriptional complex on DNA with a small-molecule inhibitor. *Proceedings of the National Academy of Sciences of the United States of America*, *116*(20), 9959–9968. https://doi.org/10.1073/pnas.1820604116

Mohanty, S., Kumar, A., Das, P., Sahu, S. K., Mukherjee, R., Ramachandranpillai, R., Nair, S. S., & Choudhuri, T. (2022). Nm23-H1 induces apoptosis in primary effusion lymphoma cells via inhibition of NF-κB signaling through interaction with oncogenic latent protein vFLIP K13 of Kaposi's sarcoma-associated herpes virus. *Cellular Oncology*, *45*(5), 967–989. https://doi.org/10.1007/s13402-022-00701-9

Morgunova, E., & Taipale, J. (2017). Structural perspective of cooperative transcription factor binding. *Current Opinion in Structural Biology*, *47*, 1–8. https://doi.org/10.1016/j.sbi.2017.03.006

Mulero, M. C., Huang, D.-B., Nguyen, H. T., Wang, V. Y.-F., Li, Y., Biswas, T., & Ghosh, G. (2017). DNA-binding affinity and transcriptional activity of the RelA homodimer of nuclear factor κB are not correlated. *Journal of Biological Chemistry*, *292*(46), 18821–18830. https://doi.org/10.1074/jbc.M117.813980

Mulero, M. C., Wang, V. Y.-F., Huxford, T., & Ghosh, G. (2019). Genome reading by the NF-κB transcription factors. *Nucleic Acids Research*, *47*(19), 9967–9989. https://doi.org/10.1093/nar/gkz739

Müller, C. W., Rey, F. A., Sodeoka, M., Verdine, G. L., & Harrison, S. C. (1995). Structure of the NF-κB p50 homodimer bound to DNA. *Nature*, *373*(6512), 311–317. https://doi.org/10.1038/373311a0

Müller, M. R., & Rao, A. (2010). NFAT, immunity and cancer: A transcription factor comes of age. *Nature Reviews Immunology*, *10*(9), 645–656. https://doi.org/10.1038/nri2818

Ngo, K. A., Kishimoto, K., Davis-Turak, J., Pimplaskar, A., Cheng, Z., Spreafico, R., Chen, E. Y., Tam, A., Ghosh, G., Mitchell, S., & Hoffmann, A. (2020). Dissecting the Regulatory Strategies of NF-κB RelA Target Genes in the Inflammatory Response Reveals Differential Transactivation Logics. *Cell Reports*, *30*(8), 2758-2775.e6. https://doi.org/10.1016/j.celrep.2020.01.108

Norman, A. W., Wedding, R. T., & Black, M. K. (1965). Detection of phosphohistidine in nucleoside diphosphokinase isolated from Jerusalem artichoke mitochondria. *Biochemical and Biophysical Research Communications*, *20*(6), 703–709. https://doi.org/10.1016/0006-291X(65)90073-2

Oeckinghaus, A., & Ghosh, S. (2009). The NF- B Family of Transcription Factors and Its Regulation. *Cold Spring Harbor Perspectives in Biology*, *1*(4), a000034–a000034. https://doi.org/10.1101/cshperspect.a000034

Pamidimukkala, N. V., Leonard, M. K., Snyder, D., Mccorkle, J. R., & Kaetzel, D. M. (2018). Metastasis Suppressor NME1 Directly Activates Transcription of the *ALDOC* Gene in Melanoma Cells. *Anticancer Research*, *38*(11), 6059–6068. https://doi.org/10.21873/anticanres.12956

Pan, L., Hao, W., Zheng, X., Zeng, X., Ahmed Abbasi, A., Boldogh, I., & Ba, X. (2017). OGG1-DNA interactions facilitate NF-κB binding to DNA targets. *Scientific Reports*, *7*, 43297. https://doi.org/10.1038/srep43297

Pan, M., Winslow, M. M., Chen, L., Kuo, A., Felsher, D., & Crabtree, G. R. (2007). Enhanced NFATc1 nuclear occupancy causes T cell activation independent of CD28 costimulation. *Journal of Immunology (Baltimore, Md.: 1950)*, *178*(7), 4315–4321. https://doi.org/10.4049/jimmunol.178.7.4315

Pan, W., Meshcheryakov, V. A., Li, T., Wang, Y., Ghosh, G., & Wang, V. Y.-F. (2023). Structures of NF-κB p52 homodimer-DNA complexes rationalize binding mechanisms and transcription activation. *ELife*, *12*, e86258. https://doi.org/10.7554/eLife.86258

Panne, D., Maniatis, T., & Harrison, S. C. (2007). An Atomic Model of the Interferon-β Enhanceosome. *Cell*, *129*(6), 1111–1123. https://doi.org/10.1016/j.cell.2007.05.019

Peng, S. L., Gerth, A. J., Ranger, A. M., & Glimcher, L. H. (2001). NFATc1 and NFATc2 Together Control Both T and B Cell Activation and Differentiation. *Immunity*, *14*(1), 13–20. https://doi.org/10.1016/S1074-7613(01)00085-1

Pham, L. V., Tamayo, A. T., Yoshimura, L. C., Lin-Lee, Y.-C., & Ford, R. J. (2005). Constitutive NF-kappaB and NFAT activation in aggressive B-cell lymphomas synergistically activates the CD154 gene and maintains lymphoma cell survival. *Blood*, *106*(12), 3940–3947. https://doi.org/10.1182/blood-2005-03-1167

Phelps, C. B., Sengchanthalangsy, L. L., Malek, S., & Ghosh, G. (2000). Mechanism of κB DNA binding by Rel/NF-κB dimers. *Journal of Biological Chemistry*, *275*(32), 24392–24399. https://doi.org/10.1074/jbc.M003784200

Ramirez-Carrozzi, V. R., & Kerppola, T. K. (2001). Dynamics of Fos-Jun-NFAT1 complexes. *Proceedings of the National Academy of Sciences*, *98*(9), 4893–4898. https://doi.org/10.1073/pnas.091095998

Rao, P., Hayden, M. S., Long, M., Scott, M. L., West, A. P., Zhang, D., Oeckinghaus, A., Lynch, C., Hoffmann, A., Baltimore, D., & Ghosh, S. (2010). IkappaBbeta acts to inhibit and activate gene expression during the inflammatory response. *Nature*, *466*(7310), 1115–1119. https://doi.org/10.1038/nature09283

Rao, S., Ahmad, K., & Ramachandran, S. (2021). Cooperative binding between distant transcription factors is a hallmark of active enhancers. *Molecular Cell*, *81*(8), 1651-1665.e4. https://doi.org/10.1016/j.molcel.2021.02.014

Ravasi, T., Suzuki, H., Cannistraci, C. V., Katayama, S., Bajic, V. B., Tan, K., Akalin, A., Schmeier, S., Kanamori-Katayama, M., Bertin, N., Carninci, P., Daub, C. O., Forrest, A. R. R., Gough, J., Grimmond, S., Han, J.-H., Hashimoto, T., Hide, W., Hofmann, O., … Hayashizaki, Y. (2010). An atlas of combinatorial transcriptional regulation in mouse and man. *Cell*, *140*(5), 744–752. https://doi.org/10.1016/j.cell.2010.01.044

Ray, S., Tillo, D., Durell, S. R., Khund-Sayeed, S., & Vinson, C. (2021). REL Domain of NFATc2 Binding to Five Types of DNA Using Protein Binding Microarrays. *ACS Omega*, *6*(6), 4147–4154. https://doi.org/10.1021/acsomega.0c04069

Sarai, A., & Kono, H. (2005). Protein-DNA Recognition Patterns and Predictions. *Annual Review of Biophysics and Biomolecular Structure*, *34*(1), 379–398. https://doi.org/10.1146/annurev.biophys.34.040204.144537

Sen, R., & Baltimore, D. (1986). Inducibility of κ immunoglobulin enhancer-binding protein NF-κB by a posttranslational mechanism. *Cell*, *47*(6), 921–928. https://doi.org/10.1016/0092-8674(86)90807-X

Shahein, A., López-Malo, M., Istomin, I., Olson, E. J., Cheng, S., & Maerkl, S. J. (2022). Systematic analysis of low-affinity transcription factor binding site clusters in vitro and in vivo establishes their functional relevance. *Nature Communications*, *13*(1), 5273. https://doi.org/10.1038/s41467-022-32971-0

Sharif, O., Bolshakov, V. N., Raines, S., Newham, P., & Perkins, N. D. (2007). Transcriptional profiling of the LPS induced NF-κB response in macrophages. *BMC Immunology*, *8*(1), 1. https://doi.org/10.1186/1471-2172-8-1

Shen, Z., Li, R. Z., Prohaska, T. A., Hoeksema, M. A., Spann, N. J., Tao, J., Fonseca, G. J., Le, T., Stolze, L. K., Sakai, M., Romanoski, C. E., & Glass, C. K. (2022). Systematic analysis of naturally occurring insertions and deletions that alter transcription factor spacing identifies tolerant and sensitive transcription factor pairs. *ELife*, *11*, e70878. https://doi.org/10.7554/eLife.70878

Sica, A., Dorman, L., Viggiano, V., Cippitelli, M., Ghosh, P., Rice, N., & Young, H. A. (1997). Interaction of NF-κB and NFAT with the Interferon-γ Promoter. *Journal of Biological Chemistry*, *272*(48), 30412–30420. https://doi.org/10.1074/jbc.272.48.30412

Siggers, T., Chang, A. B., Teixeira, A., Wong, D., Williams, K. J., Ahmed, B., Ragoussis, J., Udalova, I. A., Smale, S. T., & Bulyk, M. L. (2012). Principles of dimer-specific gene regulation revealed by a comprehensive characterization of NF-κB family DNA binding. *Nature Immunology*, *13*(1), 95–102. https://doi.org/10.1038/ni.2151

Singh, A., Martinez-Yamout, M. A., Wright, P. E., & Dyson, H. J. (2022). Structural and dynamic studies of DNA recognition by NF-κB p50 RHR homodimer using methyl NMR spectroscopy. *Nucleic Acids Research*, *50*(12), 7147–7160. https://doi.org/10.1093/nar/gkac535

Smale, S. T. (2012). Dimer-specific regulatory mechanisms within the NF-κB family of transcription factors: NF-κB dimer-specific regulatory mechanisms. *Immunological Reviews*, *246*(1), 193–204. https://doi.org/10.1111/j.1600-065X.2011.01091.x

Soto-Nieves, N., Puga, I., Abe, B. T., Bandyopadhyay, S., Baine, I., Rao, A., & Macian, F. (2009). Transcriptional complexes formed by NFAT dimers regulate the induction of T cell tolerance. *Journal of Experimental Medicine*, *206*(4), 867–876. https://doi.org/10.1084/jem.20082731

Spitz, F., & Furlong, E. E. M. (2012). Transcription factors: From enhancer binding to developmental control. *Nature Reviews Genetics*, *13*(9), 613–626. https://doi.org/10.1038/nrg3207

Steeg, P. S., Bevilacqua, G., Kopper, L., Thorgeirsson, U. P., Talmadge, J. E., Liotta, L. A., & Sobel, M. E. (1988). Evidence for a Novel Gene Associated With Low Tumor Metastatic Potential. *JNCI Journal of the National Cancer Institute*, *80*(3), 200–204. https://doi.org/10.1093/jnci/80.3.200

Stefflova, K., Thybert, D., Wilson, M. D., Streeter, I., Aleksic, J., Karagianni, P., Brazma, A., Adams, D. J., Talianidis, I., Marioni, J. C., Flicek, P., & Odom, D. T. (2013). Cooperativity and Rapid Evolution of Cobound Transcription Factors in Closely Related Mammals. *Cell*, *154*(3), 530–540. https://doi.org/10.1016/j.cell.2013.07.007

Stroud, J. C., & Chen, L. (2003). Structure of NFAT bound to DNA as a monomer. *Journal of Molecular Biology*, *334*(5), 1009–1022. https://doi.org/10.1016/j.jmb.2003.09.065

Subramanian, C., & Robertson, E. S. (2002). The Metastatic Suppressor Nm23-H1 Interacts with EBNA3C at Sequences Located between the Glutamine- and Proline-Rich Domains and Can Cooperate in Activation of Transcription. *Journal of Virology*, *76*(17), 8702–8709. https://doi.org/10.1128/JVI.76.17.8702-8709.2002

Taatjes, D. J. (2010). The human Mediator complex: A versatile, genome-wide regulator of transcription. *Trends in Biochemical Sciences*, *35*(6), 315–322. https://doi.org/10.1016/j.tibs.2010.02.004

Taniguchi, K., & Karin, M. (2018). NF-κB, inflammation, immunity and cancer: Coming of age. *Nature Reviews Immunology*, *18*(5), 309–324. https://doi.org/10.1038/nri.2017.142

Tapryal, N., Shahabi, S., Chakraborty, A., Hosoki, K., Wakamiya, M., Sarkar, G., Sharma, G., Cardenas, V. J., Boldogh, I., Sur, S., Ghosh, G., & Hazra, T. K. (2021). Intrapulmonary administration of purified NEIL2 abrogates NF-κB-mediated inflammation. *The Journal of Biological Chemistry*, *296*, 100723. https://doi.org/10.1016/j.jbc.2021.100723

Tong, A.-J., Liu, X., Thomas, B. J., Lissner, M. M., Baker, M. R., Senagolage, M. D., Allred, A. L., Barish, G. D., & Smale, S. T. (2016). A Stringent Systems Approach Uncovers Gene-Specific Mechanisms Regulating Inflammation. *Cell*, *165*(1), 165–179. https://doi.org/10.1016/j.cell.2016.01.020

Tsui, R., Kearns, J. D., Lynch, C., Vu, D., Ngo, K. A., Basak, S., Ghosh, G., & Hoffmann, A. (2015). IκBβ enhances the generation of the low-affinity NFκB/RelA homodimer. *Nature Communications*, *6*(1), 7068. https://doi.org/10.1038/ncomms8068

van Essen, D., Engist, B., Natoli, G., & Saccani, S. (2009). Two Modes of Transcriptional Activation at Native Promoters by NF-κB p65. *PLoS Biology*, *7*(3), e1000073. https://doi.org/10.1371/journal.pbio.1000073

Wagner, P. D., & Vu, N.-D. (2000). Phosphorylation of Geranyl and Farnesyl Pyrophosphates by Nm23 Proteins/Nucleoside Diphosphate Kinases. *Journal of Biological Chemistry*, *275*(45), 35570–35576. https://doi.org/10.1074/jbc.M006106200

Wan, F., Anderson, D. E., Barnitz, R. A., Snow, A., Bidere, N., Zheng, L., Hegde, V., Lam, L. T., Staudt, L. M., Levens, D., Deutsch, W. A., & Lenardo, M. J. (2007). Ribosomal Protein S3: A KH Domain Subunit in NF-κB Complexes that Mediates Selective Gene Regulation. *Cell*, *131*(5), 927–939. https://doi.org/10.1016/j.cell.2007.10.009

Wan, F., & Lenardo, M. J. (2009). Specification of DNA binding activity of NF-kappaB proteins. *Cold Spring Harbor Perspectives in Biology*, *1*(4), a000067. https://doi.org/10.1101/cshperspect.a000067

Wang, J., Zhuang, J., Iyer, S., Lin, X., Whitfield, T. W., Greven, M. C., Pierce, B. G., Dong, X., Kundaje, A., Cheng, Y., Rando, O. J., Birney, E., Myers, R. M., Noble, W. S., Snyder, M., & Weng, Z. (2012). Sequence features and chromatin structure around the genomic regions bound by 119 human transcription factors. *Genome Research*, *22*(9), 1798–1812. https://doi.org/10.1101/gr.139105.112

Wang, V. Y.-F., Huang, W., Asagiri, M., Spann, N., Hoffmann, A., Glass, C., & Ghosh, G. (2012). The transcriptional specificity of NF-κB dimers is coded within the κB DNA response elements. *Cell Reports*, *2*(4), 824–839. https://doi.org/10.1016/j.celrep.2012.08.042

Wong, D., Teixeira, A., Oikonomopoulos, S., Humburg, P., Lone, I., Saliba, D., Siggers, T., Bulyk, M., Angelov, D., Dimitrov, S., Udalova, I. A., & Ragoussis, J. (2011). Extensive characterization of NF-κB binding uncovers non-canonical motifs and advances the interpretation of genetic functional traits. *Genome Biology*, *12*(7), R70. https://doi.org/10.1186/gb-2011-12-7-r70

Wu, Y., Kröller, L., Miao, B., Boekhoff, H., Bauer, A. S., Büchler, M. W., Hackert, T., Giese, N. A., Taipale, J., & Hoheisel, J. D. (2021). Promoter Hypermethylation Promotes the Binding of Transcription Factor NFATc1, Triggering Oncogenic Gene Activation in Pancreatic Cancer. *Cancers*, *13*(18), 4569. https://doi.org/10.3390/cancers13184569

Xia, Y., Shen, S., & Verma, I. M. (2014). NF-κB, an active player in human cancers. *Cancer Immunology Research*, *2*(9), 823–830. https://doi.org/10.1158/2326-6066.CIR-14-0112

Yan, J., Enge, M., Whitington, T., Dave, K., Liu, J., Sur, I., Schmierer, B., Jolma, A., Kivioja, T., Taipale, M., & Taipale, J. (2013). Transcription factor binding in human cells occurs in dense clusters formed around cohesin anchor sites. *Cell*, *154*(4), 801–813. https://doi.org/10.1016/j.cell.2013.07.034

Yarilina, A., Xu, K., Chen, J., & Ivashkiv, L. B. (2011). TNF activates calcium–nuclear factor of activated T cells (NFAT)c1 signaling pathways in human macrophages. *Proceedings of the National Academy of Sciences*, *108*(4), 1573–1578. https://doi.org/10.1073/pnas.1010030108

Yie, J., Liang, S., Merika, M., & Thanos, D. (1997). Intra- and intermolecular cooperative binding of high-mobility-group protein I(Y) to the beta-interferon promoter. *Molecular and Cellular Biology*, *17*(7), 3649–3662. https://doi.org/10.1128/MCB.17.7.3649

You, D.-J., Park, C. R., Lee, H. B., Moon, M. J., Kang, J.-H., Lee, C., Oh, S.-H., Ahn, C., Seong, J. Y., & Hwang, J.-I. (2014). A Splicing Variant of NME1 Negatively Regulates NF-κB Signaling and Inhibits Cancer Metastasis by Interacting with IKKβ. *Journal of Biological Chemistry*, *289*(25), 17709–17720. https://doi.org/10.1074/jbc.M114.553552

Yu, H., Lin, L., Zhang, Z., Zhang, H., & Hu, H. (2020). Targeting NF-κB pathway for the therapy of diseases: Mechanism and clinical study. *Signal Transduction and Targeted Therapy*, *5*(1), 209. https://doi.org/10.1038/s41392-020-00312-6

Zabel, U., Schreck, R., & Baeuerle, P. A. (1991). DNA binding of purified transcription factor NF-kappa B. Affinity, specificity, Zn2+ dependence, and differential half-site recognition. *The Journal of Biological Chemistry*, *266*(1), 252–260.

Zhang, Q., Lenardo, M. J., & Baltimore, D. (2017). 30 Years of NF-κB: A Blossoming of Relevance to Human Pathobiology. *Cell*, *168*(1–2), 37–57. https://doi.org/10.1016/j.cell.2016.12.012

Zhao, B., Barrera, L. A., Ersing, I., Willox, B., Schmidt, S. C. S., Greenfeld, H., Zhou, H., Mollo, S. B., Shi, T. T., Takasaki, K., Jiang, S., Cahir-McFarland, E., Kellis, M., Bulyk, M. L., Kieff, E., & Gewurz, B. E. (2014). The NF-κB Genomic Landscape in Lymphoblastoid B Cells. *Cell Reports*, *8*(5), 1595–1606. https://doi.org/10.1016/j.celrep.2014.07.037

Zhao, J., Tian, M., Zhang, S., Delfarah, A., Gao, R., Rao, Y., Savas, A. C., Lu, A., Bubb, L., Lei, X., Moshirian, R., Zhu, W., Peng, C., Jiang, T., Chen, L., Graham, N. A., & Feng, P. (2020). Deamidation Shunts RelA from Mediating Inflammation to Aerobic Glycolysis. *Cell Metabolism*, *31*(5), 937-955.e7. https://doi.org/10.1016/j.cmet.2020.04.006